



JOHANNES GUTENBERG  
UNIVERSITÄT MAINZ

Complement Receptor 3 and its role in the  
interaction of primary human macrophages with  
apoptotic *Leishmania major* promastigotes

## **Dissertation**

Zur Erlangung des Grades  
Doktor der Naturwissenschaften

Am Fachbereich Biologie  
Der Johannes Gutenberg-Universität Mainz

Stefan Albrecht Schille

geboren am 03.09.1987 in Heilbronn

Mainz, 2019



Dekan:

1. Berichterstatter:

2. Berichterstatter:

Tag der mündlichen Prüfung: 18.06.2019



# Contents

Abbreviations

Summary

Zusammenfassung

|         |  |    |
|---------|--|----|
| 1.      | Introduction .....   | 1  |
| 1.1     | The neglected tropical disease leishmaniasis.....                                      | 1  |
| 1.2     | The life cycle of <i>Leishmania</i> parasites .....                                    | 3  |
| 1.3     | Myeloid cells .....  | 6  |
| 1.4     | Phagocytosis .....   | 7  |
| 1.5     | LC3-associated phagocytosis .....  | 9  |
| 1.6     | Receptors in conventional phagocytosis and LC3-associated phagocytosis .....           | 11 |
| 1.7     | Cytokine secretion of myeloid cells and activation of the adaptive immune system ..... | 13 |
| 1.8     | Uptake of <i>Leishmania</i> promastigotes by myeloid cells .....                       | 14 |
| 1.9     | The importance of apoptotic promastigotes in <i>Leishmania major</i> infection.....    | 15 |
| 2.      | Hypothesis and Aims.....   | 17 |
| 3.      | Material and Methods .....   | 19 |
| 3.1     | Material.....  | 19 |
| 3.1.1   | Consumables.....   | 19 |
| 3.1.2   | Devices .....  | 21 |
| 3.1.3   | Software.....  | 24 |
| 3.1.4   | Chemicals .....  | 25 |
| 3.1.5   | Media .....  | 28 |
| 3.1.6   | Buffers and solutions .....  | 29 |
| 3.1.7   | <i>Leishmania</i> strains .....  | 34 |
| 3.1.8   | Human cells.....   | 34 |
| 3.1.8.1 | Primary cells .....  | 34 |
| 3.1.8.2 | Cell lines.....  | 34 |
| 3.1.9   | Antibodies and antisera .....  | 35 |
| 3.1.10  | Dyes and magnetic particles .....  | 37 |

|          |  |    |
|----------|--|----|
| 3.1.11   | Enzymes .....  | 38 |
| 3.1.12   | Ready-to-use kits.....   | 38 |
| 3.1.13   | Size markers .....   | 39 |
| 3.1.14   | Plasmids .....   | 39 |
| 3.1.15   | Oligonucleotides .....   | 40 |
| 3.2      | Methods.....   | 40 |
| 3.2.1    | Cell biological methods.....   | 40 |
| 3.2.1.1  | Cell culture of primary human cells.....   | 40 |
| 3.2.1.2  | Counting of human cells .....  | 40 |
| 3.2.1.3  | Isolation of peripheral blood mononuclear cells.....                             | 41 |
| 3.2.1.4  | Plastic adherence for the generation of macrophages .....                        | 41 |
| 3.2.1.5  | Monocyte isolation by CD14-MACS.....   | 42 |
| 3.2.1.6  | Harvesting of hMDMs and hMDDCs.....  | 42 |
| 3.2.1.7  | Generation of hMDMs in Teflon bags .....   | 43 |
| 3.2.1.8  | Long-time storage and thawing of PBLs .....                                      | 44 |
| 3.2.1.9  | Cultivation of HEK 293T/17 cells.....  | 44 |
| 3.2.1.10 | Cultivation of HT1080 cells .....  | 44 |
| 3.2.2    | Cultivation of <i>Leishmania major</i> promastigotes.....                        | 45 |
| 3.2.2.1  | Counting of <i>Leishmania major</i> parasites .....                              | 45 |
| 3.2.2.2  | AnnexinA5-MACS of stationary phase <i>Leishmania major</i> promastigotes .....   | 45 |
| 3.2.3    | Cycentrifugation of hMDMs and <i>Leishmania major</i> promastigotes.....         | 46 |
| 3.2.4    | Infection experiments .....  | 47 |
| 3.2.4.1  | Infection of transduced hMDMs for live cell microscopy .....                     | 47 |
| 3.2.4.2  | Infection of hMDMs and hMDDCs for flow cytometry or fluorescence microscopy..... | 47 |
| 3.2.4.3  | Cytokine analysis upon differential infection with <i>Leishmania major</i> ...   | 48 |
| 3.2.4.4  | CFSE-based proliferation assay.....  | 48 |
| 3.2.4.5  | Determination of parasite survival by limiting dilution assay .....              | 48 |
| 3.2.4.6  | Determination of LC3 conversion by western blot analysis .....                   | 49 |

|           |  |    |
|-----------|--|----|
| 3.2.5     | Magnetic isolation of phagosomes.....  | 49 |
| 3.2.5.1   | Isolation procedure for phagosomes .....   | 49 |
| 3.2.5.2   | Label-free mass spectrometry and functional protein association<br>network-analysis..... | 51 |
| 3.2.6     | Virological methods .....  | 52 |
| 3.2.6.1   | Production and concentration of lentiviral vectors .....                                 | 52 |
| 3.2.6.1.1 | Transfection of HEK 293T/17 cells with calcium phosphate .....                           | 52 |
| 3.2.6.1.2 | Concentration of lentiviral vector particles .....                                       | 53 |
| 3.2.6.2   | Titration of lentiviral vectors .....  | 53 |
| 3.2.6.3   | Lentiviral transduction of human monocyte-derived macrophages .....                      | 54 |
| 3.2.7     | Molecular biological methods .....   | 54 |
| 3.2.7.1   | Determination of nucleic acid concentration.....   | 54 |
| 3.2.7.2   | Transfection of hMDMs with small interfering RNA .....                                   | 55 |
| 3.2.7.3   | RNA isolation from hMDMs.....  | 55 |
| 3.2.7.4   | Reverse transcription for synthesis of cDNA.....   | 55 |
| 3.2.7.5   | Quantitative real-time polymerase chain reaction .....                                   | 57 |
| 3.2.8     | Protein-biochemical methods and immunoassays.....  | 58 |
| 3.2.8.1   | Western blot analysis .....  | 58 |
| 3.2.8.1.1 | Sodium dodecyl sulfate-polyacrylamide gel electrophoresis.....                           | 58 |
| 3.2.8.1.2 | Western blotting and protein detection.....  | 58 |
| 3.2.8.2   | Enzyme-linked immunosorbent assay (ELISA) .....  | 59 |
| 3.2.8.3   | Bicinchoninic acid assay .....   | 59 |
| 3.2.9     | Labeling and staining of hMDMs or <i>Leishmania major</i> promastigotes.....             | 60 |
| 3.2.9.1   | AnnexinA5-staining of <i>Leishmania major</i> promastigotes .....                        | 60 |
| 3.2.9.2   | Staining of <i>Leishmania major</i> promastigotes for live cell microscopy...            | 60 |
| 3.2.9.3   | Staining of infected hMDM for immunofluorescence microscopy ....                         | 60 |
| 3.2.9.4   | Diff-Quick staining .....  | 61 |
| 3.2.9.5   | Magnetic labeling of apoptotic <i>Leishmania major</i> .....                             | 61 |
| 3.2.9.6   | Detection of surface proteins by antibody staining .....                                 | 62 |

|          |   |     |
|----------|---|-----|
| 3.2.9.7  | Labeling of <i>Leishmania major</i> promastigotes with CFSE or AF647-SE for infection experiments.....                                | 62  |
| 3.2.9.8  | Labeling of PBLs and hMDMs for T cell proliferation assay .....   | 63  |
| 3.2.9.9  | DAPI staining of infected hMDMs .....   | 63  |
| 3.2.10   | Flow cytometry .....  | 63  |
| 3.2.11   | Microscopy.....   | 63  |
| 3.2.11.1 | Transmitted light microscopy .....  | 63  |
| 3.2.11.2 | Fluorescence microscopy .....   | 64  |
| 3.2.11.3 | Time lapse imaging of <i>Leishmania major</i> infection in hMDMs .....  | 64  |
| 3.2.12   | Statistical analysis .....  | 65  |
| 4.       | Results.....  | 66  |
| 4.1      | <i>In vitro</i> cultures of <i>Leishmania major</i> promastigotes contain apoptotic parasites .....                                   | 66  |
| 4.2      | Purification of apoptotic and viable <i>Leishmania major</i> by AnnexinA5-MACS.....   | 67  |
| 4.3      | Comparison of infection rates upon differential infection of human monocyte-derived macrophages by flow cytometry and microscopy..... | 68  |
| 4.4      | Generation of eGFP-LC3-expressing hMDMs by lentiviral transduction and live cell imaging of <i>Leishmania major</i> infection .....   | 70  |
| 4.5      | Evaluation of a possible evasion strategy by viable <i>Leishmania major</i> promastigotes .....                                       | 75  |
| 4.6      | Magnetic isolation of apoptotic <i>Leishmania major</i> -harboring phagosomes .....   | 78  |
| 4.7      | Phenotypic characterization of human monocyte-derived phagocytes .....  | 84  |
| 4.8      | Cytokine production of antigen-presenting cells upon differential infection with <i>Leishmania major</i> promastigotes .....          | 86  |
| 4.9      | Manipulation of CD91 on human monocyte-derived macrophages .....  | 89  |
| 4.10     | The influence of CD91 knockdown on infection with apoptotic <i>Leishmania major</i> promastigotes .....                               | 92  |
| 4.11     | Manipulation of CR3 on monocyte-derived antigen-presenting cells.....   | 93  |
| 4.12     | Inhibition of CR3 significantly reduces interaction with apoptotic <i>Leishmania major</i> promastigotes .....                        | 97  |
| 4.13     | CR3 modulation prior to <i>Leishmania major</i> infection leads to alterations in TNF- $\alpha$ and IL-10 secretion.....              | 100 |



|      |   |     |
|------|---|-----|
| 4.14 | Blocking of CR3 reduces the LC3 conversion in hMDM2 upon uptake of apoptotic <i>Leishmania major</i> promastigotes.....           | 102 |
| 4.15 | Decreased uptake of apoptotic <i>Leishmania major</i> promastigotes in presence of CR3 does not affect T cell proliferation ..... | 104 |
| 4.16 | Blocking of CR3 and the effect on parasite survival .....   | 106 |
| 5.   | Discussion .....  | 108 |
| 6.   | Concluding remarks .....  | 122 |
| 7.   | Appendix .....  | 124 |
| 8.   | References .....  | 125 |
| 9.   | List of figures.....  | 142 |
| 10.  | List of tables .....  | 144 |
| 11.  | Declaration of authorship .....   | 145 |



## Abbreviations

|                               |  |
|-------------------------------|--|
| µg                            | Microgram  |
| µL                            | Microliter   |
| µM                            | Micromolar   |
| AF                            | Alexa Fluor  |
| APC                           | Antigen-presenting cell  |
| CD                            | Cluster of differentiation   |
| CFSE                          | Carboxyfluorescein succinimidyl ester  |
| CL                            | Cutaneous leishmaniasis  |
| CM                            | Complete medium  |
| CR                            | Complement Receptor  |
| d                             | Day  |
| DNA (cDNA)                    | Deoxyribonucleic acid (complementary deoxyribonucleic acid)                      |
| dpi                           | Days post infection  |
| Ds                            | <i>Discosoma sp.</i>   |
| eGFP                          | Enhanced Green Fluorescent Protein   |
| FSC                           | Forward scatter  |
| h                             | Hour   |
| ddH <sub>2</sub> O            | Double distilled water   |
| dNTP (dATP, dCTP, dGTP, dTTP) | Deoxyribonucleoside (adenosine-, cytidine-, guanosine-, thymidine-) triphosphate |
| FIB-SEM                       | Focused ion-beam scanning electron microscopy                                    |
| g                             | Gram   |
| HIV                           | Human immunodeficiency virus   |
| hMDDC                         | Human monocyte-derived dendritic cell  |
| hMDM                          | Human monocyte-derived macrophage  |
| hpt                           | Hours post transfection  |
| HRP                           | Horseradish peroxidase   |
| IF                            | Immunofluorescence microscopy  |
| IFN                           | Interferon   |
| IgG                           | Immunoglobulin G   |
| IL                            | Interleukin  |

|                |  |
|----------------|--|
| i.u.           | Infectious units                               |
| L              | Liter  |
| LAP            | LC3-associated phagocytosis                    |
| LC             | Liquid chromatography                          |
| log. ph.       | Logarithmic growth phase                       |
| <i>Lm</i>      | <i>Leishmania major</i> promastigote           |
| LPG            | Lipophosphoglycan                              |
| M              | Molar  |
| mA             | Milli ampere                                   |
| mM             | Millimolar                                     |
| MCL            | Mucocutaneous leishmaniasis                    |
| MFI            | Mean fluorescence intensity                    |
| MHC            | Major histocompatibility complex               |
| min            | Minute   |
| mL             | Milliliter                                     |
| mm             | Millimeter                                     |
| MOI            | Multiplicity of infection                      |
| MS             | Mass spectrometry                              |
| ng             | Nanogram                                       |
| nM             | Nanomolar                                      |
| NTD            | Neglected tropical disease                     |
| pg             | Picogram                                       |
| PB             | Pacific Blue                                   |
| PBL            | Peripheral blood lymphocyte                    |
| PBMC           | Peripheral blood mononuclear cell              |
| PCR            | Polymerase chain reaction                      |
| PE             | Phycoerythrin                                  |
| PKDL           | Post-Kala-Azar dermal leishmaniasis            |
| PMN            | Polymorphonuclear neutrophil                   |
| PS             | Phosphatidylserine                             |
| RNA/mRNA/siRNA | Ribonucleic acid (messenger/small interfering) |
| ROS            | Reactive oxygen species                        |

|                |   |
|----------------|---|
| RT-PCR         | Real time polymerase chain reaction       |
| SE             | Succinimidyl ester                        |
| sec            | Second                                    |
| SSC            | Side scatter                              |
| stat. ph.      | Stationary growth phase                   |
| STED           | Stimulated emission depletion microscopy  |
| STEM           | Scanning transmission electron microscopy |
| TGF            | Transforming growth factor                |
| T <sub>H</sub> | T helper cell                             |
| TLR            | Toll-like receptor                        |
| TNF            | Tumor necrosis factor                     |
| U              | Units                                     |
| V              | Volt                                      |
| VL             | Visceral leishmaniasis                    |
| vs.            | Versus                                    |
| v/v            | Volume per volume                         |
| w/v            | Weight per volume                         |
| WB             | Western blot                              |
| WHO            | World Health Organization                 |
| WT             | Wildtype                                  |
| x <i>g</i>     | Fold gravitational acceleration           |



## Summary

*Leishmania* parasites are the causative agent of the neglected tropical disease leishmaniasis. The sand fly vector-borne, disease-initiating *Leishmania* promastigote life stage (*Lm*) is comprised of viable and apoptotic parasites. Targeting of the latter by LC3-associated phagocytosis (LAP) leads to a decreased activation of the adaptive immune system. Based on these findings, this study focuses on (1) the internalization of apoptotic *Lm* by human monocyte-derived pro- (hMDM1) and anti-inflammatory (hMDM2) macrophages, (2) evasion of viable *Lm* from degradation as well as (3) identification and (4) functional characterization of factors that lead to uptake of apoptotic *Lm* and LAP induction. For detailed analysis of the apoptotic *Lm* population we separated viable from apoptotic *Lm*. Phagocytosis assays by flow cytometry in which hMDMs were differentially infected with viable or apoptotic *Lm* showed that hMDMs ingested apoptotic *Lm* more rapidly than viable parasites. Investigations of supernatants from differentially infected hMDMs and hMDDCs by ELISA revealed not only a higher release of the anti-inflammatory cytokine IL-10 but also an increase in secretion of the pro-inflammatory cytokines IL-1 $\beta$ , IL-6 and IL-8 in presence of apoptotic *Lm*. Live cell microscopy showed that LAP can be triggered by viable and apoptotic *Lm*. Phagosomes harboring apoptotic parasites were targeted more frequently and more rapidly by eGFP-LC3 in hMDM2 as compared to phagosomes containing viable parasites. To identify factors that initiate apoptotic parasite internalization and LC3 recruitment, magnetic isolation of apoptotic *Lm*-containing phagosomes was performed. Subsequent mass spectrometry and data analysis revealed the phagocytic receptors low-density lipoprotein receptor-related protein 1 (CD91) and Complement Receptor 3 (CR3) to be highly abundant in phagosomes harboring apoptotic *Lm*. Blocking of CD91 with a monoclonal antibody was not efficient and knockdown of CD91 with siRNA did not affect uptake of *Lm*, but the interaction still might be relevant and should be investigated in more detail. Inhibition of CR3 with a functional antibody significantly reduced uptake of apoptotic *Lm* by hMDMs. This receptor blocking in turn resulted in a decreased production of pro-inflammatory TNF- $\alpha$  by hMDM1 and a significantly diminished IL-10 secretion by hMDM2. Inhibition of CR3 strikingly reduced LC3 lipidation as a measure for LAP induction in hMDM2 challenged with apoptotic or stationary phase *Lm*. Intriguingly, decreased internalization of apoptotic *Lm* neither resulted in a higher T cell proliferation nor in an increased survival of viable *Lm* within

hMDMs. In conclusion, the data for the first time describe CR3 to play a significant role in the interaction of hMDM2 with especially apoptotic *Lm* and indicate a role of the receptor in LAP. Control of receptor-mediated internalization and LAP of apoptotic *Lm* could serve as a novel therapeutic approach to combat the neglected tropical disease leishmaniasis.



## Zusammenfassung

Parasiten der Gattung *Leishmania* sind die Erreger der vernachlässigten Tropenkrankheit Leishmaniose. Das durch einen Sandfliegenvektor übertragene promastigote Lebensstadium der *Leishmanien* (*Lm*) umfasst lebendige als auch apoptotische Parasiten. Aufnahme der Letzteren durch LC3-assoziierte Phagozytose (LAP) führt zu einer verminderten Aktivierung des adaptiven Immunsystems. Basierend auf diesen Erkenntnissen konzentriert sich die vorliegende Studie auf (1) die Internalisierung von apoptotischen *Lm* durch primäre, humane pro- (hMDM1) und anti-inflammatorische (hMDM2) Makrophagen, (2) das Entkommen der lebendigen Parasiten vor der Degradation in der Zelle sowie (3) die Identifizierung und (4) funktionelle Charakterisierung von Faktoren, die zur Aufnahme der apoptotischen *Lm* und einer Induktion von LAP führen. Für eine detaillierte Analyse der apoptotischen Parasiten wurden diese von lebendigen *Lm* getrennt. Phagozytose-Assays mittels Durchflusszytometrie zeigten, dass nach differenzieller Infektion von hMDMs mit apoptotischen und lebendigen *Lm* die Aufnahme apoptotischer *Lm* schneller erfolgte als die Aufnahme lebendiger Parasiten. Untersuchungen von Zellüberständen differentiell infizierter hMDMs und hMDDCs mittels ELISA zeigten nicht nur eine erhöhte Freisetzung des anti-inflammatorischen Zytokins IL-10, sondern auch eine Erhöhung der Sekretion der pro-inflammatorischen Zytokine IL-1 $\beta$ , IL-6 und IL-8 durch hMDMs in Gegenwart von apoptotischen *Lm*. Die Analyse der LAP von *Lm* mittels Lebendzell-Mikroskopie ergab, dass eGFP-LC3 in hMDM2 in größerem Maße und schneller zu Phagosomen rekrutiert wurde, die apoptotische Parasiten beinhalteten, als zu Phagosomen, die lebendige Parasiten enthielten. Um Faktoren zu identifizieren, die die Internalisierung der apoptotischen Parasiten und die Rekrutierung von LC3 auslösen, wurde eine magnetische Isolierung von apoptotischen *Lm*-enthaltenden Phagosomen durchgeführt. Markierungsfreie Massenspektrometrie und eine anschließende Datenanalyse zeigten, dass die Phagozytoserezeptoren *Lipoprotein receptor-related protein 1* (CD91) und *Complement Receptor 3* (CR3), in Phagosomen mit apoptotischem *Lm* in großer Zahl vorhanden waren. Die Blockierung von CD91 mit einem monoklonalen Antikörper war nicht effizient und auch der Knockdown des Rezeptors hatte keinen Einfluss auf die Wechselwirkung mit *Lm*. Die Inhibierung von CR3 mit einem funktionellen Antikörper hingegen reduzierte signifikant die Wechselwirkung von hMDMs mit apoptotischem *Lm*. Diese Blockierung des Rezeptors führte wiederum zu einer

verminderten Produktion von pro-inflammatorischem TNF- $\alpha$  durch hMDM1 und einer signifikant verminderten anti-inflammatorischen IL-10-Sekretion durch hMDM2. Zusätzlich verringerte die Inhibierung von CR3 die LC3-Konversion in hMDM2, welche mit apoptotischen oder stationäre Phase-*Lm* inkubiert wurden. Interessanterweise führte eine verringerte Internalisierung von apoptotischen *Lm* weder zu einer höheren T-Zell-Proliferation noch zu einem erhöhten Überleben lebendiger *Lm* in infizierten hMDMs. Zusammenfassend zeigen diese Daten zum ersten Mal, dass *Complement Receptor 3* eine signifikante Rolle in der Wechselwirkung von hMDM2 mit apoptotischen *Lm* spielt und lassen zudem auf eine Rolle des Rezeptors in LAP schließen. Rezeptor-vermittelte Internalisierung und LAP von apoptotischen *Lm* könnte als neuer therapeutischer Ansatz zur Bekämpfung der vernachlässigten Tropenkrankheit Leishmaniose dienen.

## 1. Introduction

### 1.1 The neglected tropical disease leishmaniasis

Neglected tropical diseases (NTDs) are a group of infectious diseases of humans mainly occurring in poor populations in tropical and subtropical regions throughout the world. The World Health Organization (WHO) estimates that about 1 billion people in 149 countries are affected, leaving their economies with annually costs of billions of dollars which represents a major global public health problem (WHO, 2019a). NTDs are mainly connected to poor hygiene and a lack of proper sanitation in rural areas as well as the close vicinity to livestock leading to increased risks of zoonotic NTDs. In addition, malnutrition and hence, a weakened immune system, contributes to infections (WHO, 2017a). The major NTDs, as classified by the WHO, are listed below (Table 1).

**Table 1: List of the 20 neglected tropical diseases as classified by the World Health Organization (WHO, 2019a).**

|  |                                  |
|--|----------------------------------|
| Buruli ulcer   | Lymphatic filariasis             |
| Chagas disease                                       | Onchocerciasis (river blindness) |
| Dengue and Chikungunya                               | Rabies                           |
| Dracunculiasis (guinea-worm disease)                 | Scabies and other ectoparasites  |
| Echinococcosis                                       | Schistosomiasis                  |
| Foodborne trematodiasis                              | Soil-transmitted helminthiasis   |
| Human African trypanosomiasis (sleeping sickness)    | Snakebite envenoming             |
| Mycetoma, chromoblastomycosis and other deep mycoses | Taeniasis/Cysticercosis          |
| Leishmaniasis  | Trachoma                         |
| Leprosy (Hansen's disease)                           | Yaws (Endemic treponematoses)    |

Human leishmaniasis is one of the major NTDs and endemic in 97 countries, mainly in Africa, Asia and Latin America. In addition to humans, leishmaniasis can also occur in other mammals including dogs and rodents (WHO, 2019b). It is estimated that 0.7 - 1 million new cases of the human disease occur annually resulting in 20000 - 30000 deaths per year (WHO, 2019b). Three clinical manifestations of leishmaniasis can be distinguished: the

most severe form of the disease, visceral leishmaniasis (VL, also known as Kala-Azar), the most frequent form, cutaneous leishmaniasis, (CL) and mucocutaneous leishmaniasis (MCL) (WHO, 2019a). VL results from infection of phagocytic cells of the reticuloendothelial system. It is marked by strong fever, weight loss and splenohepatomegaly and is lethal if left untreated (Figure 1A). A sequela of VL is termed post-Kala-Azar dermal leishmaniasis (PKDL) which appears as skin-rashes in 5 - 10 % of patients that overcame VL. The majority of new cases of VL (94 %) in 2017 were reported from Brazil, Ethiopia, Kenya, Somalia, South-Sudan and Sudan (Figure 1D, VL). The most recent epidemic, caused by famine and mass movement as results of civil war in South-Sudan led to approximately 30000 new cases of VL in the years 2009 - 2012 of which 900 were lethal (WHO, 2019c). CL is the most prevalent form of leishmaniasis and occurs mainly in the middle-east, Afghanistan, Algeria but also in Brazil and Columbia (Figure 1D, CL). It causes self-healing skin lesions and ulcers on limbs, leaving lifelong scars (Figure 1B). This renders the disease as a high psychological burden for the affected patient. MCL affects the mucosal tissues of nose, mouth and throat which possibly results in erosion of the tissue (Figure 1C). It is mainly prevalent in southern America, where, in addition to Ethiopia, the highest numbers of new cases were reported in 2015 (Figure 1D, MCL) (WHO, 2019a). Therapy of leishmaniasis is mainly based on administration of pentavalent antimony, amphotericin B, miltefosine or paromomycin (DNDi, 2019; WHO, 2010). Chemotherapy is the most effective way to battle all three clinical manifestations. However, the risk of drug toxicity, adverse effects and hence a low therapy compliance weaken the success of anti-leishmanial therapy (Ghorbani and Farhoudi, 2018; López et al., 2018). In addition, deficient healthcare systems in most countries that are endemic for leishmaniasis account for the restriction of access to the expensive and often unaffordable medicines (WHO, 2019d). To date, no human vaccine has been approved for clinical use (Duthie et al., 2016).

Leishmaniasis is caused by protozoan parasites of the genus *Leishmania* from the order of Trypanosomatida (Cavalier-Smith, 2016; Ross, 1903). The different clinical outcomes described above are linked to the respective parasite species infecting the host. VL is caused by *Leishmania donovani*, *L. infantum* or *L. tropica* (McGwire and Satoskar, 2014; Ready, 2014). CL is caused by infection with *L. major*, *L. mexicana*, *L. aethiopica*, *L. amazonensis*, *L. panamensis* or *L. braziliensis* (Goto and Lauletta Lindoso, 2012). Parasites of the species *L. braziliensis* are also the causative agent for MCL (De Oliveira and Brodskyn, 2012).

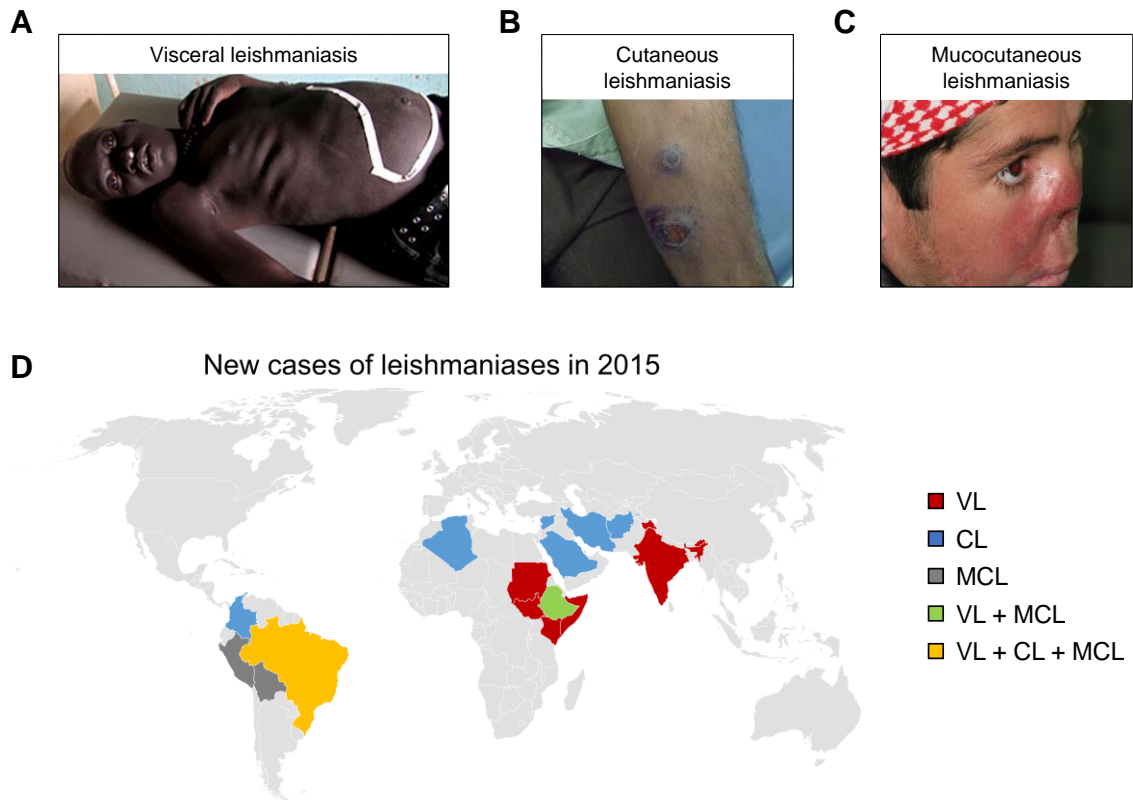


**Figure 1: Exemplary images of the three clinical manifestations of leishmaniasis and new occurrences of leishmaniasis in 2017.** Exemplary images of patients suffering from (A) visceral leishmaniasis, (B) cutaneous leishmaniasis and (C) mucocutaneous leishmaniasis (images: WHO). D Brazil was amongst the countries that reported most cases of VL, CL and MCL. Ethiopia was amongst the countries that reported most cases of VL and MCL (VL: Visceral leishmaniasis, CL: Cutaneous leishmaniasis, MCL: Mucocutaneous leishmaniasis, graph was generated according to data of the WHO, 2017b).

## 1.2 The life cycle of *Leishmania* parasites

*Leishmania* parasites are transmitted by sand flies during a blood meal. These sand flies of the genus *Phlebotomus* and *Lutzomyia* are 2 - 3 mm long (Maroli, 2013). They are mainly distributed in Asia, Africa, Australia, southern Europe and America whilst they are absent from New Zealand and the Pacific Ocean (Lane, 1993; Maroli, 2013). Recent research on the geographical distribution of phlebotomine sand flies revealed their presence in the Black Forest and near the city of Gießen in Germany (Melaun, 2014). Within the lumen of the sand fly's mid-gut, *Leishmania* promastigotes are initially non-infective with a long body and a short flagellum (pro-cyclic) but develop into an infective, metacyclic form during their growth in the vector. During this so-called process of metacyclogenesis, expression patterns of genes are altered. Abundance of the major surface component lipophosphoglycan (LPG) and the glycoposphatidylinositol-anchored zinc-dependent metalloprotease GP63 is increased. Changes in morphology include a decrease in body

length while the flagellum grows (McConville, 1992; Sacks, 1989). When the sand fly takes a blood meal, the infectious inoculum, containing the metacyclic promastigotes and the fly's saliva, is injected into the host's body (Teixeira et al., 2005).

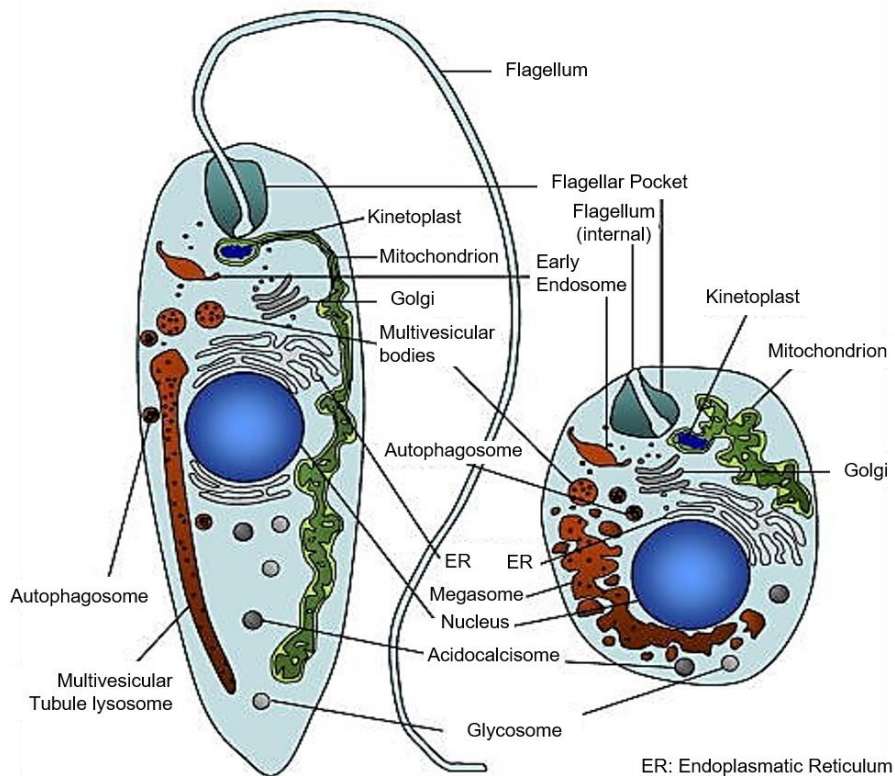


**Figure 2: Life stages of *Leishmania* sp.** Left Metacyclic *Leishmania* promastigote characterized by its long body morphology and the flagellum. Right *Leishmania* amastigote marked by its lentil-like shape and the lack of a flagellum (modified according to Besteiro, 2007).

After a given time, the parasites at the infection site are internalized by macrophages, their final host cells. Inside this antigen-presenting cell, the promastigotes transform into the aflagellated, non-motile amastigote stage (Figure 2, right drawing) and start to multiply within a compartment termed the parasitophorous vacuole (PV). Multiplication is induced by the increase of temperature and fusion of the PV with lysosomes resulting in their acidification (Alcolea et al., 2010; Moradin and Descoteaux, 2012). Infected macrophages possibly burst, releasing amastigotes that can re-infect other cells. During another sand fly's blood meal, this aflagellated, non-motile amastigote stage of the parasite is internalized by the vector through ingestion of infected host cells or free amastigotes. Within the insect they relocate to the mid-gut where they attach to the epithelium. The alkaline milieu within the digestive tract induces the re-transformation of amastigotes into

the flagellated, motile promastigote stage (Figure 2, left drawing) closing the life cycle (Dostálová and Volf, 2012). The schematic life cycle is depicted in Figure 3.

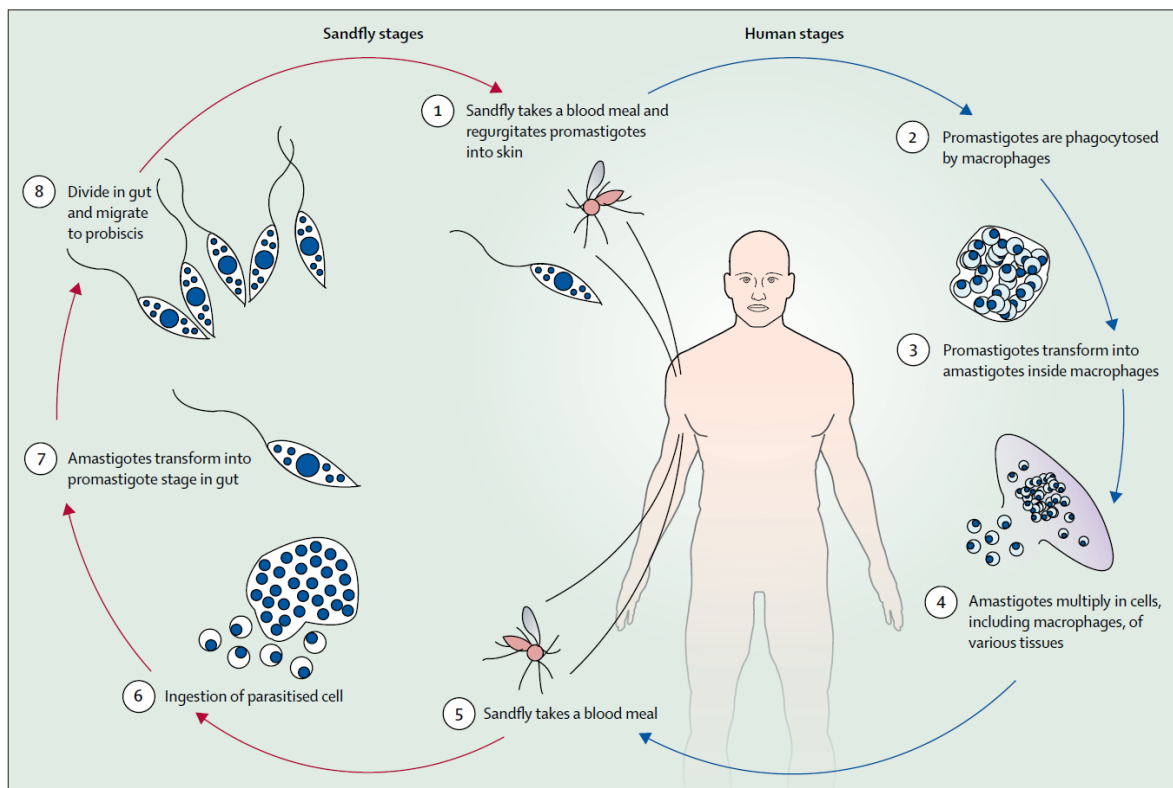


**Figure 3: Life cycle of *Leishmania* parasites.** (1) Injection of *Leishmania* promastigotes into the host by the sand fly vector of the genus *Phlebotomus* and *Lutzomyia*. (2) Phagocytosis of parasites by phagocytic cells such as macrophages. (3) Transformation into the amastigote stage. (4) Multiplication of amastigotes, burst of infected macrophages and re-infection of other cells. (5 and 6) Uptake of infected macrophages or free amastigotes by sand flies. (7 and 8) Re-transformation into the promastigote stage and multiplication in the fly's midgut (Burza et al., 2018).

In addition to direct phagocytosis of promastigotes by macrophages, parasites can also be internalized by polymorphonuclear neutrophils (PMNs) (Peters et al., 2008; van Zandbergen et al., 2004). Promastigotes do not multiply within this cell type but use PMNs as a “trojan horse” (van Zandbergen et al., 2004). Infected PMNs eventually go into apoptosis which leads to their uptake by macrophages. Subsequently, when apoptotic PMNs are degraded, *Leishmania* promastigotes are set free into the macrophage, transform into amastigotes and start to multiply (van Zandbergen et al., 2004).

### 1.3 Myeloid cells

Myeloid cells are a group of cells originating from hematopoietic stem cells in the bone marrow (Kawamoto and Minato, 2004). They are comprised of granulocytes, monocytes, the progenitor of macrophages, and myeloid dendritic cells (herein: dendritic cells). Monocytes, macrophages and dendritic cells are professional antigen-presenting cells (APCs) as they are specialized in antigen processing and presentation to T lymphocytes (Mann, 2014). Macrophages and dendritic cells belong to the innate immune system and serve as a first barrier against invading pathogens. In steady-state, monocytes, characterized by their major surface marker CD14, circulate in the blood stream. Upon pathogen invasion, they are attracted by chemokines prompting them to infiltrate the affected tissue where they differentiate into pro- or anti-inflammatory monocyte-derived macrophages (MDMs) or monocyte-derived dendritic cells (MDDCs). Differentiation into the respective cell type depends on the inflammatory microenvironment (Ginhoux and Jung, 2014; Lee et al., 2015).

Monocytes differentiate to MDDCs in presence of TNF- $\alpha$  and prostaglandin E<sub>2</sub> (Soruri et al., 2003). Dendritic cells are the major APCs, constantly sensing e.g. bacterial and viral antigens. Contact with self or foreign antigens leads to their activation that results in maturation and migration to the lymph node where they initialize the adaptive immune response. MDDCs in particular are characterized by high expression of CD1a and secretion of IL-12 (Tamoutounour et al., 2013). Stimulation of monocytes with T helper cell 1 (T<sub>H</sub>1)-derived interferon (IFN)- $\gamma$  or lipophosphosaccharides from bacteria yields classically activated type 1 macrophages (M1) with a round-shaped morphology (Biswas et al., 2012). M1 macrophages display a high level of phagocytic activity, production of reactive oxygen species (ROS) and hence efficient pathogen killing. Moreover, they have a high antigen presentation capacity by major histocompatibility complex (MHC) II (reviewed in Atri et al., 2018; Tomiotto-Pellissier et al., 2018). Establishment of a pro-inflammatory environment elicits the adaptive immune response and leads to tissue injury. M1 macrophages produce high amounts of pro-inflammatory cytokines (TNF- $\alpha$ , Interleukin (IL)-1, IL-6, IL-12, IL-23 and type I IFNs). When infiltrating monocytes are stimulated with T<sub>H</sub>2-derived IL-4 and IL-13, IL-10 or macrophage-colony stimulating factor (M-CSF), they differentiate into the anti-inflammatory type 2 macrophage subset (M2), also termed alternatively activated macrophage. These M2 macrophages have a long-shaped morphology and an important



role in clearance of apoptotic cells, resolution of inflammation and tissue healing (Anderson and Mosser, 2002; Atri et al., 2018). They are characterized by surface expression of scavenger receptor CD163 and a high production of anti-inflammatory mediators such as IL-10 and TGF- $\beta$  (Jaguin et al., 2013).

Due to the restricted number of primary, fully differentiated macrophages and dendritic cells in the blood, *in vitro* studies mainly employ MDMs and MDDCs (Haniffa et al., 2015). Thus, in the laboratory, initial differentiation from monocytes into pro-inflammatory type 1 macrophages is achieved by stimulation with granulocyte-macrophage colony stimulating factor (GM-CSF). M2 macrophages are yielded by monocyte stimulation with M-CSF whereas hMDDCs can be generated by cultivation in presence of IL-4 and GM-CSF (Ohradanova-Repic et al., 2016).

#### 1.4 Phagocytosis

Phagocytosis, first described by Metchnikoff in 1884, is defined as the internalization of particles bigger than 0.5  $\mu\text{m}$  in size (Metchnikoff, 1884; Richards and Endres, 2014). It is an important mechanism in development and cell homeostasis. The uptake of apoptotic cells (termed efferocytosis) but also foreign, pathogenic particles such as bacteria, fungi or parasites, is mainly facilitated by professional antigen presenting cells such as dendritic cells and macrophages.

In a first step that precedes phagocytosis, chemoattractants, so-called 'find-me' signals, are released by dying cells or pathogens and lead to the recruitment of phagocytes. Phosphatidylserine (PS) and calreticulin (eat-me signals) mark apoptotic cells as cargo and are recognized by specific surface receptors on phagocytic cells. Subsequent uptake of these dying cells stimulates production and secretion of anti-inflammatory mediators (reviewed in Arandjelovic and Ravichandran, 2015; Elliott et al., 2018). Phagocytosis of foreign particles or pathogens serves the inflammatory resolution of infection by destruction of the invading microbe. Here, phagocytosis is mainly initiated by binding of antibody- or complement-opsonized particles to specific receptors on the surface of phagocytic cells (Rosales and Uribe-Querol, 2017).

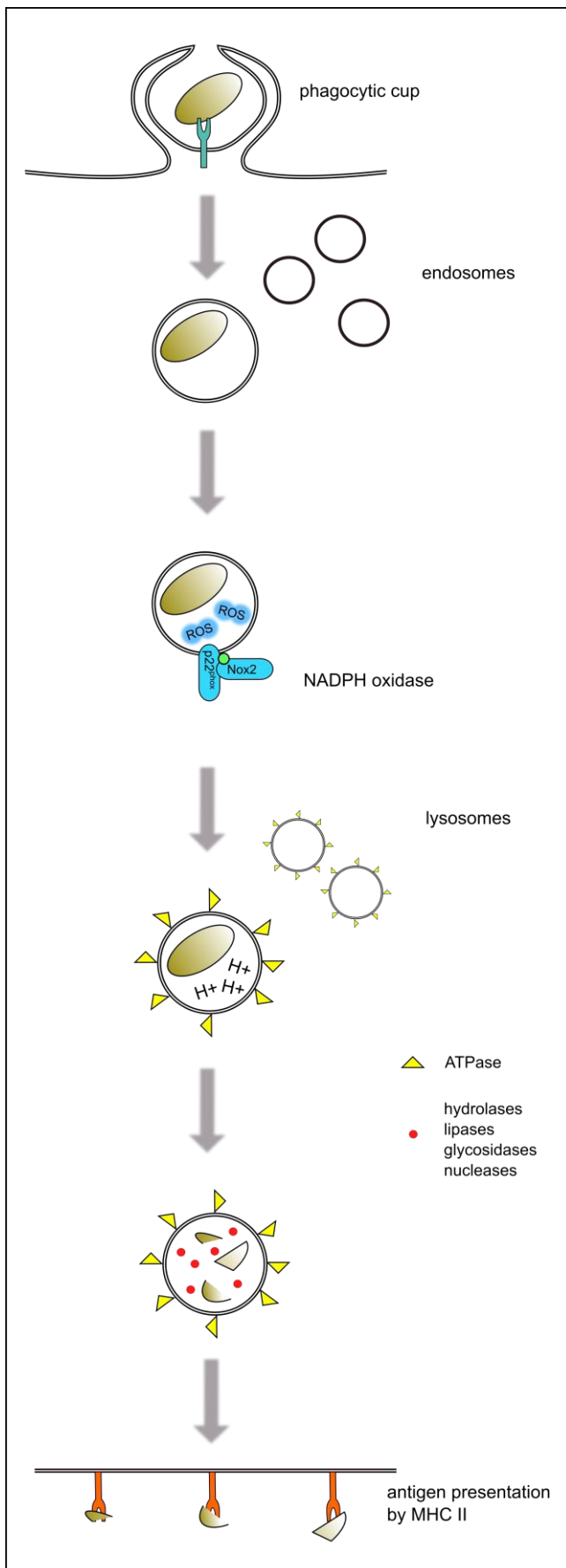


**Figure 4: Major steps in phagocytosis.** Cargo is internalized upon binding to a specific receptor. It comes to fusion and fission events with vesicles of the endosomal system which results in the acquisition of the ROS-generating NADPH oxidase which is the first step in cargo processing. The phagosome fuses with lysosomes that harbor proton-pumping ATPases. This lowers pH and activates hydrolytic enzymes, nucleases, lipases and glycosidases. Finally, processed antigens are presented on the surface of the phagocyte via MHCII molecules to activate the adaptive immune system.

In addition, antigens on the pathogen's surface can be recognized directly by receptors which prime the phagocyte and activate phagocytosis through different receptors (Pauwels et al., 2017; Rosales and Uribe-Querol, 2017). Receptor signaling leads to actin rearrangement and formation of a phagocytic cup around the yet to be internalized cargo. Upon closure of the phagocyte's membrane around the cargo, a single-membrane compartment, the phagosome, is formed (Swanson, 2008; Yeo et al., 2016). The maturation of this phagosome is characterized by fusion and fission with components of the endosomal system as well as by acquisition of proteins that support

degradation of the cargo. One important player for phagosome maturation is the NADPH oxidase which is recruited to the phagosomal membrane and generates reactive oxygen

species (ROS) within the compartment lumen. Subsequent fusion of the phagosome with lysosomes to a phagolysosome is characterized by acquisition of the marker proteins lysosome-associated membrane protein 1 and 2 (LAMP1/2). Consequently, ATPases are introduced to the compartment membrane that pump protons into the lumen, resulting in a decrease in pH. This serves the establishment of an optimal milieu for lysosomal proteases (cathepsins), nucleases, glycosidases, lipases and disulphide reductases that process antigens for presentation and hence activation of the adaptive immune system (Nunes et al., 2013; Pauwels et al., 2017; Yates et al., 2005).

### 1.5 LC3-associated phagocytosis

A decade ago, a novel discovered mechanism for pathogen elimination and apoptotic cell clearance termed LC3-associated phagocytosis has been described (Sanjuan et al., 2009, 2007). LC3-associated phagocytosis (LAP) is a process of particle internalization that links several members of the autophagy-machinery - but not all - to the process of conventional phagocytosis (Sanjuan et al., 2009, 2007). Many pathogenic microbes have been found to be, at least partially, processed by LAP (reviewed in Schille et al., 2017). Upon recognition of apoptotic cells or microbes by cell surface receptors, LAP is initiated. Binding to the receptor is followed by phagocytosis of the cargo which is sequestered within a unilamellar phagosome. Recruitment of the class III phosphatidylinositol-3-phosphate kinase (PI3K)-complex that consists of VPS15, VPS34, Beclin-1, UVRAG and Rubicon leads to introduction of phosphatidylinositol-3-phosphate into the phagosomal membrane (Figure 5).

Of note, Ulk1 a crucial protein of the autophagic pre-initiation complex, is dispensable for LAP induction (Martinez et al., 2011). As in conventional phagocytosis, the NADPH oxidase complex is recruited and generates ROS in the phagosomal lumen (Huang and Brumell, 2009; Lam et al., 2010; Martinez et al., 2015). The NADPH oxidase complex is stabilized by Rubicon (Martinez et al., 2015). Rubicon, known to be a negative regulator of canonical autophagy, activates the function of the PI3K-complex resulting in PI3P generation on the phagosome. This leads to recruitment of the NADPH oxidase subunit p40<sup>phox</sup> and hence, formation of the NADPH oxidase complex by further recruitment of the subunits gp91<sup>phox</sup> and p22<sup>phox</sup> of which the latter is directly bound by Rubicon (Boyle and Randow, 2015; Martinez et al., 2015; Matsunaga et al., 2009; Sanjuan et al., 2007).

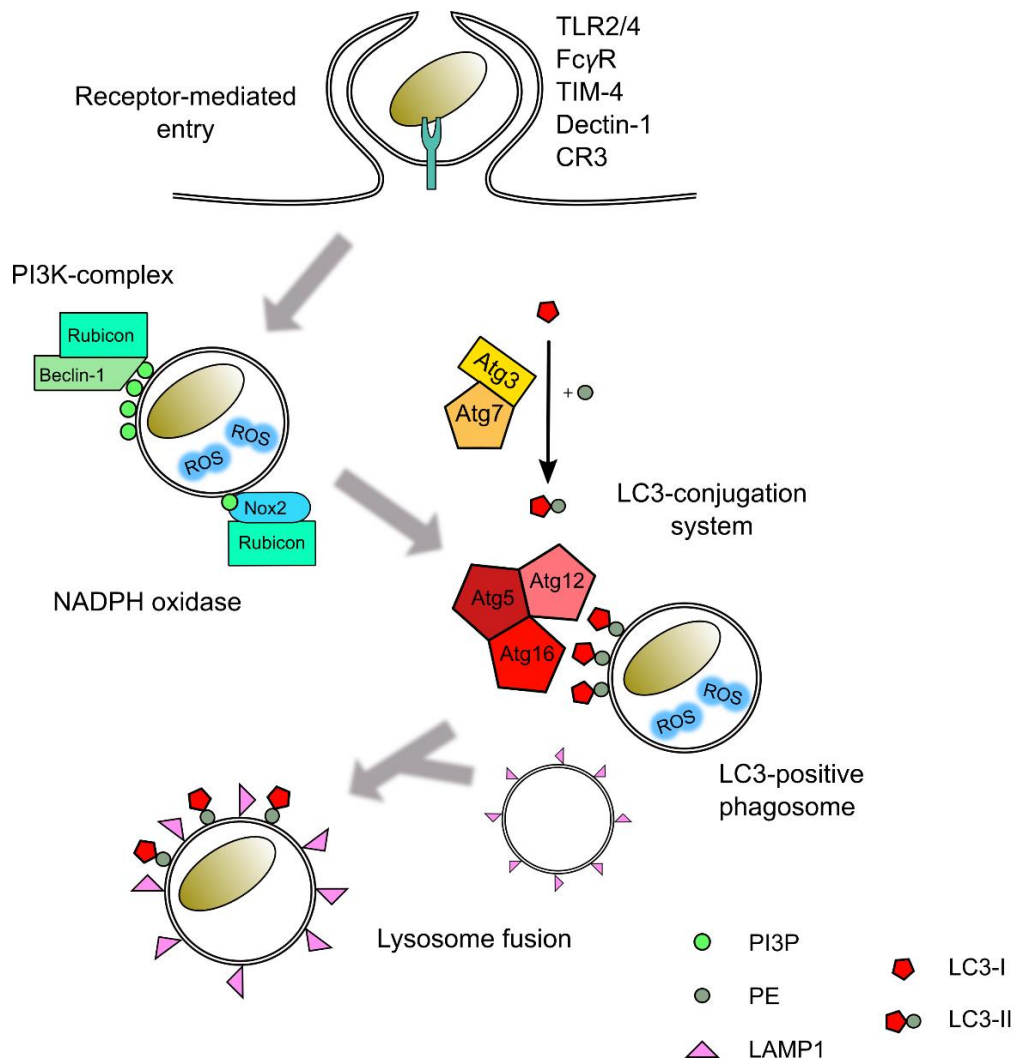


**Figure 5: LC3-associated phagocytosis.** LAP is initiated by engagement of specific receptors such as toll-like receptor (TLR) 2 and 4, FcγRs (upon antibody opsonization), TIM-4, Dectin-1 or CR3 on the phagocyte. The cargo is internalized receptor-dependent and engulfed within a single-membrane phagosome. Recruitment of the NADPH oxidase initiates production of reactive oxygen species (ROS). ROS generation leads to rapid lipidation of cytosolic LC3-I on the phagosomal membrane (LC3-II) by the autophagy protein complexes Atg3-Atg7 and Atg12-Atg-5-Atg16. The emerging LC3-positive phagosome matures by fusion with lysosomes and the cargo is degraded (modified according to Schille et al., 2017).

ROS production is essential for recruitment of the autophagic protein microtubule-associated protein 1A/1B light chain 3B (MAP1LC3B, hereafter: LC3). The soluble form of LC3 (LC3-I) is processed and conjugated to phosphatidylethanolamine (PE) on the cytosolic phagosomal surface (now termed LC3-II) by two autophagy protein complexes Atg7-Atg3 and Atg12-Atg5-Atg16 (Henault et al., 2013; Martinez et al., 2011; Sanjuan et al., 2007; Tanida et al., 2004). However, a study by Cemina et al. showed that autophagy proteins Atg5 and Atg7 are expendable at least in Fcγ receptor-mediated LAP (Cemina et al., 2016). LAP has been proposed to serve three functions: (1) Rapid phagosomal maturation by

promoting fusion of phagosomes with lysosomes, (2) cargo delivery to intravesicular pattern recognition receptors (PRRs) and (3) enhancement of antigen presentation via MHCII (Romao and Münz, 2014). Phagocytosis as well as LAP relies on the induction by receptor signaling upon antigen recognition. This is mediated by specific receptors on the surface of APCs.

### 1.6 Receptors in conventional phagocytosis and LC3-associated phagocytosis

The initiation of phagocytosis as well as LAP relies on the recognition of microbial structures or apoptotic cell-associated ligands by specific receptors. Phagocytosis or LAP of apoptotic cells is facilitated by receptors that bind 'eat-me signals' on the surface of dying cells. The best studied 'eat-me' signals are phosphatidyl-serine (PS) and calreticulin. During apoptosis, the phospholipid PS is flipped from the inner leaflet of the plasma membrane to the outer leaflet (Mariño and Kroemer, 2013). The brain-specific angiogenesis inhibitor 1 (BAI1) and T cell immunoglobulin- and mucin-domain-containing molecule (TIM4) are well studied representatives for PS receptors (Miyanishi et al., 2007; Park et al., 2007). The latter is involved in LAP induction upon engagement of apoptotic lymphocytes (Martinez et al., 2011). In addition to PS, other 'eat-me' signals, e.g. calreticulin (in a PS-bound form) or complement C1q, can serve as a recognition signal for phagocytes. The receptor for both 'eat-me' signals is the low density lipoprotein receptor-related protein 1 (LRP1/CD91) (Gardai et al., 2005; Ogden et al., 2001). In addition to calreticulin and C1q, CD91 recognizes at least 30 ligands from several protein families including complement component C3 which indicates a possible role in phagocytosis of pathogenic microbes (Herz and Strickland, 2001).

Phagocytic receptors that recognize specific microbial antigens, so-called pathogen-associated molecular patterns (PAMPs), are termed pattern-recognition receptors (PRRs). A well described PRR is the mannose receptor (CD206) which is known to specifically bind carbohydrates such as mannose, N-acetylglucosamine and fucose (Rajaram et al., 2017). Other important PRRs are represented by the family of toll-like receptors (TLRs). They sense microbial lipoproteins (TLR1, TLR2, TLR6), double stranded RNA (TLR3), lipopolysaccharide (TLR4), flagellin (TLR5), single-stranded RNA (TLR7, TLR8) and DNA (TLR9). TLRs can be exposed on the surface of phagocytic cells or associated with compartments of the

endosomal system (reviewed in Kawai and Akira 2011). TLR signaling results in the induction of inflammatory signaling by activation of nuclear factor NF- $\kappa$ B (Medzhitov, 2007). TLR2 was amongst the first PRRs described to induce LAP in response to zymosan, a yeast cell wall extract, or to the TLR ligand PAM3CSK4 (Sanjuan et al., 2007). Another well investigated PRR, Dectin-1 that recognizes polysaccharides such as  $\beta$ -glucan, initiates phagocytosis upon stimulation with fungal pathogens and was also found to trigger LAP (Akoumianaki et al., 2016; Martinez et al., 2015).

Opsonic receptors comprise the family of Fc (fragment crystallizable) receptors and complement receptors. Immunoglobulin G (IgG) is an important opsonin that induces efficient phagocytosis by Fc $\gamma$  receptors upon decoration of pathogens (Nimmerjahn and Ravetch, 2010). Complement receptors (CRs) facilitate uptake of complement-opsonized pathogens and apoptotic cells by phagocytes. Analogous to antibody opsonization, complement deposition on the surface prepares the microbe for effective phagocytosis. The complement system can be activated by three different pathways: The classical pathway, the lectin pathway and the alternative pathway (reviewed in Merle et al., 2015a, 2015b). Each pathway results in the deposition of C3b on the pathogens surface. Moreover, C3b can be further cleaved to an inactive form (iC3b) which also attaches to the surface of microbes (Amin Arnaout, 1990). Complement receptor 1 (CR1, CD35) plays an important role in clearance of immune complexes bound by C1q but also directly binds C3b (Klickstein et al., 1997; Taylor et al., 1997). Complement receptor 2 (CR2) is mainly involved in B cell immunity and not present on macrophages and dendritic cells (Weis et al., 1984). Complement receptors 3 and 4 (CR3 and CR4) both are highly expressed by macrophages. They consist of heterodimers comprising a common  $\beta_2$  (CD18) integrin subunit and a distinct  $\alpha$ -chain ( $\alpha_M$ /CD11b or  $\alpha_X$ /CD11c) (Vorup-Jensen and Jensen, 2018). The CD11b subunit of CR3 binds inactive C3b (iC3b) with high affinity leading to a silent, anti-inflammatory internalization of iC3b opsonized particles (Nakamura et al., 2017). This is also of relevance in clearance of apoptotic cells which can be decorated by iC3b and hence, phagocytosed after binding to CR3 (Hashimoto et al., 2007; Mevorach et al., 1998). Recently, Gluschko and colleagues found CR3 to induce LAP of *Listeria monocytogenes*. Interestingly, this was linked to a reduced ROS generation in cells lacking CR3 (Gluschko et al., 2018).

## 1.7 Cytokine secretion of myeloid cells and activation of the adaptive immune system

When myeloid cells are challenged with pathogen-derived stimuli or apoptotic cells, a broad repertoire of pro- or anti-inflammatory cytokines is secreted mainly by macrophages. Upon binding of an antigen to its specific receptor e.g. a surface TLR, intracellular signaling leads to activation of the transcription factor NF- $\kappa$ B. This mediates the induction of pro-inflammatory genes such as *IL-1*, *IL-6*, *IL-8* or *TNF* (reviewed in Liu et al., 2017). An interplay between these mediators in connection with chemokines results in establishment of an inflammatory milieu, an increase in vascular permeability and recruitment and activation of other cells of the adaptive or innate immune system (Arango Duque and Descoteaux, 2014). When an apoptotic cell-associated antigen binds its cognate receptor, anti-inflammatory cytokines are secreted of which the most important are IL-10 and TGF- $\beta$ . They mainly serve the suppression of pro-inflammatory cytokine production and macrophage activation. IL-10 e.g. effects other macrophages to lower their microbicidal activity (Oswald et al., 1992). TGF- $\beta$  also suppresses pro-inflammatory cytokine effects but is also a potent down-regulator of T helper cell ( $T_H$ ) 1 and  $T_H$ 2 responses (Arango Duque and Descoteaux, 2014).

Upon internalization and degradation of foreign material by the phagocyte, dendritic cells and macrophages activate the adaptive immune system by major histocompatibility complex II (MHCII)-dependent antigen presentation to antigen-specific  $CD4^+$  T cells. This mechanism is restricted to APCs whereas MHCI-dependent antigen presentation is executed by all cell types. Thus, MHCI presentation allows for constitutive presentation of proteasomal degraded self-peptides presented to antigen-specific cytotoxic  $CD8^+$  T cells (Roche and Furuta, 2015; Rossjohn et al., 2015). A characteristic feature of dendritic cells is the ability to present also internalized foreign antigens via its MHCI complex in a mechanism termed cross-presentation (reviewed in Embgenbroich and Burgdorf, 2018).

Antigen presentation to  $CD4^+$  lymphocytes is a crucial step in combatting pathogenic invaders. In phagocytosis and LAP, MHCII molecules must be located to the phagolysosome where the processed antigens can be loaded onto the complex. The MHCII-antigen complex is translocated to the plasma membrane of the APC where a  $CD4^+$  T lymphocyte can bind with its specific T cell receptor (TCR) (Neefjes et al., 2011). TCR engagement results in T cell

activation which requires an additional co-activation signal (Pagan et al., 2012). If no co-stimulatory signal is provided by the APC, T cells will go into apoptosis or become inactivated. The cytokine environment at the time of activation of CD4<sup>+</sup> T cells is directing the differentiation into T<sub>H</sub>1 or T<sub>H</sub>2 cells. In presence of IL-12 or IFN- $\gamma$ , mainly secreted by pro-inflammatory M1 macrophages, CD4<sup>+</sup> cells differentiate in T<sub>H</sub>1 cells (Hsieh et al., 1993; Lighvani et al., 2001). Presence of IL-4 during TCR-dependent antigen presentation results in differentiation into T<sub>H</sub>2 lymphocytes.

### 1.8 Uptake of *Leishmania* promastigotes by myeloid cells

Several receptors have been described to be involved in phagocytosis of *Leishmania* parasites whereas to date, no receptor has been found to specifically induce LAP of *Leishmania*. TLRs, although not directly linked to phagocytosis of *Leishmania* promastigotes, serve their uptake in a regulatory manner (reviewed in Chauhan et al., 2017). TLR2, TLR4 and TLR9 have been suggested to be involved in *Leishmania major* recognition (Abou Fakher et al., 2009; de Veer et al., 2003; Kropf et al., 2004; Liese et al., 2008). Fc $\gamma$  receptors are of particular interest in secondary infections by amastigotes, since the host already has specific IgGs that readily bind to the parasites surface. Nonetheless, in an initial infection by the promastigote stage, naturally occurring antibodies decorate the parasites which are in turn engaged by dendritic cell and macrophage Fc $\gamma$  receptors (Polando et al., 2013; Woelbing et al., 2006). It is long known that the mannose receptor CD206 is involved in phagocytosis of *Leishmania* promastigotes (Wilson and Pearson, 1988). A recent report showed that anti-inflammatory macrophages that express high levels of CD206 are permissive for parasite growth, even in pro-inflammatory environments (Lee et al., 2018). The macrophage fibronectin receptor (FnR) was suggested to be involved in parasite uptake in cooperation with complement receptors (Kane and Mosser, 2000). Intensive studies of CRs revealed major roles for CR1 and CR3 in the infection of macrophages with *Leishmania* promastigotes. CR1, the receptor for complement C3b, is involved in the internalization of viable *Leishmania major* promastigotes (Da Silva et al., 1989; Wenzel et al., 2012). In addition to C3b, CR1 directly binds *Leishmania* surface LPG (Rosenthal et al., 1996). Modulation of this receptor resulted in a decreased infection of primary human M1 macrophages but an increase of survival of promastigotes within the infected cell (Da Silva et al., 1989). CR3 is the best investigated receptor implicated in



*Leishmania* promastigote infection (Mosser and Edelson, 1985; Rosenthal et al., 1996; Schönlau et al., 2000; Wilson and Pearson, 1988). It is employed by *Leishmania* promastigotes for entry of host macrophages by three different mechanisms: (1) Binding of iC3b that is generated by cleavage of membrane-bound C3b by the *Leishmania* surface protease GP63, (2) direct binding of GP63 on the parasite surface or (3) similar to CR1, binding of *Leishmania* surface-LPG (Brittingham et al., 1995; Mosser and Edelson, 1985).

### 1.9 The importance of apoptotic promastigotes in *Leishmania major* infection

Most studies on *Leishmania* promastigote infection concentrate on viable parasites since a liquid parasite cultivation system is used which mainly restrains the apoptosis of *Leishmania* promastigotes (Grekov et al., 2011). One study showed that these viable *L. major* promastigotes are partially internalized by LAP in murine macrophages. Interestingly, targeting by LC3 could be evaded by action of the surface protease GP63 (Matte et al., 2016). Moreover, our group detected a viable promastigote to reside within a phagosome that had an opening to the extracellular space by electron microscopy possibly serving for evasion of degradation (PhD thesis M. Thomas, 2015). Of note, the infectious inoculum that is injected into the host by the sand fly is comprised of an almost equal mixture of viable and apoptotic parasites (van Zandbergen et al., 2006; Wanderley et al., 2013, 2009). This mixture is also found in a stationary growth phase (stat. ph.) of *in vitro* cultured *L. major* promastigotes (van Zandbergen et al., 2006).

Apoptosis is a fundamental mechanism in development and tissue homeostasis. In unicellular parasitic organisms it was described as altruistic process regulating parasite density within the vector and the host cell (Lüder et al., 2010). To date, the intracellular pathways that lead to apoptosis in *Leishmania* promastigotes are not known. Interestingly, the molecular factors described for classic mammalian apoptosis are not found within the parasite (Basmacıyan et al., 2018). Nonetheless, apoptotic *Leishmania* promastigotes show the same characteristics as apoptotic mammalian cells. They have a round morphology and as general characteristics of apoptotic cells, PS is exposed on their surface, they show nuclear condensation, DNA fragmentation and they are TUNEL-positive. In addition, apoptotic promastigotes have a short flagellum or lack the flagellum (Crauwels et al., 2015; van Zandbergen et al., 2006; Wanderley et al., 2009; Zangger et al., 2002). *In vivo* studies

in susceptible BALB/c mice showed a dependence of disease initiation on the apoptotic parasite population within the infectious inoculum (van Zandbergen et al., 2006). When apoptotic *Leishmania* were depleted from a stat. ph., rates of PMNs and macrophages infected with viable promastigotes were significantly reduced as compared to cells infected with a stat. ph. containing viable and apoptotic parasites. Presence of apoptotic *Leishmania* led to an increase in anti-inflammatory cytokine production in PMNs (van Zandbergen et al., 2006). The importance of the uptake of apoptotic cells was underscored by studies that found uptake of apoptotic PMNs to silence neutrophils and macrophages during *Leishmania* infection (Afonso et al., 2008; Salei et al., 2017). Our group demonstrated that anti-inflammatory macrophage infection in presence of apoptotic *L. major* promastigotes resulted in enhanced survival of the viable parasite population as compared to infection with log. ph. promastigotes that are comprised almost exclusively of viable parasites. Further, in an *in vitro* T cell assay, the co-internalization of apoptotic with viable promastigotes by anti-inflammatory macrophages led to a significant reduction of a *Leishmania*-specific T cell proliferation. Presence of apoptotic promastigotes decreased production of pro-inflammatory TNF- $\alpha$ , IL-6 and IL-1 $\beta$  by macrophages, and IFN- $\gamma$  secretion by T cells, indicating a crucial role for apoptotic parasites in host cell infection by *L. major* (Crauwels et al., 2015). The reduction in the adaptive immune response towards *L. major* was found to be dependent on LAP of these apoptotic promastigotes in the infection process. The number of dying promastigotes in the infectious mixture during infection correlated with occurrence of LC3<sup>+</sup> compartments (Crauwels et al., 2015). This study highlighted the importance of apoptotic promastigotes in *Leishmania major* infection and revealed LC3-associated phagocytosis to be of importance for initiation of leishmaniasis.

## 2. Hypothesis and Aims

*Leishmania* parasite infection causes the neglected tropical disease leishmaniasis. Accession of affected populations to cheap medicines often is challenging and to date, no vaccine is available. Therefore, understanding the molecular details of initial *Leishmania* infection is of high importance to find ways for effective treatment of leishmaniasis.

Viable *L. major* parasites were found to escape degradation by macrophages, possibly by formation of tunnel-like structures from the phagosome to the extracellular space. Apoptotic *Leishmania major* promastigotes were found to be crucial for disease development in a susceptible mouse model (van Zandbergen et al., 2006). In previous *in vitro* studies with primary human type 2 macrophages, the presence of apoptotic *L. major* promastigotes resulted in a decrease of pro-inflammatory cytokine production as well as a diminished *Leishmania*-specific T cell response (Crauwels et al., 2015). This could be linked to the internalization of apoptotic parasites into a LC3-decorated single membrane compartment by LC3-associated phagocytosis. To date, it remains elusive which factors contribute to initiation of LAP and maturation of the LC3 positive phagosome that surrounds apoptotic *L. major* promastigotes. Based on the findings of van Zandbergen and Crauwels we hypothesize:

**Viable and apoptotic *Leishmania major* promastigotes are internalized by primary human macrophages in a process termed LC3-associated phagocytosis. Viable parasites escape degradation and multiply within the phagosomal compartment whereas processing of apoptotic parasites results in an anti-inflammatory host cell response that supports survival of the viable *Leishmania* population.**

To investigate this hypothesis, we formulated the following aims:

- 1) Evaluation of differences in induction of LC3-associated phagocytosis and processing of internalized parasites by live cell imaging of eGFP-LC3 expressing pro- and anti-inflammatory primary human macrophages upon uptake of viable or apoptotic *Leishmania major* promastigotes.
- 2) Investigation of a possible evasion strategy, based on the formation of tunnel-like structures by viable promastigotes, using immunofluorescence microscopy.

- 3) Identification of host cell factors that initiate LC3-associated phagocytosis and contribute to phagosome maturation by mass spectrometric analysis of magnetically isolated phagosomes that contain apoptotic *Leishmania major* promastigotes.
- 4) Functional characterization of identified targets regarding their role in uptake of apoptotic *Leishmania major* promastigotes and their effect on the macrophage cytokine response and intracellular survival of viable parasites.

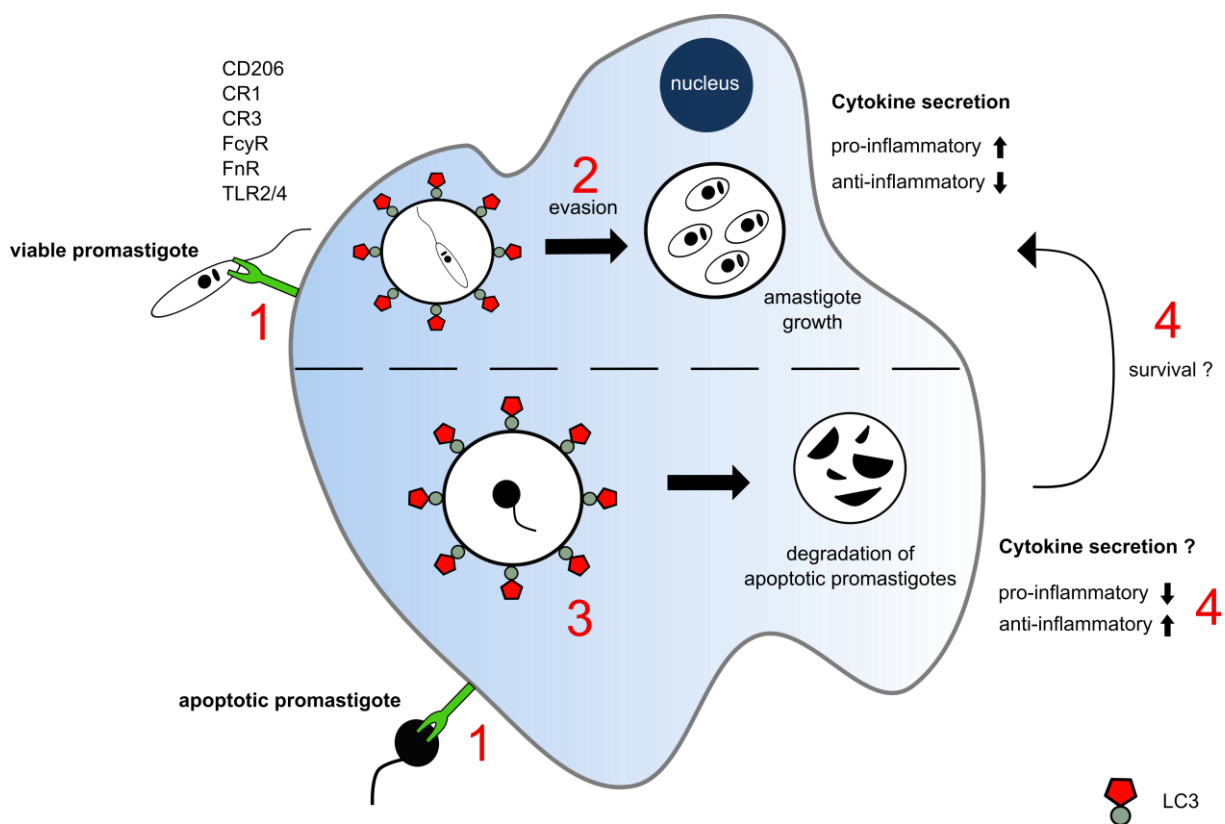


**Figure 6: Hypothesis and aims of the study.** Viable *Leishmania major* promastigotes are internalized upon recognition by several receptors. Portions of the internalized parasites are sequestered in LC3 positive phagosomes by a mechanism termed LC3-associated phagocytosis, escape degradation and transform into amastigotes and multiply. Infection with viable promastigotes induces pro-inflammatory cytokine secretion. Processing of apoptotic parasites results in an anti-inflammatory host cell response that supports survival of the viable *Leishmania* population. We aimed on (1) assessment of differences in uptake of viable and apoptotic *L. major* promastigotes, (2) investigation of an evasion strategy of viable promastigotes by formation of tunnel-like structures, (3) identification and (4) functional characterization of factors regarding LAP of apoptotic promastigotes as well as their effect on macrophage cytokine production and intracellular parasite survival.

### 3. Material and Methods

#### 3.1 Material

##### 3.1.1 Consumables

| <b>Consumable</b>  | <b>Manufacturer</b>                      |
|--|--|
| CASY cups  | OLS OMNI Life Science, Bremen, GER       |
| Cell culture flasks (25 cm <sup>2</sup> , 75 cm <sup>2</sup> , 175 cm <sup>2</sup> ) | Greiner, Frickenhausen, GER              |
| Cell culture petri dish (10 cm diameter)   | Sarstedt, Nürnbrecht, GER                |
| Cell culture plates (6-well, 24-well)  | Greiner, Frickenhausen, GER              |
| Cell funnel for cytopins   | Tharmac, Waldsolms, GER                  |
| Cell lifter (16 cm, 25 cm)   | Sarstedt, Nürnbrecht, GER                |
| Centrifuge tubes polyallomer   | Beckman Coulter, Krefeld, GER            |
| Chamber slide (8-well, 12-well), ibidi-treat   | Ibidi, Planegg-Martinsried, GER          |
| Cover slip (#1.5)  | Thermo Scientific, Dreieich, GER         |
| Cryotube (2 mL)  | Thermo Scientific, Dreieich, GER         |
| ECL X-ray film   | GE Healthcare, Buckinghamshire, UK       |
| FACS microtube (2 mL)  | Micronic, Lelystad, NL                   |
| FACS tube (5 mL)   | BD labware, Le Pont de Claix, FRA        |
| Filter card for cytopins   | Tharmac, Waldsolms, GER                  |
| Filter paper (Whatman)   | VWR, Darmstadt, GER                      |
| Free-flow column for HOKImag   | HOOCK, Kiel, GER                         |
| Hemocytometer Neubauer improved<br>(depth 0.1 mm, 0.02 mm)                           | VWR, Darmstadt, GER                      |
| LightCycler plate (96-well) with foil  | Roche Applied Science, Darmstadt,<br>GER |
| MACS column (LS/LD)  | Miltenyi, Bergisch Gladbach, GER         |
| Microscope slide for cytopins, uncoated  | Tharmac, Waldsolms, GER                  |

| <b>Consumable</b>   | <b>Manufacturer</b>                    |
|---|--|
| Microtiter plate (96-well, V-bottom/flat bottom)                              | Sarstedt, Nürnberg, GER                |
| Microtiter plate (96-well, flat bottom, medium-binding)                       | Sarstedt, Nürnberg, GER                |
| PCR tube (0.2 mL)   | Sarstedt, Nürnberg, GER                |
| Pipette filter tips<br>(0.5-10 µL, 10-200 µL, 100-1000 µL)                    | Nerbe plus, Winsen/Luhe, GER           |
| Pipette tips<br>(0.5-10 µL, 10-200 µL, 100-1000 µL)                           | Biozym, Hessisch Oldendorf, GER        |
| Pipette (Pasteur)   | Sarstedt, Nürnberg, GER                |
| Pipettes (Research Plus)<br>(0.5-10 µL, 10-100 µL, 20-200 µL,<br>100-1000 µL) | Eppendorf, Hamburg, GER                |
| Pipette Multichannel (Research Plus)<br>(10-100 µL, 20-200 µL)                | Eppendorf, Hamburg, GER                |
| Polystyrene lids, PS, high profile  | Greiner, Frickenhausen, GER            |
| Polyvinylidene difluoride (PVDF) membrane                                     | GE Healthcare, Buckinghamshire, UK     |
| Reaction tube (1.5 mL)  | Eppendorf, Hamburg, GER                |
| Reaction tube (15 mL, 50 mL)  | Greiner, Frickenhausen, GER            |
| Serological pipettes (2 mL, 5 mL, 10 mL,<br>25 mL)                            | Greiner, Frickenhausen, GER            |
| Sterile vacuum filter (0.45 µm, 0.22 µm)                                      | Merck Millipore, Billerica, USA        |
| Syringe (1 mL)  | Beckton Dickinson, Franklin Lakes, USA |

3.1.2 Devices

| <b>Device</b>   | <b>Manufacturer/equipment</b>      |
|---|------------------------------------|
| <i>Centrifuges</i>  |                                    |
| Cellspin II Universal 320R Cytocentrifuge                       | Tharmac, Waldsolms, GER            |
| Centrifuge 5430/5430R   | Eppendorf, Hamburg, GER            |
| Labofuge 200  | Thermo Scientific, Dreieich, GER   |
| Multifuge 16R with swinging bucket rotor<br>BIOliner            | Thermo Scientific, Dreieich, GER   |
| Optima L-70k Ultracentrifuge with rotor SW28                    | Beckman Coulter, Krefeld, GER      |
| <i>Electrophoresis and western blot</i>                         |                                    |
| ECL & Fluorescence Imager Chemostar                             | Intas, Göttingen, GER              |
| Electrophoresis chamber for agarose gels                        | Biotec-Fischer, Reiskirchen, GER   |
| Electrophoresis chamber for SDS-PAGE<br>Mini-Protean Tetra cell | Bio-Rad, München, GER              |
| Power Supply "PowerPac™ 200/2.0"                                | Bio-Rad, München, GER              |
| Semi-dry transfer unit TE 77 PWR                                | GE Healthcare, Buckinghamshire, UK |
| UV-transilluminator Genoview                                    | VWR International, Darmstadt, GER  |
| X-ray processor Curix 60  | AGFA, Mortsel, BE                  |
| <i>Flow cytometry</i>   |                                    |
| LSR II  | BD Biosciences, Heidelberg, GER    |
| LSR II SORP (special order research product)                    | BD Biosciences, Heidelberg, GER    |
| CytoFLEX  | Beckman Coulter, Krefeld, GER      |
| <i>Magnets</i>  |                                    |
| HOKImag free-flow magnetic chamber                              | HOOCK, Kiel, GER                   |
| MACS Separator (Midi)   | Miltenyi, Bergisch Gladbach, GER   |
| MACS magnet (Midi)  | Miltenyi, Bergisch Gladbach, GER   |

| <b>Device</b>  | <b>Manufacturer/equipment</b>   |
|--|---|
| <i>Microscopy (all microscopes were from Carl Zeiss Microscopy, Oberkochen, GER)</i> |   |
| Primo Star   | cell culture  |
| AxioVert A1  | cell culture  |
| AxioPhot   | equipped with a color camera AxioCam IC and mercury vapor lamp HBO50  |
| Observer Z.1 Fluorescence Microscope   | equipped with: ApoTome, AxioCam MRm, light source HXP120C, reflectors DIC TL, 38 HE GFP, 43 HE DsRed, 49 DAPI, 50 Cy5, 64 HE mPlum, objectives LD Achrom Plan 20x/0.4 Ph2 DICIII, LD Achrom Plan 40x/0.6 Ph2, Pln Apo 20x/0.8 DICII, PlnN 10x/0.3 Ph1 DIC I, EC PlnN 40x/1.3 Oil DICIII, Pln Apo 63x/1.4 Oil DICIII |
| Confocal Laser Scanning Microscope (LSM) 7 Live                                      | Observer Z.1 equipped with: line scanner, four laser lines (405 nm, 488 nm, 561 nm and 635 nm), AxioCam MRm, light source HXP120C, piezo z-controller 24V80CAP, incubation chamber, reflectors Pol TL, 26 AF660, 38 HE GFP, 43 DsRed, 49 DAPI, objectives Pln Apo 63x/1.4 Oil DICIII, Pln Apo 40x/0.95 DICIII       |
| <i>Incubators</i>  |   |
| Forma Series II Water Jacket   | Thermo Scientific, Dreieich, GER  |
| Heraeus Auto Zero  | Thermo Scientific, Dreieich, GER  |
| Recirculating cooler   | Julabo, Seebach, GER  |



| <b>Device</b>                    | <b>Manufacturer/equipment</b>        |
|----------------------------------|--------------------------------------|
| <i>PCR Thermo cyclers</i>        |                                      |
| LightCycler 480                  | Roche Applied Science, Mannheim, GER |
| S1000 Thermal Cycler             | Bio-Rad, München, GER                |
| <i>Sterile cabinets</i>          |                                      |
| Workbench MSC-Advantage          | Thermo Scientific, Dreieich, GER     |
| Steril Gard III Advance          | The Baker Company, Sanford, USA      |
| Steril Gard Hood                 | The Baker Company, Sanford, USA      |
| <i>Miscellaneous</i>             |                                      |
| Analytical balance KB BA 100     | Sartorius, Göttingen, GER            |
| CASY Modell TT                   | Roche Innovatis, Reutlingen, GER     |
| Freezer (-20°C)                  | Liebherr, Biberach a. d. R., GER,    |
| Freezer U725-G (-80°C)           | Eppendorf, Hamburg, GER              |
| Magnetic stirrer C-MaG HS7       | IKA, Staufen, GER                    |
| Microplate reader Infinite F50   | Tecan, Männedorf, CH                 |
| Microwave                        | Bosch, Gerlingen, GER                |
| Minipulse 3 peristaltic pump     | Gilson, Middleton, USA               |
| Nitrogen container Chronos       | Messer, Bad Soden, GER               |
| pH-meter PB-11                   | Sartorius, Göttingen, GER            |
| Spectrophotometer NanoDrop 2000c | Thermo Scientific, Dreieich, GER     |
| Sonifier Branson 450 II Classic  | Branson Ultrasonics, Danbury, USA    |
| Speed control module R2          | Gilson, Middleton, USA               |
| Thermomixer 5437                 | Eppendorf, Hamburg, GER              |
| Vortex mixer VV3                 | VWR, Darmstadt, GER                  |
| Waterbath                        | Köttermann, Darmstadt, GER           |

3.1.3 Software

| <b>Software</b>  | <b>Manufacturer</b>  |
|--|--|
| AxioVision (Version 4.8)   | Carl Zeiss Microscopy, Oberkochen, GER   |
| FACSDiva (Version 7.0.1)   | BD Biosciences, Heidelberg, GER  |
| FlowJo (Version 10)  | BD Biosciences, Heidelberg, GER  |
| Prism (Version 7/8)  | Graphpad Software, La Jolla, USA   |
| ImageJ/FIJI  | National Institutes of Health, Bethesda, USA   |
| LEGENDplex Data Analysis Software (Version 8)                      | Biolegend, San Diego, USA  |
| LightCycler LC480 Software (Version 1.5.0)                         | Roche Applied Science, Mannheim, GER   |
| Microsoft Office 2013/2019   | Microsoft, Redmont, USA  |
| NCBI Nucleotide Blast (blastn) database                            | National Library of Medicine, Bethesda, USA  |
| Protein Data Bank  | The Protein Data Bank<br>( <a href="http://www.rcsb.org/pdb/">www.rcsb.org/pdb/</a> ; Berman et al., 2000)                       |
| String database (Version 11)                                       | STRING Consortium, ELIXIR, Hinxton, UK<br>( <a href="http://www.string-db.org/">www.string-db.org</a> ; Szklarczyk et al., 2019) |
| Zeiss Efficient Navigation (ZEN) 2012 (black edition/blue edition) | Carl Zeiss Microscopy, Oberkochen, GER   |

3.1.4 Chemicals

Reagents that were obtained from the in-house facilities are marked with 'Paul-Ehrlich-Institut'.

| <b>Chemical</b>  | <b>Manufacturer</b>                        |
|--|--|
| $\beta$ -Mercaptoethanol                               | Sigma-Aldrich, Steinheim, GER              |
| Acetic acid (CH <sub>3</sub> COOH)                     | Roth, Karlsruhe, GER                       |
| Acrylamide/Bisacrylamide solution 30%                  | SERVA Electrophoresis, Heidelberg, GER     |
| Agarose LE   | Biozym Scientific, Hessisch Oldendorf, GER |
| Ammonium persulfate (APS)                              | SERVA Electrophoresis, Heidelberg, GER     |
| Aqua bidest. (ddH <sub>2</sub> O)                      | Paul-Ehrlich-Institut                      |
| Benzonase  | Merck, Darmstadt, GER                      |
| Bovine Serum Albumin (BSA)                             | Applichem, Darmstadt, GER                  |
| Brain-heart infusion agar                              | BD Biosciences, Sparks, USA                |
| Bromophenol blue                                       | Merck, Darmstadt, GER                      |
| Calcium chloride (CaCl <sub>2</sub> )                  | Sigma-Aldrich, Steinheim, GER              |
| CASYton  | OLS OMNI Life Science, Bremen, GER         |
| Chloroquine  | Sigma-Aldrich, Steinheim, GER              |
| Cytochalasin D   | Merck, Darmstadt, GER                      |
| DABCO (1,4-Diazabicyclo (2.2.2)-octan)                 | Roth, Karlsruhe, GER                       |
| Developer for X-Ray film G153 A+B                      | AGFA, Mortsel, BE                          |
| Disodium phosphate (Na <sub>2</sub> HPO <sub>4</sub> ) | Merck, Darmstadt, GER                      |
| Dimethyl sulfoxide (DMSO)                              | Sigma-Aldrich, Steinheim, GER              |
| Dithiothreitol (DTT)                                   | Sigma-Aldrich, Steinheim, GER              |
| DNA loading buffer (10x)                               | New England Biolabs, Ipswich, USA          |
| dNTPs: dATP, dCTP, dGTP, dTTP<br>(100 mM)              | PeqLab, Erlangen, GER                      |

| <b>Chemical</b>   | <b>Manufacturer</b>   |
|---|---|
| Dulbecco's Modified Eagle Medium (DMEM)                     | Sigma-Aldrich, Steinheim, GER   |
| ECL Western Blotting Detection Reagents                     | GE Healthcare, Buckinghamshire, UK  |
| Ethylenediaminetetraacetic acid (EDTA)                      | Paul-Ehrlich-Institut   |
| Ethanol (EtOH, 96 %)  | Paul-Ehrlich-Institut   |
| Fetal Calf Serum (FCS)                                      | Sigma-Aldrich, Steinheim, GER   |
| (L)-glutamine   | Biochrom, Berlin, GER   |
| Glycerol (99 %)   | Citifluor, London, UK   |
| Glycine   | Sigma-Aldrich, Steinheim, GER   |
| HEPES (4-(2-hydroxyethyl) -1-piperazineethanesulfonic acid) | Merck, Darmstadt, GER   |
| High-purity water   | Sigma-Aldrich, Steinheim, GER   |
| Histopaque 1.077 g/mL                                       | Sigma-Aldrich, Steinheim, GER   |
| Human AB serum  | Sigma-Aldrich, Steinheim, GER<br>DRK Blutspendedienst, Frankfurt a. M., GER |
| Hydrochloric acid 37 % (HCl)                                | Roth, Karlsruhe, GER  |
| Hygromycin B solution                                       | Invitrogen, San Diego, USA  |
| Immersion oil (Immersol 518F)                               | Zeiss Microscopy, Oberkochen, GER   |
| Luminata Forte Western HRP-Substrate                        | Merck, Darmstadt, GER   |
| Methanol (MeOH)   | Paul-Ehrlich-Institut   |
| Magnesium chloride (MgCl <sub>2</sub> )                     | Merck, Darmstadt, GER   |
| Mowiol 4-88   | Roth, Karlsruhe, GER  |
| Nuclease-free water   | Qiagen, Hilden, GER   |
| Pancoll 1.077 g/mL  | PAN Biotech, Aidenbach, GER   |
| Paraformaldehyde (PFA) 4 %                                  | Sigma-Aldrich, Steinheim, GER   |
| Penicillin/Streptomycin solution                            | Biochrom, Berlin, GER   |

| <b>Chemical</b>                                       | <b>Manufacturer</b>                                   |
|---|---|
| PI-103  | Sellekchem, Houston, USA                              |
| Potassium chloride (KCl)                              | Sigma-Aldrich, Steinheim, GER                         |
| Protease Inhibitor Cocktail                           | Roche, Mannheim, GER                                  |
| Rabbit blood, defibrinated                            | Elocin-Lab, Oberhausen, GER                           |
| Ringer's solution                                     | B. Braun, Melsungen, GER                              |
| Roswell Park Memorial Institute (RPMI)<br>1640        | Biowest, Nuaille, FR<br>Sigma-Aldrich, Steinheim, GER |
| Saponin (from <i>Quillaja</i> bark)                   | Sigma-Aldrich, Steinheim, GER                         |
| Skim-milk powder                                      | EDEKA, Hamburg, GER                                   |
| Sodium azide (NaN <sub>3</sub> )                      | Sigma-Aldrich, Steinheim, GER                         |
| Sodium chloride (NaCl)                                | Sigma-Aldrich, Steinheim, GER                         |
| Sodium dodecyl sulfate (SDS)                          | Paul-Ehrlich-Institut                                 |
| Sodium hydroxide (NaOH)                               | Merck, Darmstadt, GER                                 |
| Stemfect RNA Transfection Reagent                     | Stemgent, San Diego, USA                              |
| Sucrose   | Sigma Aldrich, Steinheim, GER                         |
| Sulfuric acid (H <sub>2</sub> SO <sub>4</sub> )       | Roth, Karlsruhe, GER                                  |
| TEMED (Tetramethylethylenediamine)                    | Roth, Karlsruhe, GER                                  |
| TMB High Sensitivity Substrate Solution               | Biolegend, San Diego, USA                             |
| Tris (Tris(hydroxymethyl)-aminomethan) -<br>solutions | Paul-Ehrlich-Institut                                 |
| Triton X-100  | Sigma-Aldrich, Steinheim, GER                         |
| Tween-20  | Sigma-Aldrich, Steinheim, GER                         |

3.1.5 Media

| <b>Medium</b>                                       | <b>Components</b>   |
|---|---|
| Cryo medium   | CM<br>40 % FCS (v/v)  |
| HEK293T/17/HT1080 medium (DMEM)                     | DMEM<br>10 % FCS (v/v)<br>4 mM L-glutamine<br>1 U/mL Penicillin<br>1 µg/mL Streptomycin   |
| <i>Leishmania</i> liquid medium ( <i>Lm</i> medium) | RPMI 1640<br>5 % FCS (v/v)<br>2 mM L-glutamine<br>1 U/mL Penicillin<br>1 µg/mL Streptomycin<br>10 mM HEPES buffer<br>50 µM β-Mercaptoethanol<br>(for DsRed expressing <i>L. major</i> , <i>Lm</i> medium was supplemented with 20 ng/mL Hygromycin B) |
| Macrophage complete medium (CM)                     | RPMI 1640<br>10 % FCS (v/v)<br>2 mM L-glutamine<br>1 U/mL Penicillin<br>1 µg/mL Streptomycin<br>10 mM HEPES buffer<br>50 µM β-Mercaptoethanol   |

| <b>Medium</b>                           | <b>Components</b>  |
|---|--|
| Medium for cultivation in Teflon bags   | RPMI 1640<br>2 % FCS (v/v)<br>2 mM L-glutamine<br>1 U/mL Penicillin<br>1 µg/mL Streptomycin  |
| Novy-MacNeal-Nicolle- (NNN-) blood-agar | 400 mL ddH <sub>2</sub> O<br>100 mL PBS pH 7.1<br>20.8 g Brain heart infusion agar<br>66.2 U/mL<br>66.2 µg/mL Streptomycin<br>100 mL defibrinated rabbit blood |

### 3.1.6 Buffers and solutions

Phosphate-buffered saline without Ca<sup>2+</sup> and Mg<sup>2+</sup> (PBS) pH 7.1 and pH 7.4, ddH<sub>2</sub>O and Tris-solutions were obtained from the in-house facility of the Paul-Ehrlich-Institut. All solutions used in cell culture were sterile filtered (0.45 µm or 0.22 µm sterile filter) prior to use.

| <b>Buffer/solution</b>         | <b>Components</b>   |
|--------------------------------|---|
| Ammonium chloride solution     | ddH <sub>2</sub> O<br>150 mM Ammonium chloride  |
| Blotting buffer (western blot) | ddH <sub>2</sub> O<br>50 mM Tris<br>40 mM Glycine<br>0.0375 % SDS (w/v)<br>2.5 % MeOH (v/v) |

| <b>Buffer/solution</b>  | <b>Components</b>  |
|---|--|
| Calcium chloride solution   | ddH <sub>2</sub> O<br>2.5 M CaCl <sub>2</sub>  |
| ELISA blocking buffer   | PBS pH 7.4<br>1 % BSA (w/v)  |
| ELISA wash buffer   | PBS pH 7.4<br>0.05 % Tween-20 (v/v)  |
| ELISA reagent diluent (TNF- $\alpha$ , IL-10, IL-6, IL-1 $\beta$ )                | PBS pH 7.4<br>1 % BSA (w/v)  |
| ELISA reagent diluent (IL-8)  | 20 mM Tris-HCl pH 7.4<br>150 mM NaCl<br>0.1 % BSA (w/v)<br>0.05 % Tween-20   |
| FACS blocking buffer  | PBS pH 7.1<br>10 % FCS (v/v)<br>10 % human AB serum (v/v)  |
| FACS washing/staining buffer  | PBS pH 7.1<br>1 % FCS (v/v)<br>1 % human AB serum (v/v)  |
| Hank's balanced salt solution (HBSS)<br>w/o Mg <sup>2+</sup> and Ca <sup>2+</sup> | ddH <sub>2</sub> O<br>140 mM NaCl<br>5 mM KCl<br>300 $\mu$ M Na <sub>2</sub> HPO <sub>4</sub> x 2 H <sub>2</sub> O<br>400 $\mu$ M KH <sub>2</sub> PO <sub>4</sub><br>6 mM Glucose<br>4 mM NaHCO <sub>3</sub> |



| <b>Buffer/solution</b>         | <b>Components</b>  |
|--------------------------------|--|
| HEPES-buffered saline (HBS) 2x | ddH <sub>2</sub> O<br>281 mM NaCl<br>100 mM HEPES<br>1.5 mM Na <sub>2</sub> HPO <sub>4</sub>                             |
| Homogenization buffer          | ddH <sub>2</sub> O<br>15 mM HEPES<br>0.5 mM MgCl <sub>2</sub><br>25 mM Sucrose<br>pH 7.2 - 7.4, sterile filtered 0.22 μm |
| IF blocking buffer             | PBS pH 7.1<br>10 % FCS (v/v)<br>10 % human AB serum (v/v)  |
| IF permeabilization buffer     | PBS pH 7.1<br>1 % FCS (v/v)<br>1 % human AB serum (v/v)<br>0.5 % Saponin (w/v)<br>or<br>0.5 % Triton X-100 (v/v)         |
| IF washing/staining buffer     | PBS pH 7.1<br>1 % FCS (v/v)<br>1 % human AB serum (v/v)  |

| <b>Buffer/solution</b>   | <b>Components</b>   |
|--|---|
| Laemmli buffer (6x)  | ddH <sub>2</sub> O<br>500 mM Tris-HCl pH 6.8<br>38 % Glycerol (v/v)<br>10 % SDS (w/v)<br>600 mM DTT<br>0.01 % Bromophenol blue  |
| MACS-buffer (CD14-MACS)  | PBS pH 7.2<br>0.5 % BSA (w/v)<br>0.5 mM EDTA  |
| MACS-buffer 1 (AnnexinA5-MACS)   | Ringer's solution<br>0.5 % BSA (w/v)  |
| MACS-buffer 2 (AnnexinA5-MACS)   | PBS pH 7.1<br>0.5 % BSA (w/v)   |
| Paraformaldehyde solution (4 %)  | PBS pH 7.1<br>4 % Formaldehyde (w/v)  |
| Phosphate-buffered saline (PBS) w/o Ca <sup>2+</sup> /Mg <sup>2+</sup> | ddH <sub>2</sub> O<br>140 mM NaCl (w/v)<br>10 mM Na <sub>2</sub> HPO <sub>4</sub> x 2 H <sub>2</sub> O<br>2.7 mM KCl (w/v)<br>1.8 mM KH <sub>2</sub> PO <sub>4</sub><br>pH 7.1 / pH 7.4 |
| Ringer's solution  | ddH <sub>2</sub> O<br>147 mM NaCl<br>4 mM KCl<br>2.2 mM CaCl <sub>2</sub>   |

| <b>Buffer/solution</b>                 | <b>Components</b>   |
|--|---|
| SDS-PAGE Running buffer (5x)           | ddH <sub>2</sub> O<br>125 mM Tris<br>1.25 M Glycine<br>0.5 % SDS (w/v)            |
| Stacking gel buffer                    | ddH <sub>2</sub> O<br>1.5 M Tris-HCl pH 8.8<br>0.4 % SDS (w/v)                    |
| Separating gel buffer                  | ddH <sub>2</sub> O<br>0.5 M Tris-HCl pH 6.8<br>0.4 % SDS (w/v)                    |
| TAE buffer (TAE, 20x)                  | ddH <sub>2</sub> O<br>0.8 M Tris (w/v)<br>2..25 % acetic acid (v/v)<br>20 mM EDTA |
| Tris-buffered saline + Tween-20 (TBST) | ddH <sub>2</sub> O<br>50 mM Tris-HCl pH 7.4<br>150 mM NaCl                        |
| Wash buffer (PBMC isolation)           | PBS pH 7.1<br>5 % CM (v/v)  |
| Western blot blocking solution         | 5 % BSA (w/v) + 0.01 % NaN <sub>3</sub> (v/v)<br>or<br>5 % skim-milk powder (w/v) |

### 3.1.7 Leishmania strains

*Leishmania major* wild type (WT): Isolate MHOM/IL/81/FEBNI, isolated from a skin biopsy of an Israeli patient. Kindly provided by Dr. Frank Ebert, Bernhard-Nocht-Institut, Hamburg, Germany.

*Leishmania major* DsRed: Isolate MHOM/IL/81/FEBNI transfected with DsRed (Red Fluorescent Protein from *Discosoma* sp.). A hygromycin phosphotransferase serves as selection marker (Campbell et al., 2002; Misslitz et al., 2000).

### 3.1.8 Human cells

#### 3.1.8.1 Primary cells

Human peripheral-blood mononuclear cells were isolated from buffy coats that were acquired from healthy anonymous volunteers from the blood bank of Frankfurt (DRK-Blutspendedienst Frankfurt am Main) with ethical approval #329/10. Written informed consent was obtained from the participants of these studies and the ethics committee approved the protocol, accordingly. Donations were obtained

#### 3.1.8.2 Cell lines

| Cell line   | Description  | Source         |
|-------------|--|----------------|
| HEK 293T/17 | Human embryonic kidney cells (HEK) 293T. Highly transfectable derivative of the HEK 293 cell line with SV40 T-antigen insertion. | ATCC CRL-11268 |
| HT1080      | Human fibrosarcoma cell line, epithelial-like cells. Highly susceptible to Vesicular stomatitis-virus (VSV) infection.           | ATCC CCL-121   |

### 3.1.9 Antibodies and antisera

Primary antibodies for western blot (WB) analysis were diluted in TBST + 5 % BSA, secondary, HRP-conjugated antibodies were diluted in TBST + 5 % skim-milk powder. Primary fluorophore-conjugated antibodies for flow cytometry (FACS) were diluted in FACS staining buffer. Primary and secondary antibodies for immunofluorescence (IF) were diluted in IF staining buffer.

| <b>Antibody/antiserum</b>                              | <b>Species</b>          | <b>Manufacturer</b>       | <b>Use</b>  |
|--|-------------------------|---------------------------|---|
| <i>Unconjugated primary antibodies</i>                 |                         |                           |   |
| $\alpha$ -LC3B (polyclonal)                            | rabbit                  | Cell Signaling            | WB 1:1000   |
| $\alpha$ - $\beta$ -actin (clone 8H10D10)              | mouse,<br>IgG2b         | Cell Signaling            | WB 1:2000   |
| $\alpha$ -CD11b (clone ICRF44) non-azide/low-endotoxin | mouse,<br>IgG1 $\kappa$ | BD Pharmingen             | Functional assay<br>1 $\mu$ g/1x 10 <sup>5</sup> cells    |
| $\alpha$ -CD91 (clone 8G1)                             | mouse,<br>IgG1          | Thermo<br>Scientific      | Functional assay<br>0.53 $\mu$ g/1x 10 <sup>5</sup> cells |
| $\alpha$ -Cox4 (polyclonal)                            | rabbit                  | Cell Signaling            | WB 1:1000   |
| $\alpha$ -LAMP1  | mouse,<br>IgG1 $\kappa$ | BD Pharmingen             | IF 1:100  |
| $\alpha$ -Nucleoporin p62 (clone 53)                   | mouse,<br>IgG2b         | Abcam                     | WB 1:500  |
| $\alpha$ - <i>Leishmania major</i><br>promastigote     | rabbit,<br>polyclonal   | Uwe Ritter,<br>Regensburg | WB 1:500/IF 1:200   |
| <i>Unconjugated isotype controls</i>                   |                         |                           |   |
| IgG1 $\kappa$ non-azide/low-endotoxin                  | mouse                   | Biolegend                 | Functional assay<br>1 $\mu$ g/1x 10 <sup>5</sup> cells    |
| IgG1 (clone 679.1Mc7)<br>purified                      | mouse                   | Immunotech                | Functional assay<br>0.53 $\mu$ g/1x 10 <sup>5</sup> cells |

| <b>Antibody/antiserum</b>               | <b>Species</b>           | <b>Manufacturer</b>  | <b>Use</b>                                 |
|---|--------------------------|----------------------|--|
| <i>Conjugated primary antibodies</i>    |                          |                      |  |
| FITC $\alpha$ -CD1a (clone HI149)       | mouse,<br>IgG1 $\kappa$  | BD Pharmingen        | FACS 0.1 $\mu$ g/1x 10 <sup>5</sup> cells  |
| PB $\alpha$ -CD3 (clone UCHT1)          | mouse,<br>IgG1 $\kappa$  | Biologend            | FACS 0.1 $\mu$ g/1x 10 <sup>5</sup> cells  |
| PE $\alpha$ -CD11b (clone ICRF44)       | mouse,<br>IgG1 $\kappa$  | BD Pharmingen        | FACS 16 ng/1x 10 <sup>5</sup> cells        |
| PE $\alpha$ -CD14 (clone M5E2)          | mouse,<br>IgG2a $\kappa$ | Biologend            | FACS 0.01 $\mu$ g/1x 10 <sup>5</sup> cells |
| BV421 $\alpha$ -CD163<br>(clone GHI/61) | mouse,<br>IgG1 $\kappa$  | BD Pharmingen        | FACS 0.05 $\mu$ g/1x 10 <sup>5</sup> cells |
| PE $\alpha$ -CD206 (clone 19.2)         | mouse,<br>IgG1 $\kappa$  | BD Pharmingen        | FACS 0.2 $\mu$ L/1x 10 <sup>5</sup> cells  |
| APC $\alpha$ -CD209 (clone DCN46)       | mouse<br>IgG2b $\kappa$  | BD Pharmingen        | FACS 2.5 $\mu$ L/1x 10 <sup>5</sup> cells  |
| <i>Conjugated isotype controls</i>      |                          |                      |  |
| FITC IgG1 $\kappa$ (clone MOPC-21)      | mouse                    | BD Pharmingen        | FACS 0.1 $\mu$ g/1x 10 <sup>5</sup> cells  |
| PB IgG1 $\kappa$ (clone MOPC-21)        | mouse                    | Biologend            | FACS 0.1 $\mu$ g/1x 10 <sup>5</sup> cells  |
| PE IgG1 $\kappa$ (clone MOPC-21)        | mouse                    | BD Pharmingen        | FACS 16 ng/1x 10 <sup>5</sup> cells        |
| PE IgG2a $\kappa$ (clone MOPC-173)      | mouse                    | Biologend            | FACS 0.1 $\mu$ g/1x 10 <sup>5</sup> cells  |
| BV421 IgG1 $\kappa$ (clone X40)         | mouse                    | BD Pharmingen        | FACS 0.05 $\mu$ g/1 x10 <sup>5</sup> cells |
| APC IgG2b $\kappa$ (clone 27-35)        | mouse                    | BD Pharmingen        | FACS 2.5 $\mu$ L/1x 10 <sup>5</sup> cells  |
| <i>Secondary antibodies</i>             |                          |                      |  |
| $\alpha$ -mouse IgG<br>AF488 conjugated | chicken                  | Thermo<br>Scientific | IF 1:100                                   |

| <b>Antibody/antiserum</b>                | <b>Species</b> | <b>Manufacturer</b>         | <b>Use</b> |
|--|----------------|-----------------------------|------------|
| $\alpha$ -mouse IgG<br>HRP-conjugated    | goat           | Santa Cruz<br>Biotechnology | WB 1:2000  |
| $\alpha$ -rabbit IgG<br>AF568 conjugated | goat           | Thermo<br>Scientific        | IF 1:100   |
| $\alpha$ -rabbit IgG<br>AF647 conjugated | chicken        | Thermo<br>Scientific        | IF 1:100   |
| $\alpha$ -rabbit IgG<br>HRP-conjugated   | goat           | Santa Cruz<br>Biotechnology | WB 1:2000  |

### 3.1.10 Dyes and magnetic particles

| <b>Dye</b>   | <b>Manufacturer</b>               |
|--|-----------------------------------|
| Alexa Fluor 647 succinimidyl ester (AF647-SE)              | Thermo Scientific, Dreieich, GER  |
| Bromophenol blue   | Serva, Heidelberg, GER            |
| Carboxyfluorescein succinimidyl ester (CFSE)               | Sigma-Aldrich, Steinheim, GER     |
| DAPI (4',6-Diamidin-2-phenylindole)                        | Sigma-Aldrich, Steinheim,GER      |
| Diff-Quick staining solution 1 (Eosin) and<br>2 (Thiazine) | Medion Diagnostics, Dürdingen, CH |
| FITC AnnexinA5   | Miltenyi, Bergisch Gladbach,GER   |
| GelRed   | Biotium, Fremont, USA             |
| Hoechst 33342 (Bis-benzimide)                              | Sigma-Aldrich, Steinheim,GER      |
| PKH26 + Diluent C  | Sigma-Aldrich, Steinheim, GER     |
| Phalloidin-AF488   | Thermo Scientific, Dreieich, GER  |
| Streptavidin-Cy5   | Thermo Scientific, Dreieich, GER  |
| Trypan Blue  | Lonza, Basel, CH                  |

| <b>Magnetic particle</b>  | <b>Manufacturer</b>              |
|---|----------------------------------|
| Microbeads, AnnexinA5-conjugated  | Miltenyi, Bergisch Gladbach, GER |
| Microbeads, $\alpha$ -CD14-conjugated                                   | Miltenyi, Bergisch Gladbach, GER |
| Bionized nanoferrite (BNF)-dextran beads (80 nm), Lipobiotin-conjugated | Micromod, Rostock, GER           |

### 3.1.11 Enzymes

| <b>Enzyme</b>   | <b>Manufacturer</b>               |
|---|-----------------------------------|
| Benzonase   | Merck, Darmstadt, GER             |
| Human recombinant granulocyte macrophage colony-stimulating factor (GM-CSF) | Bayer Healthcare, Leverkusen, GER |
| Human recombinant macrophage colony-stimulating factor (M-CSF)              | R&D Systems, Minneapolis, USA     |
| Human recombinant Interleukin-4 (IL-4)                                      | R&D Systems, Minneapolis, USA     |
| Recombinant RNasin Ribonuclease Inhibitor                                   | Promega, Mannheim, GER            |
| Trypsin (in PBS, supplemented with EDTA)                                    | Paul-Ehrlich-Institut             |

### 3.1.12 Ready-to-use kits

| <b>Kit</b>                          | <b>Manufacturer</b>              |
|-------------------------------------|----------------------------------|
| AnnexinA5 Microbead Kit             | Miltenyi, Bergisch Gladbach, GER |
| CD14 Microbead Kit                  | Miltenyi, Bergisch Gladbach, GER |
| Human IL-1 $\beta$ DuoSet ELISA     | R&D Systems, Minneapolis, USA    |
| Human IL-6 DuoSet ELISA             | R&D Systems, Minneapolis, USA    |
| Human IL-8 DuoSet ELISA             | R&D Systems, Minneapolis, USA    |
| Human IL-10 DuoSet ELISA            | R&D Systems, Minneapolis, USA    |
| Human IL-TNF- $\alpha$ DuoSet ELISA | R&D Systems, Minneapolis, USA    |
| ImProm II Reverse Transcription Kit | Promega, Mannheim, GER           |



| <b>Kit</b>  | <b>Manufacturer</b>          |
|---|------------------------------|
| LEGENDplex Human Inflammation Panel                 | Biolegend, San Diego, USA    |
| MESA Blue qPCR MasterMix Plus for SYBR Assay No Rox | Eurogentec, Cologne, GER     |
| Pierce BCA Protein Assay Kit                        | Thermo Fisher, Dreieich, GER |
| RNeasy Plus Mini Kit                                | Qiagen, Hilden, GER          |
| Stemfect RNA Transfection Kit                       | Stemgent, San Diego, USA     |

### 3.1.13 Size markers

| <b>Marker</b>                              | <b>Manufacturer</b>                  | <b>Use</b>            |
|--|--------------------------------------|-----------------------|
| PageRuler Prestained (Plus) protein marker | Thermo Scientific, St. Leon-Rot, GER | 5 $\mu$ L<br>SDS-PAGE |

### 3.1.14 Plasmids

| <b>Plasmid name</b> | <b>Resistance</b> | <b>Source</b>  |
|---------------------|-------------------|--|
| pPBj-SW-eGFP-LC3B   | Ampicillin        | (PhD thesis M. Thomas, 2015)   |
| pPBj-pack           | Ampicillin        | Plasmid Factory, Bielefeld, GER<br>(Wolfrum et al., 2007)                        |
| pVpxPBjsyn          | Ampicillin        | Plasmid Factory, Bielefeld, GER<br>(Kloke et al., 2010)                          |
| pMD.G2 (VSV-G)      | Ampicillin        | Plasmid Factory, Bielefeld, GER<br>(Kind gift of D. Trono; Naldini et al., 1996) |

3.1.15 Oligonucleotides

| <b>Primers</b>               | <b>5' - 3' sequence</b>       | <b>Manufacturer</b>         |
|------------------------------|-------------------------------|-----------------------------|
| CD91 forward                 | AAC GAG CAT AACT GCC TGG G    | Eurofins, Ebersberg,<br>GER |
| CD91 reverse                 | CGT ACA CTG AGC ACT CAT CAA A |                             |
| CD11b forward                | CGG CAA TAC AAG GAC ATG       |                             |
| CD11b reverse                | CAC TTG CAC ACA GAC ACT TG    |                             |
| GAPDH forward                | GAG TCA ACG GAT TTG GTC GT    |                             |
| GAPDH reverse                | TTG ATT TTG GAG GGA TCT CG    |                             |
| <b>Small interfering RNA</b> | <b>5' - 3' sequence</b>       |                             |
| siCD91                       | not available                 | Qiagen, Hilden, GER         |
| siCD11b                      | not available                 |                             |
| Allstar control RNA          | not available                 |                             |

## 3.2 Methods

3.2.1 Cell biological methods3.2.1.1 Cell culture of primary human cells

All cell culture work was performed under sterile conditions in a laminar flow workbench. If not stated differently, human cells were incubated at 37°C, 5 % CO<sub>2</sub> and centrifuged at 143x *g* for 8 min at 20°C.

3.2.1.2 Counting of human cells

If not stated differently, peripheral blood mononuclear cells (PBMCs), peripheral blood lymphocytes (PBLs), monocytes, macrophages and dendritic cells were counted using an automatic CASY cell counter equipped with a 150 µm capillary. For this, cells in CM were diluted 1:10000 in CASYton in a CASY tube and cell numbers were determined by three subsequent automatic measurements. Human embryonic kidney (HEK) 293T/17 cells and HT1080 cells were counted using a Neubauer-improved hemocytometer with a depth of 0.1 mm. HEK 293T/17 and HT1080 cells were diluted 1:1 with Trypan Blue and incubated

for 1 min at RT. A volume of 10  $\mu$ L was applied to the hemocytometer and Trypan Blue-negative cells were counted as viable. The cell number in four big squares was determined and the concentration of cells/mL was calculated by multiplication of the median number of cells per big square with the dilution-factor of 2 and the chamber-factor ( $10^4$ ).

### 3.2.1.3 Isolation of peripheral blood mononuclear cells

Peripheral blood mononuclear cells were isolated from blood donations of healthy and anonymous donors (DRK Blutspendedienst, Frankfurt) containing 30-50 mL blood. The blood was diluted with prewarmed PBS to a final volume of 100 mL. A volume of 25 mL of this suspension were layered on top of 15 mL prewarmed Histopaque leukocyte separation medium (density: 1.077 g/mL) in four 50 mL tubes to fraction the blood constituents. The tubes were centrifuged at 573x *g* for 30 min at 20°C with the minimal acceleration and deceleration, respectively. The white interphase containing the PBMCs (“buffy coat”) was collected and distributed into 6 new tubes. Wash buffer was added to a volume of 50 mL and the suspension was centrifuged to remove cell debris and thrombocytes. Further washing steps at different centrifugal forces (1084x *g*/ 573x *g*/ 143x *g*, 8 min, 20°C) were performed. Contaminating erythrocytes were lysed by incubation with 10 mL cold ammonium chloride-solution for 10-15 min at 20°C. Subsequently, the cells were washed with wash-buffer (143x *g*, 8 min, 20°C), pooled and counted using a CASY cell counter. Selection of monocytes was performed by plastic adherence or CD14-MACS.

### 3.2.1.4 Plastic adherence for the generation of macrophages

For the generation of human monocyte-derived macrophages (hMDMs) by plastic adherence, 50x 10<sup>6</sup> PBMCs were seeded in a 25 cm<sup>2</sup> cell culture flask in 5 mL CM supplemented with 1 % human AB serum. Alternatively, 150x 10<sup>6</sup> PBMCs were seeded in a 75 cm<sup>2</sup> cell culture flask in 15 mL CM supplemented with 1 % human AB serum. By incubating for 1 h, monocytes adhered to the tissue culture-treated bottom of the flask. The supernatant with the non-adherent cells, containing mainly PBLs, was discarded or collected separately for subsequent experiments (3.2.4.4). Adherent cells were washed twice with wash-buffer. To differentiate macrophages from monocytes, CM supplemented

with 10 ng/mL GM-CSF (to generate hMDM1) or 30 ng/mL M-CSF (to generate hMDM2) was added. The cells were incubated for 5-7 days at 37°C.

#### 3.2.1.5 Monocyte isolation by CD14-MACS

To yield monocytes with high purity, e.g. for siRNA-transfection or to generate hMDDCs, CD14-magnetic activated cell sorting (MACS) was performed. Freshly isolated PBMCs were washed with 50 mL MACS-buffer (322x *g*, 8 min, 20°C). Per 100x 10<sup>6</sup> PBMCs, 95 µL MACS-buffer and 5 µL α-CD14 antibody-conjugated microbeads were added. Cells were resuspended and the suspension was incubated for 15 min at 4°C. Subsequently the cells were washed with 50 mL MACS-buffer (322x *g*, 8 min, 20°C) and the pellet was resuspended in 5 mL MACS-buffer. The cell suspension was applied onto a MACS-buffer-equilibrated large separation (LS) column. After the suspension entered the column, cells were washed with 3x 3 mL MACS-buffer and the flow through, containing PBLs, was discarded or collected on ice for later experiments (3.2.4.4). CD14<sup>+</sup> monocytes were eluted on ice in 5 mL MACS-buffer with a plunger. The monocytes were counted with a CASY cell counter. For generation of hMDMs, 3x 10<sup>6</sup> cells per well were seeded in a 6-well plate in a volume of 2.5 mL CM. To stimulate the differentiation of the monocytes into hMDM1 or hMDM2, the CM was supplemented with GM-CSF (10 ng/mL) or M-CSF (30 ng/mL), respectively. To generate hMDDCs, 1.5x 10<sup>6</sup> monocytes per well were seeded in a 6-well plate in a volume of 2.5 mL CM supplemented with 5 ng/mL GM-CSF and 10 ng/mL IL-4. The cells were incubated for 5-7 days. After 3 days of cultivation, growth factors were replenished by addition of 0.5 mL CM supplemented with the concentrations of GM-CSF, M-CSF or GM-CSF/IL-4 as stated above.

#### 3.2.1.6 Harvesting of hMDMs and hMDDCs

After 5-7 days of cultivation, morphological appearance and adherence of hMDMs and hMDDCs was checked with a light microscope. Subsequently, the flasks or plates were put on ice for 20-30 min to allow the cells to detach from the surface. Macrophages were harvested using a cell lifter and were pooled in a 50 mL tube. The flasks were washed once with 2 mL cold PBS. Each well was washed with 1 mL cold PBS. Cells were pelleted

(143x *g*, 8 min, 20°C) and resuspended in an appropriate amount of CM, depending on the size of the cell pellet, and counted using a CASY cell counter.

### 3.2.1.7 Generation of hMDMs in Teflon bags

The isolation of apoptotic *Leishmania major* promastigote-containing compartments from infected hMDMs was performed in the laboratory of a cooperation partner (PD Dr. Norbert Reiling, Research Center Borstel). Hence, different protocols for isolation of monocytes and generation of macrophages were used. Here, primary macrophages were generated from monocytes by cultivation in Teflon bags (Menck et al., 2014; Reiling et al., 2001; van der Meer et al., 1982).

A blood donation containing approx. 250 mL fresh blood was diluted 1:1 with prewarmed PBS and 40 mL of this dilution were layered on top of 10 mL Pancoll (density: 1.077 g/mL) in 50 mL reaction tubes. Tubes were centrifuged at 1024x *g* for 40 min at 20°C. The plasma on top of the emerging gradient was discarded and the interphase was harvested using a Pasteur pipette. The interphases of three gradients were pooled in 50 mL reaction tubes on ice. Reaction tubes were filled with cold PBS and centrifuged (545x *g*, 10 min, 4°C). Supernatants were discarded and the pellets were washed with cold PBS. Pellets were resuspended in CM without P/S and counted using a Neubauer-improved hemocytometer. For elutriation, cells were resuspended in HBSS + 1 % BSA at a concentration of 5x 10<sup>6</sup> cells/mL. Elutriation or counter flow centrifugation, is utilizing centrifugal forces for the separation of monocytes from PBLs. This was performed by our collaboration partners according to their standard protocol (Reiling et al., 2001). After elutriation, 20-25x 10<sup>6</sup> monocytes were resuspended in differentiation medium supplemented with 10 ng/mL M-CSF and seeded in a Teflon bag, which was flushed two times with 50 mL PBS using a 50 mL syringe (Menck et al., 2014). Cells were incubated for 7 days at 37°C. To harvest hMDM2, Teflon bags were placed on ice for 1 h and cells were detached by pulling the bags over the edge of a workbench. Cell suspensions were collected in reaction tubes and centrifuged (545x *g*, 10 min, 4°C). The cell pellet was resuspended in an appropriate volume of CM depending on the pellet size prior to counting in a Neubauer hemocytometer.

#### 3.2.1.8 Long-time storage and thawing of PBLs

Supernatants collected from cell culture flasks or wash fractions from CD14-MACS that contained PBLs were centrifuged (322x *g*, 8 min, 20°C) and the pellets were resuspended in 1.8 mL cryo-medium. A volume of 900 µL was transferred to a cryo-tube and 100 µL DMSO were added. Cryotubes were rapidly transferred to -80°C and stored for further usage of the cells.

Cells were thawed by gently shaking the cryotube in a water bath at 37°C. The thawed PBLs were carefully transferred to 7 mL prewarmed CM. Residual DMSO was removed by centrifugation (143x *g*, 8 min, 20°C) and the pellet was resuspended in CM. The cells were counted using a CASY cell counter and adjusted with CM to the desired concentration for further use.

#### 3.2.1.9 Cultivation of HEK 293T/17 cells

HEK 293T/17 cells are a human embryonic kidney cell line which is highly susceptible to transfection and used for the recombinant production of retroviral. Cells were cultivated in DMEM and were sub-cultured twice a week in a 175 cm<sup>2</sup> culture flask by splitting at a ratio of 1:3. The cell supernatant was discarded and cells were washed with 10 mL prewarmed PBS. Cells were detached by addition of 3 mL trypsin/EDTA and incubation at 37°C for 5 min. Trypsinization was stopped with 9 mL culture medium. A volume of 4 mL of this cell suspension was mixed with 20 mL DMEM and transferred into a new 175 cm<sup>2</sup> flask. Cells were further incubated at 37°C.

#### 3.2.1.10 Cultivation of HT1080 cells

HT-1080 cells are a fibrosarcoma cell line highly susceptible to Vesicular stomatitis virus (VSV)-infection. The surface glycoprotein of the virus (VSV-G) is used in recombinant lentiviral vectors allowing for efficient transduction of human cells (3.2.6.2). HT1080 therefore are used to titrate lentivirus titers. Cells were cultivated in DMEM and were sub-cultured twice a week in a 75 cm<sup>2</sup> culture flask by splitting them at a ratio of 1:10. Therefore, the cell supernatant was discarded and cells were washed with 10 mL prewarmed PBS. Cells were detached by addition of 2 mL trypsin/EDTA at 37°C for 5 min. To stop the enzymatic reaction, 8 mL DMEM were added and 1 mL of this cell suspension

was transferred into a new 75 cm<sup>2</sup> flask containing 19 mL DMEM. Cells were further incubated at 37°C.

### 3.2.2 Cultivation of *Leishmania major* promastigotes

*Leishmania major* promastigotes (hereafter: *Lm*) were incubated at 27°C and 5 % CO<sub>2</sub>. If not stated differently, *Lm* were centrifuged at 2400x *g* for 8 min at 4°C.

*Lm* were cultured in Novy-MacNeal-Nicolle (NNN) modified medium, a biphasic rabbit blood-based medium consisting of a solid blood-agar slope and liquid *Lm* medium (hereafter: NNN-blood-agar) (Nicolle, 1908). For passaging, 3 wells of a 7-day-old stationary phase *Lm*-culture were diluted in 3 mL liquid *Leishmania* medium and counted as described below (3.2.2.1). Promastigotes were adjusted to a final concentration of 1x 10<sup>6</sup>/mL and 1x 10<sup>5</sup> *Lm* per well ( $\pm$  100  $\mu$ L) were transferred to a new blood-agar plate. Parasites were incubated at 27°C for 6-8 days until stationary phase *Lm* were used for AnnexinA5-MACS or infection experiments. Parasites were cultured up to 8 serial passages until they were discarded. DsRed expressing *Lm* were cultivated analogous to wild-type *Lm* whereas the *Lm* medium was supplemented with 20 ng/mL hygromycin to maintain selection pressure for keeping the DsRed-encoding plasmids.

#### 3.2.2.1 Counting of *Leishmania major* parasites

*Lm* were counted in a Neubauer-improved hemocytometer with a depth of 0.02 mm. For this, parasites from an *in vitro* culture were diluted at a ratio of 1:10 in liquid *Lm* medium and 5  $\mu$ L of the suspension were applied to the hemocytometer. Numbers of viable and apoptotic *Lm* in 16 small squares were counted. Total cell numbers per mL were calculated by multiplication of the total cell numbers with the chamber factor (5x 10<sup>4</sup>).

#### 3.2.2.2 AnnexinA5-MACS of stationary phase *Leishmania major* promastigotes

Viable and apoptotic *Lm* were separated from a wild-type stationary phase *Lm* culture by magnetic-activated cell sorting (MACS) using AnnexinA5 (AnxA5) microbeads. These beads specifically bind phosphatidylserine (PS) on the surface of apoptotic cells in presence of Ca<sup>2+</sup> ions. Microbeads are paramagnetic particles, 50 nm in size, that are conjugated to

antigen-specific antibodies or other antigen-directed proteins such as AnxA5. Due to their small size, binding of the beads to their target does not activate cells.

*Lm* were counted and set to the desired cell numbers for the respective experiment. Parasites were pelleted and washed twice with 20 mL and 10 mL MACS buffer 1, respectively. Subsequently, *Lm* were resuspended in 40  $\mu$ L MACS-buffer 1 per  $25 \times 10^6$  parasites. A volume of 10  $\mu$ L AnxA5-microbeads was added per  $25 \times 10^6$  parasites (viable and apoptotic *Lm*) and this suspension was incubated for 15 min in the refrigerator. After incubation, parasites were washed with 10 mL MACS buffer 1, resuspended in 1 mL MACS buffer 1 and applied onto a large separation (LS) column that was pre-equilibrated with MACS buffer 1. As soon as the suspension entered, the column was washed with 3x 3 mL MACS buffer 1 and the flow-through containing mainly unlabeled, AnxA5-non-binding viable *Lm*, was collected. For elution of PS-positive, AnxA5-binding apoptotic *Lm*, 1x 2 mL and 3x 3 mL MACS buffer 2 which contains no  $\text{Ca}^{2+}$  ions, were applied and the elution fraction was collected. The cell number and purity of the wash-fraction was determined by counting in a hemocytometer. To improve purity of the viable *Lm*-containing fraction, the cells were once more incubated with AnxA5-microbeads as described and separated in a large depletion (LD) column that retains labeled, apoptotic *Lm*. In principle the procedure is similar to that for separation on a LS column whereas *Lm* are applied onto the column in a volume of 500  $\mu$ L MACS buffer 1 and the viable fraction was washed out by addition of 3x 1 mL MACS buffer 1. The number of parasites in each fraction was determined by counting and cells were labeled for infection experiments and flow cytometry (3.2.4.2 and 3.2.9.7) or remained unlabeled for western blot-analysis and cytokine analysis by ELISA (3.2.4.6 and 3.2.8.2). When infection with a stationary phase was desired, an artificial 1:1 mixture of purified viable and apoptotic *Lm* was generated.

### 3.2.3 Cyto centrifugation of hMDMs and *Leishmania major* promastigotes

Cyto centrifugation is a rapid method to attach cells onto microscopy slides for microscopic analysis. Either  $1 \times 10^5$  hMDMs or  $1 \times 10^6$  *Lm* were resuspended in 100  $\mu$ L CM/*Lm* medium or PBS and centrifuged onto a microscopy slide at 75x *g* for 5 min (hMDMs) or 500x *g* for 10 min (*Lm*) at RT. Slides were air-dried and further stained by Diff-Quick or DAPI to visualize the nucleus for fluorescence microscopy analysis. Fluorescent samples were



mounted with Mowiol, supplemented with DABCO to retain fluorescence, and a glass coverslip.

### 3.2.4 Infection experiments

#### 3.2.4.1 Infection of transduced hMDMs for live cell microscopy

For dynamic imaging of *Lm* infection *in vitro*, eGFP-LC3-transduced hMDMs (3.2.6.3) were co-incubated with PKH26-stained purified viable or apoptotic *Lm*. Parasites were set to a concentration of  $15 \times 10^6$  cells/mL with CM of which 10  $\mu$ L were added to hMDMs ( $1.5 \times 10^5$  *Lm*, MOI 1). Cells were imaged as described in 3.2.11.3.

#### 3.2.4.2 Infection of hMDMs and hMDDCs for flow cytometry or fluorescence microscopy

For quantification of infection rates by immunofluorescence microscopy,  $0.1 \times 10^6$  hMDMs were seeded in 100  $\mu$ L in a well of a 12-well chamber slide. Cells were left to adhere for a minimum of 30 min and were subsequently co-incubated with viable or apoptotic *Lm* for different times as indicated in the respective experiment. hMDMs were fixed by 4 % PFA for 10 min at 4°C. Fixed macrophages were further processed for immunofluorescence microscopy as described below (3.2.9.3).

To assess infection rates of hMDMs and hMDDCs by flow cytometry,  $3 \times 10^5$  cells were seeded in 1.5 mL reaction tubes in a volume of 100  $\mu$ L CM. To investigate the role of CR3 in *Lm* infection, cells were incubated with  $\alpha$ -CD11b or the corresponding isotype-control (3.1.9) for 30 min at 37°C. Unbound antibody was removed by washing of the cells with 1 mL CM (68x *g*, 8 min, 20°C). Alternatively, CD91 knockdown cells or the corresponding controls (3.2.7.2) were used at the indicated cell numbers. Subsequently, hMDMs and hMDDCs were infected with  $3 \times 10^6$  AnxA5-MACS-purified, CFSE-labeled viable *Lm*, Alexa Fluor 647-SE-labeled apoptotic *Lm* or an artificial stat. ph. (MOI 10) for 3 h at 37°C. To remove non-internalized parasites, cells were washed twice with CM (68x *g*, 8 min, 4°C) and resuspended in 100  $\mu$ L CM or 100  $\mu$ L 1 % PFA for later analysis. Infection rates were determined by flow cytometry (3.2.10).

#### 3.2.4.3 Cytokine analysis upon differential infection with *Leishmania major*

To measure the concentrations of secreted cytokines in supernatants of infected hMDMs or hMDDCs,  $1-3 \times 10^5$  macrophages were seeded in 1.5 mL reaction tubes. Depending on the experimental setup, cells were treated with  $\alpha$ -CD11b or the corresponding isotype control. Cells were co-incubated with either purified viable or apoptotic *Lm* or an artificial stat. ph. (MOI 10) for 3 h. After co-incubation, cells were washed twice with 1 mL CM ( $68 \times g$ , 8 min,  $20^\circ\text{C}$ ). Infected cells were further incubated in 100  $\mu\text{L}$  CM per  $1 \times 10^5$  cells for 21 h at  $37^\circ\text{C}$ . Subsequently, supernatants were collected and frozen at  $-80^\circ\text{C}$  for later analysis by ELISA (3.2.8.2).

#### 3.2.4.4 CFSE-based proliferation assay

For the T cell proliferation assay,  $1.5 \times 10^5$  CFSE-stained hMDMs were seeded in 1.5 mL reaction tubes. CR3 on the surface of the cells was blocked by addition of 1.5  $\mu\text{g}$   $\alpha$ -CD11b or cells were treated with the corresponding isotype control and subsequently incubated for 30 min at  $37^\circ\text{C}$ . After washing with 900  $\mu\text{L}$  CM, cells were infected with  $1.5 \times 10^6$  log. ph. or stat. ph. DsRed *Lm* (MOI 10). Untreated hMDMs served as controls. After 3 h of incubation at  $37^\circ\text{C}$ , extracellular parasites were removed by washing the cells twice with 900  $\mu\text{L}$  CM ( $68 \times g$ , 8 min,  $20^\circ\text{C}$ ). The pellet was resuspended in 375  $\mu\text{L}$  CM and 50  $\mu\text{L}$  of the suspension were transferred to a 96-well round bottom plate in 6 replicates. The plates were incubated over night at  $37^\circ\text{C}$ .

One day post infection CFSE-stained PBLs were added at a ratio of 1:5 (hMMDM:PBL) and the cell suspensions were incubated at  $37^\circ\text{C}$  for 6 days. To determine the number of proliferated T cells after 6 days of co-incubation, 4 replicates were pooled in a 96 well V-shape plate. The plate was centrifuged ( $439 \times g$ , 8 min,  $4^\circ\text{C}$ ) and the cell pellets were resuspended in 100  $\mu\text{L}$  FACS washing buffer. T cells were stained with an  $\alpha$ -CD3 antibody and analysis was performed by flow cytometry.

#### 3.2.4.5 Determination of parasite survival by limiting dilution assay

To assess the survival of viable *Lm* within hMDMs, a limiting dilution assay was performed in NNN-blood-agar plates. By serial dilution of infected cells, the number of internalized

parasites can be determined by assessing the last dilution step in which parasite growth can be detected (Bogdan et al., 1990; Titus et al., 1985).

For this,  $7 \times 10^5$  cells were seeded in 1.5 mL reaction tubes in 100  $\mu$ L CM. Cells were treated with  $\alpha$ -CD11b or the corresponding isotype control or were left untreated prior to infection with an artificial stat. ph. comprised of CFSE or AF647-SE-labeled purified viable and apoptotic *Lm*. At 3 h post-infection, non-internalized *Lm* were removed by washing twice with 1 mL CM. Cells were further incubated in 700  $\mu$ L CM over night at 37°C. The next day, the number of cells per condition were determined with a CASY cell counter. Solutions of  $1 \times 10^4$  cells /mL were generated with *Lm* medium. Four replicates of each 200  $\mu$ L ( $\cong 2 \times 10^3$  cells) were seeded in a NNN-blood-agar plate and cells were serially diluted in 1:1.5 steps. Blood-agar plates were incubated at 27°C for 7 days. Determination of the last dilution step in which *Lm* growth could be detected was performed by light microscopy. The number of parasites per 1000 hMDMs was calculated from the last dilution that showed parasite growth and equals  $1.5 \exp$  (mean dilution with parasite growth). Remaining infected hMDMs were further incubated at 37°C for 5 days and the generation of serial dilutions was repeated as described.

#### 3.2.4.6 Determination of LC3 conversion by western blot analysis

Western blot analysis was used to assess the induction of LC3-associated phagocytosis upon co-incubation of hMDMs or hMDDCs with *Lm*. For this,  $2.5 \times 10^5$  hMDMs or hMDDCs were seeded in a 1.5 mL reaction tube in 100  $\mu$ L CM. Cells were incubated with  $\alpha$ -CD11b or the corresponding isotype control for 30 min. Excess antibody was washed away with 1 mL CM (68x *g*, 8 min, 20°C) and cells were differentially infected with purified viable, apoptotic or stat. ph. *Lm* for 3 h. Subsequently, cells were centrifuged (345x *g*, 8 min, 4°C) and the pellet was resuspended in 20  $\mu$ L 1x Laemmli buffer. Lysates were generated by heating at 95°C for 10 min. The samples were stored at -20°C.

#### 3.2.5 Magnetic isolation of phagosomes

##### 3.2.5.1 Isolation procedure for phagosomes

The isolation of phagosomes harboring apoptotic *Lm* from macrophages was performed according to the modified protocol of Steinhäuser (Steinhäuser et al., 2014, 2013). For this,

each  $10 \times 10^6$  hMDM2 generated in Teflon bags (3.2.1.7) were seeded in two petri dishes ( $60 \text{ cm}^2$ ). Adherent cells were co-incubated with  $100 \times 10^6$  (MOI 10) of purified, magnetic bead-labeled apoptotic *Lm* for 1 h at  $37^\circ\text{C}$  (3.2.9.5). Subsequently, medium was discarded and cells were gently washed with 10 mL cold PBS. Cells were further incubated with homogenization buffer (supplemented with 0.2 % EDTA) for 15 min on ice and harvested with a cell lifter. After centrifugation ( $310 \times g$ , 10 min,  $4^\circ\text{C}$ ) cells were resuspended in 500  $\mu\text{L}$  of homogenization buffer (supplemented with protease inhibitors) and collected in a 1.5 mL reaction tube. A sample of 50  $\mu\text{L}$  was taken and 1:1 diluted with homogenization buffer (supplemented with 0.2 % EDTA) for later western blot analysis and BCA assay (sample: lysate).

Gentle homogenization of cells was achieved by three rounds of sonication, each followed by centrifugation ( $500 \times g$ , 2 min,  $4^\circ\text{C}$ ) and collection of the supernatants. The approx. 600  $\mu\text{L}$  of homogenate were filled to 700  $\mu\text{L}$  with homogenization buffer (supplemented with protease inhibitors, Cytochalasin D and Benzonase). The sample was incubated at  $37^\circ\text{C}$  for 5 min to ensure degradation of nucleic acids by the supplemented Benzonase. A sample of 50  $\mu\text{L}$  was taken and 1:1 diluted with homogenization buffer (supplemented with protease inhibitors, Cytochalasin D and Benzonase) for later western blot analysis and BCA assay (sample: homogenate).

For magnetic isolation, a commercially available permanent-magnet (HOKImag) was used. The magnetic chamber is constructed with a high-intensity 2 Tesla magnetic field and a device to insert a unique free-flow separation column (Tchikov and Schütze, 2008). After loading of the homogenate, magnetically labeled phagosomes are attracted to the walls of the column. The system's advantage is the lack of ferromagnetic particles. Hence, lysates of any density can be applied and separated (Steinhäuser et al., 2013; Tchikov and Schütze, 2008).

Prior to loading of approx. 650  $\mu\text{L}$  of the homogenate, the plastic column was rinsed with homogenization buffer 3. The homogenate was incubated within the magnetic field for 90 min and washed for 5 min with homogenization buffer (supplemented with protease inhibitors) at a flow rate of 250  $\mu\text{L}/\text{min}$ . A volume of 100  $\mu\text{L}$  was withdrawn for later western blot analysis and BCA assay (sample: non-magnetic fraction). The column was washed for another 10 min. The magnetic-fraction, harboring the apoptotic *Lm*-containing phagosomes, was eluted by first releasing the column from the magnetic field. Phagosomes

adhering to the walls of the column spontaneously eluted and were collected in a 1.5 mL reaction tube. Remaining phagosomes were collected by scraping the sides of the column with a plunger of a 1 mL syringe. The eluate was centrifuged (15000x *g*, 10 min, 4°C) and the brownish pellet was resuspended in 100 µL of homogenization buffer (supplemented with protease inhibitors). Each 12.5 µL were stored for later western blot analysis and BCA assay (sample: magnetic-fraction). Western blot samples were diluted with 6x Laemmli buffer and stored at -20°C. The remaining eluate for mass spectrometry was centrifuged (15000x *g*, 10 min, 4°C), rapidly frozen in liquid nitrogen and stored at -80°C. Protein amounts of the different elution fractions and western blot samples were determined by BCA assay (3.2.8.3).

### 3.2.5.2 Label-free mass spectrometry and functional protein association network-analysis

Mass spectrometry of the isolated apoptotic *Lm*-containing phagosomes was performed by our collaboration partner (Prof. Dr. Stefan Tenzer, University Hospital Mainz). Samples were prepared and analyzed by label-free nano ultra-performance liquid chromatography-coupled mass spectrometry (nanoUPLC-MS<sup>E</sup>, hereafter: LC-MS). Prior to LC-MS, proteins of a sample were proteolytically digested to generate small peptides. These peptides were separated by LC and subsequently identified and quantified by MS (Distler et al., 2016). For each sample, three technical replicates were analyzed and data was processed with the quantification software ISOQuant (Kuharev et al., 2015). Most abundant human proteins were determined by ranking for their overall presence in all independently analyzed samples in MS Excel 2010 software. Proteins of interest were further analyzed in regard of the number of reported distinct peptides and the coverage of the respective protein sequence by these peptides. Most abundant human proteins identified were used for functional protein association network-analysis at the STRING-database (Szklarczyk et al., 2019). Interesting target proteins were further analyzed *in vitro* regarding their function in *Lm* infection.

### 3.2.6 Virological methods

#### 3.2.6.1 Production and concentration of lentiviral vectors

##### 3.2.6.1.1 Transfection of HEK 293T/17 cells with calcium phosphate

Lentiviral vectors were produced by transfection of HEK 293T/17 cells with a four-plasmid system (Kloke et al., 2010). The packaging construct (pPBj-pack) is coding for structural lentiviral genes (*gag*, *pol*) except the envelope protein. The envelope construct (pMD.G2) encodes for the surface G-protein of Vesicular stomatitis-virus (VSV-G). This pseudo-typing with the VSV-G protein allows for transduction of a wide variety of cells since it redirects vector entry through the endocytic pathway (Naldini et al., 1996). The viral accessory protein Vpx targets the host cell restriction factor SAMHD1 to proteasomal degradation what enables successful infection of myeloid cells with HIV-1 and related SIV viruses (Hrecka et al., 2011; Laguette et al., 2011). Furthermore, Vpx-mediated SAMHD1 degradation renders primary monocytes highly susceptible to HIV-1 infection and is therefore included in the transfection system (pVpxPBjsyn) (Berger et al., 2011). The desired transgene is introduced into the cells by the plasmid pPBj-trans which in our project codes for eGFP-tagged microtubule-associated protein 1A/1B light chain 3B (pPBj-SW-eGFP-LC3).

Transfection was performed with constructs that were already isolated from bacterial cells (pPBj-SW-eGFP-LC3) or that can be acquired commercially. Three days prior to transfection, each  $4.5 \times 10^6$  HEK 293T/17 cells were seeded into 24 T175-flasks in 20 mL DMEM. One hour before transfection the medium was replaced by 5 mL pre-warmed DMEM supplemented with 25  $\mu$ M chloroquine to inhibit fusion of lentiviral-containing endosomes with lysosomes and hence increasing transfection efficiency. The four different plasmids were diluted in High-purity water and 250 mM  $\text{CaCl}_2$  was added (Table 2). For 24x T175-flasks a total volume of 36 mL was prepared in a 50 mL tube and afterwards split to three tubes à 12 mL. The same volume 2x HBS-buffer was added drop wise to each tube while aspirating the DNA- $\text{CaCl}_2$  solution with a pipette. Subsequently, the precipitate was added drop wise to the cells (3 mL/flask). After 8 h and 24 h of incubation medium was replaced by 20 mL and 9 mL fresh DMEM, respectively.

**Table 2: Ratios and volumes used for a large-scale transfection of HEK293T/17 cells for lentiviral vector-production.**

| <b>Plasmid</b>    | <b>stock concentration</b> | <b>ratio/ concentration</b> | <b>24x T175 flasks</b> |                   |
|-------------------|----------------------------|-----------------------------|------------------------|-------------------|
| pPBj-SW-eGFP-LC3  | 0.431 µg/µL                | 1                           | 600 µg                 | <b>1391,95 µL</b> |
| pPBjpack          | 1 µg/µL                    | 1                           | 600 µg                 | <b>600 µL</b>     |
| pMD.G2            | 1 µg/µL                    | 0,33                        | 198 µg                 | <b>198 µL</b>     |
| pVpxPBjsyn        | 1 µg/µL                    | 0,165                       | 99 µg                  | <b>99 µL</b>      |
| CaCl <sub>2</sub> | 2.5 M                      | 250 mM                      |                        | <b>3600 µL</b>    |
| High-purity water |                            |                             |                        | <b>30,111 mL</b>  |
| 2x HBS            |                            |                             |                        | <b>36 mL</b>      |

#### 3.2.6.1.2 Concentration of lentiviral vector particles

At 48 h post-transfection cell-supernatants that contained the pseudo-typed lentiviral vector particles were harvested. The medium was replaced by 9 mL fresh DMEM and cells were further incubated for 24 h. The supernatants of four flasks were pooled and centrifuged (169x *g*, 10 min, 4°C) to remove dead cells and cell debris. Cleared supernatants were sterilized through a 0.45 µm vacuum filter. To enrich vector particles, 30 mL of the filtered supernatant was transferred to a polyallomer centrifuge tube, sub layered with 5 mL of 20 % sucrose and concentrated by ultracentrifugation (82705x *g*, 2 h, 4°C). A small aliquot of 1 mL of unconcentrated particles was withdrawn and stored at -80°C. After centrifugation, the supernatant was discarded and the pellet containing lentiviral particles was resuspended in 50-200 µL of RPMI 1640 without supplements. Pellets were dissolved by shaking at 4°C for 15 min. Concentrates were transferred to 2 mL tubes and centrifuged (7983x *g*, 1 min, 4°C). Lentiviral vector particles were stored in 10 µL-aliquots at -80°C. At 72 h and 96 h post-transfection, vectors were harvested and prepared as described.

#### 3.2.6.2 Titration of lentiviral vectors

Titers of lentiviral vector particles were determined by transduction of HT1080 cells and analysis by flow cytometry. One day prior to transduction 5x 10<sup>4</sup> cells were seeded in 1 mL DMEM per well of a 24-well plate. Concentrated vector particle stocks were serially diluted

with DMEM (1:500, 1:1000, 1:5000, 1:10000, 1:50000). A volume of 250  $\mu$ L of the respective dilution was added per well. Cells were incubated for 4 h and the medium was changed to 500  $\mu$ L DMEM. After 3-4 days cells were harvested discarding the supernatant and addition of 250  $\mu$ L of PBS/EDTA for 5 min at 37°C. Subsequently, the collected cells were washed with PBS (265x *g*, 5 min, 20°C) and cells were fixed with 200  $\mu$ L 1 % PFA. Vector titers were determined by flow cytometry. For this, dilutions of vector particles that resulted in 4-20 % of transduced HT1080 cells were used for calculation. Higher transduction efficiencies indicate double-positive cells. Titers were calculated as follows: Titer [i.u./mL] = % transduced cells / 100 % x seeded cell number ( $5 \times 10^4$ ) x dilution factor x 4.

### 3.2.6.3 Lentiviral transduction of human monocyte-derived macrophages

To generate eGFP-LC3-expressing hMDMs for western blot analysis,  $2.5 \times 10^5$  cells were seeded in 1.5 mL reaction tubes. For live cell microscopy  $1.5 \times 10^5$  cells were seeded per well of an 8-well chamber slide. hMDMs were transduced with lentiviral vector particles at a multiplicity of infection (MOI) of 1 and incubated for 4-5 days.

For western blot samples, transduced hMDMs were harvested 4 h and 24 h post-transduction. As positive controls, hMDMs were stimulated with the autophagy inducer PI-103 (10  $\mu$ M) for 1 h. Cells were centrifuged (345x *g*, 8 min, 4°C) and pellets were resuspended 20  $\mu$ L 1x Laemmli buffer and heated at 95°C for 10 min. Lysates were stored at -20°C.

### 3.2.7 Molecular biological methods

#### 3.2.7.1 Determination of nucleic acid concentration

Nucleic acid concentrations were determined with a NanoDrop 2000c UV-Vis spectrophotometer. For this, 1-2  $\mu$ L of the DNA or RNA sample were pipetted on the quartz cell of the device and concentration was measured at a wavelength of 260 nm in duplicates. Synchronous measurement at a wavelength of 280 nm allowed for determination of protein impurities of the samples.



### 3.2.7.2 Transfection of hMDMs with small interfering RNA

We performed knock down of receptors by transfection with small interfering RNA (siRNA). For transfection,  $3 \times 10^6$  CD14-MACS separated hMDMs seeded in 6-well cell culture plates were washed once with 1 ml RPMI 1640 medium and 1 ml RPMI 1640 was added per well. For the transfection, solutions A and B were prepared according to Table 3. Both solutions were mixed and incubated for 20 min at RT. The final concentration of siRNA or non-target siRNA per well was 20 nM. After 7 h of incubation, cells were washed once with 1 mL CM and 2.5 mL CM were added per well. At day 2 post-transfection, hMDMs were harvested, counted and used for RNA isolation, characterization by flow cytometry or infection experiments.

**Table 3: Preparation of solutions A and B for siRNA transfection of hMDMs per well of a 6-well cell culture plate.**

|                          | target siRNA (c=10 $\mu$ M) | non-target siRNA (c=20 $\mu$ M) |
|--------------------------|-----------------------------|---------------------------------|
| <b>Solution A</b>        |                             |                                 |
| Transfection buffer      | 20 $\mu$ L                  | 20 $\mu$ L                      |
| RNA transfection reagent | 4.6 $\mu$ L                 | 4.6 $\mu$ L                     |
| <b>Solution B</b>        |                             |                                 |
| Transfection buffer      | 20 $\mu$ L                  | 20 $\mu$ L                      |
| siRNA (final 20 nM)      | 2 $\mu$ L                   | 1 $\mu$ L                       |

### 3.2.7.3 RNA isolation from hMDMs

RNA was isolated from hMDMs with the RNeasy Plus Mini Kit according to the manufacturer's instructions. RNA was either placed on ice for subsequent cDNA synthesis or was stored at  $-80^{\circ}\text{C}$ .

### 3.2.7.4 Reverse transcription for synthesis of cDNA

For cDNA synthesis the ImProm-II Reverse Transcription System Kit was used according the manufacturer's instructions. The used reverse-transcriptase is a RNA-dependent polymerase that catalyzes the generation of cDNA from a RNA template. Annealing of

random primers serves the generation of random starting points for subsequent cDNA synthesis by the reverse-transcriptase (Table 4).

**Table 4: Preparation of RNA samples for reverse transcription by annealing of random primers.**

| Reagent                        | Volume/amount |
|--------------------------------|---------------|
| Random primer mix              | 1 $\mu$ L     |
| Template RNA                   | 50 ng         |
| Nuclease-free H <sub>2</sub> O | ad 5 $\mu$ L  |

The primer-RNA mixture was incubated for 5 min at 70°C and subsequently chilled on ice. A reverse transcription reaction mix was prepared on ice and added to each sample (Table 5).

**Table 5: Preparation of the master-mix for reverse transcription of isolated RNA with the ImPromII Reverse Transcription Kit.**

| Reagent                                       | Volume      | Final concentration |
|---|-------------|---------------------|
| Nuclease-free H <sub>2</sub> O                | 6.5 $\mu$ L |                     |
| ImPromII reaction buffer (5x)                 | 4 $\mu$ L   | 1x                  |
| MgCl <sub>2</sub> (25 mM)                     | 2 $\mu$ L   | 2.5 mM              |
| dNTP mix (10 mM each)                         | 1 $\mu$ L   | 0.5 mM              |
| RNasin Ribonuclease Inhibitor (20 U/ $\mu$ L) | 0.5 $\mu$ L | 10 U                |
| ImPromII Reverse Transcriptase                | 1 $\mu$ L   |                     |

The reverse transcription was performed in a thermal cycler with the following program (Table 6) and samples were subsequently used for quantitative real-time polymerase chain reaction (qRT-PCR) or were stored for further use at -20°C.

**Table 6: Thermo cycler program for reverse transcription using the ImPromII Reverse Transcription Kit.**

| Amplification step    | Temperature | Time     |
|-----------------------|-------------|----------|
| Annealing             | 25°C        | 5 min    |
| Reverse transcription | 42°C        | 60 min   |
| Inactivation          | 70°C        | 15 min   |
| Cooling               | 4°C         | $\infty$ |

### 3.2.7.5 Quantitative real-time polymerase chain reaction

Quantitative real-time PCR (qRT-PCR) was used to amplify DNA and quantify the *de novo* synthesized DNA molecules during analysis in real-time. This allows for determination of expression levels of genes by analysis of synthesized cDNA which correlates to the initial amount of mRNA. For this, the MESA Blue qPCR MasterMix Plus for SYBR Assay-Kit was used according to the manufacturer's instructions. A master-mix for each cDNA-specific primer pair was prepared (Table 7). GAPDH was used as housekeeping-gene for normalization. The primers used are listed in 3.1.15.

**Table 7: Preparation of the master-mix for quantitative real-time polymerase chain reaction with the MESA Blue qPCR Kit.**

| Reagent                       | Volume     | Final concentration |
|-------------------------------|------------|---------------------|
| MESA Blue qPCR MasterMix (2x) | 10 $\mu$ L | 1x                  |
| ddH <sub>2</sub> O            | 6 $\mu$ L  |                     |
| Primer forward (10 $\mu$ M)   | 1 $\mu$ L  | 0.5 $\mu$ M         |
| Primer reverse (10 $\mu$ M)   | 1 $\mu$ L  | 0.5 $\mu$ M         |
| cDNA                          | 2 $\mu$ L  |                     |

The polymerase-chain-reaction was performed in a LightCycler 480 (Table 8). Amplified DNA is quantified by detection of the fluorescent dye SYBR Green that intercalates into the DNA molecules. Based on the fluorescence-intensity that is proportional to the amount of DNA molecules, the amplification of the target genes can be measured. The more DNA was present in the beginning of the amplification, the more will be quantified. All samples were measured in duplicates. H<sub>2</sub>O instead of cDNA served as negative control.

**Table 8: Amplification program for quantitative real-time PCR in a LightCycler 480.**

| Amplification step | Temperature | Time   | Temperature change/s |
|--------------------|-------------|--------|----------------------|
| Taq activation     | 95°C        | 10 min | 4.4°C                |
| <b>45 cycles</b>   |             |        |                      |
| Denaturation       | 95°C        | 10 s   | 4.4°C                |
| Annealing          | 60°C        | 10 s   | 2.2°C                |
| Elongation         | 72°C        | 15 s   | 4.4°C                |
| Melting curve      | 60-99°C     |        | 0.11°C               |
| Cooling            | 40°C        | 20 min | 2.2°C                |

Data was analyzed for relative gene expression compared to GAPDH with the  $2^{-\Delta\Delta CT}$ -method (CT: cycle threshold; Livak and Schmittgen, 2001). For this, the cycle in which the fluorescence signal significantly exceeds the background signal for the first time is determined and normalized to the housekeeping gene.

### 3.2.8 Protein-biochemical methods and immunoassays

#### 3.2.8.1 Western blot analysis

##### 3.2.8.1.1 Sodium dodecyl sulfate-polyacrylamide gel electrophoresis

Sodium dodecyl sulfate-polyacrylamide gel electrophoreses (SDS-PAGE) is a method used to separate proteins according to their respective molecular weight (Laemmli, 1970). Proteins were separated on 15 % SDS-polyacrylamide gels that were prepared according to a standard protocol (Table 9). Alternatively, precast gradient gels (4 - 20 % polyacrylamide) were used. Samples were loaded onto the gel together with a pre-stained molecular weight marker. Separation of proteins was performed by electrophoresis in a tank containing cold 1x running buffer at constant voltage of 120 V.

**Table 9: Components and volume for the preparation of two 15 % polyacrylamide gels for SDS-PAGE.**

| Reagent                                   | Volume             |                       |
|---|--------------------|-----------------------|
|   | Stacking gel (4 %) | Separation gel (15 %) |
| ddH <sub>2</sub> O                        | 2.5 mL             | 4.5 mL                |
| Stacking gel buffer (pH 6.8)              | 1 mL               | -                     |
| Separating gel buffer (pH 8.8)            | -                  | 9 mL                  |
| Acrylamide/bis-acrylamide solution (30 %) | 0.5 mL             | 9 mL                  |
| TEMED                                     | 5 $\mu$ L          | 40 $\mu$ L            |
| APS (10 %)                                | 20 $\mu$ L         | 180 $\mu$ L           |

##### 3.2.8.1.2 Western blotting and protein detection

SDS-PAGE-separated proteins were transferred from the polyacrylamide gel onto a methanol-activated polyvinylidene difluoride (PVDF)-membrane by semi-dry blotting (Burnette, 1981). Transfer was performed in presence of western blotting-buffer for 1 h at constant 1.5 mA per cm<sup>2</sup> of gel. Immobilized proteins were detected by incubation with specific antibodies (3.1.9). Prior to incubation, the membrane was blocked in

TBST + 5% milk for 1 h at RT to saturate possible unspecific binding sites for the used antibodies. Subsequently, the membrane was rinsed with TBST to remove residual milk and the membrane was incubated with the primary antibody over night at 4°C with gentle agitation. The membrane was washed 3x 10 min with TBST and a secondary HRP-conjugated antibody was added in TBST + 5 % milk for 1-2 h at RT. The membrane was again washed 3x 10 min and proteins were detected by chemiluminescence. For this, the membrane was incubated with either ECL- or Luminata Forte-substrate for 2 min and the signal was detected by exposition to x-ray film and subsequent development or with a digital gel-documentation device. Densitometry analysis of western blot signals was performed with the software LabImage 1D or ImageJ/Fiji. Signals of the protein of interest were normalized to  $\beta$ -actin which served as loading control.

#### 3.2.8.2 Enzyme-linked immunosorbent assay (ELISA)

The concentrations of cytokines in cell supernatants of infected cells were determined by ELISA according to the manufacturer's instructions. Prior to analysis, supernatants were diluted 1:10. The optical density at a wavelength of 450 nm was recorded in duplicates in an absorbance microplate reader.

Alternatively, a LEGENDplex bead-based immunoassay kit was used to quantify cytokine concentrations. The principle is based on the ELISA but utilizes beads with different sizes and different internal fluorescence intensities. These beads are conjugated to cytokine-specific antibodies which allows for detection and quantification of multiple cytokines at a time. Read-out was performed in duplicate by flow cytometry according to the manufacturer's instructions. Data was analyzed with the LEGENDplex data analysis software.

#### 3.2.8.3 Bicinchoninic acid assay

The protein concentration of western blot samples and eluate fractions of the phagosome-isolation were determined in duplicates with a bicinchoninic acid (BCA) assay kit according to the manufacturer's instructions. BCA-reagent was prepared by mixing 6 mL of solution A with 120  $\mu$ L of solution B. Bovine serum albumin (BSA) was serially diluted 1:2 (2 mg/mL - 31,25  $\mu$ g/mL) and 10  $\mu$ L of each dilution or sample were transferred to a 96-well

flat bottom plate. Per well, 200  $\mu$ L BCA-reagent were added and incubated at 37°C for 30 min in the dark. The optical density at a wavelength of 562 nm was recorded in an absorbance microplate reader.

### 3.2.9 Labeling and staining of hMDMs or *Leishmania major* promastigotes

#### 3.2.9.1 AnnexinA5-staining of *Leishmania major* promastigotes

To assess purity of the viable and apoptotic fractions after AnxA5-MACS, parasites were labeled with FITC-conjugated AnxA5. A volume according to  $1 \times 10^6$  stat. ph., purified viable and apoptotic *Lm* were transferred in a 96-well V-plate in duplicates and centrifuged (300x *g*, 4 min, 4°C). Cells were washed with 100  $\mu$ L Ringer's solution and incubated with AnxA5-FITC diluted in Ringer's solution at 4°C for 20 min. Cells were again washed once with Ringer's solution and transferred to microtubes for flow cytometry analysis. Samples washed and incubated with PBS that contained no  $\text{Ca}^{2+}$  ions served as negative controls.

#### 3.2.9.2 Staining of *Leishmania major* promastigotes for live cell microscopy

AnxA5-MACS purified viable and apoptotic parasites were labeled with the PKH26 Red Fluorescent Cell Linker Kit. In brief, 1  $\mu$ L of fluorescent dye was diluted in 600  $\mu$ L of Diluent C. Parasites were resuspended in this dilution and incubated for 10 min at 27°C. Cells were washed once with 1 mL CM (2400x *g*, 8 min, RT) and resuspended in the desired volume of CM and used for infection of eGFP-LC3 transduced hMDMs.

#### 3.2.9.3 Staining of infected hMDM for immunofluorescence microscopy

For the determination of infection rates by microscopy, infected and PFA fixed macrophages were permeabilized with 100  $\mu$ L IF permeabilization buffer per well that contained 0.5 % Triton X-100 or 0.5 % Saponin for 10 min at 4°C. This step serves the disruption of cellular membranes and enable penetration of antibodies directed against intracellular targets. Following two washing steps with IF washing buffer, cells were blocked with 100  $\mu$ L IF blocking buffer containing 10 % FCS and 10 % human AB serum for 15 min at 4°C to avoid unspecific binding of the used antibodies. For some experiments, macrophages were directly blocked without previous permeabilization. Cells were

incubated with primary antibodies directed against the respective target (see 3.1.9) diluted in 100  $\mu$ L IF staining buffer for 30 min at 4°C and washed once with IF staining buffer. For fluorescent labeling of primary antibodies, incubation with fluorophore-coupled secondary antibodies in 100  $\mu$ L IF staining buffer was performed for 30 min at 4°C and followed by three washes with IF washing buffer. hMDMs were counterstained with DAPI together with the secondary antibodies to visualize the nucleus. Buffers were aspirated and the samples were mounted with Mowiol, supplemented with DABCO to retain fluorescence, and a glass coverslip. Analysis was performed by fluorescence microscopy.

#### 3.2.9.4 Diff-Quick staining

Diff-Quick staining is usually used to stain histological samples. It can also be of use to stain myeloid cells and eukaryotic pathogens. The kit consists of three different solutions. Air-dried cytopsin-slides were incubated for 2 min in fixation solution containing methanol. Subsequently, fixed cells were incubated in Staining Solution 1 for 2 min. This eosinophilic dye stains proteins in the cytoplasm. Cells were further incubated for 2 min in Staining Solution 2, a basophilic dye to stain nucleic acids of the nucleus and the parasites kinetoplast. The slides were rinsed in tap water and air-dried for microscopical analysis using an AxioPhot microscope.

#### 3.2.9.5 Magnetic labeling of apoptotic *Leishmania major*

For magnetic isolation of apoptotic *Lm*-containing phagosomes,  $200 \times 10^6$  purified apoptotic *Lm* were labeled with magnetic Bionized NanoFerrite (BNF)-dextran beads, 150 nm in size, that are conjugated with lipobiotin (LB) on their surface (hereafter: LB-beads). LB integrates into cellular membranes and hence can be used to label cells. To assess an optimal concentration of beads to label apoptotic *Lm*, parasites were diluted in 2 mL RPMI 1640 without supplements and LB-beads were added. Cells were incubated at 4°C over night. Labeled apoptotic parasites were centrifuged (3800x *g*, 6 min, 4°C) and resuspended in 200  $\mu$ L CM that were added to 10 mL CM for infection of hMDMs (3.2.5).

Labeling efficiency was assessed by staining of magnetically labeled apoptotic *Lm* with streptavidin-Cy5, which has a high affinity to biotin. Hence, this molecule binds LB residues that were not integrated into the cell membrane and its fluorescence intensity correlates

with membrane-bound LB-beads. Apoptotic *Lm* ( $2 \times 10^6$ ) that were incubated with different concentrations of magnetic LB-conjugated microbeads were labeled for 30 min at 4°C in the dark in presence of streptavidin-Cy5 diluted 1:200 in RPMI 1640. Cells were washed once with 1 mL RPMI 1640 and resuspended in 100  $\mu$ L PBS. Labeling efficiency was determined by flow cytometry.

#### 3.2.9.6 Detection of surface proteins by antibody staining

$1 \times 10^5$  cells were transferred into each well of a 96-well V-plate and washed with 100  $\mu$ L FACS buffer (300x *g*, 4°C, 4 min). To avoid unspecific antibody binding, cells were incubated with 100  $\mu$ L FACS blocking buffer at 4°C for 10 min. Cells were washed once more and incubated with the respective fluorophore-conjugated antibodies for 30 min at 4°C in the dark. After washing as described above, cells were resuspended in 100  $\mu$ L FACS buffer or 1 % PBS and transferred to microtubes for flow cytometry analysis. As controls, untreated cells and cells that were incubated with a fluorophore-conjugated isotype antibody were used.

#### 3.2.9.7 Labeling of *Leishmania major* promastigotes with CFSE or AF647-SE for infection experiments

For determination of *L. major* infection rates in hMDMs and hMDDCs, AnxA5-MACSpurified parasites were labeled with fluorescent dyes for later flow cytometry analysis. The desired number of parasites was transferred to a 15 mL reaction tube and centrifuged (2400x *g*, 8 min, 4°C). Apoptotic *Lm* were resuspended in 6 mL PBS containing 0.5  $\mu$ g of Alexa Fluor 647-conjugated succinimidylester (AF647-SE). Viable *Lm* were resuspended in a 4  $\mu$ M carboxyfluorescein-conjugated succinimidylester (CFSE)-PBS solution. For efficient and rapid labeling, cells were incubated for 10 min at 27°C. After incubation, labeled parasites were washed once with 6 mL PBS and were resuspended in the desired volume of CM. If an artificial stationary phase was needed, labeled parasites were mixed in a 1:1 ratio.



### 3.2.9.8 Labeling of PBLs and hMDMs for T cell proliferation assay

For the T cell proliferation assay, thawed PBLs were labeled with CFSE which is transferred to daughter cells during proliferation and hence can be used to identify proliferating cells by a decrease in staining intensity. For labeling,  $12 \times 10^6$  PBLs were transferred in 1 mL CM containing 4  $\mu$ M CFSE. The cells were incubated for 15 min at 37°C. To remove excessive CFSE, 7 mL CM were added and the tube was centrifuged (143x *g*, 8 min, 20°C). The pellet was resuspended in 12 mL CM resulting in a concentration of  $1 \times 10^6$  PBLs/mL. The hMDMs were labeled analogue to that.

### 3.2.9.9 DAPI staining of infected hMDMs

Prior to cyto centrifugation,  $0.1 \times 10^5$  infected hMDMs were incubated with 25 ng/mL of DAPI in PBS for 30 min on ice.

### 3.2.10 Flow cytometry

Determination of the presence of cellular surface proteins (3.2.9.6) as well as infection rates (3.2.4.2, 3.2.4.4) was performed by flow cytometry. Cells were treated as described in the given experiment and resuspended in either PBS, CM, FACS buffer or fixed in 1 % PFA for later analysis. By flow cytometry, cells can be distinguished by their size (forward scatter, FSC) or granularity (side scatter, SSC) by their ability to refract light of a certain wavelength. This is used to determine a specific cell population. Moreover, staining of cells with a specific fluorophore-conjugated antibody or a fluorescent dye also allows for identification of a specific cell-population. In this study, hMDMs and hMDDCs or *Leishmania major* promastigotes were gated by their FSC/SSC properties. For hMDMs/hMDDCs and PBLs a minimum of 10000 cells (counts) and for *Leishmania* promastigotes, at least 20000 cells were recorded.

### 3.2.11 Microscopy

#### 3.2.11.1 Transmitted light microscopy

Light microscopy was used in cell culture for analysis of cell growth (Zeiss AxioVert.A1) or counting of *L. major* promastigotes (Zeiss Primo Star). For analysis of Diff-Quick-stained

cytospins, a Zeiss AxioPhot-microscope equipped with a high-quality color camera (AxioCam IC) and AxioVision 4.8 software was used.

#### 3.2.11.2 Fluorescence microscopy

Cytospins containing hMDMs infected with fluorescent parasites were imaged with a Zeiss Apotome fluorescence microscope equipped with an AxioCam MRM. Appropriate filter sets to detect CFSE and Alexa Fluor 647 were used. Data was acquired with AxioVision 4.8 software.

Samples that were prepared for immunofluorescence microscopy were analyzed on a Zeiss LSM 7 *Live* confocal microscope with a Plan-Apochromat 63x/1.40 Oil DICIII objective. The LSM 7 *Live* is equipped with a slit instead of a pinhole to eliminate light that is not coming from the focal plane. This scanner allows for the illumination of the sample in a line, not in a single point, and therefore enables a rapid scan of the specimen. The spatial resolution is lower as for point-scanning confocal microscopes but image acquisition speeds are superior. This is of importance, especially in live cell imaging experiments (3.2.11.3). The respective fluorophores used were excited with light-emitting diode (LED)-Lasers of the following specific wavelengths: 405 nm (DAPI/Hoechst), 488 nm (AF488, eGFP, CFSE), 561 nm (AF568, PKH24), 635 nm (AF647). Emitted light was collected with a high sensitivity detector by setting the specific filter sets for the respective fluorophores. Data was analyzed with ZEN 2012 Black/Blue or ImageJ software.

#### 3.2.11.3 Time lapse imaging of *Leishmania major* infection in hMDMs

To visualize infection dynamics, live cell imaging was performed with a Zeiss LSM 7 *Live* confocal microscope equipped with a Zeiss Plan-Apochromat 63x/1.40 Oil DICIII objective with immersion oil. Image acquisition was controlled with ZEN 2012 Black software. Appropriate lasers (488 nm, 561 nm) and filter sets for eGFP and PKH26 were used. Laser power was set to 0.2 - 1.5 % to reduce phototoxicity. Data were acquired by Z-stacks (number of planes depended on the cells and conditions) over a minimum of 15 h with 5 min intervals. The incubation-chamber was kept at 37°C and cells were gassed with 5 % CO<sub>2</sub>. Data was analyzed and processed in ZEN 2012 Black or ZEN 2012 Blue software. Characteristics of infection were manually quantified in ZEN 2012 Black.

### 3.2.12 Statistical analysis

All data are presented as mean  $\pm$  standard deviation (SD). The results were analyzed by Prism software. Gaussian distribution was tested by d'Agostino normality test. For non-normal distributed data, the paired Wilcoxon matched-pairs signed-rank test was used when all experimental conditions were covered by each group compared. The unpaired Mann-Whitney U-test was used when the groups compared did not cover all experimental conditions. For normal-distributed data, the paired or unpaired t-test was used (two-tailed distribution). The respective test used is indicated in the figure legends. Values of  $p < 0.05$  (\*),  $p < 0.01$  (\*\*),  $p < 0.001$  (\*\*\*) and  $p < 0.0001$  (\*\*\*\*) were considered significant.

## 4. Results

4.1 *In vitro* cultures of *Leishmania major* promastigotes contain apoptotic parasites

For axenic *in vitro* cultivation of *Leishmania major* promastigotes (*Lm*), a blood agar system is used (Nicolle, 1908). Similar to their growth *in vivo* in the sand fly vector, parasites show two different growth phases during *in vitro* cultivation (Figure 7A). The first 4-5 days of cultivation, *Lm* grow exponentially. Therefore, this growth phase comprising almost exclusively elongated, flagellated and hence motile viable *Lm* is termed logarithmic phase (log. ph.) (Figure 7B, upper panel). From day 4 on, *Lm* growth enters a plateau phase in which proportions of viable parasites eventually undergo apoptosis leading to a round-shaped morphology of the parasites. These apoptotic *Lm* are aflagellated, non-motile and the apoptosis marker phosphatidylserine (PS) is exposed on their surface. This phase, termed stationary phase (stat. ph.) comprises an approximate 1:1 ratio of viable and apoptotic *Lm* (Figure 7B, lower panel).

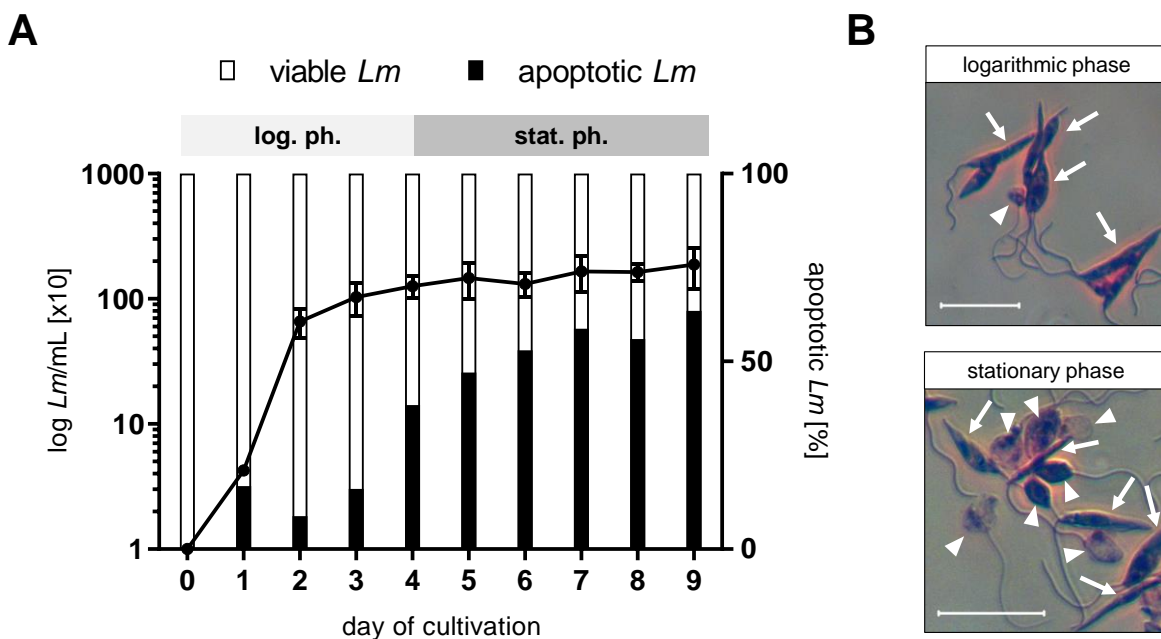


**Figure 7: Growth curve of *Leishmania major* promastigotes.** **A** Parasites were seeded in 96-well NNN-blood-agar plates and cultivated for 9 days. Total cell numbers per mL (line) and the proportion of viable and apoptotic parasites (bars) were determined by manual counting in a hemocytometer. Data are presented as mean  $\pm$  SD for 3-5 independent experiments. **B** Micrographs show cytopins of log. ph. or stat. ph. *Lm* stained by Diff-Quick. Viable *Lm* are marked with an arrow, apoptotic *Lm* are marked with an arrow head (scale bars: 5  $\mu$ m).

4.2 Purification of apoptotic and viable *Leishmania major* by AnnexinA5-MACS

To investigate the advantageous role of apoptotic *Lm* in establishment of infection, viable and apoptotic *Lm* were separated from a stationary phase *in vitro* culture by AnnexinA5 (AnxA5)-MACS. This method utilizes the ability of AnxA5 to bind to PS on the surface of apoptotic cells in a calcium-dependent manner (Figure 8A).

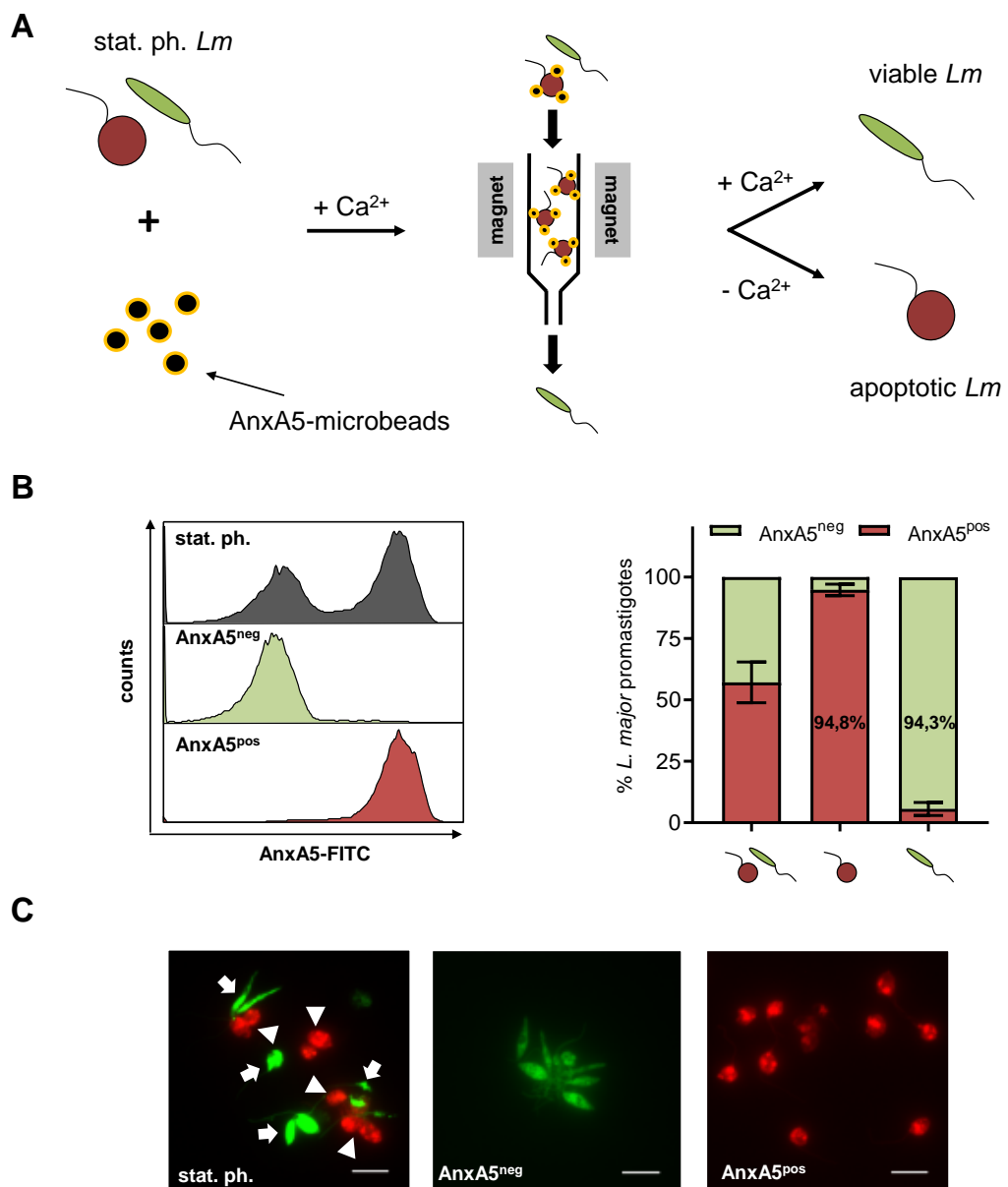


**Figure 8: AnnexinA5-MACS separation yields pure apoptotic and viable *L. major* promastigotes.** **A** Schematic presentation of AnxA5-MACS of a stat. ph. *L. major* parasite culture. Parasites were incubated with AnxA5-conjugated microbeads in presence of calcium ions. The suspension was applied onto a magnetic LS-MACS-column in which labeled apoptotic *Lm* are retained. Viable, non-AnxA5 binding *Lm* were washed out and apoptotic AnxA5-bead decorated *Lm* were eluted in absence of calcium ions. To further enrich viable parasites, the procedure was repeated using a LD-MACS-column. **B** Purity of the fractions was assessed by labeling of the eluted parasite fractions with AnxA5-FITC and flow cytometry analysis. Exemplary data from 6-7 independent experiments are presented as mean  $\pm$  SD. **C** Representative micrographs of the fractions that were labeled with CFSE (AnxA5<sup>neg</sup>) or AF647-SE (AnxA5<sup>pos</sup>) are shown (arrows: viable *Lm*, arrow heads: apoptotic *Lm*, scale bar: 10  $\mu\text{m}$ ).

For this, a 6-8-day old *Lm* culture was incubated with AnxA5-conjugated microbeads. Separation of the viable and apoptotic *Lm* by AnxA5-MACS in a magnetic field resulted in a fraction containing non-AnxA5-binding, elongated, viable *Lm* (Figure 8B, green) and a population of AnxA5-binding, round, apoptotic *Lm* (Figure 8B, red). Subsequent AnxA5-FITC staining and flow cytometry analysis showed a purity of the viable *Lm* fraction of  $94.3 \pm 2.6\%$  whereas purity of the apoptotic fraction was  $94.8 \pm 2.3\%$  (Figure 8C). This method was used throughout the study to separate apoptotic from viable *Lm* for subsequent differential infection and investigations on the effects of apoptotic promastigotes on myeloid cell infection.

#### 4.3 Comparison of infection rates upon differential infection of human monocyte-derived macrophages by flow cytometry and microscopy

To investigate whether there are differences in the velocity of uptake between viable and apoptotic *Lm* by hMDM1 and hMDM2, macrophages were co-incubated with purified viable or apoptotic *Lm*. For quantification, we assessed infection rates by flow cytometry and fluorescence microscopy and tested the suitability of both methods for further studies (Figure 9).

Quantification by flow cytometry revealed a significantly more rapid interaction of hMDM1 with apoptotic *Lm* as compared to the interaction with viable *Lm* after 30 min of co-incubation (Figure 9A). Interaction of macrophages with apoptotic and viable *Lm* did not further increase after 90 min of co-incubation. At this timepoint  $46.7 \pm 32.3\%$  and  $63.0 \pm 12.2\%$  of hMDM1 were detected to be positive for viable or apoptotic *Lm*, respectively. As expected, interaction of hMDM2 with *Lm* was in general higher than in the pro-inflammatory phenotype which can be attributed to their higher phagocytic capacity (Rószler, 2015). Initially, apoptotic parasites interacted more rapidly with hMDM2 as viable *Lm* whereas after 180 min of co-incubation, a higher interaction of viable *Lm* ( $89.7 \pm 8\%$ ) was found as compared to apoptotic *Lm* ( $78.3 \pm 12\%$ ). Microscopic determination showed lower internalization of viable *Lm* by hMDM1 ( $16.1 \pm 5.5\%$ ) and apoptotic *Lm* ( $9.2 \pm 3.6\%$ ) after 30 min as compared to flow cytometry (viable *Lm*:  $22.6 \pm 27.5\%$ , apoptotic *Lm*:  $47.7 \pm 16.9\%$ ) and revealed a more rapid internalization of viable *Lm* over time (Figure 9B). The latter was also observed in hMDM2. After 180 min of co-incubation, rates of

internalization were almost equal for viable and apoptotic parasites ( $83.3 \pm 5.6\%$  vs.  $76.7 \pm 3.3\%$ ). When infection rates were compared between the two different methods of quantification, it was clear that even though there were differences in the velocity of interaction of hMDMs with viable and apoptotic *Lm*, infection rates after 180 min were almost equal in hMDM2 whereas higher infection rates for apoptotic *Lm* were found by flow cytometry in hMDM1.

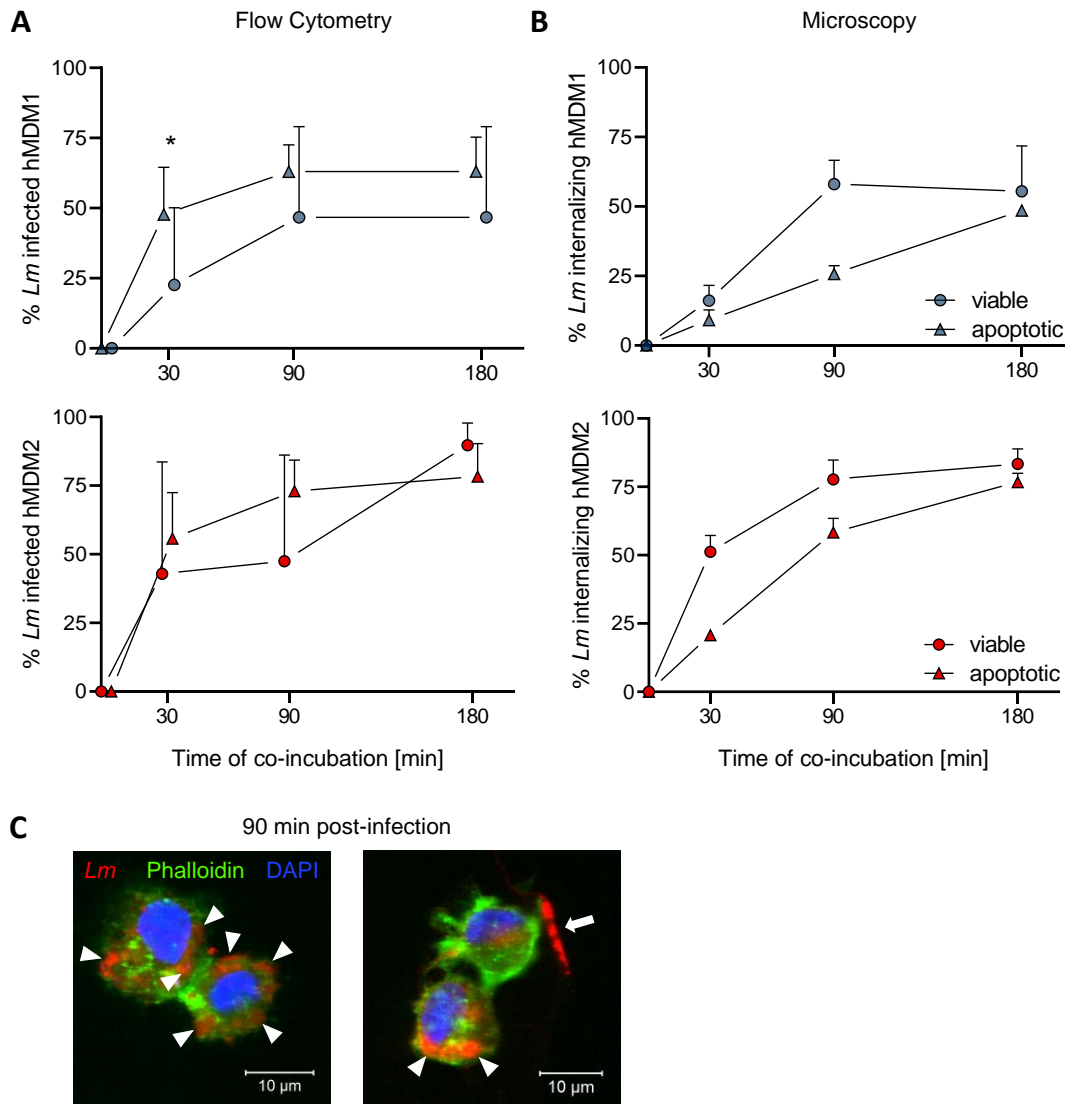


**Figure 9: Investigation of interaction upon differential infection of hMDM with viable and apoptotic *Lm* and quantification by flow cytometry or microscopy.** Pro- and anti-inflammatory macrophages were seeded in reaction tubes or chamber slides and infected with purified viable or apoptotic *Lm*. **A** Purified viable and apoptotic *Lm* were stained by CFSE or AF637-SE and co-incubated with hMDM1 (blue) or hMDM2 (red) for the indicated times. Infection rates were determined by flow cytometry. hMDMs were gated by their FCS/SSC-properties ( $n=4-12$  donors). **B** hMDMs were co-incubated with purified viable or apoptotic *Lm* and fixed with 4 % PFA at the indicated timepoints. Actin was stained with phalloidin-AF488 and *Lm* were stained with a specific antiserum. Infection rates were determined by manual counting of 100 hMDMs ( $n=2$ ). **C** Exemplary micrographs show hMDMs that fully internalized *Lm* (left, arrow heads) or hMDMs that were not fully internalizing *Lm* (right, arrow) at 90 min post infection. Data are represented as mean  $\pm$  SD of a minimum of 2 donors from at least 2 two independent experiments and were analyzed by Mann-Whitney U-test (\*  $p < 0.05$ ). Data were generated with help of Mr. Naphang Ho.

Of note, microscopic analysis indicated that *Lm* promastigotes can stick to the surface of macrophages (Figure 9C). This could bias the determination of infection rates by flow cytometry since also incompletely internalized parasites are detected by this method. Nonetheless, flow cytometry offers a more rapid experimental processing. Moreover, in our lab's standard experimental setup, we infect hMDMs for 3 h. Here it was shown that at this time point differences between flow cytometry and microscopy were not striking. Hence, we used flow cytometry analysis in most of the following experiments and defined the interaction of myeloid cells with viable and apoptotic *Lm* as "infection" whereas we described quantification of infection rates by microscopy as "internalization".

#### 4.4 Generation of eGFP-LC3-expressing hMDMs by lentiviral transduction and live cell imaging of *Leishmania major* infection

We and others (Matte et al., 2016) showed that during *Leishmania major* infection, apoptotic and viable *Lm* are located within unilamellar phagosomes that are positive for the autophagy marker protein microtubule-associated protein 1A/1B light chain 3B (hereafter: LC3). Ulk1, an autophagic protein that is crucial for canonical autophagy, was dispensable for LC3 recruitment towards apoptotic *Lm*-containing phagosomes (PhD thesis M. Thomas, 2015). These studies suggested the non-canonical autophagic process of LC3-associated phagocytosis (LAP) to play a role in apoptotic parasite uptake and processing (Crauwels et al., 2015). Importantly, we and others observed that portions of phagocytosed viable *Lm* that were targeted by LAP escape degradation (Matte et al., 2016; PhD thesis M. Thomas, 2015). Hence, we were interested in the fate of LC3-positive, *Lm*-containing phagosomes within the macrophage host cell. To dynamically follow the formation of LC3-decorated phagosomes and to analyze the effect of LC3 recruitment to the *Lm*-containing compartments, we employed macrophages expressing green fluorescent LC3. To this end, macrophages were transduced with lentiviral vectors coding for LC3 which is N-terminally fused to the enhanced Green Fluorescent Protein (eGFP-LC3).

Vectors were produced in a human kidney cell line and particle titers were evaluated by titration in HT1080 cells and flow cytometry analysis (data not shown). With the determined percentage of eGFP-positive cells, titers were calculated as described in the methods section. The calculation gave high titers of  $1.72 \times 10^8$  i.u. (infectious units) of the



produced lentiviral vectors. Successful transduction was confirmed by fluorescence microscopy of transduced, and hence, eGFP-LC3 expressing HT1080 cells (Figure 10A). Since we wanted to investigate LC3 recruitment in the context of LAP, we tested whether transduction with lentiviral particles alone already induced conversion of cytosolic LC3 (LC3-I) to the membrane-bound, lipidated form (LC3-II) in hMDMs. To do so, hMDM1 and hMDM2 were transduced, harvested and prepared for SDS-PAGE at 4 h and 24 h post-transduction (hpt). Lysates were analyzed for endogenous LC3-II by western blot (Figure 10B). We detected induction of LC3 conversion 4 h post-transfection in both hMDM subtypes. This LC3 conversion was comparable to the samples where control cells were stimulated with the canonical autophagy inducer PI-103. After 24 h, the LC3 conversion was decreased in hMDM1. We assumed the detected LC3 lipidation shortly after transduction to be connected to transduction-induced cell stress. In hMDM2, LC3 conversion was as low as in non-transduced cells. In our setting, transduced hMDMs were used 4 days post-transduction.

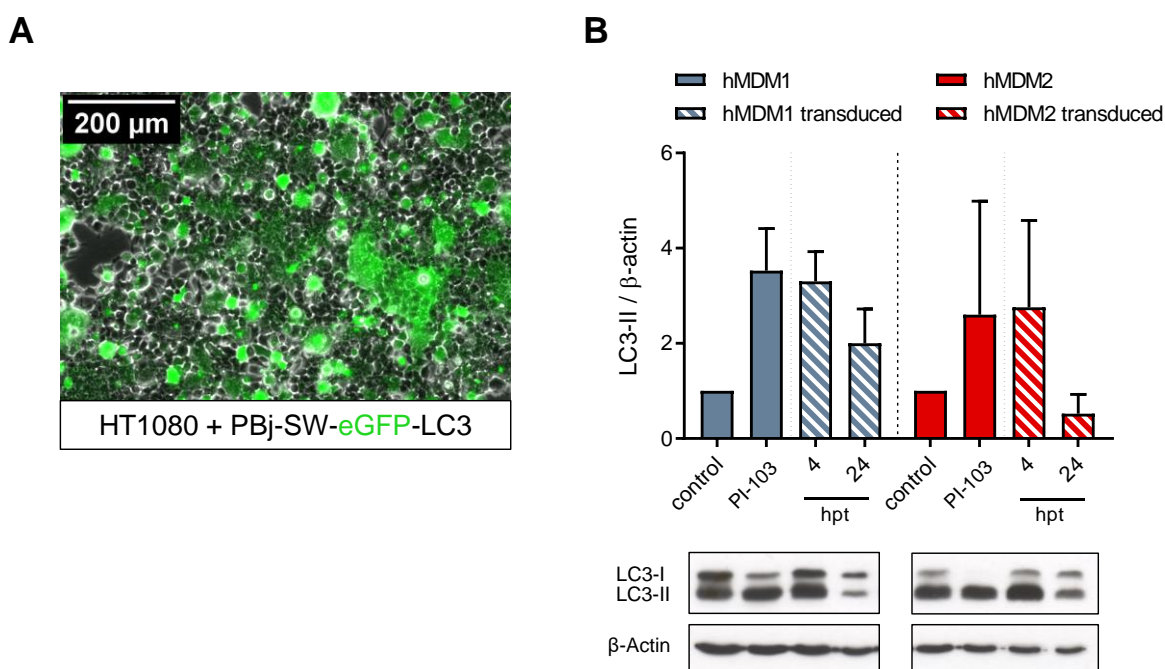


**Figure 10: Transduction with eGFP-LC3 lentiviral particles transiently induces conversion of endogenous LC3 in hMDMs.** PBJ-SW-eGFP-LC3 vector particles were produced with a four-plasmid system in HEK 293T/17 cells as described in the methods section. **A** Lentiviral vector-transduction was tested in HT1080 cells and verified by fluorescence microscopy. **B** To assess a possible induction of endogenous LC3 conversion by transduction, hMDM1 and hMDM2 were transduced with PBJ-SW-eGFP-LC3 lentiviral vectors for 4 or 24 h (hpt: hours post-transduction). The canonical autophagy inducer PI-103 served as positive control for conversion of endogenous LC3. Lysates were analyzed by SDS-PAGE and immunoblotting for LC3 and  $\beta$ -actin. LC3-II to  $\beta$ -actin levels were determined by densitometry and ratios were normalized to untreated control cells. Western blots are representative for one experiment. Data represent the mean  $\pm$  SD of three donors from two independent experiments.

To investigate LAP induction in real-time, hMDM1 and hMDM2 were transduced with the lentiviral vectors and co-incubated with either purified and labeled apoptotic or viable *Lm* to follow their intracellular fate (Figure 11A). As expected, time-lapse imaging of eGFP-LC3-expressing hMDMs showed the accumulation of eGFP-LC3 around proportions of viable as well as apoptotic *Lm*, indicating internalization of these parasites by LAP. The elongated morphology of viable parasites was not altered after being sequestered in a LC3<sup>+</sup> phagosome (Figure 11A). In line with literature, this indicated that, at least partially, viable *Lm* were not degraded within macrophages (Matte et al., 2016). In contrast, parts of apoptotic *Lm* seemed to be processed within LC3<sup>+</sup> phagosomes since red-labeled parasites disintegrated into smaller particles at a given time after the eGFP signal disappeared around the apoptotic parasite (Figure 11B).

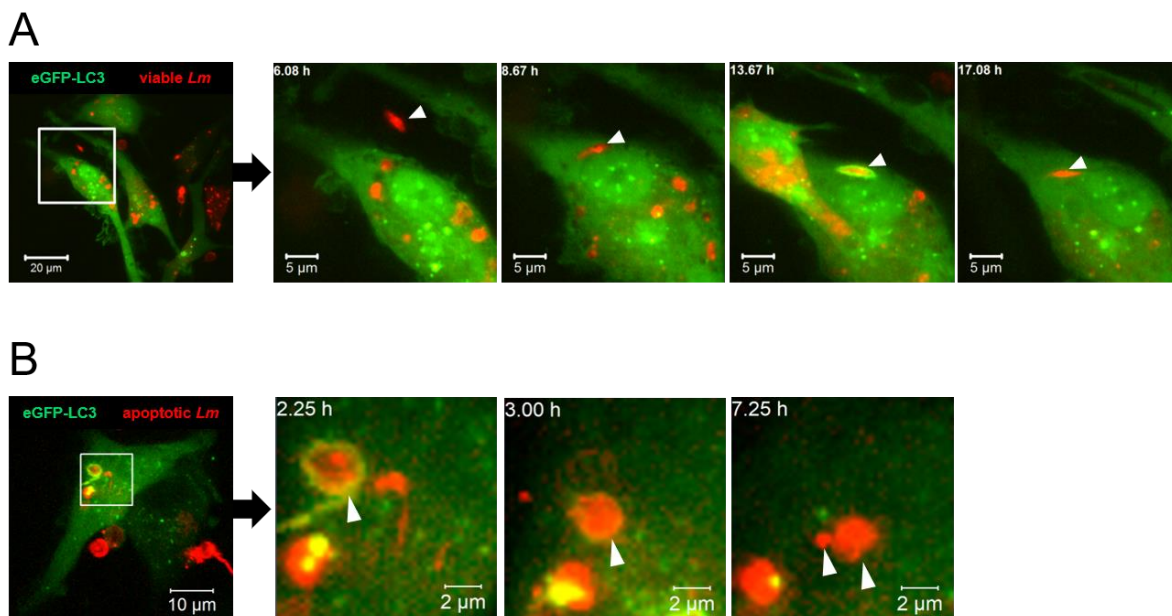


**Figure 11: Purified viable and apoptotic *Lm* are sequestered in LC3<sup>+</sup> phagosomes in hMDMs.** Purified viable *Lm* or apoptotic *Lm* were labeled with PKH26 and co-incubated with eGFP-LC3-transduced hMDM1 or hMDM2 (MOI 1). 3D time-lapse imaging was performed for at least 15 h (1 frame/5 min) on a ZEISS LSM 7 Live confocal microscope. **A** Viable *Lm* in a LC3-positive phagosome with an unaltered morphology after LC3 is absent. **B** Apoptotic *Lm* in a LC3 positive phagosome is degraded over time. Scale bars: as indicated in the images. Videos were acquired with help of Mrs. Sylvia Panitz.

It was shown in murine macrophages, that only a small part of internalized viable *Lm* are sequestered within LC3<sup>+</sup> phagosomes (Matte et al., 2016). It is not known if the same is true in the human system. Hence, we were interested in quantification of LC3<sup>+</sup> phagosomes upon differential *Lm* infection and the temporal characteristics of LC3 recruitment by analysis of time-lapse videos (Figure 12). To do so, transduced cells of at least 3 donors were infected with purified viable or apoptotic *Lm*. A minimum of 40 cells from each donor

were imaged by time-lapse confocal microscopy. The generated video data was quantified for eGFP-LC3 recruitment towards emerging phagosomes and the temporal aspects of eGFP-LC3 presence and its impact on degradation of *Lm* (Figure 12). In hMDM1 we found  $4.7 \pm 5.6$  % of viable and  $6.7 \pm 10$  % of apoptotic *Lm* to be sequestered in LC3<sup>+</sup> phagosomes (Figure 12A). Of note, in M1 macrophages from two of the four donors tested, no LC3 recruitment towards the phagosome was detected. As expected, in hMDM2 that have a higher phagocytic capacity (Biswas et al., 2012),  $12.6 \pm 8.5$  % of viable and  $22.8 \pm 21.8$  % of apoptotic *Lm* were sequestered in LC3<sup>+</sup> phagosomes. This was strongly dependent on the donor as indicated by the heterogenous distribution. We further determined the temporal aspects of LC3 recruitment and whether there are differences between phagosomes harboring viable or apoptotic *Lm* in pro- or anti-inflammatory macrophages. Therefore, we assessed the time from internalization of *Lm* to the detection of green fluorescent signal around the parasites (Figure 12B). Only two viable *Lm* and four apoptotic *Lm* were found within LC3<sup>+</sup> phagosomes in hMDM1 over the 15 h period of imaging. Nonetheless, these compartments were scored and an average of  $22 \pm 18$  min and  $138 \pm 222$  min passed before LC3 recruitment to phagosomes around viable *Lm* or apoptotic *Lm*, respectively, became visible. In hMDM2 that sequestered more viable and apoptotic parasites in LC3<sup>+</sup> phagosomes than hMDM1 (Figure 12A), an average of  $70 \pm 113$  min (viable *Lm*) and a significantly shorter time of  $34 \pm 75$  min (apoptotic *Lm*) passed until LC3 was present on the emerging phagosomes. Fusion of LC3<sup>-</sup> and LC3<sup>+</sup> phagosomes with lysosomes is a heavily orchestrated event. During LAP, fusion with lysosomes only occurs when LC3 is still present on the phagosomal membrane. Thus, loss of LC3 would implement lysosomal fusion (Martinez et al., 2015). We quantified the time span that LC3 was accumulated on the compartments which indicates a rapid or prolonged fusion with lysosomes (Figure 12C). In hMDM1 eGFP-LC3 could be detected for  $23 \pm 25$  min on phagosomes around viable *Lm* and for  $116 \pm 77$  min on phagosomes harboring apoptotic *Lm* (Figure 12C). In hMDM2, LC3 was present on viable *Lm*-containing phagosomes for  $71 \pm 75$  min. In comparison, transient presence of LC3 on phagosomes that harbored apoptotic *Lm* was  $57 \pm 76$  min. Higher numbers of LC3<sup>+</sup> phagosomes surrounding apoptotic *Lm* in hMDM2 as compared to viable *Lm* and a significantly faster LC3 recruitment but shorter presence of the marker protein indicated enhanced lysosomal fusion. This prompted us to also quantify the duration from internalization to the onset of degradation with respect to presence or absence of eGFP-LC3 on the compartment membrane in hMDM2 (Figure 12D). Degradation was defined as

disintegration of the apoptotic parasites into smaller particles. When LC3 was absent from phagosomes, degradation occurred after  $558 \pm 347$  min. By sequestration of apoptotic *Lm* in LC3<sup>+</sup> phagosomes, the time to degradation was reduced to  $435 \pm 246$  min. It has to be considered, that only few parasites could be tracked until degradation due to restrictions in the time frame of imaging.

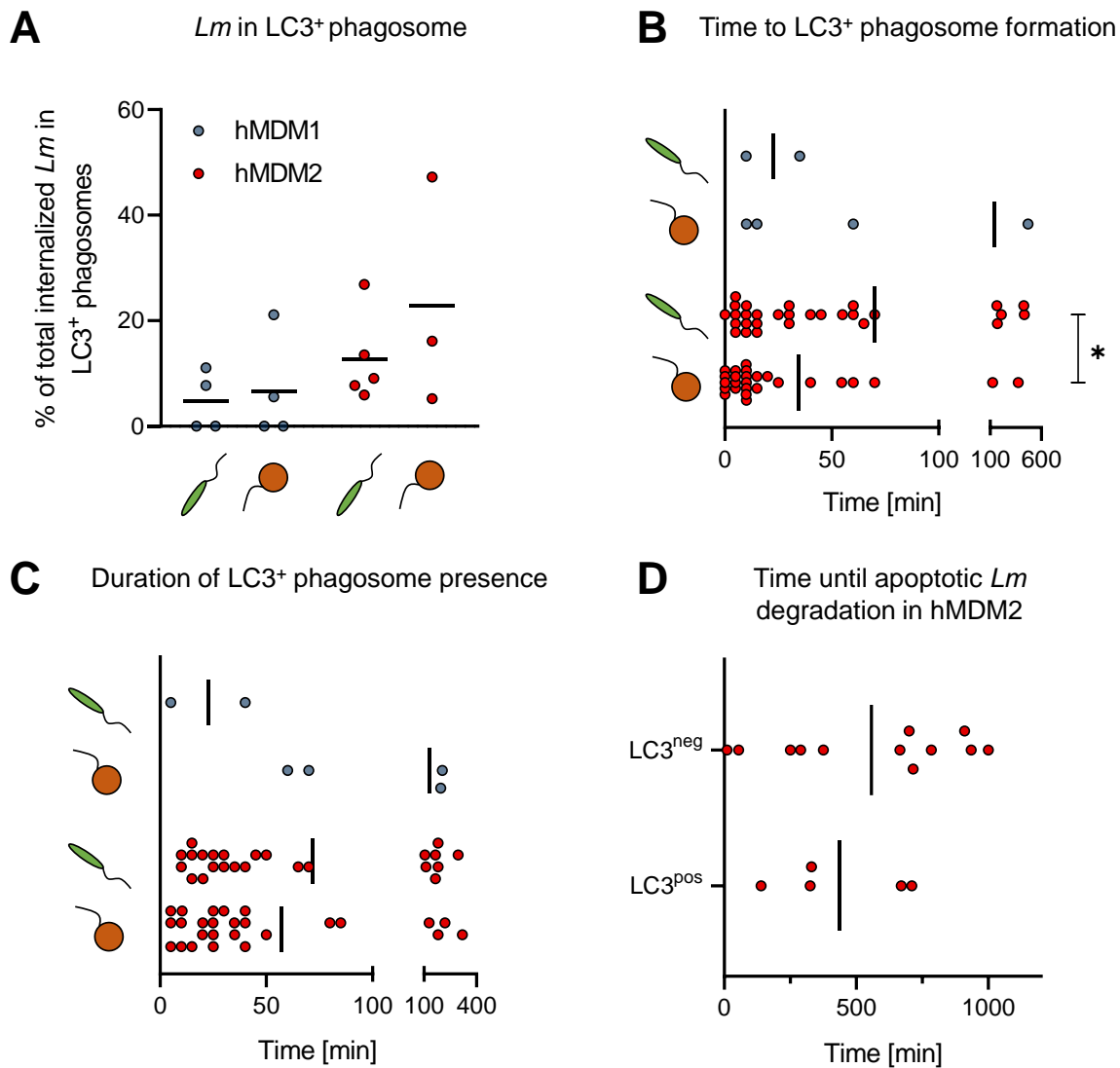


**Figure 12: Quantification of time-lapse imaging of eGFP-LC3-positive compartments within hMDMs.** Macrophages were co-incubated with PKH26- labeled viable or apoptotic *Lm* (MOI 1) for 15 h with 1 frame/5 min. The characteristics of infection were determined by analysis of time lapse videos. **A** Relative number of LC3<sup>+</sup> phagosomes in hMDM1 and hMDM2 from 3-5 donors. **B** Time from infection of hMDMs to LC3-recruitment to the phagosome. **C** Presence of LC3 on the emerging phagosomes. **D** Time from infection to degradation of apoptotic parasites in dependence of absence or presence of LC3 on the phagosomes in hMDM2. Data are presented as mean  $\pm$  SD of a minimum of 40 cells from at least three donors analyzed in 3-5 independent experiments. The means are indicated by vertical lines. Data was analyzed by unpaired Mann-Whitney U-test (\*  $p < 0.05$ ). Imaging and quantification were performed with the help of Mrs. Sylvia Panitz.

Taken together, we found few parasites to be sequestered within LC3<sup>+</sup> phagosomes in hMDM1. In hMDM2, more apoptotic *Lm* were present in LC3<sup>+</sup> phagosomes as compared to

viable *Lm* and the time to LC3 recruitment was significantly lower. Degradation was accelerated when LC3 was recruited towards these compartments. This indicated an enhanced internalization of apoptotic *Lm* by LAP in hMDM2 which results in quicker degradation of the dying parasites. Based on these findings, we wanted to further elucidate the role of LC3 recruitment, hence, LAP of apoptotic *Lm*, and the molecular factors that trigger this mechanism. In addition, we observed unaltered morphologies of viable *Lm* that were targeted by LC3 indicating resistance to LAP-mediated degradation.

#### 4.5 Evaluation of a possible evasion strategy by viable *Leishmania major* promastigotes

During time-lapse imaging of viable *Lm*, we observed an unaltered morphology of viable *Lm* in phagosomes that were targeted by LC3. This was already described by Matte et al. and suggests an evasion of LAP which supports the survival of viable parasites. In former studies we identified tunnel-like structures that protruded from the viable *Lm* harboring compartment, of which one was found to be connected to the extracellular space (PhD thesis M. Thomas, 2015, Figure 13). Before the present project started, only the electron microscopy data set (generated by G. Neusser, University Ulm) of this observation was available, the 3D reconstruction (performed by A. Weiner, Institut Pasteur, Paris) was finished shortly before the beginning of this project.

We hypothesized these tunnel-like structures to serve the delayed acidification of the compartment and possibly mediate dilution of lysosomal hydrolases from the phagosome into the extracellular space. Hence, it would serve the inhibition of proteolytic degradation of viable *Lm*. Based on this, we wanted to quantify possible tunnel-structures by immunofluorescence staining on viable *Lm*-infected hMDM2. To increase the chance to find tunnel-structures we infected with a MOI of 20. We stained for *Lm* and the lysosomal marker LAMP1 on PFA-fixed macrophages without permeabilization of the plasma membranes. This would allow the antibody to only stain the intracellular parasite and LAMP1 if it can enter the phagosome through a connection with the extracellular space. Further, we scored only parasites/phagosomes that were stained with both, the anti-*Lm* antiserum and anti-LAMP1 (Figure 14A).

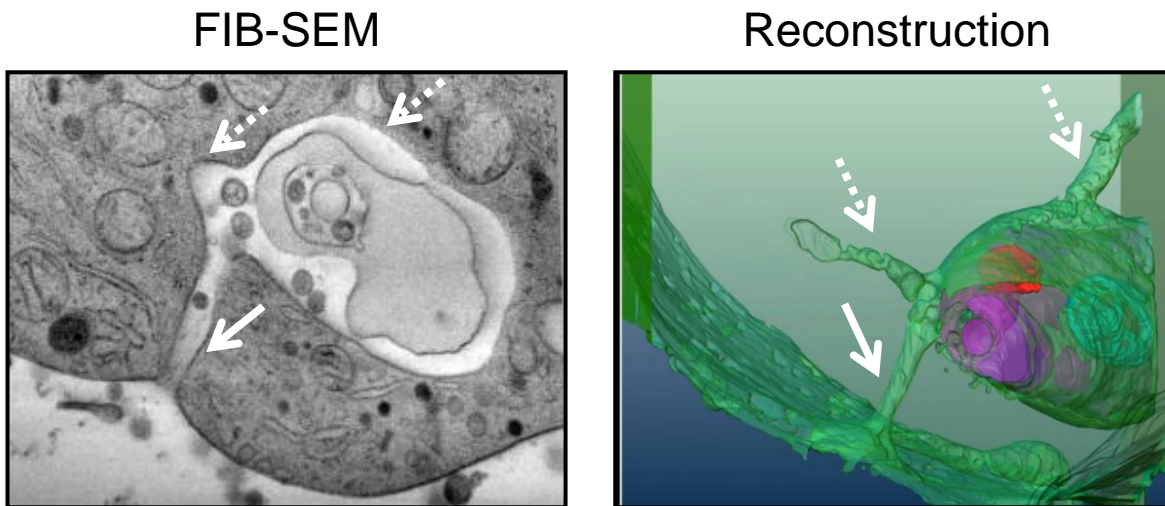
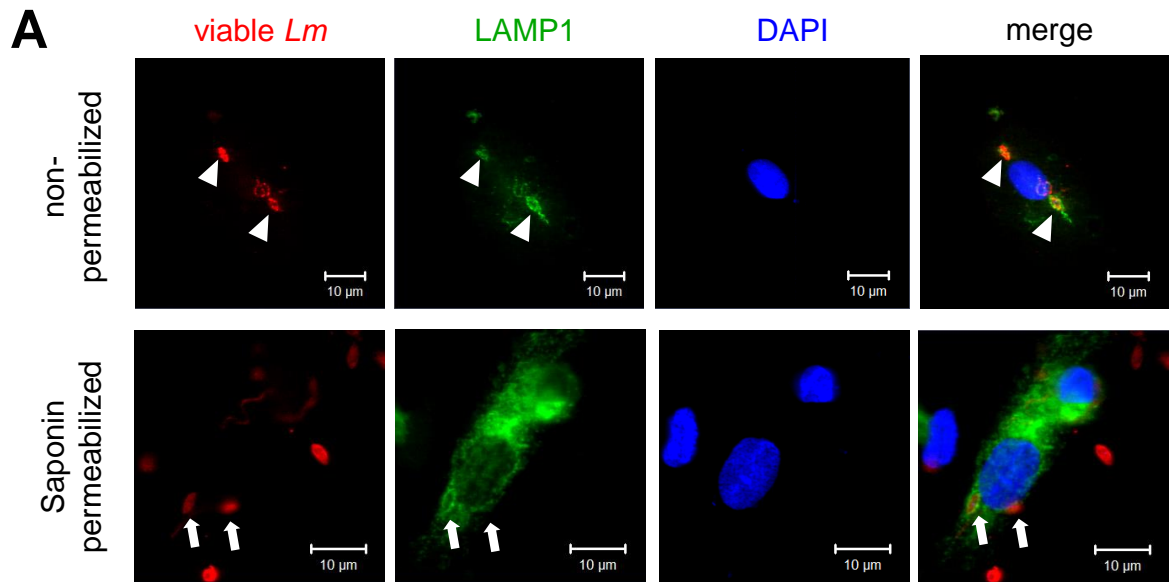


**Figure 13: 3D reconstruction of a viable *Lm* within a phagosome connected to the extracellular space.** *Left* Viable *Lm* infected hMDM2 were high pressure frozen and processed for focused ion beam scanning electron microscopy (FIB-SEM). Image shows one representative slice through the viable *Lm*-containing phagosome. Samples were generated by M. Thomas and FIB-SEM was performed in cooperation with G. Neusser at the Institute of Analytical and Bioanalytical Chemistry, University Ulm and P. Walther at the Core Facility for Electron Microscopy, University Ulm. *Right* 3D reconstruction of FIB-SEM data, performed by A. Weiner from the group of J. Enninga, Institut Pasteur, Paris. Purple, red and blue structures are part of the *Leishmania* parasite which is tightly enclosed by the green phagosomal membrane. Solid arrows in both images indicate tunnel-like structures that are connected to the outside of the cell. Dotted arrows indicate tunnel-structures protruding to the inside of the macrophage.

As controls served viable *Lm*-infected macrophages that were permeabilized with the detergent saponin before immunofluorescence staining. In hMDM2 from two donors we found  $26.9 \pm 10.8$  % compartments positive for both stains accumulating after 30 min of infection (Figure 14B). 60 min post infection, the proportion of double positive compartments was  $25.5 \pm 2.4$  %. At later time points from 1.5 h on ( $12.7 \pm 6.9$  %), a sharp decline in double positive stains was detected. After 3 h of infection, only  $4.6 \pm 2.5$  % double positive phagosomes were found. In addition to microscopical analyses of tunnel-like structures, we tried to verify possible tunnel-like structures by detection of released intraphagosomal proteins in the supernatants of viable *Lm* infected hMDMs by western blot. We hypothesized that e.g. the lysosomal protease cathepsin B were introduced into the viable *Lm*-containing phagolysosome which are in turn led to the outside of the cell by the opening. In an initial experiment from one donor we detected weak signals for cathepsin B in supernatants from hMDM1 of one donor (data not shown). Taken together, preliminary data from two donors suggests that 0.5-1 h post infection, about one quarter of infected hMDM2 do form tunnel-like structures connecting the *Lm*-harboring phagosomes to the extracellular space. This might indeed suggest formation of openings to be a novel evasion strategy but needs more detailed investigations in the

future. In the further course of the project, based on the live cell imaging data, we focused on apoptotic *Lm* and the factors that mediate their uptake and processing in human primary macrophages.



**B** Quantification of *Lm* and LAMP1 positive compartments

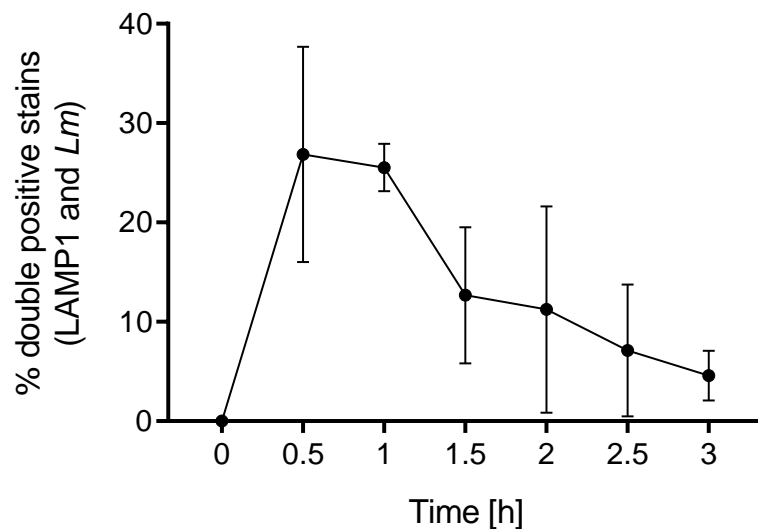


**Figure 14: Quantification of *Lm*- and LAMP1-positive staining, indicating possible tunnel structures.** **A** hMDM2 were infected with purified viable *Lm* (MOI 20). Cells were fixed with PFA and processed for immunofluorescence microscopy without permeabilization of the macrophage membranes (upper panel). Infected control cells were permeabilized prior to staining by incubation with the detergent saponin (lower panel). **B** Cells that were fixed at the indicated timepoints after infection were quantified for double positive stainings for *Lm* and the lysosome marker LAMP1. Approximately 100 phagosomes were counted. Data are presented as mean  $\pm$  SD of 2 donors from 2 independent experiments. Data were generated with help of Mr. Kevin Brück.

#### 4.6 Magnetic isolation of apoptotic *Leishmania major*-harboring phagosomes

Dying parasites play a key role in initiation of leishmaniasis (van Zandbergen et al., 2006). Based on this and the above findings from live cell imaging, we aimed on the identification of receptors and maturation markers that induce or contribute to LAP of apoptotic *Lm* and play a role in biogenesis of the emerging phagosomes. To this end, we magnetically isolated apoptotic *Lm*-containing phagosomes from infected hMDM2. For phagosome isolation, a rapid and contaminant-free method, established by Steinhäuser and colleagues, was instrumental. In this method, the pathogen is labeled with lipobiotin (LB)-coated magnetic microbeads and can be magnetically isolated from a cell lysate together with the surrounding phagosomal membrane (Steinhäuser et al., 2014, 2013) (Figure 15). In previous experiments we already showed that LB-microbead-coated apoptotic *Lm* can be sequestered within LC3<sup>+</sup> phagosomes in hMDMs (PhD thesis M. Thomas, 2015).

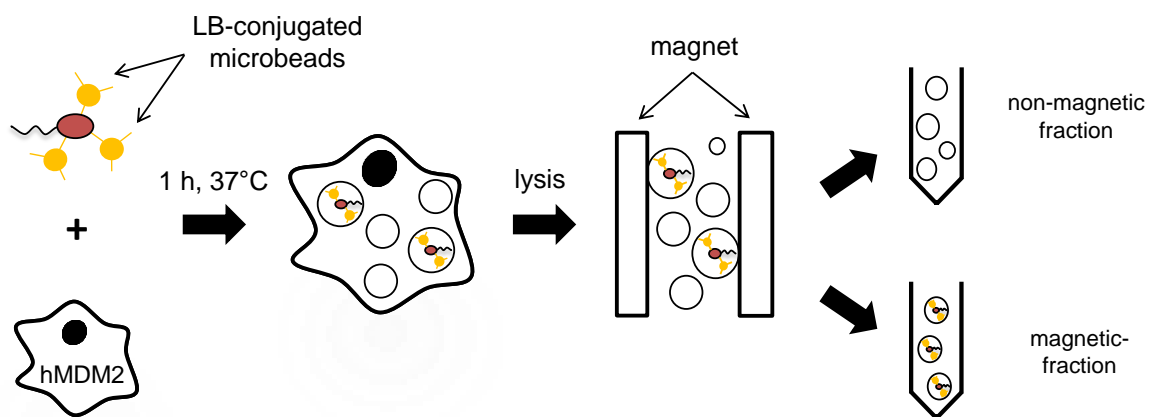


**Figure 15: Schematic presentation of the magnet-based compartment isolation.** AnxA5-MACS purified apoptotic *Lm* were labeled with lipobiotin (LB)-coated magnetic beads and co-incubated with hMDM2 for 1 h. Cells were lysed by sonication and lysates were applied onto a column in a strong magnetic field. Phagosomes containing magnetically labeled apoptotic *Lm* were retained within the magnetic field. Washing of the column yielded a non-magnetic fraction and the apoptotic *Lm*-harboring phagosomes were eluted (magnetic fraction).

To yield high amounts of apoptotic *Lm*-containing phagosomes, we first determined the optimal amount of LB-microbeads to efficiently label purified apoptotic parasites by testing increasing microbead concentrations (Figure 16). A concentration of 200  $\mu\text{g}/\text{mL}$  led to the highest grade of *Lm* labeling without aggregation of the parasites. A proportion of 89 % of the apoptotic *Lm* were conjugated to LB-microbeads as found by Streptavidin (SA)-Cy5 labeling of remaining LB-residues on the surface of the microbeads. Efficient LB-microbead labeling was further demonstrated by determination of the mean fluorescence intensity (MFI) of SA-Cy5 which was highest at a concentration of 200  $\mu\text{g}/\text{mL}$ . Thus, this



concentration of beads was used to label AnxA5-MACS purified apoptotic parasites in the following isolation procedure. The isolated amounts of protein for mass spectrometry analysis were determined by BCA assay (Table 10).

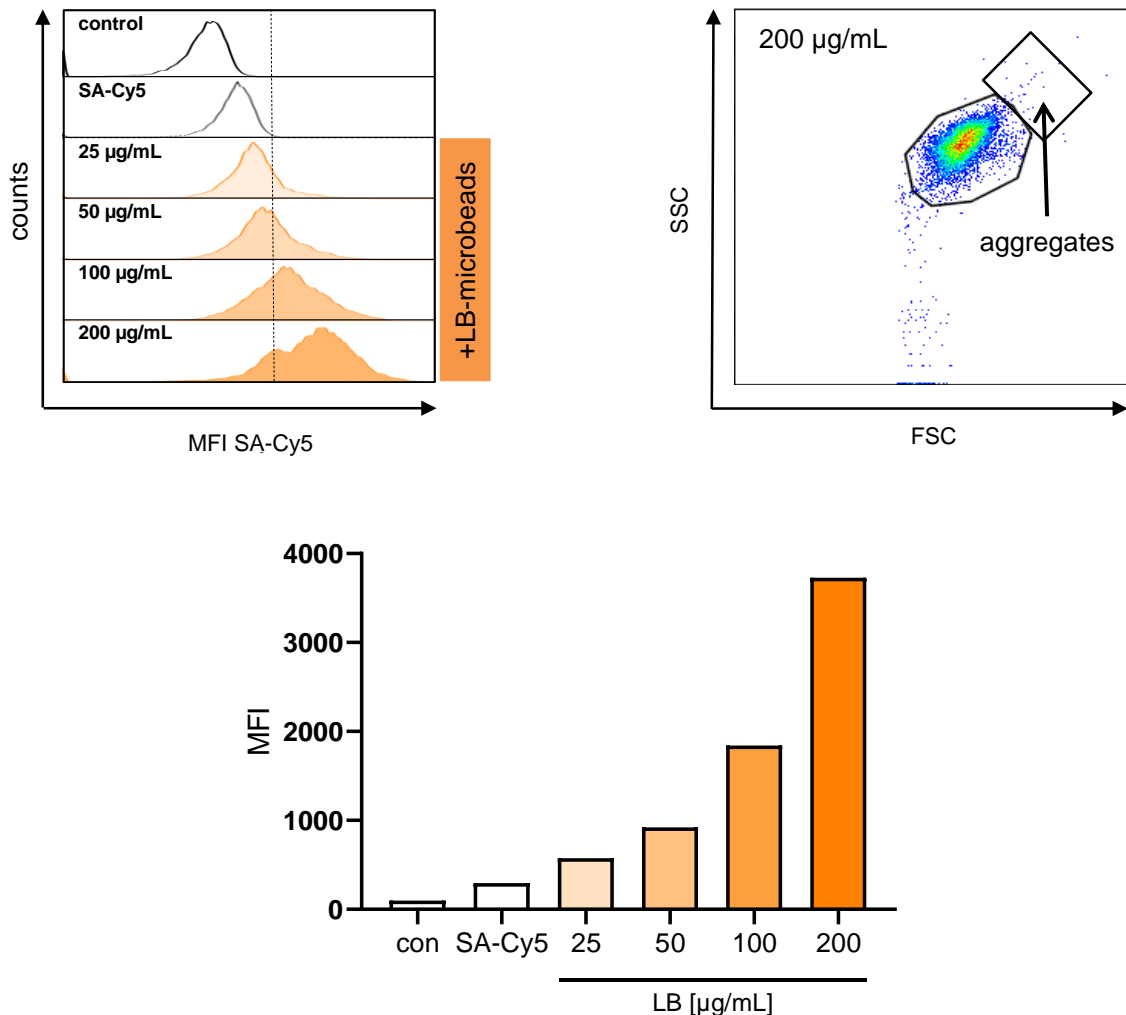


**Figure 16: Apoptotic *Lm* are efficiently labeled with lipobiotin-coated magnetic microbeads.** AnxA5-MACS-purified apoptotic *Lm* were incubated with 25-200 µg/mL lipobiotin (LB)-coated magnetic beads at 4°C overnight. Labeling efficiency was assessed by staining of non-integrated residues of LB with Streptavidin (SA)-Cy5 and flow cytometry. Formation of aggregates was assessed by gating apoptotic *Lm* by their FSC/SSC-properties (con: unstained control; n=1).

During phagosome isolation, aliquots of the cell lysate, the homogenate after sonication, the non-magnetic and the eluted magnetic fraction were collected and analyzed by western blot for enrichment of *Lm*-specific proteins within the magnetic fraction (Figure 17). As expected, analysis revealed high amounts of *Lm*-specific proteins within the magnetic fraction (M). The presence of the mitochondrial protein Cox4 as well as the nuclear pore complex component Nup62 in the magnetic fraction indicated a possible partial co-isolation of components of mitochondrial and nuclear compartments. In addition, the lipidated form of LC3 (LC3-II) could be detected on isolated phagosomes. Of

note, almost no cytosolic, non-lipidated LC3 (LC3-I) was present in the magnetic fraction indicating isolation of LC3<sup>-</sup> phagosomes as well as the portion of LC3<sup>+</sup> phagosomes (see 4.4, Figure 12A).

**Table 10: Amount of protein measured in isolated phagosomes as quantified by BCA assay.**

| Donor | Amount of isolated protein for mass spectrometry |
|-------|--|
| 1     | 26 µg  |
| 2     | 31 µg  |
| 3     | 25 µg  |
| 4     | 4 µg   |
| 5     | 44 µg  |
| 6     | 60 µg  |

The phagosome isolation was performed for six donors and the magnetic fractions were analyzed for their proteome by label-free liquid chromatography-coupled mass spectrometry (LC-MS) in cooperation with Stefan Tenzer (University Hospital Mainz, Germany). By LC-MS and subsequent data analysis, 1015 *Leishmania*-specific as well as 1998 human host cell-derived, proteins were identified. The quantity of human proteins was determined within each sample and the 40 most abundant proteins throughout all the samples were used for a functional protein association network (STRING-) analysis (Figure 18, Table 11). In accordance with western blot analysis, mitochondrial proteins such as mitochondrial ATPases ATP5A1 and ATP5B, IMMT (inner membrane protein MIC60, part of the MICOS complex) or mitochondrial heat-shock proteins (HSPA5, HSP90) could be detected in high amounts within the lysates of the magnetic fraction. Many more peptides with a mainly high sequence coverage for 216 mitochondrial proteins indicated co-isolation of phagosomes with mitochondria or a connection of both compartments (data not shown).

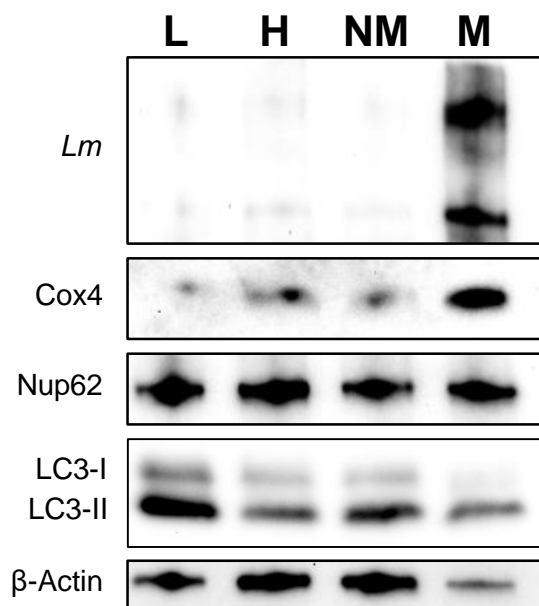


**Figure 17: Western blot analysis of samples collected during magnetic isolation of phagosomes.** Samples of the phagosome isolation were analyzed by SDS-PAGE and western blot with the indicated antibodies/antisera regarding enrichment of Lm and cellular proteins (L: lysate, H: homogenate, NM: non-magnetic fraction, M: magnetic fraction; 5  $\mu$ g protein/lane). Western blot analysis was performed for two donors used in the isolation procedure and is representative for one donor.

Of note, LC3 was not detected in our MS screen. Intriguingly, alongside proteins of the cytoskeleton, such as Talin-1, Filamin-A or Dystonin, we identified the phagocytic receptors Low-density lipoprotein receptor-related protein 1 (LRP1, CD91) and the Complement Receptor 3 subunits Integrin  $\alpha$ M (ITGAM, CD11b) and Integrin  $\beta$ 2 (ITGB2, CD18). For CD91, 80 peptides with a sequence coverage of 30 % were discovered. For CD11b, 38 peptides with a coverage of 71 % and for CD18, 39 peptides with a coverage of 48 % were identified. Interestingly, CD91, in conjunction with calreticulin that binds to complement component C1q, is described to be involved in the phagocytosis of apoptotic cells (Ogden et al., 2001). Complement Receptor 3 is known to be one of the major receptors that facilitate internalization of viable *Leishmania* promastigotes as well as *L. major* amastigotes (Mosser and Edelson, 1985; Rosenthal et al., 1996; Wenzel et al., 2012). Moreover, high amounts of Talin-1, known to be crucial for CR3-mediated phagocytosis, further suggest a role for this receptor in uptake of apoptotic *Lm* (Lim et al., 2007).

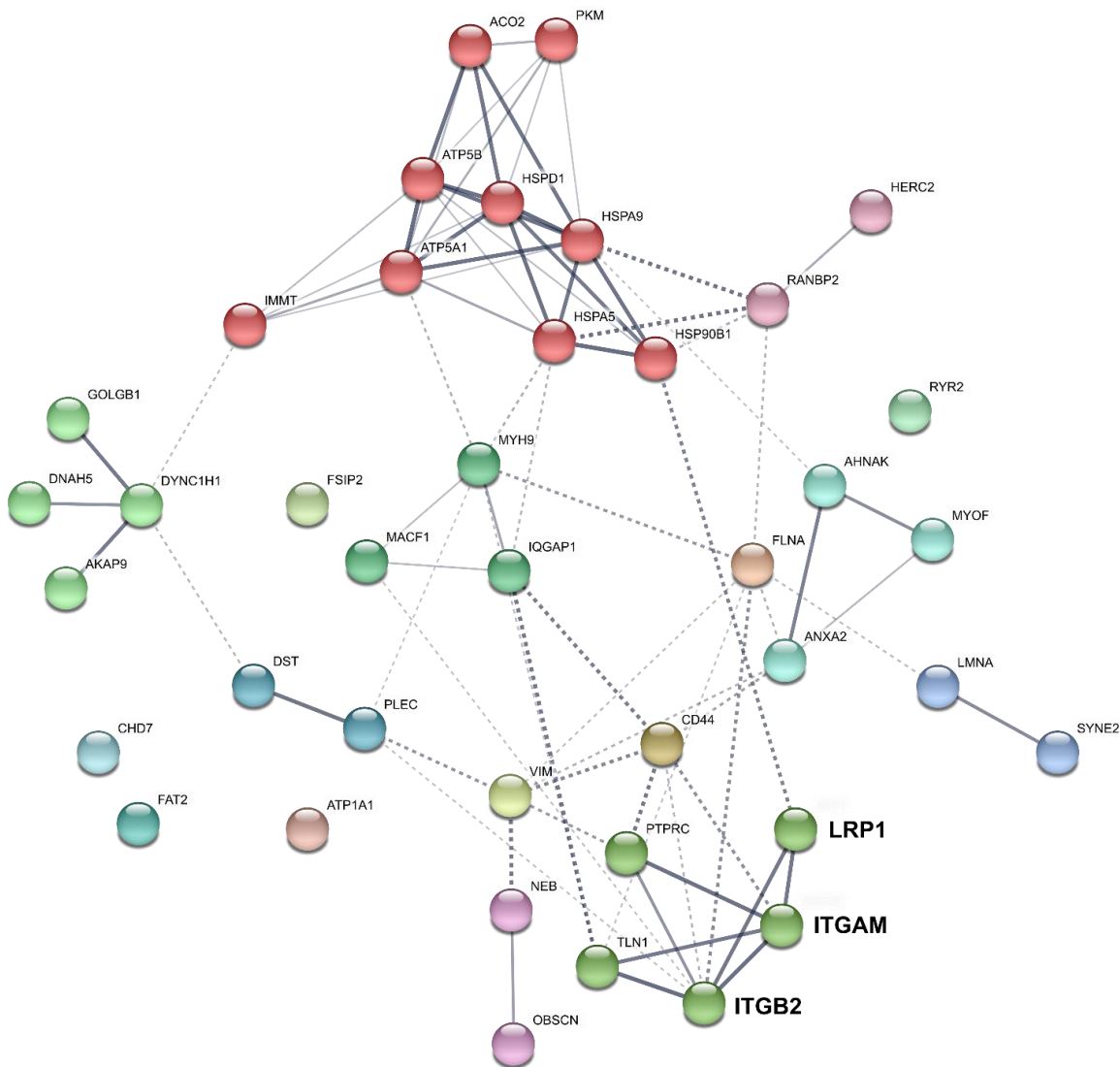


**Figure 18: STRING analysis of the 40 most abundant host cell-derived proteins as identified by LC-MS.** Complement Receptor 3 subunits ITGAM (Integrin  $\alpha$ M; CD11b) and ITGB2 (Integrin  $\beta$ 2; CD18) as well as LRP1 (Low-density lipoprotein receptor-related protein 1; CD91) are in bold. MS data represent 6 donors from 4 independent experiments.

Taken together, phagosome isolation showed enrichment of *Lm* proteins and LC3<sup>+</sup> compartments in the eluted fraction. As expected from our live cell imaging data we could not exclusively isolate LC3<sup>+</sup> compartments as anticipated on the basis of former observations at the beginning of the project (Crauwels et al., 2015). Mass spectrometry revealed proteins of the phagocytosis and autophagy machinery to be present in the compartment which indicated at least partial isolation of LAP compartments which was supported by the presence of lipidated LC3-II in the magnetic fraction in western blot analysis. The expected detection of LC3 by MS was absent whereas the apoptotic cell receptors CD91 and CR3 were found in high abundance within the compartment and were further investigated regarding their role in the interaction with apoptotic *Lm*.

**Table 11: Mass spectrometric identification of highly abundant proteins in isolated compartments.** Protein and gene name and PDB accession of proteins identified by LC-MS in phagosomes harboring apoptotic *Lm* sorted by declining amounts. Proteins that were investigated in more detail in this study are written in bold (PDB: Protein Data Bank, [www.rcsb.org/pdb](http://www.rcsb.org/pdb)).

|  | Description  | Gene              | PDB entry         |
|--|--|-------------------|-------------------|
| abundance                                    | Neuroblast differentiation-associated protein                | AHNAK             | AHNAK_HUMAN       |
|  | Myosin-9   | MYH9              | MYH9_HUMAN        |
|  | Filamin-A  | FLNA              | FLNA_HUMAN        |
|  | Golgin subfamily B member 1                                  | GOLGB1            | GOLGB1_HUMAN      |
|  | Ryanodine receptor 2   | RYR2              | RYR2_HUMAN        |
|  | Talin-1  | TLN1              | TLN1_HUMAN        |
|  | Microtubule-actin cross-linking factor 1, isoforms 1/2/3/5   | MACF1             | MACF1_HUMAN       |
|  | Plectin  | PLEC              | PLEC_HUMAN        |
|  | Ras GTPase-activating-like protein IQGAP1                    | IQGAP1            | IQGA1_HUMAN       |
|  | Nebulin NEB  | NEB               | NEBU_HUMAN        |
|  | <b>Prolow-density lipoprotein receptor-related protein 1</b> | <b>LRP1</b>       | <b>LRP1_HUMAN</b> |
|  | Dystonin   | DST               | DYST_HUMAN        |
|  | Vimentin   | VIM               | VIME_HUMAN        |
|  | Myoferlin  | MYOF              | MYOF_HUMAN        |
|  | ATP synthase subunit beta, mitochondrial                     | ATP5B             | ATPB_HUMAN        |
|  | Fibrous sheath-interacting protein 2                         | FSIP2             | FSIP2_HUMAN       |
|  | <b>Integrin beta-2</b>                                       | <b>ITGB2</b>      | <b>ITB2_HUMAN</b> |
|  | ATP synthase subunit alpha, mitochondrial                    | ATP5A1            | ATPA_HUMAN        |
|  | A-kinase anchor protein 9 AKAP9                              | AKAP9             | AKAP9_HUMAN       |
|  | Sodium/potassium-transporting ATPase subunit alpha-1         | ATP1A1            | AT1A1_HUMAN       |
|  | Stress-70 protein, mitochondrial                             | HSPA9             | GRP75_HUMAN       |
|  | Nesprin-2  | SYNE2             | SYNE2_HUMAN       |
|  | Pyruvate kinase PKM  | PKM               | KPYM_HUMAN        |
|  | Endoplasmic  | HSP90B1           | ENPL_HUMAN        |
|  | E3 ubiquitin-protein ligase HERC2                            | HERC2             | HERC2_HUMAN       |
|  | 78 kDa glucose-regulated protein                             | HSPA5             | GRP78_HUMAN       |
|  | CD44 antigen   | CD44              | CD44_HUMAN        |
|  | Cytoplasmic dynein 1 heavy chain 1                           | DYNC1H1           | DYHC1_HUMAN       |
|  | Obscurin   | OBSCN             | OBSCN_HUMAN       |
|  | Annexin A2   | ANXA2             | ANXA2_HUMAN       |
|  | E3 SUMO-protein ligase RanBP2                                | RANBP2            | RBP2_HUMAN        |
|  | 60 kDa heat shock protein, mitochondrial                     | HSPD1             | CH60_HUMAN        |
|  | Protocadherin Fat 2  | FAT2              | FAT2_HUMAN        |
|  | Chromodomain-helicase-DNA-binding protein 7                  | CHD7              | CHD7_HUMAN        |
| <b>Integrin alpha-M</b>                      | <b>ITAM</b>  | <b>ITAM_HUMAN</b> |                   |
| Dynein heavy chain 5, axonemal               | DNAH5  | DYH5_HUMAN        |                   |
| Aconitate hydratase, mitochondrial           | ACO2   | ACON_HUMAN        |                   |
| Prelamin-A/C                                 | LMNA   | LMNA_HUMAN        |                   |
| MICOS complex subunit MIC60                  | IMMT   | MIC60_HUMAN       |                   |
| Receptor-type tyrosine-protein phosphatase C | PTPRC  | PTPRC_HUMAN       |                   |

#### 4.7 Phenotypic characterization of human monocyte-derived phagocytes

Prior to investigations on the function of CD91 and CR3 in apoptotic *Lm* internalization, we sought to confirm the presence of both receptors on monocyte-derived macrophages. We further checked the two receptors' expression by monocyte-derived dendritic cells (hMDDCs) which were previously shown to lack LC3 recruitment upon stimulation with *Lm* (PhD thesis P. Crauwels, 2015). To ensure the correct *in vitro* polarization of hMDM1 and hMDM2 and generation of hMDDCs, we additionally checked the expression of known surface proteins of the professional APCs employed in this study. Characterization was performed by antibody staining of the respective markers (Figure 19). The mannose receptor CD14, which is generally accepted as marker for monocytes and macrophages (Collin et al., 2013), was present on hMDM1 and highly abundant on hMDM2. In accordance with literature, the scavenger receptor CD163 which is known to be specific for anti-inflammatory macrophages, was highly abundant on hMDM2 (Biswas et al., 2012). CD1a, a dendritic cell receptor capable of glycolipid presentation, was mainly found on hMDDCs as well as in minor amounts on hMDM1 (Ohradanova-Repic et al., 2016; Sloma et al., 2008). The C-type lectin receptor CD209 (DC-SIGN) was highly expressed by hMDDCs and present in lower numbers on hMDM2. The mannose receptor CD206 is described as a pro-inflammatory macrophage marker and relevant for phagocytosis of viable *Lm* (Chakraborty et al., 2001, 1998). We detected this receptor in high numbers on hMDM1 and on hMDDCs and to lower extend on hMDM2. Furthermore, Complement Receptor 3 (subunit CD11b) was detected on all three cell types, showing a stronger expression on hMDM1 and hMDDCs than on hMDM2. CD91 could be confirmed on the surface of hMDM1 as well as hMDM2 (Costales et al., 2013). Interestingly, hMDDCs lack this receptor.

Taken together, by measuring the expression of cell type-specific surface markers, we could confirm the expected phenotypes of our *in vitro*-generated hMDM1, hMDM2 and hMDDC. Similar to CD206, CR3 is expressed in higher amounts in hMDM1, suggesting a higher phagocytosis capacity of this cell type which does not correlate with our previous observations (Figure 11A). hMDDCs, although expressing similar amounts of CD206 and CR3 as hMDM1, are known to be relevant for anti-leishmanial immune reactions but do not serve as host cell for parasite growth (Zahn et al., 2010). Interestingly, in hMDDCs, LAP was not induced upon *Lm* infection (PhD thesis P. Crauwels, 2015). This raised the question if CD91, not present on hMDDCs, may play a role in LAP of apoptotic *Lm* in hMDMs.

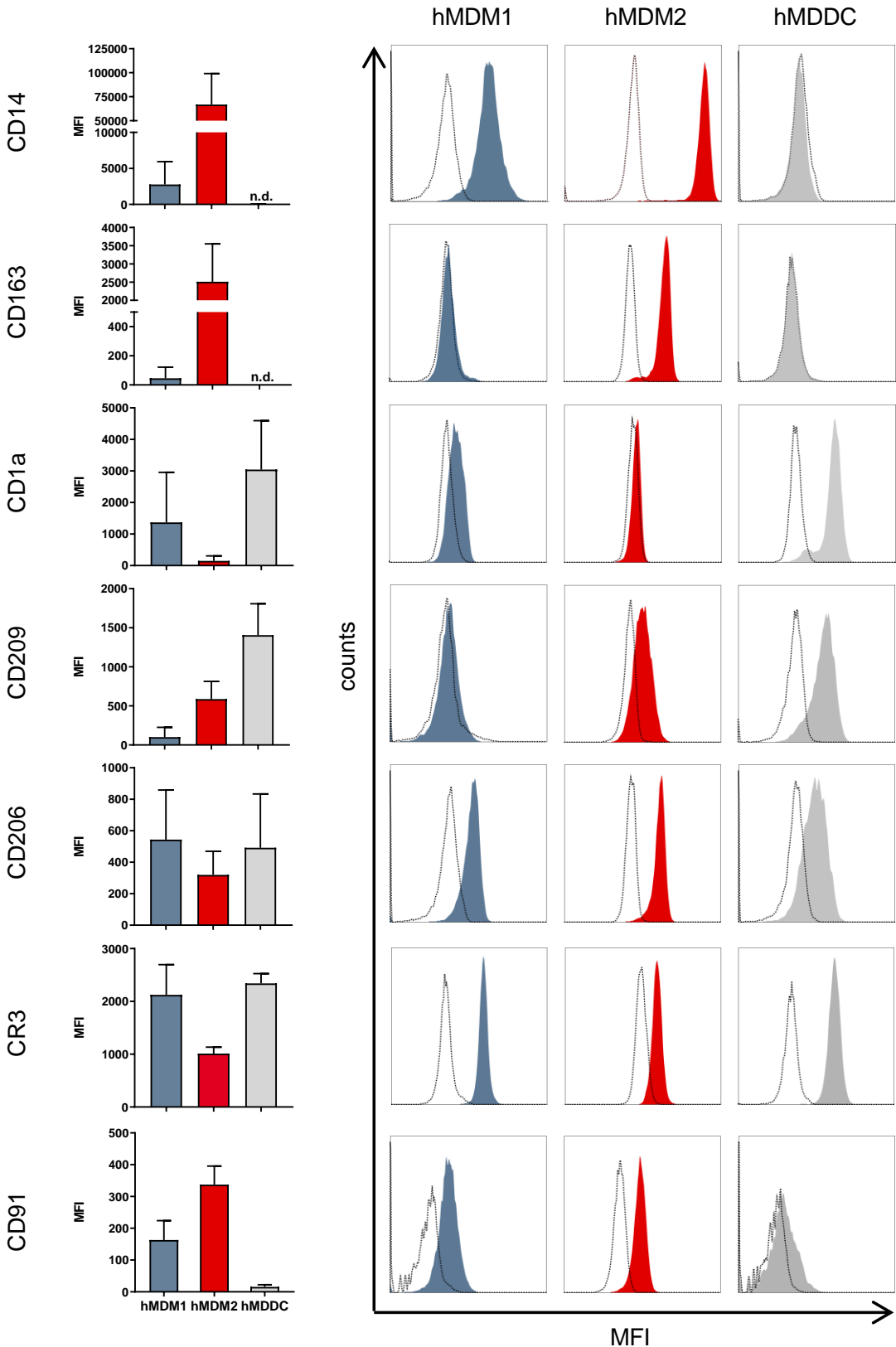


**Figure 19: Characterization of *in vitro*-generated human monocyte-derived macrophages and dendritic cells.** Monocytes were isolated from blood donations. hMDM1 (blue), hMDM2 (red) and hMDDCs were generated by cultivation for 5-7 days in presence of either GM-CSF, M-CSF or GM-CSF and IL-4, respectively. Characterization of the generated cells was performed by antibody staining of the specific cell surface markers CD14, CD206, CD163, CD1a, and CD209 as well as of CR3 and CD91 and subsequent analysis by flow cytometry. Data are presented as mean  $\pm$  SD of 3-33 donors from at least 3 independent experiments. No statistical evaluation was performed. Histograms are representative for one donor (n.d. = not detectable).

#### 4.8 Cytokine production of antigen-presenting cells upon differential infection with *Leishmania major* promastigotes

In addition to the phenotypical characterization by antibody staining of surface markers, we employed ELISA to check for the cytokine profiles of the generated monocyte-derived cells upon differential infection with purified viable or apoptotic *Lm* or an artificial stat. ph. of the parasites. hMDM1 are described to produce high amounts of pro-inflammatory mediators whereas hMDM2 are characterized by high release of IL-10, depending on the stimuli (Italiani and Boraschi, 2014). Infection with viable *Lm* was expected to trigger pro-inflammatory cytokine release whereas co-incubation of antigen-presenting cells with apoptotic *Lm* was expected to induce secretion of anti-inflammatory mediators. In addition, we hypothesized that the presence of apoptotic *Lm* in a stat. ph. *Lm* culture counteracts the pro-inflammatory response that is induced by viable *Lm* upon infection. This in turn could lead to decreased inflammation as a prerequisite that allows viable *Lm* to survive within hMDMs.

To get an overview of cytokine production upon *Lm* infection, we used a bead-based multiplex assay for the analysis of supernatants from viable or apoptotic *Lm*-infected cells (Appendix A). Multiplex data revealed strong differences in secretion of the pro-inflammatory cytokines IL-1 $\beta$ , IL-8, IL-6 and TNF- $\alpha$ . In addition, the anti-inflammatory IL-10 was found to be altered between viable and apoptotic *Lm*-infected hMDMs. These cytokines were analyzed in more detail by ELISA (Figure 20, Figure 21). IL-1 $\beta$ , an important pro-inflammatory cytokine in leishmaniasis (Maspi et al., 2016), was secreted by pro-inflammatory hMDM1 that were infected with purified viable *Lm* (Figure 20A). Compared to this, secretion of IL-1 $\beta$  was elevated in the presence of apoptotic *Lm* alone or stat. ph. *Lm*. The same was observed for differentially infected hMDM2 whereas in hMDDCs, IL-1 $\beta$  production compared to viable or stat. ph. *Lm* infected cells, was increased when challenged with purified apoptotic *Lm*. Production of IL-6, a cytokine that can act in a pro- and anti-inflammatory manner, was highly induced in hMDM1 in presence of purified viable or apoptotic *Lm* (Figure 20B). Stat. ph. infected hMDM1 showed a strongly reduced IL-6 secretion. In anti-inflammatory hMDM2, production of IL-6 was increased in presence of viable *Lm* as compared to cells that were incubated with pure apoptotic *Lm* or stat. ph. parasites. In hMDDCs, IL-6 expression slightly increased when viable *Lm* were absent during infection. The very potent pro-inflammatory cytokine IL-8 plays a key role in early stages of



*Lm* infection *in vivo* by triggering the recruitment of PMNs (Alexander et al., 1999). In general, IL-8 was present in high concentrations in supernatants from infected hMDMs and hMDDCs (Figure 20C). Production by hMDM1 was increased in presence of apoptotic *Lm* as compared to viable *Lm*-infected hMDM1. In supernatants of hMDM2, IL-8 was detected in equal amounts when cells were incubated with purified viable or apoptotic *Lm* whereas the challenge with a stat. ph. *Lm* even increased production. Low amounts of IL-8 were already present in uninfected cells.

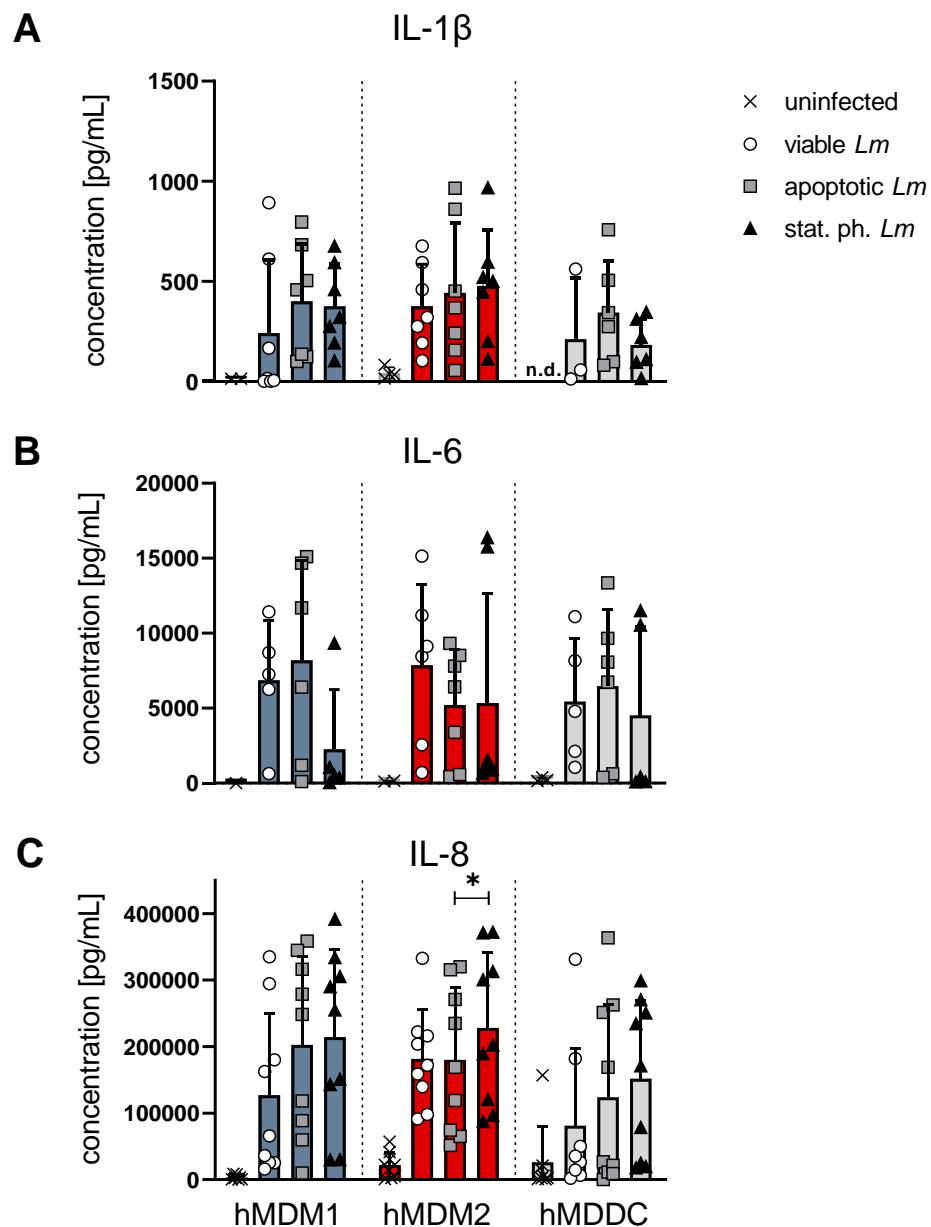


**Figure 20: Analyses of IL-1 $\beta$ , IL-6 and IL-8 secretion of differentially *Lm*-infected hMDMs and hMDDC.** hMDMs and hMDDCs were co-incubated with a MOI 10 of either purified viable *Lm* (circle) or apoptotic *Lm* (square) or an artificial stationary phase (triangle). Three hours post-infection, cells were washed twice and further incubated for 21 h. Supernatants were harvested and analyzed by ELISA for their respective content of (A) IL-1 $\beta$ , (B) IL-6, (C) IL-8. Data are presented as mean  $\pm$  SD of 7-9 donors from at least 3 independent experiments (n.d.: not detectable). Data was analyzed by unpaired Mann-Whitney U-test (A, B) and paired t-test (C) (\*  $p < 0.05$ ). Data were generated with the help of Mr. Naphang Ho.

TNF- $\alpha$  is an essential pro-inflammatory cytokine during infection and is long known to play an important role in leishmaniasis (Liew et al., 1990; Nashleanas et al., 1998). In supernatants of hMDM1 that were infected with only viable *Lm*, we detected  $700 \pm 909$  pg/mL TNF- $\alpha$ . Other than expected, concentrations increased to  $1090 \pm 959$  pg/mL and  $1146 \pm 935$  pg/mL in presence of either purified apoptotic *Lm* or stat. ph. *Lm* (Figure 21A). Moreover, the amount of TNF- $\alpha$  in supernatants of viable *Lm*-infected hMDM2 was significantly higher ( $1481 \pm 1605$  pg/mL) as compared to pro-inflammatory hMDM1. TNF- $\alpha$  production was significantly decreased ( $483 \pm 452$  pg/mL) as compared to viable *Lm*-infected hMDM2 when cells were co-incubated with purified apoptotic *Lm*. Infection with stat. ph. *Lm* resulted in a significant increase of TNF- $\alpha$  secretion similar to viable *Lm*-infected cells ( $1340 \pm 1303$  pg/mL). In hMDDCs, concentrations of TNF- $\alpha$  upon infection with only viable *Lm* were comparable to hMDM1. In comparison, presence of only apoptotic *Lm* or an artificial stationary phase strongly increased TNF- $\alpha$  secretion. The anti-inflammatory cytokine IL-10 was detected to a similar extend upon infection of hMDM1 and hMDM2 with viable *Lm* ( $2237 \pm 2028$  pg/mL and  $2318 \pm 2712$  pg/mL) (Figure 21B). In both cell types, challenge with pure apoptotic *Lm* increased IL-10 production. This increase was significant for hMDM1 ( $6881 \pm 5099$  pg/mL) and hMDM2 ( $5612 \pm 2724$  pg/mL), both infected with an artificial stat. ph. as compared to viable *Lm*-infected cells. In hMDDCs, secretion of IL-10 was lower for all conditions but was also slightly increased in presence of apoptotic *Lm* alone or stat. ph. *Lm*.

Altogether, we found no significant differences in secretion of the pro-inflammatory mediators IL-1 $\beta$  and IL-6 between the macrophage phenotypes or dendritic cells. In hMDM2, stat. ph. *Lm* infection increased release of IL-8. Of interest, between the differential infection conditions within a cell type, no expected reduction of secretion of IL-1 $\beta$ , IL-6 or IL-8 in presence of apoptotic *Lm* was observed. For TNF- $\alpha$  and IL-10 significant changes in release upon the differential infection conditions were found. In presence of apoptotic *Lm* TNF- $\alpha$  secretion in hMDM2 was downregulated and a release of IL-10 was significantly increased in both macrophage subtypes. This indicated that presence of apoptotic *Lm* effectively modulates the release of these important cytokines in human macrophages.

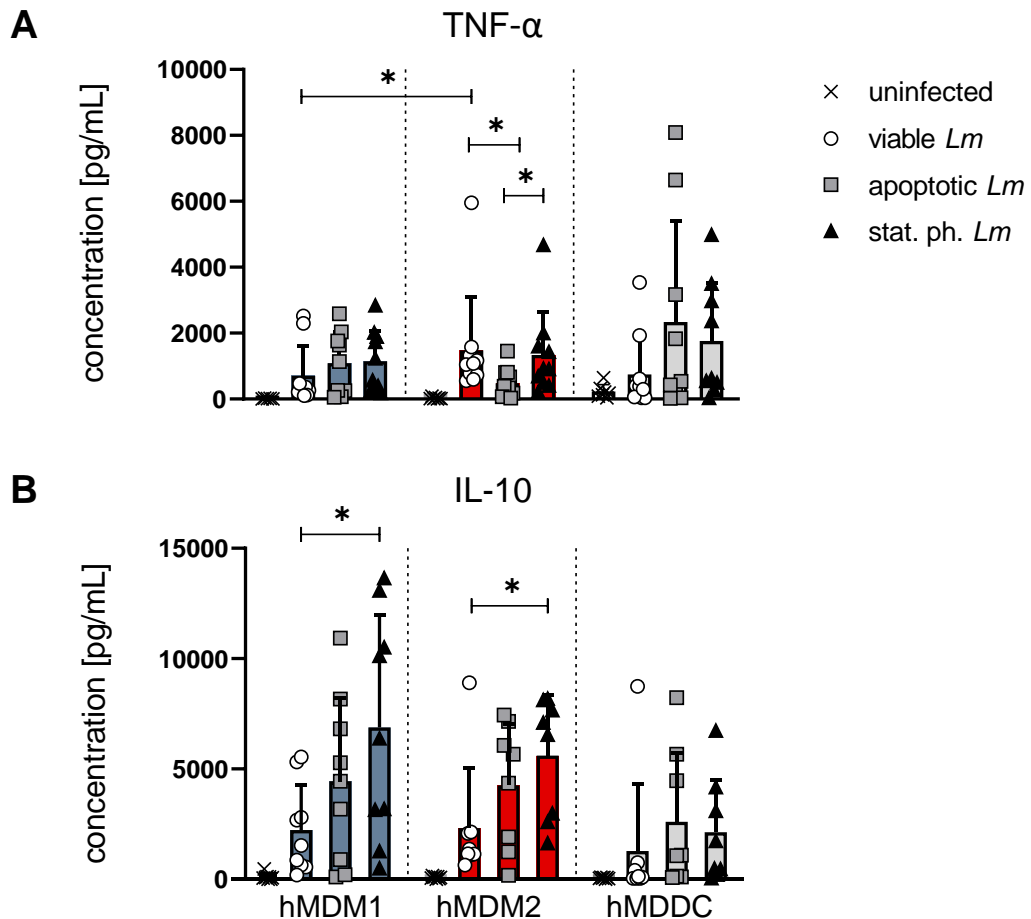


**Figure 21: Analyses of TNF- $\alpha$  and IL-10 secretion by differentially *Lm*-infected hMDMs and hMDDC.** hMDMs and hMDDC were co-incubated with a MOI 10 of either purified viable *Lm* (circle) or apoptotic *Lm* (square) or an artificial stationary phase (triangle). Three hours post-infection, cells were washed twice and further incubated for 21 h. Supernatants were harvested and analyzed by ELISA for their respective content of **(A)** TNF- $\alpha$  and **(B)** IL-10. Data are presented as mean  $\pm$  SD of 8-10 donors from at least 3 independent experiments and were analyzed by Mann-Whitney U-test (\*  $p < 0.05$ ). Data were generated with the help of Mr. Naphang Ho.

#### 4.9 Manipulation of CD91 on human monocyte-derived macrophages

Since we could demonstrate the correct differentiation of the generated monocyte-derived macrophages and dendritic cells based on surface marker characterization, we aimed on investigation of the role of CD91 in uptake of apoptotic *Lm*. To do so, we sought to manipulate the receptor on hMDM1 and hMDM2 by blocking it with a specific  $\alpha$ -CD91 functional monoclonal antibody ( $\alpha$ -CD91). As controls, isotype antibody-treated cells were used. We first tested the blocking efficiency as well as stability of blocking over time (Figure 22A). Dendritic cells were not addressed here, since CD91 was not expressed on this cell type (see Figure 19). Blocking was checked by flow cytometry after staining of the receptor with PE-conjugated  $\alpha$ -CD91 that recognizes the same epitope as the blocking

antibody. Thus, the PE-conjugated  $\alpha$ -CD91 antibody could only bind to the receptor if the latter had not been occupied by the blocking antibody. After 90 min of incubation with  $\alpha$ -CD91, hMDM1 and hMDM2 showed a decrease in  $\alpha$ -CD91-PE-specific staining of  $86 \pm 3 \%$  and  $84 \pm 10 \%$ , respectively, as compared to the isotype-treated control cells. The time of infection with *Lm* in our experimental setting is 3 h. Hence, the staining of  $\alpha$ -CD91-treated hMDMs was also assessed 3 h post-incubation. Interestingly, the capacity to stain CD91 with the PE-conjugated  $\alpha$ -CD91 after 3 h was strongly increased as compared to the 90 min post-incubation for both hMDM1 ( $35 \pm 12 \%$ ) and hMDM2 ( $40 \pm 4 \%$ ). This indicated that binding of the functional antibody to the receptor was not stable over time and therefore, inhibition of ligand binding was not given. To assess the functional role of CD91, we employed a small interfering RNA (siRNA)-based knockdown approach. Specific siRNA can be introduced into the cell by transfection and binds to its complementary mRNA molecule which in turn gets degraded by a specialized protein cascade (Whitehead et al., 2011). hMDMs were transfected with CD91-specific siRNA or non-target siRNA or were left untreated. Two days post transfection, knockdown-efficiency was checked on the protein-level by staining with  $\alpha$ -CD91-PE and flow cytometry and on the RNA level by RT-PCR (Figure 22B). Treatment with non-target control RNA resulted in a slight decrease of RNA and protein-levels in hMDM1 and a high heterogeneity between donors was observed. In hMDM2, transfection with non-target siRNA showed no effect. Upon CD91 siRNA treatment, the amounts of CD91-specific mRNA were decreased by  $80 \pm 12 \%$  in hMDM1 and by  $63 \pm 12 \%$  in hMDM2. This was confirmed by flow cytometry analysis which revealed decreased presence of the receptor on the cell surface by  $87 \pm 7 \%$  on hMDM1 and by  $76 \pm 5 \%$  on hMDM2 as compared to untreated macrophages. The successful knockdown of CD91 allowed us to investigate the receptor's role in internalization of apoptotic *Lm*.

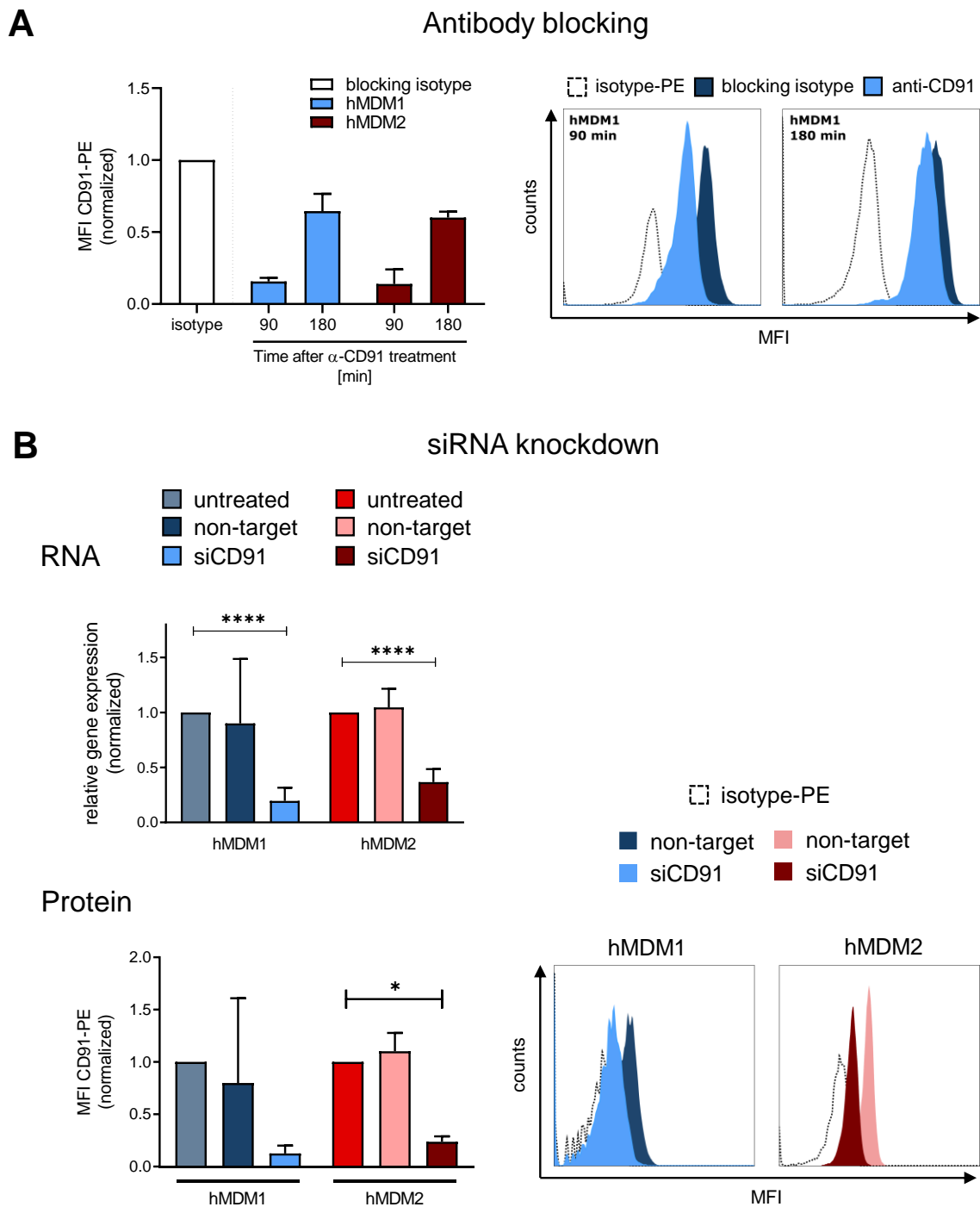


**Figure 22: Analysis of blocking or siRNA-mediated knockdown of CD91 on hMDMs.** **A** hMDMs were incubated in the absence or presence of  $\alpha$ -CD91 or an isotype control for 30 min. Excess antibody was removed by washing. Blocking of CD91 was assessed by staining of the cells with a fluorophore-conjugated  $\alpha$ -CD91-PE antibody of the same clone after 90 min and 180 min. Histograms are exemplary for hMDM1 and are representative for one donor ( $n=2-5$ ). **B** hMDMs were transfected with CD91-specific siRNA, a non-target control siRNA or were left untreated. Two days post-transfection, knockdown efficiency was determined on the RNA level by quantitative RT-PCR using CD91-specific primers ( $n=8-9$ ). Presence of CD91 protein was assessed by flow cytometry by staining of surface CD91 with  $\alpha$ -CD91-PE ( $n=5-6$ ). Histograms are representative for one donor. Data are presented as mean  $\pm$  SD from at least 3 independent experiments and were analyzed by paired t-test (**B RNA**) or Wilcoxon matched-pairs signed-rank test (**B Protein**) (\*  $p < 0.05$ , \*\*\*\*  $p < 0.0001$ ). Data were generated with the help of Mr. Marcel Seibert.

#### 4.10 The influence of CD91 knockdown on infection with apoptotic *Leishmania major* promastigotes

It is known that viable *Lm* are recognized and phagocytosed by a wide variety of receptors (Ueno and Wilson, 2012). Hence, to assess whether CD91 might also be involved in the interaction with viable parasites, CD91-knockdown cells were infected with viable *Lm* (Figure 23A). As controls served non-target siRNA-treated or untreated hMDMs. In hMDM1, we found that  $75 \pm 10\%$  of the cells interacted with viable *Lm* which was slightly decreased in knockdown macrophages (Figure 23B).

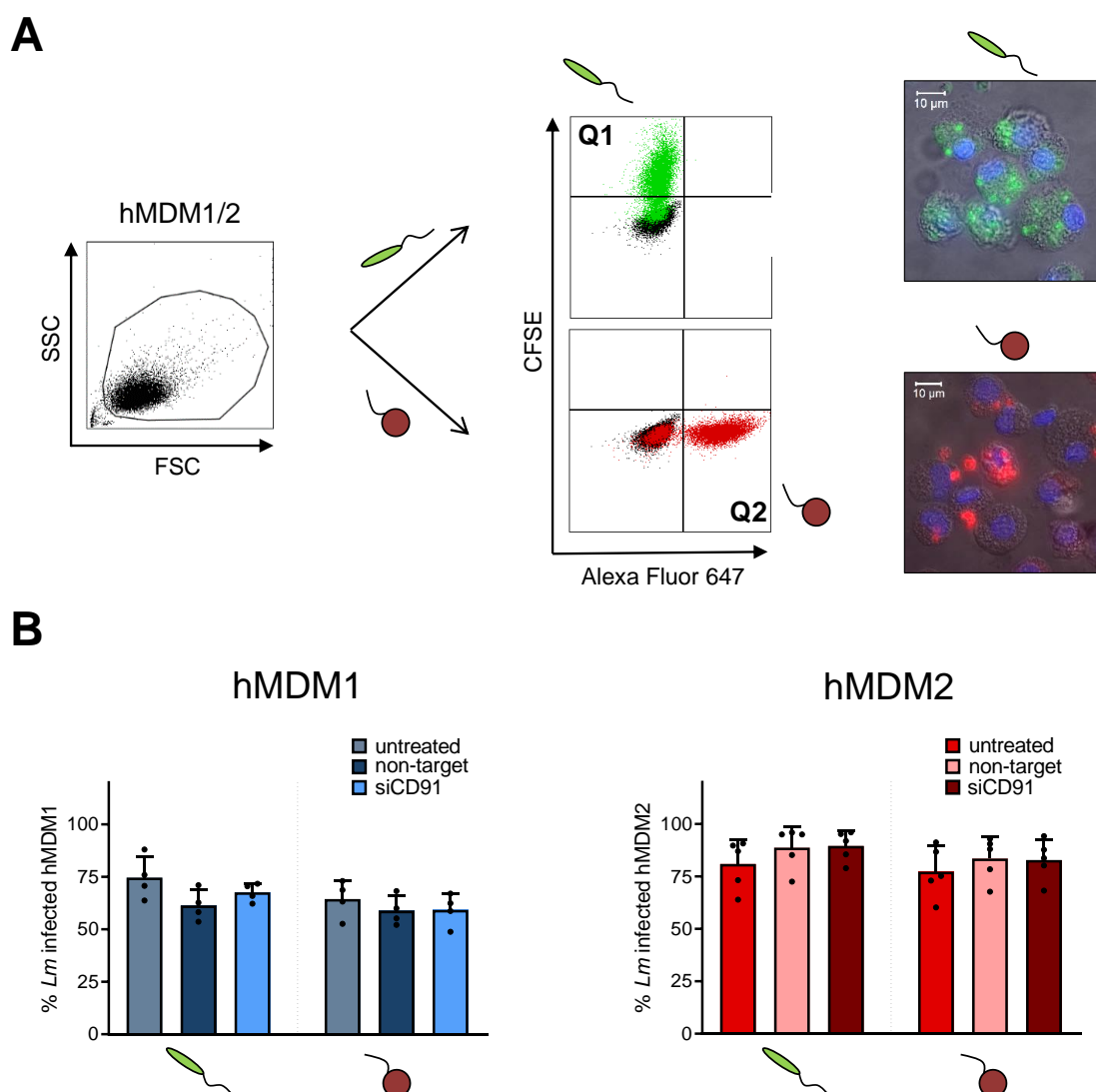


**Figure 23: Knockdown of CD91 does not alter *Lm* infection rates of hMDMs.** **A** CD91-specific siRNA-transfected hMDM1 and hMDM2 were co-incubated with purified apoptotic or viable *Lm* (MOI 10) for 3 h. Infection rates were determined by flow cytometry. hMDMs were gated by their FSC/SSC-properties. Prior to infection, viable and apoptotic *Lm* were labeled with CFSE or AF647-SE, respectively. Viable or apoptotic *Lm*-infected cells were detected in Q1 or Q2. **B** Quantification of infection rates of untreated, non-target RNA- or CD91-specific siRNA transfected hMDMs co-incubated with either purified viable or apoptotic *Lm*. Data are presented as mean  $\pm$  SD of 4-5 donors from at least 3 independent experiments.

With apoptotic *Lm*, infection rates were slightly lower and, similar to infection with viable *Lm*, downregulation of CD91 had no effect. As expected, in hMDM2 infection rates were higher than in hMDM1. Nevertheless, when untreated hMDM2 were compared to knockdown cells, no significant differences in rates of cells that interacted with viable or apoptotic *Lm* were found. Co-incubation of control siRNA-treated cells showed the same effect as CD91-specific siRNA treatment in both cell types.

Taken together, our results suggest that CD91 is not involved in the phagocytosis of viable or apoptotic *Lm* by human monocyte-derived pro- and anti-inflammatory macrophages. Hence, in the course of the study we concentrated on CR3 which was also identified within isolated apoptotic *Lm*-containing phagosomal compartments and which is known to be involved in the uptake of viable *Lm* (Ueno and Wilson, 2012).

#### 4.11 Manipulation of CR3 on monocyte-derived antigen-presenting cells

Since we did not observe an effect of CD91 downregulation on the infection rates of hMDMs we aimed on assessing the role of CR3 in phagocytosis of apoptotic *Lm* as, so far, CR3 has only been described to be of importance for the internalization of viable *Lm* (Mosser and Edelson, 1985; Rosenthal et al., 1996). We modulated the receptor by siRNA knockdown on hMDM1 and hMDM2 (Figure 24). Cells were transduced with siRNA that specifically targets mRNA that codes for the CR3 subunit CD11b/integrin  $\alpha_M$ , with non-target siRNA or were left untreated. Downregulation of CD11b to  $27 \pm 19.5\%$  and  $14.7 \pm 9.6\%$  of the untreated control in hMDM1 and hMDM2 was detected by qRT-PCR. A decreased surface expression of the receptor was confirmed by antibody staining and flow cytometry ( $27.3 \pm 14.9\%$  in hMDM1,  $47 \pm 8.3\%$  in hMDM2). Similar to the knockdown of CD91, we detected a strong off-target effect in hMDM1 that were transfected with non-target siRNA as indicated by a high heterogeneity between the donors.

To assess a possible effect of siRNA transfection on the polarization of macrophages, surface expression of CD14, CD163, CD1a and CD209 were investigated (Figure 25). CD14 was not altered between untreated and non-target siRNA- or CD11b siRNA-transfected hMDM1 and hMDM2. Higher expression of CD14 on the latter was in line with our previous results (Figure 19).

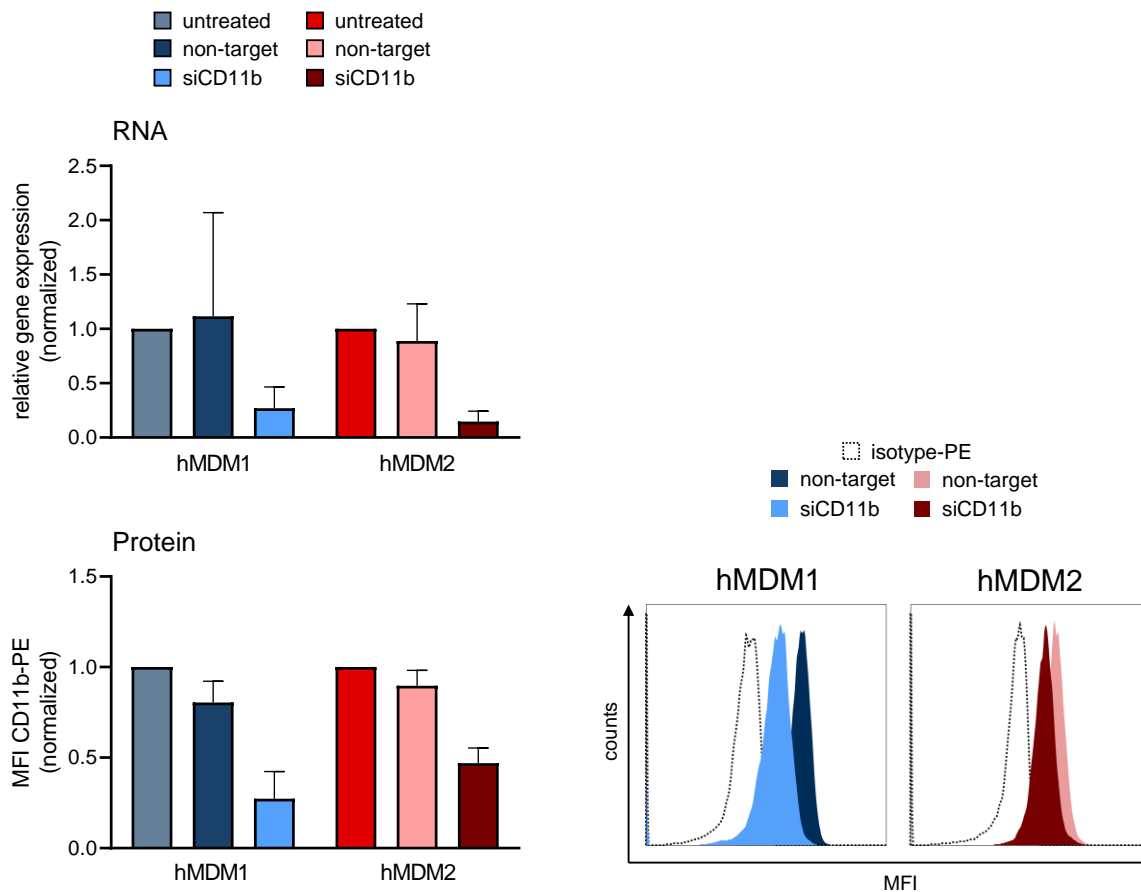


**Figure 24: Knockdown of CR3 by specific siRNA.** hMDMs were transfected with CD11b-specific siRNA, a non-target control siRNA or were left untreated. Two days post-transfection, knockdown efficiency was determined on the RNA level by quantitative RT-PCR using CD11b-specific primers (n=4). Presence of CD11b protein was assessed by flow cytometry and staining of surface CR3 with  $\alpha$ -CD11b-PE (n=5). Histograms are representative for one donor. Data are presented as mean  $\pm$  SD of 4 donors from at least 2 independent experiments and were analyzed by Wilcoxon matched-pairs signed-rank test. Data were generated with the help of Mr. Marcel Seibert and Mr. Naphang Ho.

CD163, the marker for anti-inflammatory M2 phenotype was found to be highly expressed by hMDM2. Its presence on the surface was not altered upon siRNA treatment. Interestingly, the expression of the dendritic cell marker CD1a, also found to be present in low amounts on hMDM1, was increased by 2.7-fold upon transfection of this macrophage phenotype with siCD11b whereas transfection with the non-target siRNA did not affect its expression. Moreover, when hMDM2 were treated with non-target siRNA or CD11b-specific siRNA, surface expression of the DC marker CD209 that was also detected on hMDM2 before, was reduced by 50 %.



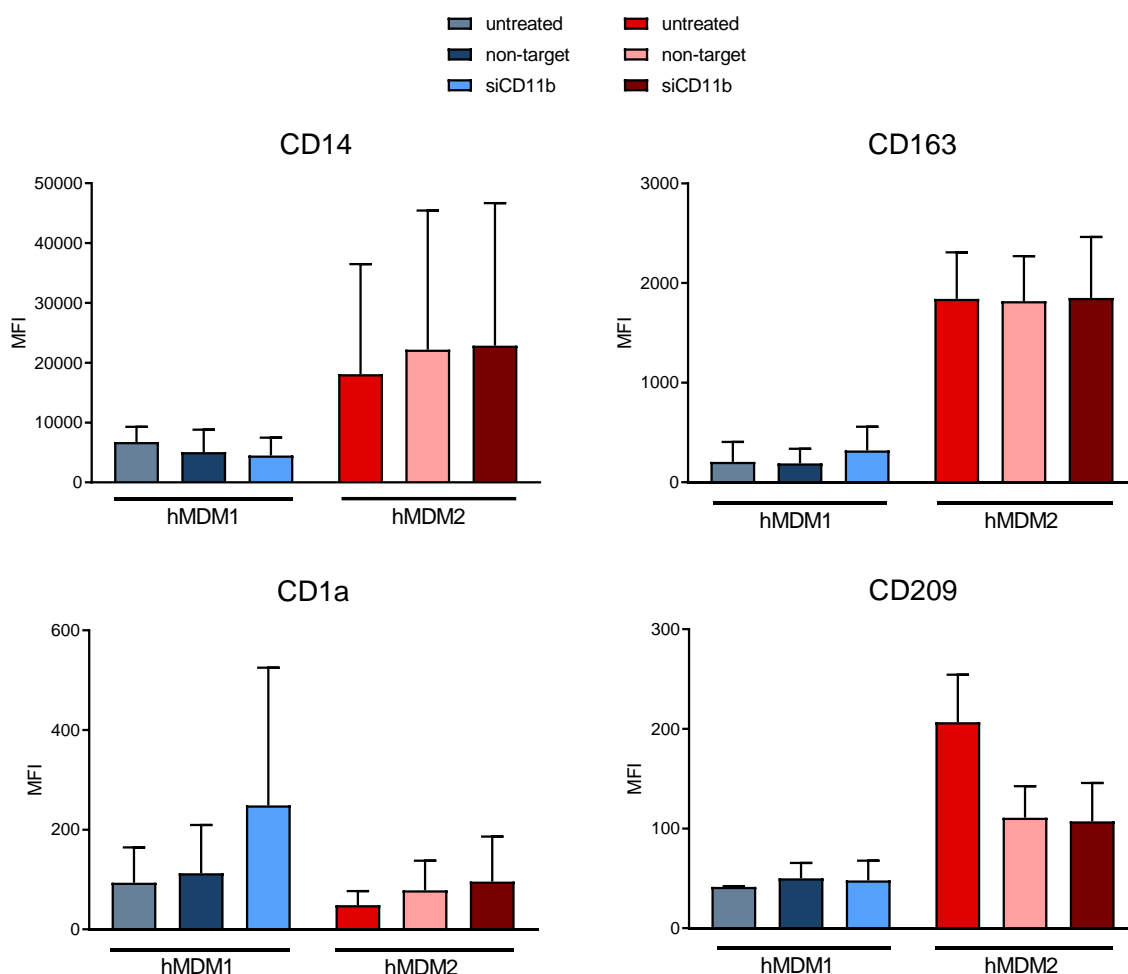


**Figure 25: Characterization of siCD11b-transfected human monocyte-derived macrophages.** hMDM1 (blue) and hMDM2 (red) were generated from isolated monocytes by cultivation for 5-7 days in presence of GM-CSF or M-CSF, respectively. Cells were transfected with siRNA and characterization was performed by antibody staining of the specific cell surface markers CD14, CD163, CD1a, and CD209 and subsequent analysis by flow cytometry. Data present the mean  $\pm$  SD of 4 donors from 2 independent experiments. No statistical analysis was performed. Data was generated with the help of Mr. Naphang Ho.

Since we found only small interference of RNA transfection on the polarization of hMDMs, we first determined infection rates of hMDM1 and hMDM2 that were co-incubated with viable or apoptotic *Lm* by fluorescence microscopy. Infected hMDMs were stained for actin with fluorophore-conjugated phalloidin and visualization of *Lm* was performed by staining with a *Lm*-specific antiserum (Figure 26). In hMDM1 we observed reduction of infection rates for both, viable and apoptotic *Lm* in siCD11b treated knockdown cells. Internalization of apoptotic *Lm* by knockdown hMDM1 as compared to untreated macrophages was strongly decreased ( $76.9 \pm 4.2\%$  vs.  $46.7 \pm 17.3\%$ ). Infection rates of hMDM1 that were treated with a non-target control siRNA were also found to be slightly reduced. In anti-inflammatory hMDM2, no reduction of infection rates with viable *Lm* were observed whereas a decrease from  $74.2 \pm 12.7\%$  in untreated to  $61.3 \pm 5.2\%$  in knockdown hMDM2 challenged with apoptotic *Lm* was found.

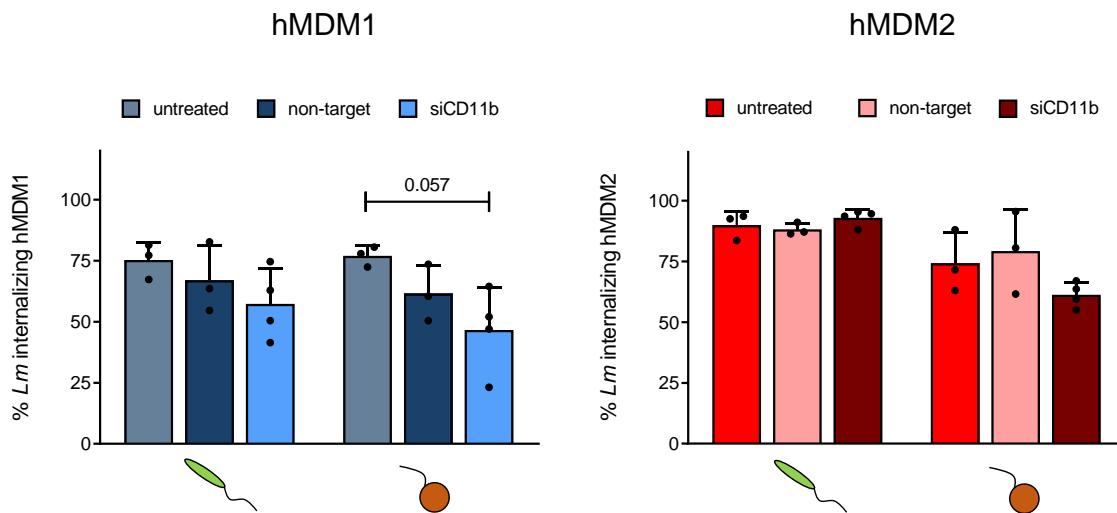


**Figure 26: Knockdown of CD11b decreases infection rates of apoptotic *Lm* in hMDM1 and hMDM2.** Untreated, non-target siRNA or CD11b-specific siRNA-transfected hMDM1 and hMDM2 were co-incubated with purified apoptotic or viable *Lm* (MOI 10) for 3 h. Cells were fixed and processed for immunofluorescence staining. Infection rates were quantified manually by fluorescence microscopy on a Zeiss LSM 7 Live confocal microscope. Data are presented as mean  $\pm$  SD of 4 donors from 2 independent experiments and were analyzed by unpaired Mann-Whitney U-test. Data were generated with the help from Mr. Naphang Ho.

Nonetheless, we also checked the influence of an  $\alpha$ -CD11b specific monoclonal antibody that had been used in other studies from our group and showed to efficiently inhibit the binding of viable *Lm* to primary human pro- and anti-inflammatory macrophages (PhD thesis S. Machado de Oliveira, 2016). As we defined flow cytometry to be the method of choice for determination of infection rates between monocyte-derived phagocytes and *Lm*, we employed this unbiased method in the following experiment. As controls served cells of the same subtype that were left untreated or that were co-incubated with an isotypic antibody. To check the efficiency and stability of receptor blocking,  $\alpha$ -CD11b-treated and control cells were incubated with a PE-conjugated  $\alpha$ -CD11b-antibody of the same clone directly after CD11b treatment or 3 h later (Figure 27). Compared to controls, we detected a strong decrease in the mean fluorescence intensities (MFI) of 70 % for hMDM1 and hMDM2 when treated with functional  $\alpha$ -CD11b directly after 30 min of incubation with the blocking antibody. The capacity to stain for CR3 at 3 h after  $\alpha$ -CD11b treatment even decreased further indicating a very stable blocking of the receptor. The MFI of CR3 on hMDDCs was decreased by 50 %. This indicated partial blocking of CR3 on all three cell types which was pronounced on hMDMs.

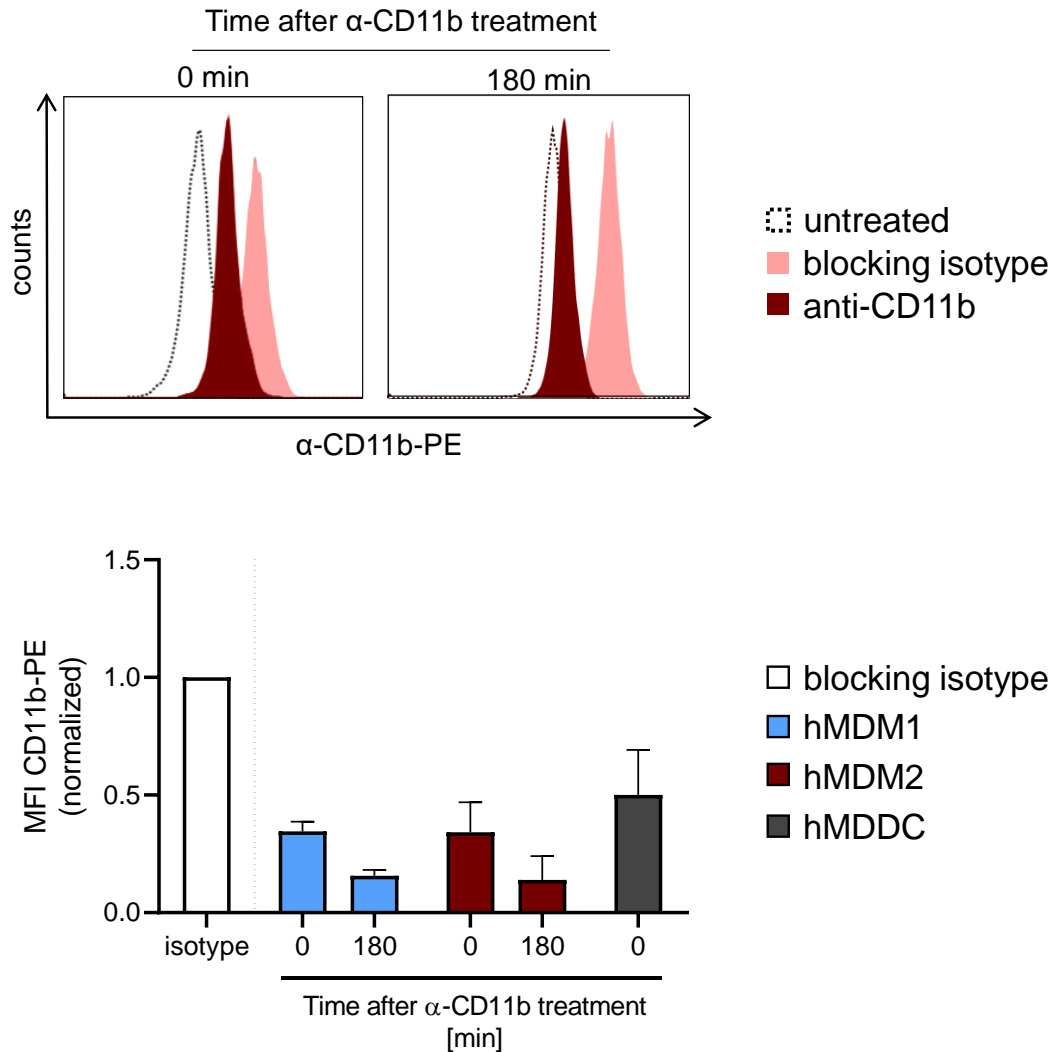


**Figure 27: Efficient blocking of Complement Receptor 3 with an  $\alpha$ -CD11b antibody.** hMDMs and hMDDCs were incubated with the  $\alpha$ -CD11b antibody or an isotype control for 30 min. Blocking stability was assessed by staining of the cells with a phycoerythrin (PE)-conjugated  $\alpha$ -CD11b antibody of the same clone (dashed line: PE-conjugated isotype control) and flow cytometry analysis directly and 180 min after co-incubation with the functional antibody. Data are presented as mean  $\pm$  SD of 3-8 donors from at least 3 independent experiments. Histograms are representative for hMDM2 from one donor. Data were generated with the help of Mr. Marcel Seibert.

#### 4.12 Inhibition of CR3 significantly reduces interaction with apoptotic *Leishmania major* promastigotes

To assess the role of the receptor for phagocytosis of apoptotic *Lm*,  $\alpha$ -CD11b or isotypic antibody treated cells or untreated control cells were co-incubated with purified apoptotic *Lm*. As controls, purified viable *Lm* or an artificial 1:1 mixture of viable and apoptotic *Lm*, resembling a stat. ph. promastigote culture (stat. ph., Figure 7), were used. Cells were gated as shown in Figure 28. When  $\alpha$ -CD11b-treated hMDM1 were infected with stat. ph. *Lm*, infection rates of cells with viable *Lm* (Q1) or only apoptotic *Lm* (Q2) were not altered as

compared to equally infected control cells (Figure 29A). Interestingly, a significant reduction in the number of hMDM1 that interacted with both, apoptotic and viable *Lm*, was found ( $27 \pm 11$  % vs.  $20 \pm 8$  %). A proportion of 57 % of hMDM1 challenged with only viable *Lm* were infected and no reduction in infection rates was observed when cells were pre-treated with  $\alpha$ -CD11b. Of note, a strong but no significant decline in infection rates from  $51 \pm 9$  % to  $43 \pm 10$  % was found in cells co-incubated with apoptotic *Lm* alone.

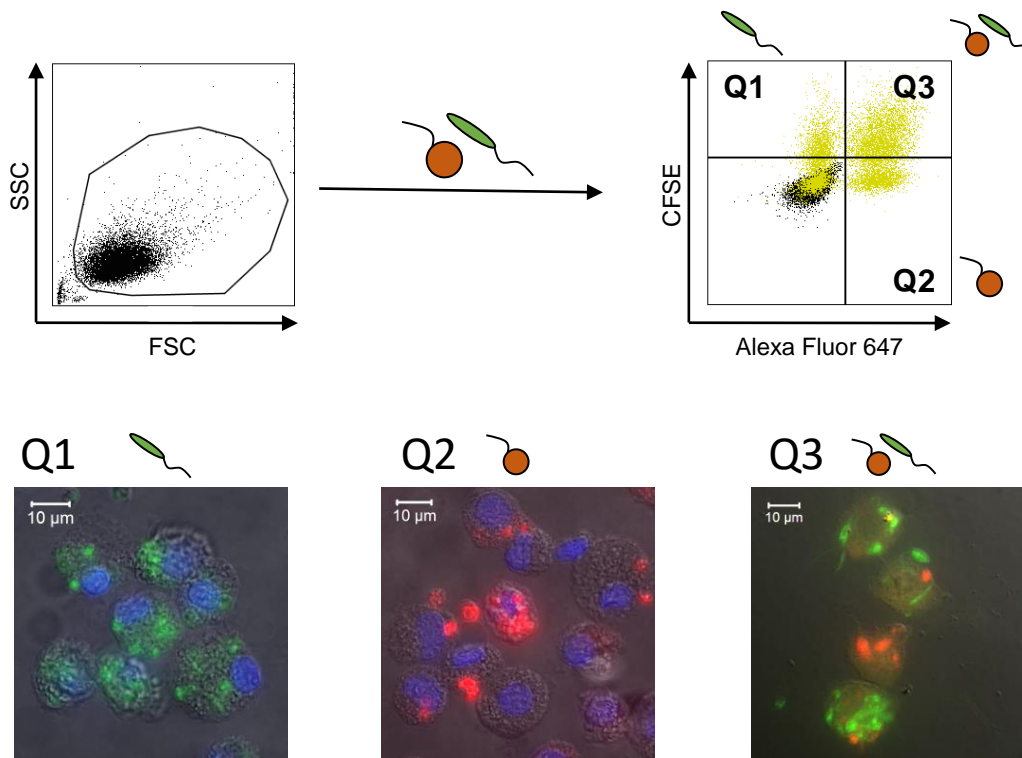


**Figure 28: Gating strategy to identify infection of hMDMs or hMDDCs with *Lm*.** Infection of hMDMs/hMDDCs with *Lm* was determined by gating hMDMs and hMDDCs by their FSC/SSC-properties. Viable or apoptotic *Lm*-positive phagocytes were detected in Q1 or Q2, respectively. Double positive cells were detected in Q3. Micrographs exemplary show infected cells from Q1, Q2 and Q3. Prior to infection, viable and apoptotic *Lm* were labeled with CFSE or AF647-SE, respectively.

Anti-inflammatory hMDM2 play a role in tissue homeostasis and apoptotic cell removal (Tomiotto-Pellissier et al., 2018). In line with this, in anti-inflammatory hMDM2 we found an enhanced interaction of macrophages with apoptotic *Lm* or with both, viable and apoptotic *Lm*, upon challenge with a stat. ph. *Lm* mixture, as compared to hMDM1 (Figure 29B). The number of stat. ph. infected cells that interacted only with apoptotic *Lm* was significantly reduced from  $31 \pm 11$  % to  $22 \pm 12$  % in the presence of  $\alpha$ -CD11b. As expected, in hMDM2 that were challenged with only apoptotic *Lm*, infection rates were higher by 22 % than in hMDM1. Moreover, co-incubation with pure apoptotic *Lm* in the presence of  $\alpha$ -CD11b resulted in a significant decrease of infection rates ( $73 \pm 4$  % to  $64 \pm 8$  %).

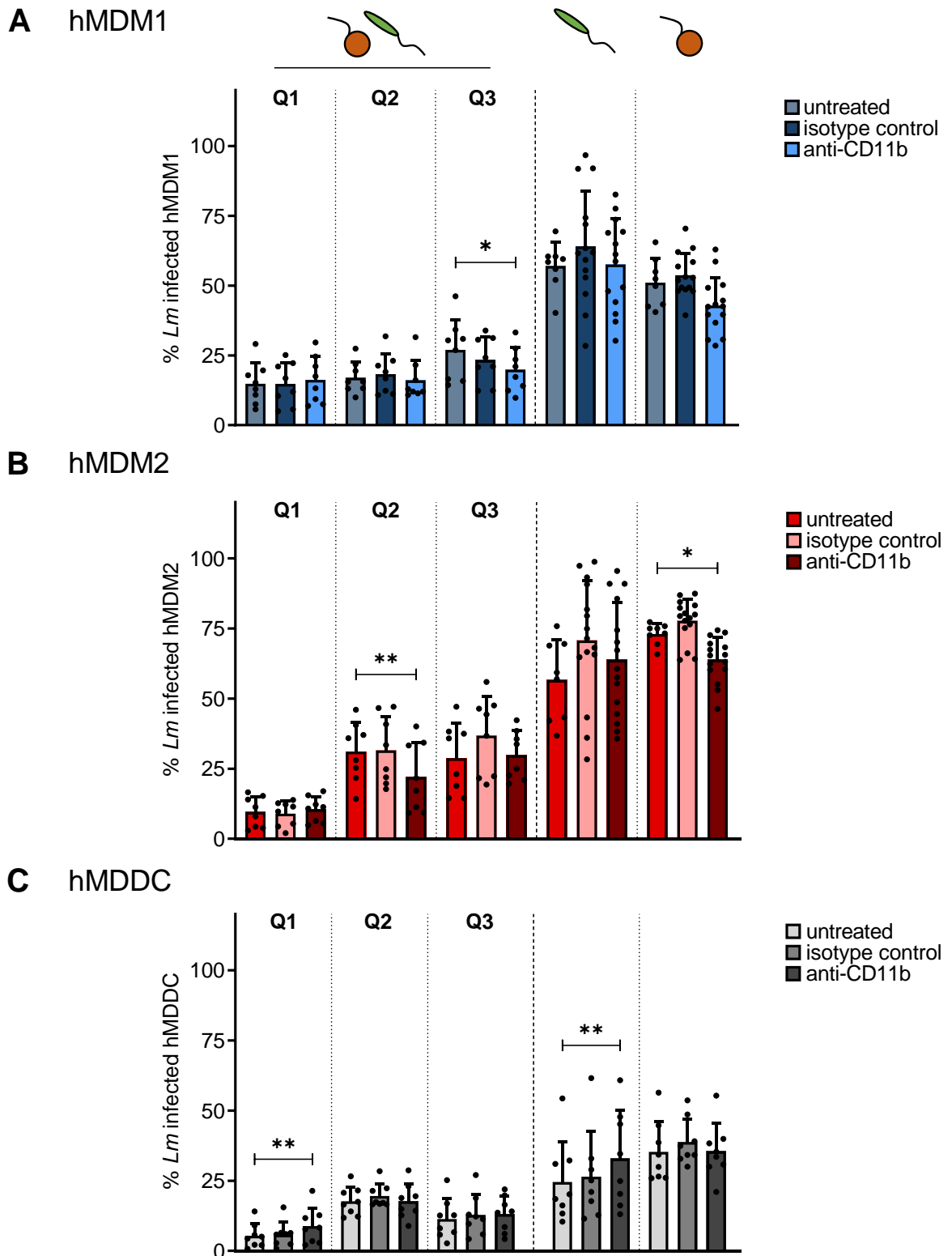


**Figure 29: Blocking of CR3 results in decreased interaction of apoptotic *Lm* with hMDMs.** hMDM1 (blue), hMDM2 (red) or hMDDCs (grey) were left untreated or incubated with  $\alpha$ -CD11b or an isotype control prior to co-incubation with either an artificial stat. ph. or purified viable or apoptotic *Lm*. Viable *Lm* were stained with CFSE, apoptotic *Lm* were stained with AF647-SE. Infection rates were determined by flow cytometry. Viable *Lm* infected cells were detected in Q1, apoptotic *Lm* positive cells in Q2 and cells that internalized viable and apoptotic *Lm* were detected in Q3. Data are presented as mean  $\pm$  SD of a minimum of 8-14 donors from at least 6 independent experiments and was analyzed by paired t-test (\*  $p < 0.05$ , \*\*  $p < 0.01$ ).

In hMDDCs, we detected a significantly higher infection of the cells with viable parasites when cells were co-incubated with stat. ph. *Lm* in presence of  $\alpha$ -CD11b ( $5 \pm 4\%$  to  $9 \pm 6\%$ , Figure 29C). In hMDDCs infected with viable *Lm* alone, blocking of CR3 also significantly increased the interaction ( $25 \pm 14\%$  vs.  $33 \pm 17\%$ ).

Taken together, the data point to a functional role of Complement Receptor 3 in the interaction of hMDDCs with apoptotic *Lm* but not in hMDDCs. Based on the immune silencing properties of apoptotic cell uptake, we further hypothesized that the diminished interaction and hence a decreased phagocytosis of apoptotic *Lm* upon inhibition of CR3 inhibits the production of anti-inflammatory cytokines.

#### 4.13 CR3 modulation prior to *Leishmania major* infection leads to alterations in TNF- $\alpha$ and IL-10 secretion

We observed significant alterations in TNF- $\alpha$  release in hMDDC2 and in IL-10 secretion by pro- and anti-inflammatory macrophages when we co-incubated these cells with apoptotic *Lm* (Figure 21). This raised the question whether the decreased interaction of primary monocyte-derived macrophages with apoptotic *Lm* and the connected lower internalization as shown by flow cytometry analysis upon CR3 receptor blocking affects the production of pro- and anti-inflammatory cytokines. To this end, hMDDCs were differentially infected in the presence or absence of  $\alpha$ -CD11b or the isotype control and secretion of TNF- $\alpha$  and IL-10 was analyzed by ELISA (Figure 30). Dendritic cells were not investigated since neither a significant reduction in interaction with apoptotic *Lm* nor significant alterations in cytokine production were observed in previous experiments in the present study (Figure 21 and Figure 29).

When hMDDC1 were treated with  $\alpha$ -CD11b and infected with purified viable *Lm*, secretion of TNF- $\alpha$  was strongly reduced ( $324 \pm 471$  pg/mL) as compared to untreated control cells ( $581 \pm 867$  pg/mL) (Figure 30A). The same trend was observed for hMDDC1 that were challenged with only apoptotic *Lm* ( $226 \pm 230$  pg/mL vs.  $92 \pm 117$  pg/mL) or stat. ph. parasites ( $623 \pm 764$  pg/mL vs.  $257 \pm 326$  pg/mL). In hMDDC2, the production of TNF- $\alpha$  was diminished upon co-incubation of the cells with viable or stat. ph. *Lm* in presence of  $\alpha$ -CD11b. Apoptotic *Lm* in general induced only a weak secretion of TNF- $\alpha$  in hMDDC2 ( $156 \pm 191$  pg/mL), which was not altered in presence of  $\alpha$ -CD11b.

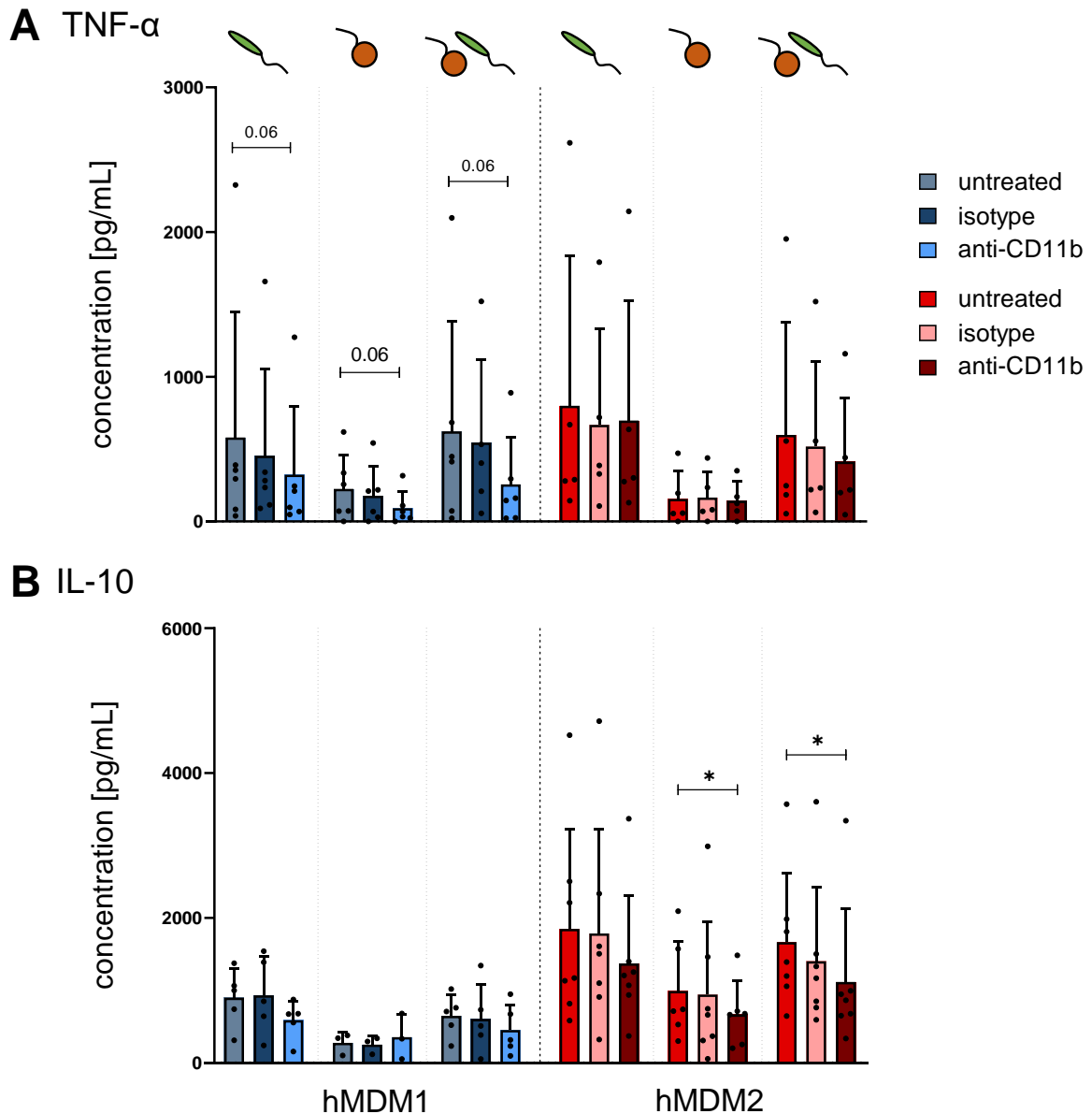


**Figure 30: Blocking of CR3 results in strong reduction of TNF- $\alpha$  and IL-10 secretion by hMDMs.** hMDM1, hMDM2 and hMDDC generated from CD14 MACS-purified monocytes were treated with  $\alpha$ -CD11b or its corresponding isotype control for 30 min. Cells were differentially infected for 3 h and non-internalized parasites were removed. 24 h post-infection, supernatants were collected and analyzed for **(A)** TNF- $\alpha$  and **(B)** IL-10 by ELISA. Data are presented as mean  $\pm$  SD from 3-7 donors of at least 3 independent experiments and were analyzed by paired Wilcoxon matched-pairs signed-rank test (\*  $p < 0.05$ ). Data were generated with the help of Mr Naphang Ho.

IL-10 production by untreated hMDM1 that were co-incubated with viable or apoptotic *Lm* was generally weaker in this experiment (Figure 30B) as compared to the previously obtained data (Figure 21B). In presence of  $\alpha$ -CD11b, we detected a reduced production of IL-10 in hMDM1 infected with viable *Lm* ( $590 \pm 270$  pg/mL) as compared to untreated hMDM1 ( $900 \pm 400$  pg/mL). Other than described before, higher amounts of IL-10 were secreted by hMDM2 as compared to hMDM1. Nonetheless, as expected, co-incubation of hMDM2 with apoptotic *Lm* alone ( $990 \pm 690$  pg/mL) or stat. ph. *Lm* ( $1660 \pm 950$  pg/mL) in

presence of  $\alpha$ -CD11b led to a significant reduction of cytokine secretion to  $660 \pm 460$  pg/mL (apoptotic *Lm*) and  $1120 \pm 1000$  pg/mL (stat. ph. *Lm*), respectively.

Taken together, blocking of CR3 had a significant effect on secretion of anti-inflammatory IL-10 in hMDM2 when challenged with pure apoptotic parasites or an infectious stat. ph. *Lm* mixture. This further indicated a connection between the diminished interaction with apoptotic *Lm* in presence of  $\alpha$ -CD11b and the establishment of an anti-inflammatory milieu *in vitro*. Based on this we further evaluated the effect of CR3 blocking on the induction of LC3 conversion and hence the ability of CR3 to trigger LC3-associated phagocytosis of apoptotic *Lm*.

#### 4.14 Blocking of CR3 reduces the LC3 conversion in hMDM2 upon uptake of apoptotic *Leishmania major* promastigotes

Blocking of CR3 significantly reduced the interaction of hMDM2 with apoptotic *Lm* and the production of anti-inflammatory IL-10 by hMDM2. In former studies from our group as well as in time-lapse microscopy experiments of differentially infected hMDMs (4.4), we observed that *Lm* can be internalized by LAP. Portions of both, viable and apoptotic promastigotes, resided within LC3<sup>+</sup> phagosomes in which they are eventually degraded (Figure 11 and Figure 12). Interestingly, Gluschko et al. showed that engagement of CR3 by the food-borne bacterium *Listeria monocytogenes* on murine macrophages resulted in LAP induction which helped in resolution of infection (Gluschko et al., 2018). Hence, we wanted to examine whether blocking of CR3 also leads to a diminished induction of LC3 conversion during *Leishmania major* promastigote infection. In former studies we already excluded LC3 lipidation after *Lm* infection to be a result of canonical autophagy, hence determination of LC3 conversion by western blot correlates to induction of LC3-associated phagocytosis of *Lm* (PhD thesis R. Bohn, 2017; PhD thesis M. Thomas, 2015). In hMDM1, infection with viable or stat. ph. *Lm* resulted in slightly increased LC3-II to  $\beta$ -Actin ratios, indicating an enhanced conjugation of LC3 to phagosomal membranes (Figure 31A). In hMDM1 challenged with apoptotic *Lm* alone, no LC3 conversion was detected compared to uninfected control cells. These data are in line with previous observations by live cell imaging in this study in which LC3 recruitment to *Lm*-containing phagosomes was almost exclusively observed in hMDM2. In accordance, LC3 conversion in infected hMDM2 was



overall higher as compared to hMDM1 and almost no differences were detectable between the infection conditions in untreated macrophages (viable *Lm*: 1.9-fold induction, apoptotic *Lm*: 2.2-fold induction, stat. ph. *Lm*: 2.1-fold induction) (Figure 31B). Upon treatment with  $\alpha$ -CD11b, LC3 lipidation significantly declined in presence of apoptotic (1.3-fold induction) or stat. ph. *Lm* (1.3-fold induction) as compared to untreated controls. In CR3-modulated hMDM2 harboring viable *Lm*, we detected only weak changes in LC3 conversion.

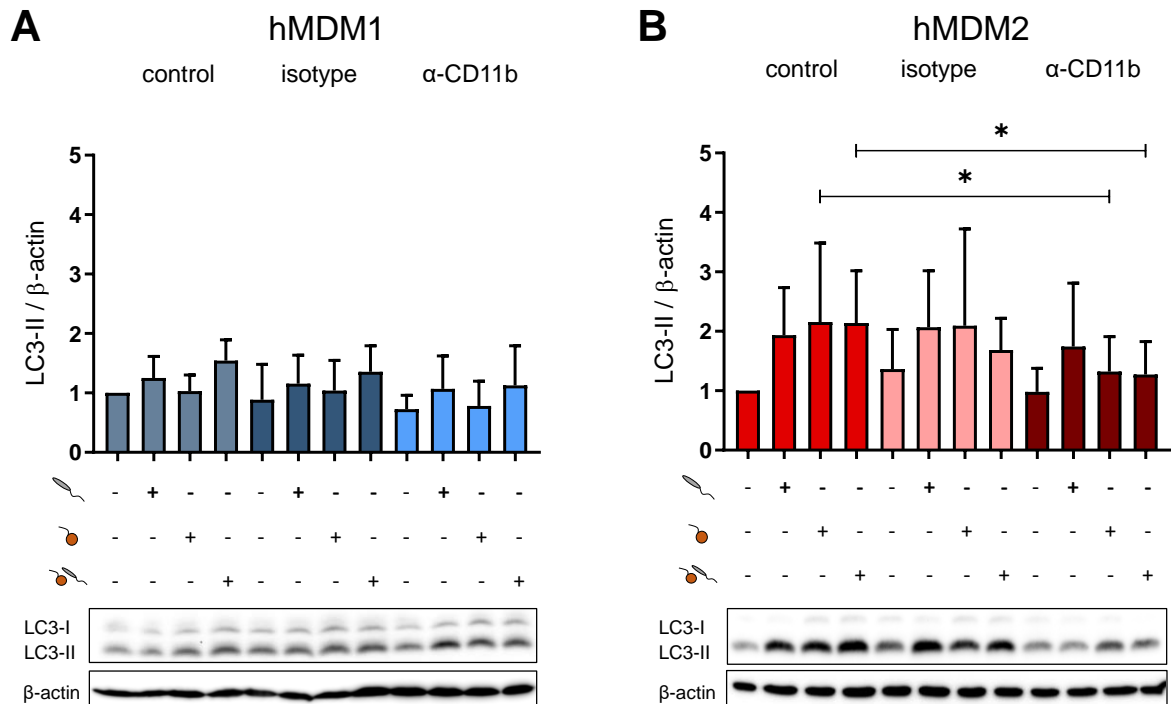


**Figure 31: LC3-associated phagocytosis of apoptotic *L. major* promastigotes is reduced by inhibition of CR3 in hMDM2.** hMDMs were pre-incubated with either  $\alpha$ -CD11b, its corresponding isotype control or were left untreated. Cells were co-incubated with viable, apoptotic or stat. ph. *Lm* (MOI 10) for 3 h. Lysates were analyzed by SDS-PAGE and immunoblotting for LC3 and  $\beta$ -Actin. LC3-II to  $\beta$ -Actin levels were determined by densitometry. Ratios were normalized to untreated control cells. Western blots are representative for one experiment. Data are presented as mean  $\pm$  SD of a minimum of 5-14 donors of at least 2 independent experiments and was analyzed by unpaired Mann-Whitney U-test (\*  $p < 0.05$ ).

Taken together our data reveal a significant reduction of LC3 conversion in hMDM2 upon treatment with  $\alpha$ -CD11b in the presence of apoptotic *Lm* alone or a stat. ph. infectious *Lm* mixture. This indicates a possible role of CR3 in induction of LC3-associated phagocytosis of apoptotic *L. major* promastigotes. It was now of interest whether a decreased uptake of apoptotic *Lm* and hence, the reduced induction of IL-10 production and LC3 conversion had an effect on the activation of the adaptive immune system.

#### 4.15 Decreased uptake of apoptotic *Leishmania major* promastigotes in presence of CR3 does not affect T cell proliferation

Crauwels et al. showed that during infection, the presence of apoptotic *Lm* within a stat. ph. reduced the *Lm*-specific T cell proliferation (Crauwels et al., 2015). In the present study, we observed that TNF- $\alpha$  production was strongly decreased in presence of the CR3 inhibiting antibody. In addition, release of the potent anti-inflammatory cytokine IL-10 was significantly downregulated by CR3 inhibition in stat. ph. *Lm*-infected hMDM2. Based on these findings, we hypothesized that modulation of CR3 inhibits uptake of apoptotic *Lm* and hence, secretion of IL-10 is decreased. This in turn could result in higher T cell proliferation stimulated by e.g. TNF- $\alpha$ . To investigate this, we infected hMDM1 and hMDM2 with stat. ph. *Lm* in presence of  $\alpha$ -CD11b or an isotype control. Log. ph. parasites, comprised almost exclusively of viable *Lm*, served as positive control since they were found to induce a high T cell proliferation (Crauwels et al., 2015). 24 h post infection, CFSE-labeled autologous PBLs were added. Six days later, CD3-positive T cells were identified by antigen staining and their proliferation was assessed by determination of the CFSE<sub>low</sub> cells within the population using flow cytometry (Figure 32A). In the presence of log. ph. or stat. ph. *Lm*-infected hMDMs, lymphocytes clustered around the macrophages indicating close vicinity for receptor binding and PBL activation (Figure 32B).

In hMDM1, as expected, log. ph. *Lm* induced a high T cell proliferation ( $47.1 \pm 21.2$  %) whereas in the presence of apoptotic *Lm*, proliferation was significantly reduced ( $33.6 \pm 20.7$  %) (Figure 33A). Other than anticipated, the blocking of CR3 did not lead to a decrease of CFSE<sub>low</sub> T cells ( $32.1 \pm 22.8$  %). In the presence of the isotype control, no interference with T cell proliferation was observed. Infection of hMDM2 with log. ph. *Lm* also resulted in proliferation of  $34.6 \pm 10.1$  % of the T cell population. Equally to hMDM1, the T cell proliferation in presence of a stat. ph. *Lm* infected hMDM2 was significantly decreased to  $21.3 \pm 9.0$  %. Treatment of hMDM2 with  $\alpha$ -CD11b prior to infection showed no effect on T cell proliferation ( $20.5 \pm 9.2$  %).

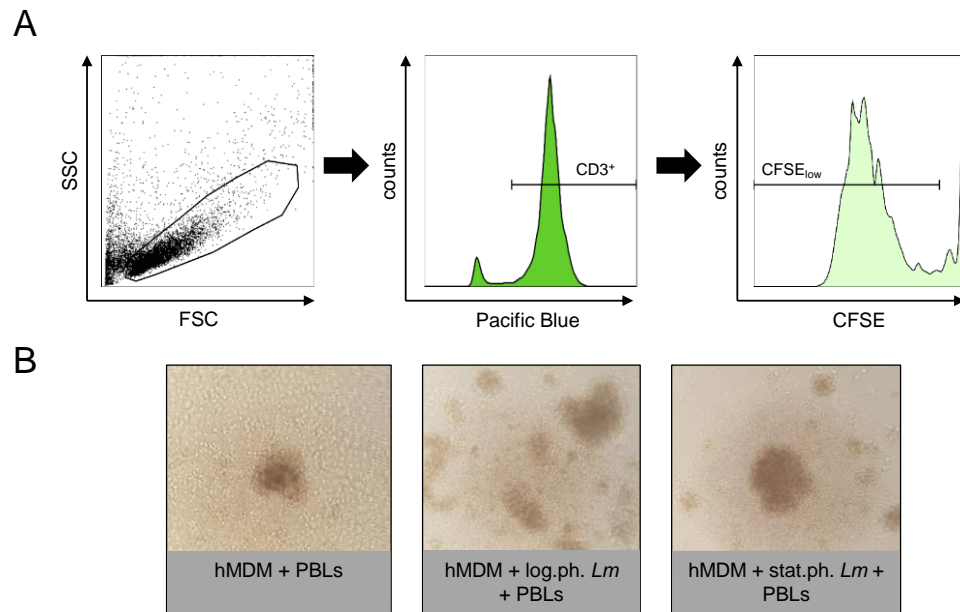


**Figure 32: Gating strategy for determination of proliferated T cells.** **A** hMDMs were treated with  $\alpha$ -CD11b or the isotype control for 30 min or were left untreated. Cells were infected with a log. ph. *Lm* or stat. ph. *Lm* (MOI 10) for 3h. At 24 h post-infection autologous, CFSE-labeled lymphocytes (PBLs) were added in a ratio of 1:5. After 6 days of co-culture T cells were analyzed by flow cytometry. Cells were gated by their FSC/SSC-properties and proliferation was assessed by determination of CFSE<sub>low</sub>-cells. **B** Micrographs exemplary show PBLs in co-culture with hMDMs infected with log. ph. or stat. ph. *Lm* after 6 days. Data were generated by Mrs. M. Boeck.

It is notable that T cell proliferation in presence of log. ph. *Lm*- and stat. ph. *Lm*-infected hMDM2 was lower than in hMDM1. Co-incubation of both macrophage subtypes with the isotypic antibody or  $\alpha$ -CD11b without subsequent infection did not result in T cell stimulation.

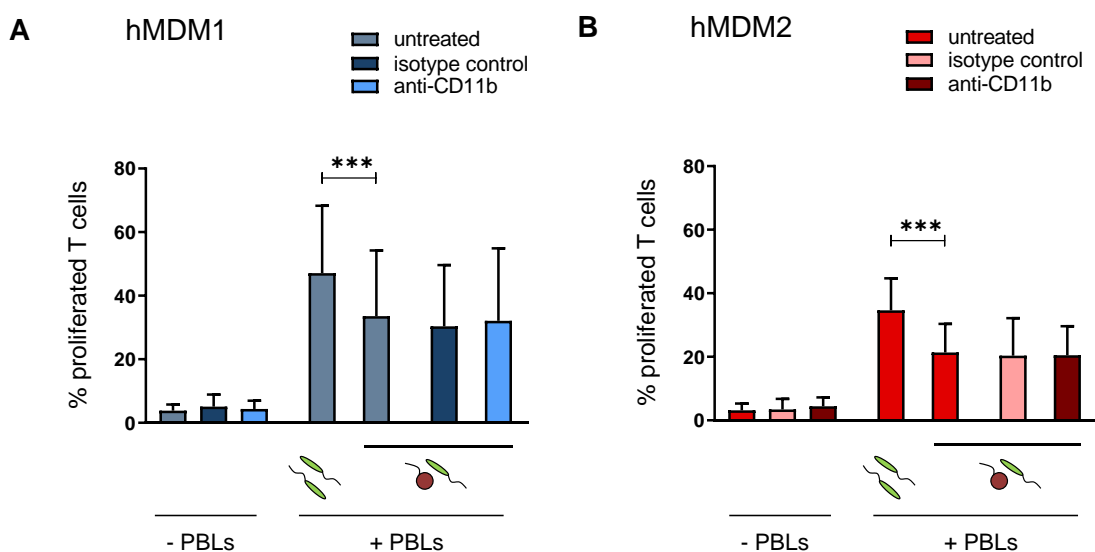


**Figure 33: T cell proliferation is unaltered in presence of  $\alpha$ -CD11b.** hMDMs were co-incubated with log. ph. or stat. ph. *Lm* (MOI 10) in presence or absence of  $\alpha$ -CD11b or in presence of an isotype control. Proliferation was determined as described in Figure 32A. Data are presented as mean  $\pm$  SD of 11 donors from at least 3 independent experiments and were analyzed by paired t-test (\*\*\*)  $p < 0.001$ ). Data were generated by Miriam Boeck.

Contrary to our hypothesis, reduced phagocytosis of apoptotic *Lm* by blocking of CR3 and thus, a decrease in anti-inflammatory IL-10 production and LC3 conversion, did not alter the activation of an adaptive immune response.

#### 4.16 Blocking of CR3 and the effect on parasite survival

Inhibition of CR3 did not influence T cell proliferation. Thus, we addressed the question whether uptake of apoptotic *Lm* via CR3 affects survival of viable *Lm* within the host macrophages. We hypothesized that during infection, apoptotic *Lm* support transformation of viable *Lm* into the amastigote stage and multiplication. Hence, diminished uptake of apoptotic *Lm* by CR3 blocking could lead to a decrease in parasite growth.

To study this, hMDMs were infected with stat. ph. *Lm*, with or without pre-incubation with  $\alpha$ -CD11b or the isotypic control, and differences in survival of the viable portion were assessed by limiting dilution assay 1 and 6 days post infection (dpi). One day post infection, we found more viable parasites per 1000 cells in CD11b-blocked hMDM1 ( $1270 \pm 1320$ ) as compared to untreated or isotype treated cells ( $960 \pm 250$  and  $930 \pm 1160$ ) (Figure 34). As expected, in hMDM1, after 6 days of cultivation, the number of parasites declined in untreated control cells ( $422 \pm 190$ ) indicating parasite killing. An even higher decrease in viable *Lm* was found in hMDM1 that were treated with  $\alpha$ -CD11b ( $120 \pm 110$ ) suggesting the decrease in apoptotic *Lm* uptake negatively affects survival of viable *Lm*. Of note, preincubation of the cells with the isotypic control resulted in the same decrease of parasites per 1000 hMDM1 ( $71 \pm 46$ ). In hMDM2, the initial parasite load 1 dpi was  $260 \pm 240$  parasites per 1000 untreated hMDM2. This was reduced in isotype-treated as well as in  $\alpha$ -CD11b-treated macrophages ( $108 \pm 49$  and  $106 \pm 54$  parasites per 1000 hMDM2). After 6 days, the number of intracellular viable *Lm* was decreased to  $171 \pm 70$  in untreated control cells. Compared to this, we observed a slight reduction of parasite numbers in hMDM2 that were pre-treated with  $\alpha$ -CD11b ( $130 \pm 105$  parasites). Isotype treatment of hMDM2 also impacted survival of viable *Lm* in this subtype.

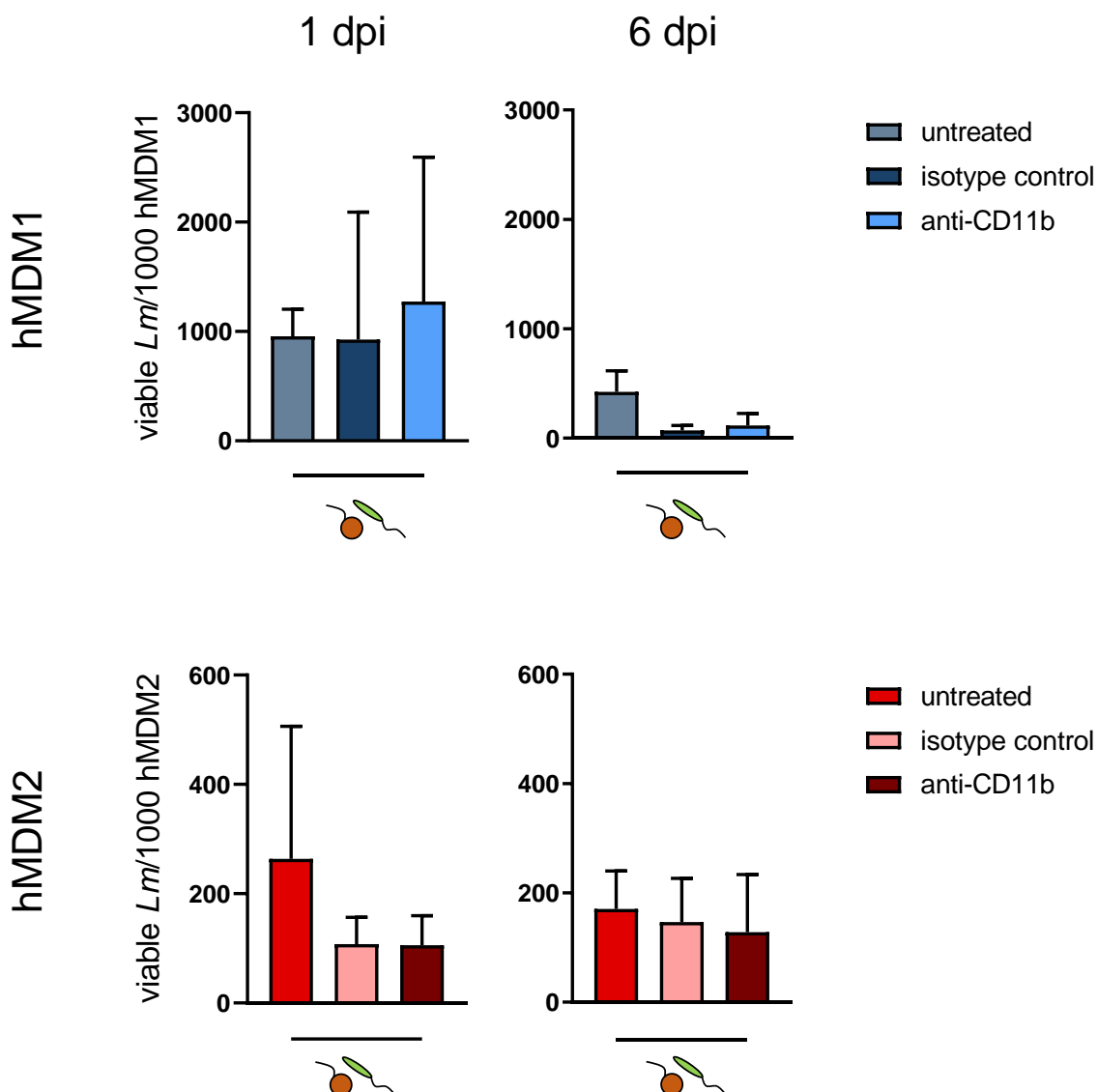


**Figure 34: Survival of viable *Lm* is not altered upon inhibition of CR3.** hMMDM1 and hMMDM2 were infected with stat. ph. *Lm* (MOI 10) for 3 h in the presence or absence of  $\alpha$ -CD11b or the isotype control. 21 h post infection,  $2 \times 10^3$  hMMDMs were serially diluted in quadruplicate wells (1.5-fold dilutions) in NNN-blood-agar plates and incubated for 7 days at 27°C (1 dpi). The serial dilution was repeated 6 days post infection (6 dpi). Parasite survival was determined by calculation from the last dilution that showed parasite growth and equals  $1.5^{\text{EXP}}$  (mean dilution with parasitic growth). Data are presented as mean  $\pm$  SD from 3-6 donors from at least 2 independent experiments and were analyzed by paired Wilcoxon matched-pairs signed-rank test.

In summary, as expected, we found parasite killing in hMMDM1 which was enhanced when cells were treated with  $\alpha$ -CD11b. In hMMDM2 survival of viable *Lm* was slightly diminished 6 dpi upon CR3 blocking indicating no strong effect on the intracellular survival and multiplication of viable *Lm*. This suggests – at least in our setting - no particular role for apoptotic *Lm* internalization by CR3 in augmenting viable parasite survival. Notably, treatment of hMMDMs with isotype control antibodies also influenced survival of the viable population.

## 5. Discussion

We hypothesized that viable and apoptotic *Leishmania major* promastigotes are internalized by primary human macrophages in a process termed LC3-associated phagocytosis. Viable parasites escape degradation and multiply within the phagosomal compartment whereas processing of apoptotic parasites results in an anti-inflammatory host cell response that supports survival of the viable *Leishmania* population.

Using live cell imaging, we demonstrated that indeed portions of viable and apoptotic *L. major* promastigotes (*Lm*) are targeted by LC3-associated phagocytosis (LAP) in human monocyte-derived macrophages (hMDMs). Quantification of live cell imaging videos revealed a more rapid recruitment of LC3 to phagosomes that contained apoptotic *Lm* in hMDM2. Data suggested that apoptotic promastigotes are degraded in LAP-compartments but viable *Lm* resist degradation. We investigated the presence of openings from the phagosome to the extracellular space as possible evasion strategy for viable promastigotes by immunofluorescence staining of infected, non-permeabilized macrophages. Quantification indicated tunnel-structures to be present on a quarter of all viable *Lm*-containing phagosomes. With the focus on cytokine production, we found that in addition to secretion of anti-inflammatory IL-10, and other than hypothesized, apoptotic *Lm* also induced production of pro-inflammatory cytokines in hMDMs and human monocyte-derived dendritic cells (hMDDCs). Successful purification of apoptotic *Lm*-containing phagosomes and subsequent mass spectrometric analyses of their proteome revealed approximately 1000 leishmanial and 2000 human proteins within the compartments and identified the host phagocytic receptors CD91 and CR3 to be highly abundant. We did not find connections between CD91 and LAP of *Lm* since knockdown of the receptor showed no influence on the internalization of viable or apoptotic *Lm* by hMDMs. Modulation of CR3 by siRNA knockdown or with a functional antibody was successful and decreased uptake of apoptotic *Lm*. Antibody blocking resulted in downregulation of TNF- $\alpha$  and IL-10 production in both hMDM phenotypes and a reduced LC3 conversion upon co-incubation of hMDM2 with apoptotic or stationary phase (stat. ph.) *Lm*. However, the reduced internalization of apoptotic *Lm* was not affecting *Lm*-specific T cell proliferation. After infection of hMDMs with stat. ph. *Lm*, intracellular survival of viable *Lm* was reduced when hMDM1 were treated with the inhibitory antibody. Survival was slightly reduced when uptake of apoptotic *Lm* was inhibited by antibody treatment of hMDM2.

**Live cell imaging of *Leishmania major* promastigote infection**

Apoptotic promastigotes, present in the infectious *Leishmania* inoculum, are targeted by LC3-associated phagocytosis which results in downregulation of the adaptive immune response (Crauwels et al., 2015). From several investigations on infection with pathogenic bacteria, fungi and parasites, but also from studies addressing uptake of apoptotic cells, it was reported that LAP targets, at least temporally, only portions of internalized microbes or cells (reviewed in Schille et al., 2017). This is in line with our findings from live cell microscopy in which only few phagosomes that contained apoptotic *Lm* but also phagosomes that harbored viable *Lm* were detected to be LC3-positive. Disparities in LC3 recruitment between the present study and previous data from our group, in which a majority of apoptotic *Lm* were found to be in compartments positive for LC3 (Crauwels et al., 2015), might be attributed to the different infection conditions, imaging techniques and sample preparations. In contrast to the analysis of LC3 compartments in *Lm*-infected macrophages at a fixed time point of 3 h post infection, we employed 3D live cell microscopy to image viable or apoptotic *Lm* uptake by transduced macrophages. It is eminent that LC3 recruitment occurs within less than 3 h after parasite internalization. Thus, live cell imaging is the superior method since the dimension of time can be taken in account providing a surplus of information as compared to fixed samples (Stephens and Allan, 2003).

In hMDM2, LC3 was recruited significantly quicker towards apoptotic *Lm*-containing compartments than to compartments harboring viable *Lm*. Martinez et al. described that apoptotic SVEC epithelial cells are targeted by LC3 as early as 35 min post-internalization in murine macrophages *in vitro* and LAP resulted in rapid degradation of apoptotic SVEC cells within 2 h post LC3 recruitment. This is in line with the mean duration of 35 min for LC3 recruitment towards apoptotic *Lm*-containing phagosomes in hMDM2 observed in our study. For apoptotic *Lm*, degradation following LC3 recruitment was also enhanced as compared to degradation of apoptotic *Lm* within phagosomes that lack LC3. The fact that LC3 dissociated from phagosomes before the onset of degradation is confirmed by data by Romao et al. who investigated zymosan-containing LC3<sup>+</sup> phagosomes in hMDMs (Romao et al., 2013). In contrast, Martinez and colleagues reported that LC3 has to be present on the phagosome to facilitate lysosomal fusion in murine macrophages (Martinez et al., 2011). These contradicting data show that it must be considered that there are strong differences

in LAP between the murine and the human system. In the murine system, LAP is more rapidly and LC3<sup>+</sup> phagosomes are short-lived (Martinez et al., 2011; Sanjuan et al., 2007). In human macrophages, LC3 compartments were shown to persist for 4 h and more (Romao et al., 2013) which is in line with our observations. Romao et al. further propose LAP vesicles to be stabilized and serve the prolonged MHCII antigen presentation (Romao et al., 2013; Romao and Münz, 2014). In contrast, our data suggest a more rapid decoration of phagosomes with LC3 which mediates an accelerated fusion with lysosomes. To clarify this, a higher number of LC3<sup>+</sup> phagosomes that contain apoptotic *Lm* should be analyzed regarding degradation of the cargo. For this, apoptotic *Lm* conjugated to pHrodo, a pH sensitive dye, could be used (Miksa et al., 2009). The fluorescence of this dye gradually increases with decreasing phagosomal pH, indicating fusion with lysosomes. This should be combined with automated particle tracking to evaluate the data in an unbiased manner. Hence, a more detailed analysis of apoptotic *Lm* uptake and degradation could be performed.

We found viable *Lm* to resist degradation within LC3-positive compartments which is in concordance with previous studies showing that viable *Lm* escape LAP by the action of the *Leishmania* surface metalloprotease GP63 (Matte et al., 2016). This evasion could also be the reason for the small number of viable parasites in LC3<sup>+</sup> compartments as detected by live cell imaging in the present study but does not explain the impaired degradation of viable *Lm* in phagosomes that were already LC3-decorated. Viable *Lm* are highly active and dynamic during uptake by macrophages. Forestier et al. described the flagellar movement of viable *L. donovani* promastigotes to serve the re-orientation within the cell. As a result, continuous oscillatory parasite movement leads to host cell membrane wounding (Forestier et al., 2011). This might explain the detection of a compartment harboring a viable *Lm* parasite which was connected to the extracellular space by a tunnel-like structure in former studies. In the present study, a first attempt to quantify such tunnel-like structures by immunofluorescence microscopy revealed their presence for a quarter of all viable *Lm*-harboring phagosomes early after infection. This further strengthens our assumption that tunnel-structures, connecting the phagosome with the extracellular space, could delay or impair acidification of the phagolysosome or serve the exclusion of hydrolytic enzymes that would otherwise facilitate parasite degradation. For a more detailed analysis of this, one could employ inducible expression of a fluorescent marker by



viable *Lm* (Taheri et al., 2015). Expression could be induced by a low molecular weight compound that is not membrane permeable and exclusively internalized by viable promastigotes. If there was a connection from the outside of the cell to the phagosome, the compound could be internalized by the parasite and initiate transcription of the fluorescent protein-coding gene whereas absence of a tunnel-like structure would deny induction of fluorescent protein synthesis. Inducible recombinant production of proteins in non-pathogenic *L. tarentolae* is already in use (Niimi, 2012). Alternatively, a synthetic substrate for the leishmanial surface protease GP63 could be used which fluoresces upon cleavage (Bouvier et al., 1993). The respective reporter system should be combined with high resolution light microscopy techniques on live cells such as STED (Vicidomini et al., 2018) or a correlative light and electron microscopy (CLEM) approach using live cell confocal imaging together with FIB-SEM or STEM to confirm openings from the phagosome to the outside of the cell on the ultrastructural level.

We conclude that the mechanism of LAP is preferred for uptake of portions of viable and apoptotic *Lm* by anti-inflammatory hMDM2 which allows for rapid processing of the internalized apoptotic parasites. Our data emphasize that live cell imaging is the method of choice to quantify compartment formation during *Lm* infection since temporal information is included. Light microscopy confirmed tunnel structures within the infected host macrophage that might serve viable *Lm* survival but need to be investigated in detail by combination of reporter systems with more sophisticated microscopy methods in future studies.

### **Cytokine secretion upon differential infection with *Leishmania major* promastigotes**

We confirmed the correct differentiation of *in vitro*-generated macrophages and dendritic cells by antigen staining which is in line with reports from literature (Biswas et al., 2012; Collin et al., 2013; Sloma et al., 2008; Tomiotto-Pellissier et al., 2018). We further categorized hMDMs and hMDDCs by their cytokine profiles upon *Lm* infection. Intriguingly, we found pro-inflammatory cytokine production upon stimulation with apoptotic *Lm*. This contradicts not only our hypothesis but also *in vitro* studies from Fadok and colleagues that showed that uptake of apoptotic cells inhibits production of IL-1 $\beta$  and IL-8 (Fadok et al., 1998). However, in line with our findings, in a study from Kurosaka et al. it was reported

that the secretion of pro-inflammatory mediators is enhanced in macrophages that were co-incubated with apoptotic thymocytes (Kurosaka et al., 2001). Niessen and colleagues described apoptotic cell-derived microparticles in combination with IFN- $\alpha$  to induce inflammatory responses in human monocytes (Niessen et al., 2015). Of note, in our multiplex data set, IFN- $\alpha$  was found to be secreted by hMDM2 in response to apoptotic *Lm*. Induction of pro-inflammatory signaling upon apoptotic cell ingestion can also be caused by an inefficient degradation (Fadok et al., 2001) which in our study might be linked to a high burden of apoptotic *Lm* and impaired capability to degrade all internalized apoptotic promastigotes. This should be tested by co-incubation of macrophages with differing MOIs of *Leishmania* parasites followed by ELISA analysis of cell supernatants.

We detected a high TNF- $\alpha$  release upon infection of macrophages with viable parasites which was increased in hMDM2, probably due to the more efficient uptake of *Lm* as compared to hMDM1. TNF- $\alpha$  is described to be reduced upon internalization of apoptotic cells (Michlewska et al., 2009). In line with this, TNF- $\alpha$  production upon stimulation of hMDM2 with apoptotic *Lm* was reduced. Data from Crauwels and Caldas indicated an increased production of IL-10 in presence of viable *Lm* in human macrophages. This was proposed to counteract an overwhelming pro-inflammatory response by TNF- $\alpha$  or IFN- $\gamma$  but could not be confirmed by our experiments on characterization of myeloid cells (Caldas et al., 2005; Crauwels et al., 2015).

An augmented IL-10 release after co-incubation of hMDMs with apoptotic or stat. ph. *Lm* confirms studies by van Zandbergen that showed the other major anti-inflammatory cytokine TGF- $\beta$  to be secreted by phagocytes in response to purified apoptotic *Lm* (Zandbergen et al., 2006). Further supporting our observations, Freire-de-Lima and colleagues reported that upon investigations of *Trypanosoma cruzi* infection, that apoptotic parasites severely increased production of anti-inflammatory cytokines which supported viable parasite growth (Freire-de-Lima et al., 2000). Also, *in vitro* studies on *Lm*-infected murine macrophages revealed that release of the potent anti-inflammatory IL-10 upon internalization of apoptotic PMNs enabled parasite replication and suggests crucial roles for IL-10 in parasite survival by counteracting inflammation (Filardy et al., 2010).

In our study, secretion of IL-1 $\beta$ , IL-6 and IL-8 by monocyte-derived myeloid cells occurred upon infection with pure viable but also upon co-incubation with apoptotic or stat. ph. *Lm* and independently of the infected monocyte-derived cell type. *In vivo* infection with viable

*Lm* induces the production of pro-inflammatory mediators such as IL-1 $\beta$ , IL-8, IL-6 and TNF- $\alpha$  (Maspi et al., 2016). *In vitro*, Crauwels et al. found an increased production of pro-inflammatory IL-1 $\beta$ , IL-6 and TNF- $\alpha$  in log. ph. *Lm*-infected hMDM2 whereas production of these cytokines was decreased in presence of apoptotic *Lm* (Crauwels et al., 2015). Induction of pro-inflammatory cytokine secretion might serve the recruitment of more phagocytes which increases uptake of viable *Lm* from the infectious inoculum. This auto-adjuvant function might allow more viable *Lm* to reside within host cells, transform into amastigotes and multiply.

In conclusion, IL-10 which was secreted in higher amount upon uptake of apoptotic *Lm* might counteract an overwhelming inflammatory response. It is of interest whether the release of IL-10 is sufficient to facilitate a balance of the cytokine response. Therefore, more investigations on cytokine secretion (e.g. on the potent anti-inflammatory cytokine TGF- $\beta$ ) in response to differential infection are needed. We assume that a high pro-inflammatory cytokine production by hMDMs and hMDDCs upon internalization of apoptotic *Lm* could serve the recruitment of more phagocytes to the site of infection, enhancing uptake of viable *Lm*. Modulation of single cytokines by use of neutralizing antibodies could further decipher the impact of the single mediators and their role in human *Leishmania* infection.

### **Phagosome isolation and mass spectrometry**

The isolation of pathogen-containing phagosomes for identification and characterization of molecules involved in cargo internalization has been used for decades (Berton et al., 1982; Zeichner, 1983). The method employed here was established by Steinhäuser et al. and allowed to enrich phagosomes from a relatively small number of murine macrophages as previously demonstrated for *Listeria monocytogenes*- and *Mycobacteria*-containing compartments (Steinhäuser et al., 2013). The phagosomal proteome was screened for host cell-derived proteins which provided a dataset of about 2000 targets of which we focused on the most abundant proteins, as discussed below. Unexpectedly, western blot analysis and MS also revealed presence of high amounts of mitochondrial proteins within the isolated compartments (data not shown, available on request). Enrichment of some of these mitochondrial proteins within the samples makes it unlikely to be a simple

contamination. Recent research suggests that mitochondria-derived vesicles (MDVs) transport mitochondrial ROS to phagosomes that contain *Staphylococcus aureus*. It was shown that this mechanism contributes to killing and degradation of the bacteria (Abuaita et al., 2018). Surprisingly, in our study, e.g. Cox4 and mitochondrial ATPases that were found to be highly abundant in the phagosomes, as identified by MS, are all located at the inner mitochondrial membrane which makes it unlikely that these proteins are part of MDVs. In a study from West et al. they found that engagement of TLRs leads to recruitment of mitochondria to phagosomes, thereby augmenting antimicrobial ROS production within the compartment (West et al., 2011). TLR2, which was present in our isolated phagosomes, could account for this observation in our study. Moreover, fusion of mitochondria with components of the endolysosomal system, independent from mitophagy, has been reported earlier which could also be a reason for co-isolation of parts of this organelle (McLelland et al., 2016). Investigating a possible connection of apoptotic *Lm*-containing phagosomes with mitochondria by microscopy could provide first insights in elucidating the presence of numerous mitochondrial proteins within samples of the isolated phagosomes.

The LAP marker protein LC3 was detected almost exclusively in its PE-conjugated form (LC3-II) within the magnetic fraction after phagosome isolation, indicating isolation of LC3<sup>+</sup> phagosomes. However, the proportion of LC3-decorated phagosomes within the total amount of isolated phagosomes remained unclear. The initial hypothesis of this study was based on the finding that a vast majority of all apoptotic *Lm* in hMDM2 reside within LC3<sup>+</sup> phagosomes (Crauwels et al., 2015). Hence, we expected to almost exclusively isolate these LAP compartments. As observed by live cell microscopy, only a small proportion of phagosomes are decorated with LC3. To improve enrichment of only LC3<sup>+</sup> compartments in future experiments, phagosomes could be labeled for LC3 with fluorophore-conjugated antibodies and separated from LC3<sup>-</sup> phagosomes by fluorescence-activated cell sorting. The drawback of this approach would be the very likely degradation of the compartments' proteome since devices for cell sorting are usually not cooled. Also, in the non-magnetic fraction of our present isolation, we detected LC3-II which could be attributed to autophagosomes or an incomplete isolation of parasite-containing phagosomes. Possible co-isolation of autophagosomes should be excluded by verification of absence of the autophagy specific protein p62/sequestosome-1 in the magnetic fraction by western blot as it is known to be dispensable for phagocytosis and LAP of apoptotic *Lm* or *Listeria*

*monocytogenes* (Crauwels et al., 2015; Lam et al., 2013). Remarkably, no LC3 but the Atg3 component of the LC3 lipidation machinery (Atg7-Atg3) was detected by MS. The absence of LC3 is very likely to be caused by MS-specific features, since LC3 was identified using a well-established and specific antibody in western blot analysis. It is known that lipidated proteins and peptides, like LC3-II, can be hard to ionize (ion suppression) which denies detection by MS (Tate et al., 2015). In addition, lipid-interacting proteins often resist complete proteolytic digestion prior to mass spectrometry, or the associated lipids make MS-analysis challenging (Hoofnagle and Heinecke, 2009).

Concluding, the performed magnetic isolation technique allowed for specific enrichment of *Lm*-containing phagosomes from hMDM2. Moreover, MS analysis of the phagosomal proteome serves as powerful tool to determine candidates for characterization of phagocytic pathways and compartment maturation providing numerous targets for detailed investigation of phagosome biogenesis and maturation. An assumed connection between apoptotic *Lm*-containing phagosomes and mitochondria could be investigated by microscopical analyses of *Lm*-phagosomes in connection with e.g. the mitochondria-specific fluorescent probe MitoTracker.

### **Function of CD91 and CR3 in *Leishmania major* promastigote phagocytosis**

MS identified the phagocytic receptors CD91 and CR3 to be present in high amounts within isolated phagosomes. Both receptors are known for phagocytosis of apoptotic cells (Mevorach et al., 1998; Ogden et al., 2001). We detected CD91 exclusively on hMDMs contradicting observations that found CD91 to be highly present on monocyte-derived dendritic cells (Cappelletti et al., 2015). In contrast to the present study in which we determined expression of CD91 on immature hMDDCs, Cappelletti et al. examined activated, mature monocyte-derived dendritic cells. Stat. ph. *Lm*-infected hMDDCs lack LAP (PhD thesis P. Crauwels, 2015), thus, we hypothesized that this receptor might trigger LAP of apoptotic *Lm* in hMDMs.

Binding of an  $\alpha$ -CD91 antibody for blocking of the receptor seemed to be a transient event which could be the result of a high turnover of the receptor. The amount of LRP4, a structurally closely related receptor of the same family, was shown to be decreased by more than 50 % after 3 h of incubation in a pulse-chase experiment (Melman et al., 2002).

In the present study, downregulation of CD91 synthesis in hMDMs by specific siRNA was efficient but did not affect the internalization of viable or apoptotic *Lm*. It is known that CD91 also serves as a main regulator of inflammation in macrophages (Gaultier et al., 2008). CD91 signaling inhibits NF- $\kappa$ B activation and includes downregulation of the TNF receptor on the cell surface of macrophages, prohibiting autocrine TNF- $\alpha$  signaling (Gaultier et al., 2008). In CD91-deficient macrophages, the response to the inflammatory agent LPS is enhanced as compared to CD91 positive cells (Mantuano et al., 2016). In addition, CD91 affects murine macrophage polarization by promoting the anti-inflammatory phenotype, giving further hints for a functional role of the receptor in establishment of an anti-inflammatory microenvironment (May et al., 2013). These reports suggest a negative regulation of inflammatory mediators by CD91 signaling which could serve the establishment of the anti-inflammatory response elicited by engagement by apoptotic cells. To proof this hypothesis, supernatants of CD91 knockdown cells and untreated hMDMs should be analyzed regarding possible alterations in the secretion of pro-inflammatory cytokines such as TNF- $\alpha$  upon co-incubation with apoptotic *Lm*.

For decades, CR3 is known to mediate phagocytosis of viable *Lm* (Mosser and Edelson, 1985) and is described as receptor for apoptotic cells (Mevorach et al., 1998; Skoberne et al., 2006). To date, all studies addressing the role of CR3 in phagocytosis of *Leishmania* by macrophages use purified metacyclic parasites from liquid cultures and neglect the presence of apoptotic promastigotes within the infectious inoculum in the natural route of infection (Polando et al., 2013; Rosenthal et al., 1996; Ueno et al., 2009). However, it was recently shown that in PMNs infection with viable *Lm* increases the expression of CR3. This in turn leads to an enhanced uptake of apoptotic PMNs and thus higher viable *Lm* survival showing the relevance of apoptotic cell uptake by CR3 for *Lm* infection (Salei et al., 2017). Mevorach et al. reported that uptake of apoptotic thymocytes or PMNs by human macrophages is decreased by ~60 % when CR3 was blocked with a functional antibody (Mevorach et al., 1998). Further, phagocytosis of apoptotic Jurkat cells opsonized with iC3b was strongly decreased in presence of a functional blocking antibody (Takizawa et al., 1996). In line with this, blocking of CR3 with an antibody significantly inhibited internalization of apoptotic *Lm* by hMDMs in the present study. In contrast to earlier investigations (Beller et al., 1982; Cooper et al., 1988; Mosser and Edelson, 1985), phagocytosis of viable *Lm* was not inhibited by CR3 blocking in our experiments. Only when

CR3 was knocked down by siRNA treatment, an effect on viable *Lm* internalization could be observed. Previous studies employed a different clone of the functional monoclonal CR3 specific antibody and focused on murine macrophages which could be causative for the varying results. As reported by Wilson and Pearson, the  $\alpha$ -CD11b clone used in the present study was not as effective in inhibition of viable *L. donovani* promastigote-attachment to hMDMs which could account for the poor or non-detectable inhibition of interaction of viable *Lm* (Wilson and Pearson, 1988).

The low but significant differences in interaction of hMDMs with apoptotic *Lm* upon CR3 blocking could be explained by availability of several receptors on the macrophage surface facilitating internalization of the apoptotic parasites, similar to viable *Lm* (Ueno and Wilson, 2012). This is in line with our MS screen of phagosomes which revealed presence of multiple receptors known to be involved in phagocytosis (data not shown). Further, treatment of macrophages and dendritic cells with  $\alpha$ -CD11b did not block all CD11b receptor subunits on the surface of the cells. Since, we do not know how few un-blocked receptors might be sufficient to facilitate binding and entry of a *Lm* parasite, the incomplete blocking of CR3 might explain the low but clear inhibition of apoptotic *Lm* uptake. In addition to the infection rates that display the percentage of infected cells, also the parasite load per cell should be determined microscopically which would allow to assess possible differences in the number of internalized viable and apoptotic *Lm*.

In this study, hMDDCs internalized viable as well as apoptotic *Lm* but to a lower extent than hMDMs. CR3 blocking on DCs resulted in significantly higher uptake of viable *Lm*, indicating elevated susceptibility. This might be explained by an increased usage of other receptors upon CR3 blocking as reported from studies on murine DCs and macrophages (Schönlau et al., 2000; von Stebut and Tenzer, 2018). In addition, blocking with a monoclonal antibody could stimulate DCs, activate them and result in an even higher phagocytosis. Further, in *Leishmania* infection, monocyte-derived DCs preferably internalize the amastigote life stage and mainly serve the antigen presentation at the inflammatory site explaining low infection rates (Feijó et al., 2016; Woelbing et al., 2006). Nonetheless, DCs are a crucial player in *Leishmania* promastigote infection since they are the major antigen-presenting cells and effective mediators for the activation of the adaptive immune system (von Stebut and Tenzer, 2018).

In sum, we found CD91 not to contribute to uptake of viable or apoptotic *Lm* but literature suggests that it could play a role in anti-inflammatory signaling in macrophages on which should be aimed at in future studies. Our data, for the first time, provide evidence that CR3 is involved in the internalization of apoptotic *Lm*. For viable *Lm*, inaccessibility of CR3 due to antibody blocking might be compensated by usage of other receptors by allowing for unimpeded entry into the cell. Our data indicate, as known for viable *Lm*, that not only a single receptor is responsible for internalization of the apoptotic parasites. Other receptors found in the MS screen should be investigated by modulation analogous to CD91 and CR3.

### **CR3 blocking and the effect on cytokine secretion**

The high secretion of TNF- $\alpha$  by macrophages in presence of viable *Lm* was strongly decreased in  $\alpha$ -CD11b treated cells. This indicates a functional role of CR3 in the induction of TNF- $\alpha$  signaling as reported by Huang et al. who found CR3 depletion resulting in decreases in TNF- $\alpha$  upon infection with *Histoplasma capsulatum* (Huang et al., 2015). Moreover, our observations in the present study are in agreement with results from Crauwels et al. who detected a diminished TNF- $\alpha$  production in hMDM2 infected with stat. ph. *Lm* as compared to infection with viable, log. ph. *Lm*. Our data also show that in hMDM2 apoptotic *Lm* downregulate TNF- $\alpha$  production and are in line with the report from Voll et al. in which apoptotic PBLs inhibit LPS-induced TNF- $\alpha$  release (Voll et al., 1997). Interestingly, when we treated hMDM2 with the CR3-specific functional antibody, IL-10 production in presence of purified viable or apoptotic *Lm* or stat. ph. promastigotes was drastically reduced. This indicates a role for CR3-mediated phagocytosis in modulation of the anti-inflammatory cytokine response towards *Leishmania* infection and is supported by the fact, that CR3 facilitates silent entry of cargo into the macrophage first described by the group of David Sacks (Da Silva et al., 1989). Murine macrophages deficient for Atg7, which is part of the LC3 conjugation machinery in LAP, also showed reduced IL-10 production in presence of apoptotic cells which was accompanied by an increase in pro-inflammatory IL-1 $\beta$  and IL-6 (Martinez et al., 2011). This, in regard of the decreased IL-10 production in presence of  $\alpha$ -CD11b, points to a possible role of CR3 in LAP induction serving the rapid degradation of apoptotic *Lm* as described above.



It should be mentioned that our study gives contradicting results for release of TNF- $\alpha$  and IL-10 in untreated but differentially infected hMDMs. Higher TNF- $\alpha$  secretion induced by viable *Lm*, as detected in the latter experiments regarding cytokine production in connection with CR3 inhibition is in line with literature (Afonso et al., 2008; Crauwels et al., 2015). It is in so far unexpected, that the parasite and cell preparations as well as conditions of infection were the same throughout the study. It might be speculated that infection rates were different or that the strong heterogeneity between the donors tested is connected to different outcomes of TNF- $\alpha$  and IL-10 secretion. Blood donations for monocyte isolation come from healthy but anonymous donors with an unknown disease-history and lifestyle which surely could affect experimental results (ter Horst et al., 2016). Of note, in CR3 blocking-experiments, TNF- $\alpha$  secretion seems to depend on IL-10 secretion and *vice versa* in both macrophage subtypes. This further strengthens the proposed mechanism of counteraction of an overwhelming inflammation by IL-10 (Crauwels et al., 2015).

In conclusion, despite contradicting data on cytokine production, data infers that the viable *Lm*-induced TNF- $\alpha$  production in hMDM1 can be modulated by CR3 inhibition. Significant reduction in IL-10 secretion upon CR3 blocking in apoptotic *Lm*-challenged hMDM2 further strengthens the evidence for the anti-inflammatory character of CR3 which suggests an immune regulating role in *Lm* infection.

### **CR3 and LAP induction**

In accordance with our findings from live cell imaging experiments, LC3 lipidation was elevated in hMDM2 and occurred equally often upon infection with viable, apoptotic or stat. ph. *Lm*. Gluschko et al. recently found CR3 to induce LAP in mice that are infected with *Listeria monocytogenes* (Gluschko et al., 2018). Concordantly, here we showed that inhibition of CR3 clearly reduced LC3 lipidation and hence LAP of apoptotic *Lm*. This could implicate either that the reduced uptake of apoptotic *Lm* also decreases the proportion of LC3 targeted phagosomes or that CR3 is responsible for induction of LAP. The latter is supported by the fact, that LC3 conversion is almost reduced to the level of non-infected hMDM2 upon challenge with apoptotic or stat. ph. *Lm*. In contrast, the weak detected residual LC3 conversion after CR3 blocking and infection could implicate that a co-receptor is involved in induction of LAP. Several receptors are described to trigger LAP e.g. TLR2,

Fc receptors, Dectin-1 or Tim-4 (Huang et al., 2009; Kyrmizi et al., 2013; Martinez et al., 2011; Sanjuan et al., 2007). TLR2 was identified in our MS screen (data not shown) and it could be assumed that TLR2 and CR3 might function in a cooperative manner. TLR2 interacts with surface LPG of *Lm*. To assess a functional role of TLR2 in LAP of apoptotic *Lm* and the possible engagement of LPG, the presence of LPG on the surface needs to be verified.

In line with the claim that CR3 induces LAP is a report from Li et al. who found CR3 to trigger phagocyte ROS production, crucial for LC3 recruitment, downstream of Shp2 and Erk signaling (Li et al., 2015). For a more detailed elucidation of CR3-mediated LAP, recruitment of other factors that are important for LAP such as the NADPH oxidase (and subsequent ROS generation) and Rubicon should be quantified by immunofluorescence (IF) with or without modulation of CR3 (Martinez et al., 2015). Western blot analyses as performed in the present study should be employed in addition to fluorescence microscopy using either antibody staining or transduction of hMDMs with lentiviral particles, that code for the respective fluorescence-coupled protein to be analyzed, for elucidation of the LAP pathway during apoptotic *Lm* uptake as suggested by Klionsky et al. (Klionsky et al., 2016).

In conclusion, with the present study we provide first evidence for CR3-mediated LC3-associated phagocytosis in *Leishmania* pathogenesis. CR3 extends the list of receptors that induce LAP in infection scenarios and should be analyzed in more detail by means of quantification of differences in recruitment of LAP hallmarks such as Rubicon and the NADPH oxidase towards phagosomes by microscopy and modulation of the intracellular signaling cascades of CR3.

### **The effect of CR3 blocking on T cell proliferation and *Leishmania major* survival**

T cell proliferation upon infection of hMDMs with log. ph. *Lm* or stat. ph. *Lm* is in line with our previous report in which Crauwels et al. showed that *in vitro* infection of hMDM2 with stat. ph. *Lm* partly inhibited *Lm*-specific T-cell proliferation as compared to infection with log. ph. *Lm* (Crauwels et al., 2015). The capacity to stimulate T cells is more pronounced in hMDM1 than in hMDM2 which is in concordance with higher MHCII expression and pro-inflammatory cytokine production in this cell type (Mills and Ley, 2014). Upon blocking of CR3 and the resulting decrease in apoptotic *Lm* uptake, we expected T cell proliferation to

be increased as compared to infection of untreated macrophages which we did not detect in our T cell proliferation assay. As reported by Chandra et al., human macrophages infected with stat. ph. *L. donovani* promastigotes can induce a shift from TLR2 triggered T<sub>H</sub>1 responses to T<sub>H</sub>2 responses (Chandra and Naik, 2008). Further, *L. major*-specific T<sub>H</sub>1 cells could be polarized to T<sub>H</sub>2 T cells by stimulation with the anti-inflammatory IL-4 *in vitro* (Mocci and Coffman, 1997). A possible shift from T<sub>H</sub>2 to T<sub>H</sub>1 should be investigated by characterization of the CD3<sup>+</sup> population that were co-incubated with infected CR3 antibody-blocked or non-blocked hMDMs. To do so, intracellular staining for STAT4/T-bet (T<sub>H</sub>1 specific transcription factors) and STAT6/GATA3 (T<sub>H</sub>2 specific transcription factors) could be performed (Levine et al., 2017).

When we investigated the effect of reduced apoptotic *Lm* internalization upon CR3 blocking on survival of the viable population within macrophages, we expected that a decreased uptake of apoptotic *Lm* from the stat. ph. inoculum diminishes survival of viable *Lm*. *Lm*-infected macrophages are able to not only activate T cells but also to modulate inflammation in a paracrine fashion by activating neighboring macrophages. In limiting dilution assays viable promastigotes showed an enhanced survival in hMDM2 on day 6 post-infection as compared to hMDM1 which is in line with the lower microbicidal and inflammatory activity of the M2 subtype (Atri et al., 2018; Tomiotto-Pellissier et al., 2018). Interestingly, blocking of CR3 even decreased parasite survival within hMDM1 but the isotype control antibody had the same effect. Treatment of cells with isotype antibodies might stimulate Fc receptors which can negatively regulate intracellular growth of viable promastigotes by induction of pro-inflammatory signaling (Newton and Dixit, 2012). *Leishmania* survival in anti-inflammatory macrophages and upon CR3 inhibition tended to decrease which is in line with the previous observations from this study of reduced uptake and IL-10 release upon CR3 blocking. Nonetheless, the limiting dilution assay might not be sensitive enough to detect the expected effects of CR3 modulation. PCR-based methods are more specific and reliable but make it hard to differentiate between amastigotes and promastigotes by the lack of an equally expressed housekeeping gene across the life stages (Ouakad et al., 2007). In addition, presence of apoptotic *Lm*-derived nucleic acids might bias the results. A way to determine viable parasite loads within cells would be manual counting of parasite nuclei of Diff-Quick stained samples. This could be extended by

immunofluorescence staining of generated cytopins and automated, computer-aided counting.

Concluding, activation of the adaptive immune system was not found to be altered by a decreased internalization of apoptotic *Lm* upon inhibition of CR3. Future experiments should examine  $T_H1/T_H2$  polarization with focus on manipulation of CR3 but also other receptors e.g. CD91. The same accounts for the assessment of survival of viable *L. major* promastigotes, especially to circumvent antibody-induced stimulations whereas here, a more sensitive and reliable method of read-out could be found in PCR applications. Hence, one could verify the observed results that indicate enhanced killing of *L. major* promastigotes in pro-inflammatory macrophages when uptake of the apoptotic *Lm* fraction is impaired.

## 6. Concluding remarks

With the present study we confirmed LC3-associated phagocytosis to be responsible for internalization of a portion of viable and apoptotic *Lm* by hMDM2. The latter are targeted more rapid by LC3 resulting in efficient degradation. *Leishmania* infection is a highly dynamic process and it is obvious that analysis of infection by live cell microscopy is superior to investigations of fixed samples. Viable parasites might resist degradation by establishment of tunnel-like structures suggesting an unknown evasion strategy of viable *Leishmania major* promastigotes. Characterization of phagocytes confirmed our hypothesis that apoptotic *Lm* induce an anti-inflammatory cytokine response in hMDMs possibly serving to balance action of pro-inflammatory mediators. Identification of CR3 and CD91 in isolated phagosomes that contained apoptotic *Lm* by mass spectrometry and subsequent functional characterization in a human infection model for the first time revealed an important role for CR3 in internalization of apoptotic *Lm*. In contrast, CD91 was neither involved in phagocytosis of viable nor apoptotic *Lm* but may serve the control of the inflammatory microenvironment upon apoptotic *Lm* internalization which we suggest to be investigated in future studies. The reduced uptake of apoptotic *Lm* by inhibition of CR3 downregulated the anti-inflammatory cytokine response in subsequent infection in hMDM2 further emphasizing CR3 to be of importance in establishment of leishmaniasis in humans. Moreover, CR3 is a trigger for LC3-associated phagocytosis of apoptotic *L. major*

promastigotes in human monocyte-derived anti-inflammatory macrophages. Induction of LAP and the inhibitory effects of CR3 modulation on apoptotic parasite uptake and cytokine production were more pronounced in hMDM2. Data suggest hMDM2 to be the preferred target cell for *Leishmania* promastigotes and indicates a major role for CR3 on anti-inflammatory macrophages in initial *Leishmania* infection.

Future research will focus on in-detail microscopical elucidation of LAP of apoptotic *Lm* in hMDM2. It will further aim on (1) the role of CD91 in inflammation during *Leishmania* infection and (2) investigations on other factors that are involved in apoptotic *Lm*-processing found by our mass spectrometry screen. Ultrastructural analyses will determine the role of tunnel structures in evasion of degradation by viable promastigotes and might define a possible target for therapeutic intervention to treat leishmaniasis.

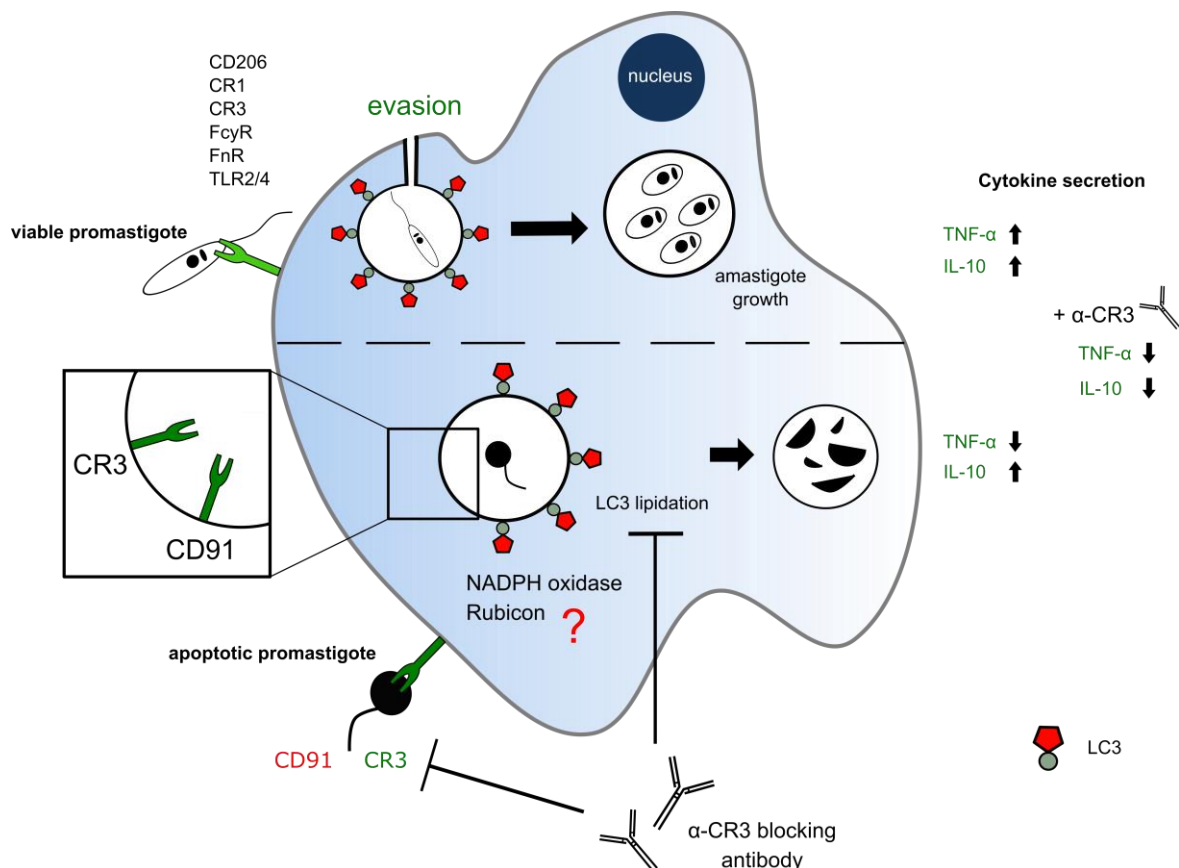
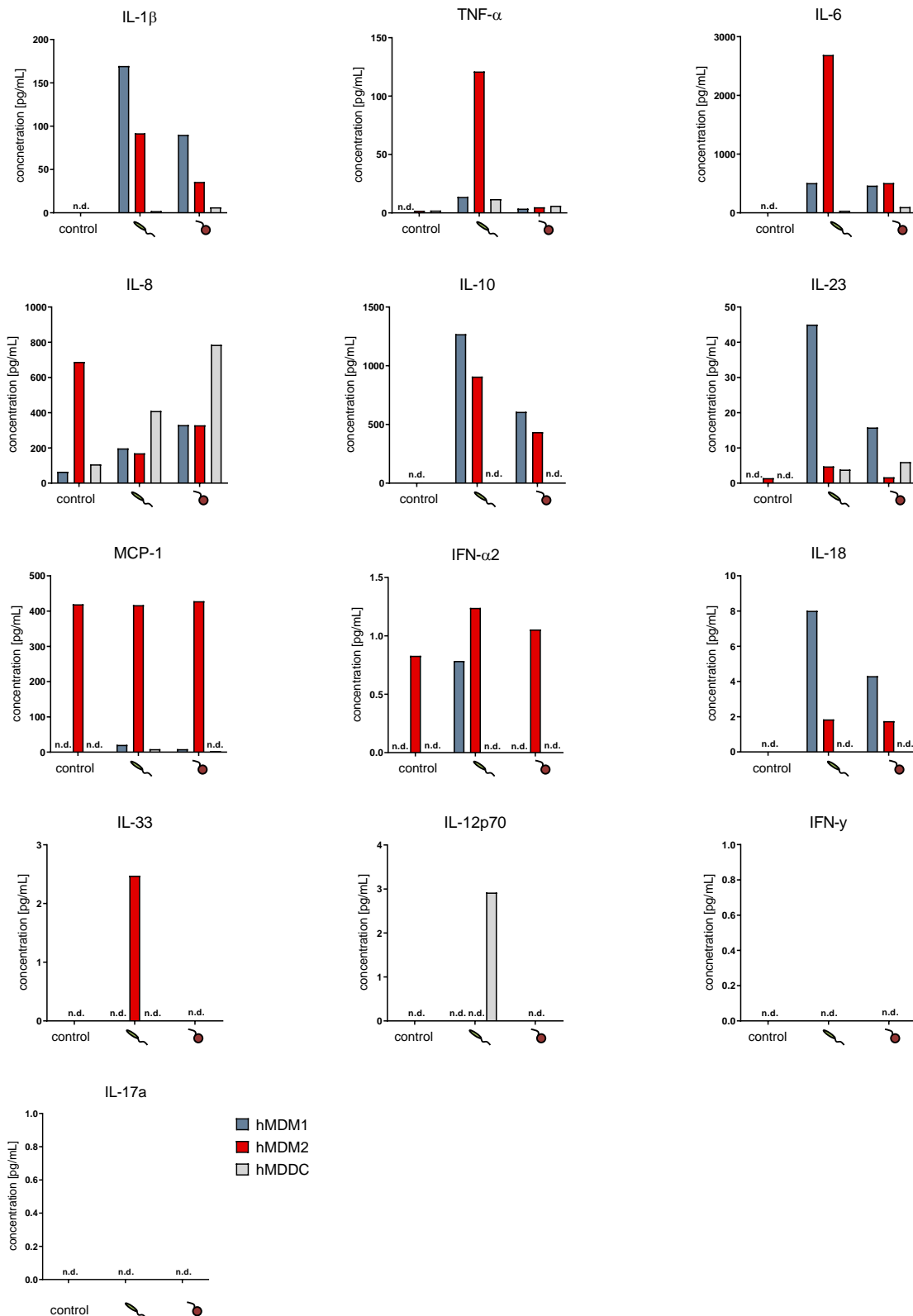


**Figure 35: Conclusion.** Portions of viable and apoptotic *Lm* are internalized by LAP which is more pronounced in hMDM2. Live cell imaging confirms that viable *Lm* are able to resist degradation possibly facilitated by tunnel-structures found on a quarter of viable *Lm*-containing phagosomes. Uptake of apoptotic *Lm* resulted in decreased production of TNF-α and upregulation of IL-10 in hMDM2 whereas viable *Lm* increased TNF-α and IL-10 production. CD91 and CR3 are highly abundant in phagosomes harboring apoptotic parasites. CD91 is not involved in *Leishmania* internalization but might serve the control of the inflammatory environment during infection. CR3 blocking inhibits uptake of apoptotic promastigotes and reduces secretion of TNF-α and IL-10. LC3 conversion is inhibited by blocking of CR3 which indicates LAP of apoptotic *Lm* to be triggered by CR3. Further hallmarks of LAP such as the NADPH oxidase or Rubicon should be investigated in following studies.

## 7. Appendix



**Appendix A: Cytokine profiles of hMDMs and hMDDCs upon infection with purified viable or apoptotic *Lm*.** Cells were co-incubated with either purified viable or apoptotic *Lm* or left untreated. Cytokine concentrations were determined by flow cytometry using a LEGENDplex™ Multi-analyte Flow Assay Kit (Biolegend) according to the manufacturer's instructions (n=1; n.d.: not detectable). Data were generated with the help of Mr Naphang Ho.

## 8. References

- Abou Fakher, F.H., Rachinel, N., Klimczak, M., Louis, J., Doyen, N., 2009. TLR9-dependent activation of dendritic cells by DNA from *Leishmania major* favors Th1 cell development and the resolution of lesions. *J. Immunol.* 182, 1386–96.
- Abuaita, B.H., Schultz, T.L., O’Riordan, M.X., 2018. Mitochondria-Derived Vesicles Deliver Antimicrobial Reactive Oxygen Species to Control Phagosome-Localized *Staphylococcus aureus*. *Cell Host Microbe* 24, 625–636.e5. <https://doi.org/10.1016/j.chom.2018.10.005>
- Afonso, L., Borges, V.M., Cruz, H., Ribeiro-Gomes, F.L., DosReis, G.A., Dutra, A.N., Clarencio, J., de Oliveira, C.I., Barral, A., Barral-Netto, M., Brodskyn, C.I., 2008. Interactions with apoptotic but not with necrotic neutrophils increase parasite burden in human macrophages infected with *Leishmania amazonensis*. *J. Leukoc. Biol.* 84, 389–396. <https://doi.org/10.1189/jlb.0108018>
- Akoumianaki, T., Kyrmizi, I., Valsecchi, I., Gresnigt, M.S., Samonis, G., Drakos, E., Boumpas, D., Muszkieta, L., Prevost, M.C., Kontoyiannis, D.P., Chavakis, T., Netea, M.G., Van De Veerdonk, F.L., Brakhage, A.A., El-Benna, J., Beauvais, A., Latge, J.P., Chamilos, G., 2016. *Aspergillus* Cell Wall Melanin Blocks LC3-Associated Phagocytosis to Promote Pathogenicity. *Cell Host Microbe* 19, 79–90. <https://doi.org/10.1016/j.chom.2015.12.002>
- Alcolea, P.J., Alonso, A., Gómez, M.J., Sánchez-Gorostiaga, A., Moreno-Paz, M., González-Pastor, E., Toraño, A., Parro, V., Larraga, V., 2010. Temperature increase prevails over acidification in gene expression modulation of amastigote differentiation in *Leishmania infantum*. *BMC Genomics* 11. <https://doi.org/10.1186/1471-2164-11-31>
- Alexander, J., Satoskar, A.R., Russell, D.G., 1999. *Leishmania* species: models of intracellular parasitism. *J. Cell Sci.* 112 Pt 18, 2993–3002.
- Amin Arnaut, M., 1990. Structure and Function of the Leukocyte Adhesion Molecules CD11/CD18. *Blood* 75, 1037–1050.
- Anderson, C.F., Mosser, D.M., 2002. A novel phenotype for an activated macrophage: the type 2 activated macrophage. *J. Leukoc. Biol.* 72, 101–6.
- Arandjelovic, S., Ravichandran, K.S., 2015. Phagocytosis of apoptotic cells in homeostasis. *Nat. Immunol.* 16, 907.
- Arango Duque, G., Descoteaux, A., 2014. Macrophage cytokines: Involvement in immunity and infectious diseases. *Front. Immunol.* 5, 1–12. <https://doi.org/10.3389/fimmu.2014.00491>
- Atri, C., Guerfali, F.Z., Laouini, D., 2018. Role of human macrophage polarization in inflammation during infectious diseases. *Int. J. Mol. Sci.* 19. <https://doi.org/10.3390/ijms19061801>
- Basmaciyan, L., Azas, N., Casanova, M., 2018. Different apoptosis pathways in *Leishmania* parasites. *Cell Death Discov.* 4, 4–6. <https://doi.org/10.1038/s41420-018-0092-z>
- Beller, D.I., Springer, T.A., Schreiber, R.D., 1982. Anti-Mac-1 selectively inhibits the mouse and human type three complement receptor. *J. Exp. Med.* 156, 1000–9.

- Berger, A., Sommer, A.F.R., Zwarg, J., Hamdorf, M., Welzel, K., Esly, N., Panitz, S., Reuter, A., Ramos, I., Jatiani, A., Mulder, L.C.F., Fernandez-Sesma, A., Rutsch, F., Simon, V., König, R., Flory, E., 2011. SAMHD1-deficient CD14<sup>+</sup> cells from individuals with Aicardi-Goutières syndrome are highly susceptible to HIV-1 infection. *PLoS Pathog.* 7, e1002425. <https://doi.org/10.1371/journal.ppat.1002425>
- Berman, H.M., Westbrook, J., Feng, Z., Gilliland, G., Bhat, T.N., Weissig, H., Shindyalov, I.N., Bourne, P.E., 2000. The Protein Data Bank. *Nucleic Acids Res.* 28, 235–42. <https://doi.org/10.1093/nar/28.1.235>
- Berton, G., Bellavite, P., de Nicola, G., Dri, P., Rossi, F., 1982. Plasma membrane and phagosome localisation of the activated NADPH oxidase in elicited peritoneal macrophages of the guinea-pig. *J. Pathol.* 136, 241–252. <https://doi.org/10.1002/path.1711360307>
- Besteiro, S., Williams, R.A.M., Coombs, G.H., Mottram, J.C., 2007. Protein turnover and differentiation in *Leishmania*. *Int. J. Parasitol.* 37, 1063–1075. <https://doi.org/10.1016/j.ijpara.2007.03.008>
- Biswas, S.K., Chittechath, M., Shalova, I.N., Lim, J.Y., 2012. Macrophage polarization and plasticity in health and disease. *Immunol. Res.* 53, 11–24. <https://doi.org/10.1007/s12026-012-8291-9>
- Bogdan, C., Schröppel, K., Lohoff, M., Röllinghoff, M., Solbach, W., 1990. Immunization of susceptible hosts with a soluble antigen fraction from *Leishmania major* leads to aggravation of murine Leishmaniasis mediated by CD4<sup>+</sup> T cells. *Eur. J. Immunol.* 20, 2533–40. <https://doi.org/10.1002/eji.1830201202>
- Bohn, R., 2017. Canonical and non-canonical autophagy modulation in human primary macrophages and its effect on the adaptive immune system. University Mainz.
- Bouvier, J., Schneider, P., Malcolm, B., 1993. A fluorescent peptide substrate for the surface metalloprotease of *Leishmania*. *Exp. Parasitol.* 76, 146–155. <https://doi.org/10.1006/expr.1993.1017>
- Boyle, K.B., Randow, F., 2015. Rubicon swaps autophagy for LAP. *Nat. Cell Biol.* 17, 843–845. <https://doi.org/10.1038/ncb3197>
- Brittingham, A., Morrison, C.J., McMaster, W.R., McGwire, B.S., Chang, K.P., Mosser, D.M., 1995. Role of the *Leishmania* surface protease gp63 in complement fixation, cell adhesion, and resistance to complement-mediated lysis. *J. Immunol.* 155, 3102–11.
- Burnette, W.N., 1981. “Western Blotting”: Electrophoretic transfer of proteins from sodium dodecyl sulfate-polyacrylamide gels to unmodified nitrocellulose and radiographic detection with antibody and radioiodinated protein A. *Anal. Biochem.* 112, 195–203. [https://doi.org/10.1016/0003-2697\(81\)90281-5](https://doi.org/10.1016/0003-2697(81)90281-5)
- Burza, S., Croft, S.L., Boelaert, M., 2018. Leishmaniasis. *Lancet* 392, 951–970. [https://doi.org/10.1016/S0140-6736\(18\)31204-2](https://doi.org/10.1016/S0140-6736(18)31204-2)
- Campbell, R.E., Tour, O., Palmer, A.E., Steinbach, P.A., Baird, G.S., Zacharias, D.A., Tsien, R.Y., 2002. A monomeric red fluorescent protein. *Proc. Natl. Acad. Sci.* 99, 7877–7882. <https://doi.org/10.1073/pnas.082243699>



- Cappelletti, M., Presicce, P., Calcaterra, F., Mavilio, D., Della Bella, S., 2015. Bright expression of CD91 identifies highly activated human dendritic cells that can be expanded by defensins. *Immunology* 144, 661–667. <https://doi.org/10.1111/imm.12418>
- Cavalier-Smith, T., 2016. Higher classification and phylogeny of Euglenozoa. *Eur. J. Protistol.* 56, 250–276. <https://doi.org/10.1016/j.ejop.2016.09.003>
- Cemna, M., Grinstein, S., Brumell, J.H., 2016. Autophagy proteins are not universally required for phagosome maturation. *Autophagy* 12, 1440–1446. <https://doi.org/10.1080/15548627.2016.1191724>
- Chandra, D., Naik, S., 2008. *Leishmania donovani* infection down-regulates TLR2-stimulated IL-12p40 and activates IL-10 in cells of macrophage/monocytic lineage by modulating MAPK pathways through a contact-dependent mechanism. *Clin. Exp. Immunol.* 154, 224–234. <https://doi.org/10.1111/j.1365-2249.2008.03741.x>
- Chauhan, P., Shukla, D., Chattopadhyay, D., Saha, B., 2017. Redundant and regulatory roles for Toll-like receptors in *Leishmania* infection. *Clin. Exp. Immunol.* 190, 167–186. <https://doi.org/10.1111/cei.13014>
- Collin, M., MCGovern, N., Haniffa, M., 2013. Human dendritic cell subsets. *Immunology* 140, 22–30. <https://doi.org/10.1111/imm.12117>
- Cooper, A., Rosen, H., Blackwell, J.M., 1988. Monoclonal antibodies that recognize distinct epitopes of the macrophage type three complement receptor differ in their ability to inhibit binding of *Leishmania* promastigotes harvested at different phases of their growth cycle. *Immunology* 65, 511–4.
- Crauwels, P., 2015. The interaction of *Leishmania major* parasites with human myeloid cells and its consequence for adaptive immunity. University Mainz.
- Crauwels, P., Bohn, R., Thomas, M., Gottwalt, S., Jäckel, F., Krämer, S., Bank, E., Tenzer, S., Walther, P., Bastian, M., Zandbergen, G. van, 2015. Apoptotic-like *Leishmania* exploit the host's autophagy machinery to reduce T-cell-mediated parasite elimination. *Autophagy* 11, 285–297. <https://doi.org/10.1080/15548627.2014.998904>
- Da Silva, R.P., Hall, B.F., Joiner, K.A., Sacks, D.L., 1989. CR1, the C3b receptor, mediates binding of infective *Leishmania major* metacyclic promastigotes to human macrophages. *J. Immunol.* 143, 617–22.
- De Oliveira, C.I., Brodskyn, C.I., 2012. The immunobiology of *Leishmania braziliensis* infection. *Front. Immunol.* 3, 1–9. <https://doi.org/10.3389/fimmu.2012.00145>
- de Veer, M.J., Curtis, J.M., Baldwin, T.M., DiDonato, J.A., Sexton, A., McConville, M.J., Handman, E., Schofield, L., 2003. MyD88 is essential for clearance of *Leishmania major*: possible role for lipophosphoglycan and Toll-like receptor 2 signaling. *Eur. J. Immunol.* 33, 2822–2831. <https://doi.org/10.1002/eji.200324128>
- Distler, U., Kuharev, J., Navarro, P., Tenzer, S., 2016. Label-free quantification in ion mobility-enhanced data-independent acquisition proteomics. *Nat. Protoc.* 11, 795–812. <https://doi.org/10.1038/nprot.2016.042>

- DNDi, D. for neglected diseases initiative, 2019. Current Treatments of Leishmaniasis [WWW Document]. URL <https://www.dndi.org/diseases-projects/Leishmaniasis/leish-current-treatments/> (accessed 2/7/19).
- Dostálová, A., Volf, P., 2012. *Leishmania* development in sand flies: Parasite-vector interactions overview. *Parasites and Vectors* 5, 1–12. <https://doi.org/10.1186/1756-3305-5-276>
- Duthie, M.S., Favila, M., Hofmeyer, K.A., Tutterrow, Y.L., Reed, S.J., Laurance, J.D., Picone, A., Guderian, J., Bailor, H.R., Vallur, A.C., Liang, H., Mohamath, R., Vergara, J., Howard, R.F., Coler, R.N., Reed, S.G., 2016. Strategic evaluation of vaccine candidate antigens for the prevention of Visceral Leishmaniasis. *Vaccine* 34, 2779–2786. <https://doi.org/10.1016/j.vaccine.2016.04.067>
- Elliott, M.R., Koster, K.M., Murphy, P.S., 2017. Efferocytosis Signaling in the Regulation of Macrophage Inflammatory Responses. *J. Immunol.* 198, 1387–1394. <https://doi.org/10.4049/jimmunol.1601520>
- Embgenbroich, M., Burgdorf, S., 2018. Current concepts of antigen cross-presentation. *Front. Immunol.* 9. <https://doi.org/10.3389/fimmu.2018.01643>
- Fadok, V.A., Bratton, D.L., Guthrie, L., Henson, P.M., 2001. Differential effects of apoptotic versus lysed cells on macrophage production of cytokines: role of proteases. *J. Immunol.* 166, 6847–54.
- Fadok, V.A., Bratton, D.L., Konowal, A., Freed, P.W., Westcott, J.Y., Henson, P.M., 1998. Macrophages that have ingested apoptotic cells in vitro inhibit proinflammatory cytokine production through autocrine/paracrine mechanisms involving TGF-beta, PGE2, and PAF. *J. Clin. Invest.* 101, 890–898. <https://doi.org/10.1172/JCI1112>
- Feijó, D., Tibúrcio, R., Ampuero, M., Brodskyn, C., Tavares, N., 2016. Dendritic cells and *Leishmania* infection: Adding layers of complexity to a complex disease. *J. Immunol. Res.* 2016. <https://doi.org/10.1155/2016/3967436>
- Filardy, A.A., Pires, D.R., Nunes, M.P., Takiya, C.M., Freire-de-Lima, C.G., Ribeiro-Gomes, F.L., DosReis, G.A., 2010. Pro-inflammatory clearance of apoptotic neutrophils induces an IL-12(low)IL-10(high) regulatory phenotype in macrophages. *J. Immunol.* 185, 2044–50. <https://doi.org/10.4049/jimmunol.1000017>
- Forestier, C.L., MacHu, C., Loussert, C., Pescher, P., Späth, G.F., 2011. Imaging host cell-*Leishmania* interaction dynamics implicates parasite motility, lysosome recruitment, and host cell wounding in the infection process. *Cell Host Microbe* 9, 319–330. <https://doi.org/10.1016/j.chom.2011.03.011>
- Freire-de-Lima, C.G., Nascimento, D.O., Soares, M.B.P., Bozza, P.T., Castro-Faria-Neto, H.C., de Mello, F.G., DosReis, G.A., Lopes, M.F., 2000. Uptake of apoptotic cells drives the growth of a pathogenic trypanosome in macrophages. *Nature* 403, 199–203. <https://doi.org/10.1038/35003208>
- Gardai, S.J., McPhillips, K.A., Frasc, S.C., Janssen, W.J., Starefeldt, A., Murphy-Ullrich, J.E., Bratton, D.L., Oldenborg, P.A., Michalak, M., Henson, P.M., 2005. Cell-surface calreticulin initiates clearance of viable or apoptotic cells through trans-activation of LRP on the phagocyte. *Cell* 123, 321–334. <https://doi.org/10.1016/j.cell.2005.08.032>

- Gaultier, A., Arandjelovic, S., Niessen, S., Overton, C.D., Linton, M.F., Fazio, S., Campana, W.M., Cravatt, B.F., Gonias, S.L., 2008. Regulation of tumor necrosis factor receptor-1 and the IKK-NF- $\kappa$ B pathway by LDL receptor-related protein explains the anti-inflammatory activity of this receptor. *Blood* 111, 5316–5325. <https://doi.org/10.1182/blood-2007-12-127613>
- Ghorbani, M., Farhoudi, R., 2018. Leishmaniasis in humans: Drug or vaccine therapy? *Drug Des. Devel. Ther.* 12, 25–40. <https://doi.org/10.2147/DDDT.S146521>
- Ginhoux, F., Jung, S., 2014. Monocytes and macrophages: developmental pathways and tissue homeostasis. *Nat. Rev. Immunol.* 14, 392–404. <https://doi.org/10.1038/nri3671>
- Gluschko, A., Herb, M., Wiegmann, K., Krut, O., Neiss, W.F., Utermöhlen, O., Krönke, M., Schramm, M., 2018. The  $\beta$ 2-Integrin Mac-1 Induces Protective LC3-Associated Phagocytosis of *Listeria monocytogenes*. *Cell Host Microbe* 23, 324–337.e5. <https://doi.org/10.1016/j.chom.2018.01.018>
- Goto, H., Lauletta Lindoso, J.A., 2012. Cutaneous and Mucocutaneous Leishmaniasis. *Infect. Dis. Clin. North Am.* 26, 293–307. <https://doi.org/10.1016/j.idc.2012.03.001>
- Grekov, I., Svobodová, M., Nohýnková, E., Lipoldová, M., 2011. Preparation of highly infective *Leishmania* promastigotes by cultivation on SNB-9 biphasic medium. *J. Microbiol. Methods* 87, 273–277. <https://doi.org/10.1016/j.mimet.2011.08.012>
- Haniffa, M., Bigley, V., Collin, M., 2015. Human mononuclear phagocyte system reunited. *Semin. Cell Dev. Biol.* 41, 59–69. <https://doi.org/10.1016/j.semcdb.2015.05.004>
- Hashimoto, Y., Moki, T., Takizawa, T., Shiratsuchi, A., Nakanishi, Y., 2007. Evidence for Phagocytosis of Influenza Virus-Infected, Apoptotic Cells by Neutrophils and Macrophages in Mice. *J. Immunol.* 178, 2448–2457. <https://doi.org/10.4049/jimmunol.178.4.2448>
- Henault, J., Martinez, J., Riggs, J.M., Tian, J., Mehta, P., Sasai, M., Latz, E., Brinkmann, M.M., Iwasaki, A., Anthony, J., Kolbeck, R., Green, D.R., Sanjuan, M.A., 2013. Noncanonical autophagy is required for type I interferon secretion in Response to DNA-Immune Complexes 37, 986–997. <https://doi.org/10.1016/j.immuni.2012.09.014>
- Herz, J., Strickland, D.K., 2001. Multiligand receptors LRP : a multifunctional scavenger and signaling receptor. *J.Clin.Invest* 108, 779–784. <https://doi.org/10.1172/JCI200113992>
- Hoofnagle, A.N., Heinecke, J.W., 2009. Lipoproteomics: using mass spectrometry-based proteomics to explore the assembly, structure, and function of lipoproteins. *J. Lipid Res.* 50, 1967–1975. <https://doi.org/10.1194/jlr.R900015-JLR200>
- Hrecka, K., Hao, C., Gierszewska, M., Swanson, S.K., Kesik-Brodacka, M., Srivastava, S., Florens, L., Washburn, M.P., Skowronski, J., 2011. Vpx relieves inhibition of HIV-1 infection of macrophages mediated by the SAMHD1 protein. *Nature* 474, 658–661. <https://doi.org/10.1038/nature10195>
- Hsieh, C.S., Macatonia, S.E., Tripp, C.S., Wolf, S.F., O'Garra, A., Murphy, K.M., 1993. Development of TH1 CD4+ T cells through IL-12 produced by *Listeria*-induced macrophages. *Science* 260, 547–9.

- Huang, J.-H., Lin, C.-Y., Wu, S.-Y., Chen, W.-Y., Chu, C.-L., Brown, G.D., Chuu, C.-P., Wu-Hsieh, B.A., 2015. CR3 and Dectin-1 Collaborate in Macrophage Cytokine Response through Association on Lipid Rafts and Activation of Syk-JNK-AP-1 Pathway. *PLoS Pathog.* 11, e1004985. <https://doi.org/10.1371/journal.ppat.1004985>
- Huang, J., Brumell, J.H., 2009. NADPH oxidases contribute to autophagy regulation. *Autophagy* 5, 887–889. <https://doi.org/10.1073/pnas.0811045106>
- Huang, J., Canadien, V., Lam, G.Y., Steinberg, B.E., Dinauer, M.C., Magalhaes, M. a O., Glogauer, M., Grinstein, S., Brumell, J.H., 2009. Activation of antibacterial autophagy by NADPH oxidases. *Proc. Natl. Acad. Sci. U. S. A.* 106, 6226–31. <https://doi.org/10.1073/pnas.0811045106>
- Italiani, P., Boraschi, D., 2014. From Monocytes to M1/M2 Macrophages: Phenotypical vs. Functional Differentiation. *Front. Immunol.* 5, 1–22. <https://doi.org/10.3389/fimmu.2014.00514>
- Jaguin, M., Houlbert, N., Fardel, O., Lecureur, V., 2013. Polarization profiles of human M-CSF-generated macrophages and comparison of M1-markers in classically activated macrophages from GM-CSF and M-CSF origin. *Cell. Immunol.* 281, 51–61. <https://doi.org/10.1016/j.cellimm.2013.01.010>
- Kane, M.M., Mosser, D.M., 2000. *Leishmania* parasites and their ploys to disrupt macrophage activation. *Curr. Opin. Hematol.* 7, 26–31.
- Kawamoto, H., Minato, N., 2004. Myeloid cells. *Int. J. Biochem. Cell Biol.* 36, 1374–1379. <https://doi.org/10.1016/j.biocel.2004.01.020>
- Klickstein, L.B., Barbashov, S.F., Liu, T., Jack, R.M., Nicholson-Weller, A., 1997. Complement Receptor Type 1 (CR1, CD35) Is a Receptor for C1q. *Immunity* 7, 345–355. [https://doi.org/10.1016/S1074-7613\(00\)80356-8](https://doi.org/10.1016/S1074-7613(00)80356-8)
- Klionsky, D.J., Abdelmohsen, K., Abe, A., Abedin, M.J., Abeliovich, H., Arozena, A.A., Adachi, H., Adams, C.M., Adams, P.D., Adeli, K., et al., 2016. Guidelines for the use and interpretation of assays for monitoring autophagy (3rd edition). *Autophagy* 12, 1–222. <https://doi.org/10.1080/15548627.2015.1100356>
- Kloke, B.-P., Schüle, S., Mühlebach, M.D., Wolfrum, N., Cichutek, K., Schweizer, M., 2010. Functional HIV-2- and SIVsmmPBj- derived lentiviral vectors generated by a novel polymerase chain reaction-based approach. *J. Gene Med.* 12, 446–452. <https://doi.org/10.1002/jgm.1454>
- Kropf, P., Freudenberg, M.A., Modolell, M., Price, H.P., Herath, S., Antoniazzi, S., Galanos, C., Smith, D.F., Müller, I., 2004. Toll-like receptor 4 contributes to efficient control of infection with the protozoan parasite *Leishmania major*. *Infect. Immun.* 72, 1920–8.
- Kuharev, J., Navarro, P., Distler, U., Jahn, O., Tenzer, S., 2015. In-depth evaluation of software tools for data-independent acquisition based label-free quantification. *Proteomics* 15, 3140–3151. <https://doi.org/10.1002/pmic.201400396>
- Kurosaka, K., Watanabe, N., Kobayashi, Y., 2001. Production of Proinflammatory Cytokines by Resident Tissue Macrophages after Phagocytosis of Apoptotic Cells. *Cell. Immunol.* 211, 1–7. <https://doi.org/10.1006/cimm.2001.1824>

- Kyrmizi, I., Gresnigt, M.S., Akoumianaki, T., Samonis, G., Sidiropoulos, P., Boumpas, D., Netea, M.G., van de Veerdonk, F.L., Kontoyiannis, D.P., Chamilos, G., 2013. Corticosteroids Block Autophagy Protein Recruitment in *Aspergillus fumigatus* Phagosomes via Targeting Dectin-1/Syk Kinase Signaling. *J. Immunol.* 191, 1287–1299. <https://doi.org/10.4049/jimmunol.1300132>
- Laemmli, U.K., 1970. Cleavage of structural proteins during the assembly of the head of bacteriophage T4. *Nature* 227, 680–5. <https://doi.org/10.1038/227680a0>
- Laguet, N., Sobhian, B., Casartelli, N., Ringeard, M., Chable-Bessia, C., Ségéral, E., Yatim, A., Emiliani, S., Schwartz, O., Benkirane, M., 2011. SAMHD1 is the dendritic- and myeloid-cell-specific HIV-1 restriction factor counteracted by Vpx. *Nature* 474, 654–657. <https://doi.org/10.1038/nature10117>
- Lam, G.Y., Cemma, M., Muise, A.M., Higgins, D.E., Brumell, J.H., 2013. Host and bacterial factors that regulate LC3 recruitment to *Listeria monocytogenes* during the early stages of macrophage infection. *Autophagy* 9, 985–995. <https://doi.org/10.4161/auto.24406>
- Lam, G.Y., Huang, J., Brumell, J.H., 2010. The many roles of NOX2 NADPH oxidase-derived ROS in immunity 415–430. <https://doi.org/10.1007/s00281-010-0221-0>
- Lane, R.P., 1993. Sandflies (Phlebotominae), in: *Medical Insects and Arachnids*. Springer Netherlands, Dordrecht, pp. 78–119. [https://doi.org/10.1007/978-94-011-1554-4\\_4](https://doi.org/10.1007/978-94-011-1554-4_4)
- Lee, J., Breton, G., Oliveira, T.Y.K., Zhou, Y.J., Aljoufi, A., Pühr, S., Cameron, M.J., Sékaly, R.-P., Nussenzweig, M.C., Liu, K., 2015. Restricted dendritic cell and monocyte progenitors in human cord blood and bone marrow. *J. Exp. Med.* 212, 385–399. <https://doi.org/10.1084/jem.20141442>
- Lee, S.H., Charmoy, M., Romano, A., Paun, A., Chaves, M.M., Cope, F.O., Ralph, D.A., Sacks, D.L., 2018. Mannose receptor high, M2 dermal macrophages mediate nonhealing *Leishmania major* infection in a Th1 immune environment. *J. Exp. Med.* 215, 357–375. <https://doi.org/10.1084/jem.20171389>
- Levine, A.G., Medoza, A., Hemmers, S., Moltedo, B., Niec, R.E., Schizas, M., Hoyos, B.E., Putintseva, E. V., Chaudhry, A., Dikiy, S., Fujisawa, S., Chudakov, D.M., Treuting, P.M., Rudensky, A.Y., 2017. Stability and function of regulatory T cells expressing the transcription factor T-bet. *Nature* 546, 421–425. <https://doi.org/10.1038/nature22360>
- Li, X.J., Goodwin, C.B., Nabinger, S.C., Richine, B.M., Yang, Z., Hanenberg, H., Ohnishi, H., Matozaki, T., Feng, G.-S., Chan, R.J., 2015. Protein-tyrosine Phosphatase Shp2 Positively Regulates Macrophage Oxidative Burst. *J. Biol. Chem.* 290, 3894–3909. <https://doi.org/10.1074/jbc.M114.614057>
- Liese, J., Schleicher, U., Bogdan, C., 2008. The innate immune response against *Leishmania* parasites. *Immunobiology* 213, 377–387. <https://doi.org/10.1016/j.imbio.2007.12.005>
- Liew, F.Y., Parkinson, C., Millott, S., Severn, A., Biotech, W., Carrier, M., 1990. Tumour necrosis factor (TNF alpha) in Leishmaniasis. I. TNF alpha mediates host protection against cutaneous Leishmaniasis. *Immunology* 69, 570–573. <https://doi.org/10.1016/j.ijpara.2010.03.011>

- Lighvani, A.A., Frucht, D.M., Jankovic, D., Yamane, H., Aliberti, J., Hissong, B.D., Nguyen, B. V., Gadina, M., Sher, A., Paul, W.E., O'Shea, J.J., 2001. T-bet is rapidly induced by interferon-gamma in lymphoid and myeloid cells. *Proc. Natl. Acad. Sci. U. S. A.* 98, 15137–42. <https://doi.org/10.1073/pnas.261570598>
- Lim, J., Wiedemann, A., Tzircotis, G., Monkley, S.J., Critchley, D.R., Caron, E., 2007. An Essential Role for Talin during  $\alpha$ M $\beta$ 2 -mediated Phagocytosis. *Mol. Biol. Cell* 18, 976–985. <https://doi.org/10.1091/mbc.e06-09-0813>
- Liu, T., Zhang, L., Joo, D., Sun, S.-C., 2017. NF- $\kappa$ B signaling in inflammation. *Signal Transduct. Target. Ther.* 2, 17023. <https://doi.org/10.1038/sigtrans.2017.23>
- Livak, K.J., Schmittgen, T.D., 2001. Analysis of Relative Gene Expression Data Using Real-Time Quantitative PCR and the  $2^{-\Delta\Delta CT}$  Method. *Methods* 25, 402–408. <https://doi.org/10.1006/meth.2001.1262>
- López, L., Vélez, I., Asela, C., Cruz, C., Alves, F., Robledo, S., Arana, B., 2018. A phase II study to evaluate the safety and efficacy of topical 3% amphotericin B cream (Anfoleish) for the treatment of uncomplicated cutaneous Leishmaniasis in Colombia. *PLoS Negl. Trop. Dis.* 12, 1–12. <https://doi.org/10.1371/journal.pntd.0006653>
- Lüder, C.G., Campos-Salinas, J., Gonzalez-Rey, E., Van Zandbergen, G., 2010. Impact of protozoan cell death on parasite-host interactions and pathogenesis. *Parasites and Vectors* 3, 116. <https://doi.org/10.1186/1756-3305-3-116>
- Machado de Oliveira, S.A., 2016. Complement receptor 1 mediated control of *Leishmania* infection in inflammatory human macrophages. PhD thesis, University Mainz.
- Mann, E.R., 2014. Intestinal antigen-presenting cells in mucosal immune homeostasis: Crosstalk between dendritic cells, macrophages and B-cells. *World J. Gastroenterol.* 20, 9653. <https://doi.org/10.3748/wjg.v20.i29.9653>
- Mantuano, E., Brifault, C., Lam, M.S., Azmoon, P., Gilder, A.S., Gonias, S.L., 2016. LDL receptor-related protein-1 regulates NF $\kappa$ B and microRNA-155 in macrophages to control the inflammatory response. *Proc. Natl. Acad. Sci.* 113, 1369–1374. <https://doi.org/10.1073/pnas.1515480113>
- Mariño, G., Kroemer, G., 2013. Mechanisms of apoptotic phosphatidylserine exposure. *Cell Res.* 23, 1247–1248. <https://doi.org/10.1038/cr.2013.115>
- Maroli, M., Feliciangeli, M.D., Bichaud, L., Charrel, R.N., Gradoni, L., 2013. Phlebotomine sandflies and the spreading of Leishmaniasis and other diseases of public health concern. *Med. Vet. Entomol.* 27, 123–147. <https://doi.org/10.1111/j.1365-2915.2012.01034.x>
- Martinez, J., Almendinger, J., Oberst, A., Ness, R., Dillon, C.P., Fitzgerald, P., Hengartner, M.O., Green, D.R., 2011. Microtubule-associated protein 1 light chain 3 alpha (LC3)-associated phagocytosis is required for the efficient clearance of dead cells. *Proc. Natl. Acad. Sci. U. S. A.* 108, 17396–17401. <https://doi.org/10.1073/pnas.1113421108>

- Martinez, J., Malireddi, R.K.S., Lu, Q., Cunha, L.D., Pelletier, S., Gingras, S., Orchard, R., Guan, J.-L., Tan, H., Peng, J., Kanneganti, T.-D., Virgin, H.W., Green, D.R., 2015. Molecular characterization of LC3-associated phagocytosis reveals distinct roles for Rubicon, NOX2 and autophagy proteins. *Nat. Cell Biol.* 17, 893–906. <https://doi.org/10.1038/ncb3192>
- Maspi, N., Abdoli, A., Ghaffarifar, F., 2016. Pro- and anti-inflammatory cytokines in cutaneous Leishmaniasis: a review. *Pathog. Glob. Health* 110, 247–260. <https://doi.org/10.1080/20477724.2016.1232042>
- Matsunaga, K., Saitoh, T., Tabata, K., Omori, H., Satoh, T., Kurotori, N., Maejima, I., Shirahama-Noda, K., Ichimura, T., Isobe, T., Akira, S., Noda, T., Yoshimori, T., 2009. Two Beclin 1-binding proteins, Atg14L and Rubicon, reciprocally regulate autophagy at different stages. *Nat. Cell Biol.* 11, 385–396. <https://doi.org/10.1038/ncb1846>
- Matte, C., Casgrain, P.A., Séguin, O., Moradin, N., Hong, W.J., Descoteaux, A., 2016. *Leishmania major* Promastigotes Evade LC3-Associated Phagocytosis through the Action of GP63. *PLoS Pathog.* 12, 1–17. <https://doi.org/10.1371/journal.ppat.1005690>
- May, P., Bock, H.H., Nofer, J.-R., 2013. Low density receptor-related protein 1 (LRP1) promotes anti-inflammatory phenotype in murine macrophages. *Cell Tissue Res.* 354, 887–889. <https://doi.org/10.1007/s00441-013-1699-2>
- McConville, M.J., Turco, S.J., Ferguson, M.A., Sacks, D.L., 1992. Developmental modification of lipophosphoglycan during the differentiation of *Leishmania major* promastigotes to an infectious stage. *EMBO J.* 11, 3593–3600. <https://doi.org/10.1002/j.1460-2075.1992.tb05443.x>
- McGwire, B.S., Satoskar, A.R., 2014. Leishmaniasis: clinical syndromes and treatment. *QJM* 107, 7–14. <https://doi.org/10.1093/qjmed/hct116>
- McLelland, G.-L., Lee, S.A., McBride, H.M., Fon, E.A., 2016. Syntaxin-17 delivers PINK1/parkin-dependent mitochondrial vesicles to the endolysosomal system. *J. Cell Biol.* 214, 275–291. <https://doi.org/10.1083/jcb.201603105>
- Medzhitov, R., 2007. Recognition of microorganisms and activation of the immune response. *Nature* 449, 819–826. <https://doi.org/10.1038/nature06246>
- Melaun, C., Krüger, A., Werblow, A., Klimpel, S., 2014. New record of the suspected Leishmaniasis vector *Phlebotomus (Transphlebotomus) mascittii* Grassi, 1908 (Diptera: Psychodidae: Phlebotominae) - The northernmost phlebotomine sandfly occurrence in the Palearctic region. *Parasitol. Res.* 113, 2295–2301. <https://doi.org/10.1007/s00436-014-3884-y>
- Melman, L., Geuze, H.J., Li, Y., McCormick, L.M., van Kerkhof, P., Strous, G.J., Schwartz, A.L., Bu, G., 2002. Proteasome Regulates the Delivery of LDL Receptor-related Protein into the Degradation Pathway. *Mol. Biol. Cell* 13, 3325–3335. <https://doi.org/10.1091/mbc.e02-03-0152>
- Menck, K., Behme, D., Pantke, M., Reiling, N., Binder, C., Pukrop, T., Klemm, F., 2014. Isolation of human monocytes by double gradient centrifugation and their differentiation to macrophages in teflon-coated cell culture bags. *J. Vis. Exp.* e51554. <https://doi.org/10.3791/51554>

- Merle, N.S., Church, S.E., Fremeaux-Bacchi, V., Roumenina, L.T., 2015a. Complement system part I - molecular mechanisms of activation and regulation. *Front. Immunol.* 6, 1–30. <https://doi.org/10.3389/fimmu.2015.00262>
- Merle, N.S., Noe, R., Halbwachs-Mecarelli, L., Fremeaux-Bacchi, V., Roumenina, L.T., 2015b. Complement system part II: Role in immunity. *Front. Immunol.* 6, 1–26. <https://doi.org/10.3389/fimmu.2015.00257>
- Metchnikoff, I., 1884. A disease of *Daphnia* caused by a yeast. A contribution to the theory of phagocytes as agents for attack on disease-causing organisms. *Milestones Microbiol.* Prentice-Hall, Englewood 1961, 177–195.
- Mevorach, D., Mascarenhas, J.O., Gershov, D., Elkon, K.B., 1998. Complement-dependent clearance of apoptotic cells by human macrophages. *J. Exp. Med.* 188, 2313–20. <https://doi.org/10.5137/1019-5149.JTN.4165-11.2>
- Miksa, M., Komura, H., Wu, R., Shah, K.G., Wang, P., 2009. A novel method to determine the engulfment of apoptotic cells by macrophages using pHrodo succinimidyl ester. *J. Immunol. Methods* 342, 71–77. <https://doi.org/10.1016/j.jim.2008.11.019>
- Mills, C.D., Ley, K., 2014. M1 and M2 Macrophages: The Chicken and the Egg of Immunity. *J. Innate Immun.* 6, 716–726. <https://doi.org/10.1159/000364945>
- Misslitz, A., Mottram, J.C., Overath, P., Aebischer, T., 2000. Targeted integration into a rRNA locus results in uniform and high level expression of transgenes in *Leishmania* amastigotes. *Mol. Biochem. Parasitol.* 107, 251–61.
- Miyanishi, M., Tada, K., Koike, M., Uchiyama, Y., Kitamura, T., Nagata, S., 2007. Identification of Tim4 as a phosphatidylserine receptor. *Nature* 450, 435–439. <https://doi.org/10.1038/nature06307>
- Mocci, S., Coffman, R.L., 1997. The mechanism of in vitro T helper cell type 1 to T helper cell type 2 switching in highly polarized *Leishmania major*-specific T cell populations. *J. Immunol.* 158, 1559–64.
- Moradin, N., Descoteaux, A., 2012. *Leishmania* promastigotes: building a safe niche within macrophages. *Front. Cell. Infect. Microbiol.* 2, 1–7. <https://doi.org/10.3389/fcimb.2012.00121>
- Mosser, D.M., Edelson, P.J., 1985. The mouse macrophage receptor for C3bi (CR3) is a major mechanism in the phagocytosis of *Leishmania* promastigotes. *J. Immunol.* 135, 2785–9.
- Nakamura, K., Kusama, K., Bai, R., Ishikawa, S., Fukushima, S., Suda, Y., Imakawa, K., 2017. Increase in complement iC3b is associated with anti-inflammatory cytokine expression during late pregnancy in mice. *PLoS One* 12, e0178442. <https://doi.org/10.1371/journal.pone.0178442>
- Naldini, L., Blömer, U., Gallay, P., Ory, D., Mulligan, R., Gage, F.H., Verma, I.M., Trono, D., 1996. *In vivo* gene delivery and stable transduction of nondividing cells by a lentiviral vector. *Science* 272, 263–7.
- Nashleanas, M., Kanaly, S., Scott, P., 1998. Control of *Leishmania major* infection in mice lacking TNF receptors. *J. Immunol.* 160, 5506–13.



- Neefjes, J., Jongasma, M.L.M., Paul, P., Bakke, O., 2011. Towards a systems understanding of MHC class I and MHC class II antigen presentation. *Nat. Rev. Immunol.* 11, 823–836. <https://doi.org/10.1038/nri3084>
- Newton, K., Dixit, V.M., 2012. Signaling in Innate Immunity and Inflammation. *Cold Spring Harb. Perspect. Biol.* 4, a006049–a006049. <https://doi.org/10.1101/cshperspect.a006049>
- Nicolle, C., 1908. Culture du parasite du bouton d’Orient., in: *Comptes Rendus Hebdomadaires Des Séances de l’Académie Des Sciences*. Bachelier, Paris, pp. 842–843.
- Niessen, A., Heyder, P., Krienke, S., Blank, N., Tykocinski, L.-O., Lorenz, H.-M., Schiller, M., 2015. Apoptotic-cell-derived membrane microparticles and IFN- $\alpha$  induce an inflammatory immune response. *J. Cell Sci.* 128, 2443–2453. <https://doi.org/10.1242/jcs.162735>
- Niimi, T., 2012. Recombinant protein production in the eukaryotic protozoan parasite *Leishmania tarentolae*: A review. *Methods Mol. Biol.* [https://doi.org/10.1007/978-1-61779-433-9\\_15](https://doi.org/10.1007/978-1-61779-433-9_15)
- Nimmerjahn, F., Ravetch, J. V., 2010. Fc $\gamma$ Rs in Health and Disease. pp. 105–125. [https://doi.org/10.1007/82\\_2010\\_86](https://doi.org/10.1007/82_2010_86)
- Nunes, P., Demaurex, N., Mary, C., 2013. Regulation of the NADPH Oxidase and Associated Ion Fluxes During Phagocytosis 1118–1131. <https://doi.org/10.1111/tra.12115>
- Ogden, C.A., DeCathelineau, A., Hoffmann, P.R., Bratton, D., Ghebrehiwet, B., Fadok, V.A., Henson, P.M., 2001. C1q and Mannose Binding Lectin Engagement of Cell Surface Calreticulin and Cd91 Initiates Macropinocytosis and Uptake of Apoptotic Cells. *J. Exp. Med.* 194, 781–796. <https://doi.org/10.1084/jem.194.6.781>
- Ohradanova-Repic, A., Machacek, C., Fischer, M.B., Stockinger, H., 2016. Differentiation of human monocytes and derived subsets of macrophages and dendritic cells by the HLDA10 monoclonal antibody panel. *Clin. Transl. Immunol.* 5, e55-9. <https://doi.org/10.1038/cti.2015.39>
- Oswald, I.P., Wynn, T.A., Sher, A., James, S.L., 1992. Interleukin 10 inhibits macrophage microbicidal activity by blocking the endogenous production of tumor necrosis factor alpha required as a costimulatory factor for interferon gamma-induced activation. *Proc. Natl. Acad. Sci.* 89, 8676–8680. <https://doi.org/10.1073/pnas.89.18.8676>
- Ouakad, M., Bahi-Jaber, N., Chenik, M., Dellagi, K., Louzir, H., 2007. Selection of endogenous reference genes for gene expression analysis in *Leishmania major* developmental stages. *Parasitol. Res.* 101, 473–477. <https://doi.org/10.1007/s00436-007-0491-1>
- Pagan, A.J., Pepper, M., Chu, H.H., Green, J.M., Jenkins, M.K., 2012. CD28 Promotes CD4+ T Cell Clonal Expansion during Infection Independently of Its YMNM and PYAP Motifs. *J. Immunol.* 189, 2909–2917. <https://doi.org/10.4049/jimmunol.1103231>
- Park, D., Tosello-Tramont, A.C., Elliott, M.R., Lu, M., Haney, L.B., Ma, Z., et al., 2007. BAI1 is an engulfment receptor for apoptotic cells upstream of the ELMO/Dock180/Rac module. *Nature* 450, 430–434. <https://doi.org/10.1038/nature06329>

- Pauwels, A.M., Trost, M., Beyaert, R., Hoffmann, E., 2017. Patterns, Receptors, and Signals: Regulation of Phagosome Maturation. *Trends Immunol.* 38, 407–422. <https://doi.org/10.1016/j.it.2017.03.006>
- Peters, N.C., Egen, J.G., Secundino, N., Debrabant, A., Kimblin, N., Kamhawi, S., Lawyer, P., Fay, M.P., Germain, R.N., Sacks, D., 2008. In Vivo Imaging Reveals an Essential Role for Neutrophils in Leishmaniasis Transmitted by Sand Flies. *Science* 321, 970–974. <https://doi.org/10.1126/science.1159194>
- Polando, R., Dixit, U.G., Carter, C.R., Jones, B., Whitcomb, J.P., Ballhorn, W., Harintho, M., Jerde, C.L., Wilson, M.E., McDowell, M.A., 2013. The roles of complement receptor 3 and Fcγ receptors during *Leishmania* phagosome maturation. *J. Leukoc. Biol.* 93, 921–932. <https://doi.org/10.1189/jlb.0212086>
- Rajaram, M.V.S., Arnett, E., Azad, A.K., Guirado, E., Ni, B., Gerberick, A.D., He, L.-Z., Keler, T., Thomas, L.J., Lafuse, W.P., Schlesinger, L.S., 2017. *M. tuberculosis*-Initiated Human Mannose Receptor Signaling Regulates Macrophage Recognition and Vesicle Trafficking by FcRγ-Chain, Grb2, and SHP-1. *Cell Rep.* 21, 126–140. <https://doi.org/10.1016/j.celrep.2017.09.034>
- Ready, P.D., 2014. Epidemiology of visceral Leishmaniasis. *Clin. Epidemiol.* 6, 147–54. <https://doi.org/10.2147/CLEP.S44267>
- Reiling, N., Blumenthal, A., Flad, H.-D., Ernst, M., Ehlers, S., 2001. Mycobacteria-Induced TNF and IL-10 Formation by Human Macrophages Is Differentially Regulated at the Level of Mitogen-Activated Protein Kinase Activity. *J. Immunol.* 167, 3339–3345. <https://doi.org/10.4049/jimmunol.167.6.3339>
- Richards, D.M., Endres, R.G., 2014. The mechanism of phagocytosis: Two stages of engulfment. *Biophys. J.* 107, 1542–1553. <https://doi.org/10.1016/j.bpj.2014.07.070>
- Roche, P.A., Furuta, K., 2015. The ins and outs of MHC class II-mediated antigen processing and presentation. *Nat. Rev. Immunol.* 15, 203–216. <https://doi.org/10.1038/nri3818>
- Romao, S., Gasser, N., Becker, A.C., Guhl, B., Bajagic, M., Vanoaica, D., Ziegler, U., Roesler, J., Dengjel, J., Reichenbach, J., Münz, C., 2013. Autophagy proteins stabilize pathogen-containing phagosomes for prolonged MHC II antigen processing. *J. Cell Biol.* 203, 757–766. <https://doi.org/10.1083/jcb.201308173>
- Romao, S., Münz, C., 2014. LC3-associated phagocytosis. *Autophagy* 10, 526–528. <https://doi.org/10.4161/auto.27606>
- Rosales, C., Uribe-Querol, E., 2017. Phagocytosis: A Fundamental Process in Immunity. *Biomed Res. Int.* 2017. <https://doi.org/10.1155/2017/9042851>
- Rosenthal, L.A., Sutterwala, F.S., Kehrl, M.E., Mosser, D.M., 1996. *Leishmania major*-human macrophage interactions: Cooperation between Mac-1 (CD11b/CD18) and complement receptor type 1 (CD35) in promastigote adhesion. *Infect. Immun.* 64, 2206–2215.
- Ross, R., 1903. Further notes on Leishman's bodies. *Br. Med. J.* 2, 1401.
- Rossjohn, J., Gras, S., Miles, J.J., Turner, S.J., Godfrey, D.I., McCluskey, J., 2015. T cell antigen receptor recognition of antigen-presenting molecules. *Annu. Rev. Immunol.* 33, 169–200. <https://doi.org/10.1146/annurev-immunol-032414-112334>

- Rószter, T., 2015. Understanding the Mysterious M2 Macrophage through Activation Markers and Effector Mechanisms. *Mediators Inflamm.* 2015, 1–16. <https://doi.org/10.1155/2015/816460>
- Sacks, D.L., 1989. Metacyclogenesis in *Leishmania* promastigotes. *Exp. Parasitol.* 69, 100–103. [https://doi.org/10.1016/0014-4894\(89\)90176-8](https://doi.org/10.1016/0014-4894(89)90176-8)
- Salei, N., Hellberg, L., Köhl, J., Laskay, T., 2017. Enhanced survival of *Leishmania major* in neutrophil granulocytes in the presence of apoptotic cells. *PLoS One* 12, 1–15. <https://doi.org/10.1371/journal.pone.0171850>
- Sanjuan, M.A., Dillon, C.P., Tait, S.W.G., Moshiah, S., Dorsey, F., Connell, S., Komatsu, M., Tanaka, K., Cleveland, J.L., Withoff, S., Green, D.R., 2007. Toll-like receptor signalling in macrophages links the autophagy pathway to phagocytosis. *Nature* 450, 1253–1257. <https://doi.org/10.1038/nature06421>
- Sanjuan, M.A., Milasta, S., Green, D.R., 2009. Toll-like receptor signaling in the lysosomal pathways. *Immunol. Rev.* 227, 203–220. <https://doi.org/10.1111/j.1600-065X.2008.00732.x>
- Schille, S., Crauwels, P., Bohn, R., Bagola, K., van Zandbergen, G., 2017. LC3-associated phagocytosis in microbial pathogenesis. *Int. J. Med. Microbiol.* <https://doi.org/10.1016/j.ijmm.2017.10.014>
- Schönlau, F., Scharffetter-Kochanek, K., Grabbe, S., Pietz, B., Sorg, C., Sunderkötter, C., 2000. In experimental Leishmaniasis deficiency of CD18 results in parasite dissemination associated with altered macrophage functions and incomplete Th1 cell response. *Eur. J. Immunol.* 30, 2729–2740. [https://doi.org/10.1002/1521-4141\(200009\)30:9<2729::AID-IMMU2729>3.0.CO;2-3](https://doi.org/10.1002/1521-4141(200009)30:9<2729::AID-IMMU2729>3.0.CO;2-3)
- Skoberne, M., Somersan, S., Almodovar, W., Truong, T., Petrova, K., Henson, P.M., Bhardwaj, N., 2006. The apoptotic-cell receptor CR3, but not alphavbeta5, is a regulator of human dendritic-cell immunostimulatory function. *Blood* 108, 947–955. <https://doi.org/10.1182/blood-2005-12-4812>
- Sloma, I., Zilber, M.-T., Vasselon, T., Setterblad, N., Cavallari, M., Mori, L., De Libero, G., Charron, D., Mooney, N., Gelin, C., 2008. Regulation of CD1a Surface Expression and Antigen Presentation by Invariant Chain and Lipid Rafts. *J. Immunol.* 180, 980–987. <https://doi.org/10.4049/jimmunol.180.2.980>
- Soruri, A., Riggert, J., Schlott, T., Kiafard, Z., Dettmer, C., Zwirner, J., 2003. Anaphylatoxin C5a Induces Monocyte Recruitment and Differentiation into Dendritic Cells by TNF- $\alpha$  and Prostaglandin E2-Dependent Mechanisms. *J. Immunol.* 171, 2631–2636. <https://doi.org/10.4049/jimmunol.171.5.2631>
- Steinhäuser, C., Dallenga, T., Tchikov, V., Schaible, U.E., Schütze, S., Reiling, N., 2014. Immunomagnetic isolation of pathogen-containing phagosomes and apoptotic blebs from primary phagocytes. *Curr. Protoc. Immunol.* 105, 14.36.1-14.36.26. <https://doi.org/10.1002/0471142735.im1436s105>
- Steinhäuser, C., Heigl, U., Tchikov, V., Schwarz, J., Gutschmann, T., Seeger, K., Brandenburg, J., Fritsch, J., Schroeder, J., Wiesmüller, K.H., Rosenkrands, et al., 2013. Lipid-Labeling facilitates a novel magnetic isolation procedure to characterize pathogen-containing phagosomes. *Traffic* 14, 321–336. <https://doi.org/10.1111/tra.12031>

- Stephens, D.J., Allan, V.J., 2003. Light microscopy techniques for live cell imaging. *Science* 300, 82–86. <https://doi.org/10.1126/science.1082160>
- Swanson, J.A., 2008. Shaping cups into phagosomes and macropinosomes. *Nat. Rev. Mol. Cell Biol.* 9, 639–649. <https://doi.org/10.1038/nrm2447>
- Szklarczyk, D., Gable, A.L., Lyon, D., Junge, A., Wyder, S., Huerta-Cepas, J., Simonovic, M., Doncheva, N.T., Morris, J.H., Bork, P., Jensen, L.J., Mering, C. von, 2019. STRING v11: protein–protein association networks with increased coverage, supporting functional discovery in genome-wide experimental datasets. *Nucleic Acids Res.* 47, D607–D613. <https://doi.org/10.1093/nar/gky1131>
- Taheri, T., Saberi Nik, H., Seyed, N., Doustdari, F., Etemadzadeh, M.-H., Torkashvand, F., Rafati, S., 2015. Generation of stable *L. major*+EGFP-LUC and simultaneous comparison between EGFP and luciferase sensitivity. *Exp. Parasitol.* 150, 44–55. <https://doi.org/10.1016/j.exppara.2015.01.008>
- Takizawa, F., Tsuji, S., Nagasawa, S., 1996. Enhancement of macrophage phagocytosis upon iC3b deposition on apoptotic cells. *FEBS Lett.* 397, 269–72.
- Tamoutounour, S., Guilleims, M., Montanana Sanchis, F., Liu, H., Terhorst, D., Malosse, C., Pollet, E., Ardouin, L., Luche, H., Sanchez, C., Dalod, M., Malissen, B., Henri, S., 2013. Origins and Functional Specialization of Macrophages and of Conventional and Monocyte-Derived Dendritic Cells in Mouse Skin. *Immunity* 39, 925–938. <https://doi.org/10.1016/j.immuni.2013.10.004>
- Tanida, I., Ueno, T., Kominami, E., 2004. LC3 conjugation system in mammalian autophagy. *Int. J. Biochem. Cell Biol.* 36, 2503–2518. <https://doi.org/10.1016/j.biocel.2004.05.009>
- Tate, E.W., Kalesh, K.A., Lanyon-Hogg, T., Storck, E.M., Thinon, E., 2015. Global profiling of protein lipidation using chemical proteomic technologies. *Curr. Opin. Chem. Biol.* 24, 48–57. <https://doi.org/10.1016/j.cbpa.2014.10.016>
- Taylor, R.P., Ferguson, P.J., Martin, E.N., Cooke, J., Greene, K.L., Grinspun, K., Guttman, M., Kuhn, S., 1997. Immune complexes bound to the primate erythrocyte complement receptor (CR1) via anti-CR1 mAbs are cleared simultaneously with loss of CR1 in a concerted reaction in a rhesus monkey model. *Clin. Immunol. Immunopathol.* 82, 49–59.
- Tchikov, V., Schütze, S., 2008. Immunomagnetic isolation of tumor necrosis factor receptosomes. *Methods Enzymol.* 442, 101–23. [https://doi.org/10.1016/S0076-6879\(08\)01405-5](https://doi.org/10.1016/S0076-6879(08)01405-5)
- Teixeira, C.R., Teixeira, M.J., Gomes, R.B.B., Santos, C.S., Andrade, B.B., Raffaele-Netto, I., Silva, J.S., Guglielmotti, A., Miranda, J.C., Barral, A., Brodskyn, C., Barral-Netto, M., 2005. Saliva from *Lutzomyia longipalpis* Induces CC Chemokine Ligand 2/Monocyte Chemoattractant Protein-1 Expression and Macrophage Recruitment. *J. Immunol.* 175, 8346–8353. <https://doi.org/10.4049/jimmunol.175.12.8346>
- ter Horst, R., Jaeger, M., Smeekens, S.P., Oosting, M., Swertz, M.A., Li, Y., Kumar, V., Diavatopoulos, D.A., Jansen, A.F.M., Lemmers, H., Toenhake-Dijkstra, H., van Herwaarden, A.E., Janssen, M., van der Molen, R.G., Joosten, et al., 2016. Host and Environmental Factors Influencing Individual Human Cytokine Responses. *Cell* 167, 1111–1124.e13. <https://doi.org/10.1016/j.cell.2016.10.018>

- Thomas, M., 2015. *Leishmania major* promastigote entry of an autophagy-like compartment and amastigote escape from the parasitophorous vacuole. PhD thesis, University Mainz.
- Titus, R.G., Marchand, M., Boon, T., Louis, J.A., 1985. A limiting dilution assay for quantifying *Leishmania major* in tissues of infected mice. *Parasite Immunol.* 7, 545–55.
- Tomiotto-Pellissier, F., Bortoleti, B.T. da S., Assolini, J.P., Gonçalves, M.D., Carloto, A.C.M., Miranda-Sapla, M.M., Conchon-Costa, I., Bordignon, J., Pavanelli, W.R., 2018. Macrophage Polarization in Leishmaniasis: Broadening Horizons. *Front. Immunol.* 9, 2529. <https://doi.org/10.3389/fimmu.2018.02529>
- Ueno, N., Bratt, C.L., Rodriguez, N.E., Wilson, M.E., 2009. Differences in human macrophage receptor usage, lysosomal fusion kinetics and survival between logarithmic and metacyclic *Leishmania infantum chagasi* promastigotes. *Cell. Microbiol.* 11, 1827–1841. <https://doi.org/10.1111/j.1462-5822.2009.01374.x>
- Ueno, N., Wilson, M.E., 2012. Receptor-mediated phagocytosis of *Leishmania*: implications for intracellular survival. *Trends Parasitol.* 28, 335–344. <https://doi.org/10.1016/j.pt.2012.05.002>
- van der Meer, J.W., van de Gevel, J.S., Blussé van Oud Alblas, A., Kramps, J.A., van Zwet, T.L., Leijh, P.C., van Furth, R., 1982. Characteristics of human monocytes cultured in the Teflon culture bag. *Immunology* 47, 617–25.
- van Zandbergen, G., Bollinger, A., Wenzel, A., Kamhawi, S., Voll, R., Klinger, M., Müller, A., Hölscher, C., Herrmann, M., Sacks, D., Solbach, W., Laskay, T., 2006. *Leishmania* disease development depends on the presence of apoptotic promastigotes in the virulent inoculum. *Proc. Natl. Acad. Sci. U. S. A.* 103, 13837–42. <https://doi.org/10.1073/pnas.0600843103>
- van Zandbergen, G., Klinger, M., Mueller, A., Dannenberg, S., Gebert, A., Solbach, W., Laskay, T., 2004. Cutting Edge: Neutrophil Granulocyte Serves as a Vector for *Leishmania* Entry into Macrophages. *J. Immunol.* 173, 6521–6525. <https://doi.org/10.4049/jimmunol.173.11.6521>
- Vicidomini, G., Bianchini, P., Diaspro, A., 2018. STED super-resolved microscopy. *Nat. Methods* 15, 173–182. <https://doi.org/10.1038/nmeth.4593>
- Voll, R.E., Herrmann, M., Roth, E.A., Stach, C., Kalden, J.R., Girkontaite, I., 1997. Immunosuppressive effects of apoptotic cells. *Nature* 390, 350–351. <https://doi.org/10.1038/37022>
- von Stebut, E., Tenzer, S., 2018. Cutaneous Leishmaniasis: Distinct functions of dendritic cells and macrophages in the interaction of the host immune system with *Leishmania major*. *Int. J. Med. Microbiol.* 308, 206–214. <https://doi.org/10.1016/j.ijmm.2017.11.002>
- Vorup-Jensen, T., Jensen, R.K., 2018. Structural immunology of complement receptors 3 and 4. *Front. Immunol.* 9, 1–20. <https://doi.org/10.3389/fimmu.2018.02716>

- Wanderley, J.L.M., da Silva, L.H.P., Deolindo, P., Soong, L., Borges, V.M., Prates, D.B., de Souza, A.P.A., Barral, A., de Freitas Balanco, J.M., do Nascimento, M.T.C., Saraiva, E.M., Barcinski, M.A., 2009. Cooperation between apoptotic and viable metacyclics enhances the pathogenesis of Leishmaniasis. *PLoS One* 4, 1–11. <https://doi.org/10.1371/journal.pone.0005733>
- Wanderley, J.L.M., Thorpe, P.E., Barcinski, M.A., Soong, L., 2013. Phosphatidylserine exposure on the surface of *Leishmania amazonensis* amastigotes modulates in vivo infection and dendritic cell function. *Parasite Immunol.* 35, 109–19. <https://doi.org/10.1111/pim.12019>
- Weis, J.J., Tedder, T.F., Fearon, D.T., 1984. Identification of a 145,000 Mr membrane protein as the C3d receptor (CR2) of human B lymphocytes. *Proc. Natl. Acad. Sci. U. S. A.* 81, 881–5.
- Wenzel, U.A., Bank, E., Florian, C., Förster, S., Zimara, N., Steinacker, J., Klinger, M., Reiling, N., Ritter, U., van Zandbergen, G., 2012. *Leishmania major* parasite stage-dependent host cell invasion and immune evasion. *FASEB J.* 26, 29–39. <https://doi.org/10.1096/fj.11-184895>
- West, A.P., Brodsky, I.E., Rahner, C., Woo, D.K., Erdjument-Bromage, H., Tempst, P., Walsh, M.C., Choi, Y., Shadel, G.S., Ghosh, S., 2011. TLR signalling augments macrophage bactericidal activity through mitochondrial ROS. *Nature* 472, 476–480. <https://doi.org/10.1038/nature09973>
- Whitehead, K.A., Dahlman, J.E., Langer, R.S., Anderson, D.G., 2011. Silencing or Stimulation? siRNA Delivery and the Immune System. *Annu. Rev. Chem. Biomol. Eng.* 2, 77–96. <https://doi.org/10.1146/annurev-chembioeng-061010-114133>
- WHO, 2019a. Neglected tropical diseases [WWW Document]. URL [https://www.who.int/neglected\\_diseases/diseases/en/](https://www.who.int/neglected_diseases/diseases/en/) (accessed 2/7/19).
- WHO, 2019b. Fact sheet on Leishmaniasis [WWW Document]. URL [www.who.int/en/news-room/fact-sheets/detail/Leishmaniasis](http://www.who.int/en/news-room/fact-sheets/detail/Leishmaniasis) (accessed 2/7/19).
- WHO, 2019c. Leishmaniasis - Epidemics [WWW Document]. URL <https://www.who.int/Leishmaniasis/epidemic/epidemics/en> (accessed 2/7/19).
- WHO, 2019d. Leishmaniasis - Research [WWW Document]. URL <https://www.who.int/Leishmaniasis/research/en/> (accessed 2/7/19).
- WHO, 2017a. Integrating neglected tropical diseases into global health and development: fourth WHO report on neglected tropical diseases. Geneva.
- WHO, 2017b. Leishmaniasis - Burden [WWW Document]. URL <https://www.who.int/Leishmaniasis/burden/en/> (accessed 2/20/19).
- WHO, 2010. Report of a meeting of the WHO Expert Committee on the Control of Leishmaniases, Geneva, Switzerland, 22-26 March 2010. World Health Organization, Geneva, pp. 1–186.
- Wilson, M.E., Pearson, R.D., 1988. Roles of CR3 and mannose receptors in the attachment and ingestion of *Leishmania donovani* by human mononuclear phagocytes. *Infect. Immun.* 56, 363–369.

- Woelbing, F., Kostka, S.L., Moelle, K., Belkaid, Y., Sunderkoetter, C., Verbeek, S., Waisman, A., Nigg, A.P., Knop, J., Udey, M.C., von Stebut, E., 2006. Uptake of *Leishmania major* by dendritic cells is mediated by Fcγ receptors and facilitates acquisition of protective immunity. *J. Exp. Med.* 203, 177–188. <https://doi.org/10.1084/jem.20052288>
- Wolfrum, N., Mühlebach, M.D., Schüle, S., Kaiser, J.K., Kloke, B.-P., Cichutek, K., Schweizer, M., 2007. Impact of viral accessory proteins of SIVsmmPBj on early steps of infection of quiescent cells. *Virology* 364, 330–41. <https://doi.org/10.1016/j.virol.2007.03.008>
- Yates, R.M., Hermetter, A., Russell, G., 2005. The Kinetics of Phagosome Maturation as a Function of Phagosome / Lysosome Fusion and Acquisition of Hydrolytic Activity. *Traffic* 5, 413–420. <https://doi.org/10.1111/j.1600-0854.2005.00284.x>
- Yeo, J.C., Wall, A.A., Luo, L., Stow, J.L., 2016. Sequential recruitment of Rab GTPases during early stages of phagocytosis. *Cell. Logist.* 6, 1–12. <https://doi.org/10.1080/21592799.2016.1140615>
- Zahn, S., Kirschsiefen, P., Jonuleit, H., Steinbrink, K., Von Stebut, E., 2010. Human primary dendritic cell subsets differ in their IL-12 release in response to *Leishmania major* infection. *Exp. Dermatol.* 19, 924–926. <https://doi.org/10.1111/j.1600-0625.2010.01149.x>
- Zangger, H., Mottram, J.C., Fasel, N., 2002. Cell death in *Leishmania* induced by stress and differentiation: programmed cell death or necrosis? *Cell Death Differ.* 9, 1126–39. <https://doi.org/10.1038/sj.cdd.4401071>
- Zeichner, S.L., 1983. Isolation and characterization of macrophage phagosomes containing infectious and heat-inactivated *Chlamydia psittaci*: two phagosomes with different intracellular behaviors. *Infect. Immun.* 40, 956–66.

## 9. List of figures

|   |    |
|---|----|
| Figure 1: Exemplary images of the three clinical manifestations of Leishmaniasis and new occurrences of Leishmaniasis in 2017 .....                                     | 3  |
| Figure 2: Life stages of <i>Leishmania</i> sp.....  | 4  |
| Figure 3: Life cycle of <i>Leishmania</i> parasites.....  | 5  |
| Figure 4: Major steps in phagocytosis .....   | 8  |
| Figure 5: LC3-associated phagocytosis. ....   | 10 |
| Figure 6: Hypothesis and aims of the study .....  | 18 |
| Figure 7: Growth curve of <i>Leishmania major</i> promastigotes .....   | 66 |
| Figure 8: AnnexinA5-MACS separation yields pure apoptotic and viable <i>L. major</i> promastigotes .....  | 67 |
| Figure 9: Investigation of interaction upon differential infection of hMDM with viable and apoptotic <i>Lm</i> and quantification by flow cytometry or microscopy ..... | 69 |
| Figure 10: Transduction with eGFP-LC3 lentiviral particles transiently induces conversion of endogenous LC3 in hMDMs.....   | 71 |
| Figure 11: Purified viable and apoptotic <i>Lm</i> are sequestered in LC3 <sup>+</sup> phagosomes in hMDMs.....   | 72 |
| Figure 12: Quantification of time-lapse imaging of eGFP-LC3-positive compartments within hMDMs.....   | 74 |
| Figure 13: 3D reconstruction of a viable <i>Lm</i> within a phagosome connected to the extracellular space .....  | 76 |
| Figure 14: Quantification of <i>Lm</i> and LAMP1 positive staining, indicating possible tunnel structures. ....   | 77 |
| Figure 15: Schematic presentation of the magnet-based compartment isolation. ....   | 78 |
| Figure 16: Apoptotic <i>Lm</i> are efficiently labeled with lipobiotin-coated magnetic microbeads.....  | 79 |
| Figure 17: Western blot analysis of samples collected during magnetic isolation of phagosomes .....   | 81 |
| Figure 18: STRING analysis of the 40 most abundant host cell-derived proteins as identified by LC-MS .....  | 82 |
| Figure 19: Characterization of <i>in vitro</i> -generated human monocyte-derived macrophages and dendritic cells .....  | 85 |



|  |     |
|--|-----|
| Figure 20: Analyses of IL-1 $\beta$ , IL-6 and IL-8 secretion of differentially <i>Lm</i> -infected hMDMs and hMDDC.....         | 87  |
| Figure 21: Analyses of TNF- $\alpha$ and IL-10 secretion by differentially <i>Lm</i> -infected hMDMs and hMDDC.....              | 89  |
| Figure 22: Analysis of blocking or siRNA-mediated knockdown of CD91 on hMDMs.....  | 91  |
| Figure 23: Knockdown of CD91 does not alter <i>Lm</i> infection rates of hMDMs.....  | 92  |
| Figure 24: Knockdown of CR3 by specific siRNA.....   | 94  |
| Figure 25: Characterization of siCD11b-transfected human monocyte-derived macrophages.....                                       | 95  |
| Figure 26: Knockdown of CD11b decreases infection rates of apoptotic <i>Lm</i> in hMDM1 and hMDM2 .....                          | 96  |
| Figure 27: Efficient blocking of Complement Receptor 3 with an $\alpha$ -CD11b antibody .....                                    | 97  |
| Figure 28: Gating-strategy to identify infection of hMDMs or hMDDCs with <i>Lm</i> .....   | 98  |
| Figure 29: Blocking of CR3 results in decreased interaction of apoptotic <i>Lm</i> with hMDMs .....                              | 99  |
| Figure 30: Blocking of CR3 results in strong reduction of TNF- $\alpha$ and IL-10 secretion by hMDMs .....                       | 101 |
| Figure 31: LC3-associated phagocytosis of apoptotic <i>L. major</i> promastigotes is reduced by inhibition of CR3 in hMDM2. .... | 103 |
| Figure 32: Gating strategy for determination of proliferated T cells. ....   | 105 |
| Figure 33: T cell proliferation is unaltered in presence of $\alpha$ -CD11b .....  | 105 |
| Figure 34: Survival of viable <i>Lm</i> is not altered upon inhibition of CR3.....   | 107 |
| Figure 35: Conclusion.....   | 123 |

## 10. List of tables

|  |    |
|--|----|
| Table 1: List of the 20 neglected tropical diseases as classified by the World Health Organization (WHO, 2019a).....               | 1  |
| Table 2: Ratios and volumes needed for a large-scale transfection of HEK293T/17 cells for lentiviral vector-production. ....       | 53 |
| Table 3: Preparation of solutions A and B for siRNA transfection of hMDMs per well of a 6-well cell culture plate.....             | 55 |
| Table 4: Preparation of RNA samples for reverse transcription by annealing of random primers. ....                                 | 56 |
| Table 5: Preparation of the master-mix for reverse transcription of isolated RNA with the ImPromII Reverse Transcription Kit. .... | 56 |
| Table 6: Thermo cycler program for reverse transcription using the ImPromII Reverse Transcription Kit.....                         | 56 |
| Table 7: Preparation of the master-mix for quantitative real-time polymerase chain reaction with the MESA Blue qPCR Kit.....       | 57 |
| Table 8: Amplification-program for quantitative real-time PCR in a LightCycler 480. ....   | 57 |
| Table 9: Components and volume for the preparation of two 15 % polyacrylamide gels for SDS-PAGE. ....                              | 58 |
| Table 10: Amount of protein present in isolated phagosomes as quantified by BCA assay. ....  | 80 |
| Table 11: Mass spectrometric identification of highly abundant proteins in isolated compartments.....                              | 83 |

## 11. Declaration of authorship

I hereby certify that I have written the present dissertation with the topic:

“Complement Receptor 3 and its role in interaction of primary human macrophages with apoptotic *Leishmania major* promastigotes”

independently, using no other aids than those I have cited. I have clearly mentioned the source of the passages that are taken word for word or paraphrased from other works. Experiments that were performed with or from other persons are indicated in the respective figure legends.

The presented thesis has not been submitted in this or any other form to another faculty or examination institution.

### Eidesstattliche Versicherung

Hiermit versichere ich, dass ich die vorgelegte Dissertation mit dem Titel

“Complement Receptor 3 and its role in interaction of primary human macrophages with apoptotic *Leishmania major* promastigotes”

selbstständig verfasst habe und keine anderen als die angegebenen Quellen und Hilfsmittel verwendet habe. Die Stellen der Dissertation, die anderen Werken und Veröffentlichungen dem Wortlaut oder dem Sinn nach entnommen wurden, sind durch Quellenangaben gekennzeichnet. Von, oder gemeinsam mit, anderen Personen durchgeführte Experimente sind in der jeweiligen Abbildungsunterschrift kenntlich gemacht.

Diese Dissertation wurde in der jetzigen oder in ähnlicher Form noch an keiner anderen Hochschule eingereicht und hat noch keinen sonstigen Prüfungszwecken gedient.

Frankfurt, 9 July 2019

Stefan A. Schille







